BARRIERS TO PROGRESS IN THE SIMULATION OF VISCOELASTIC FLOWS OF MOLTEN PLASTICS

by

Marie-Claude Heuzey

Department of Chemical Engineering

McGill University

Montreal, Canada

September 1999

A Thesis submitted to the Faculty of Graduate Studies and Research in partial fulfillment of the requirements of the degree of Doctor of Philosophy

0-612-55341-8

ABSTRACT

Polymer melts exhibit some degree of viscoelasticity in most industrial forming operations, and elasticity is particularly important in flows involving an abrupt contraction or expansion in the flow direction. However, the incorporation of a viscoelastic constitutive equation into computer models for polymer processing poses many problems, and for this reason inelastic models have been used almost exclusively to represent rheological behavior for flow simulation in the plastics industry.

In order to explore the limits of viscoelastic flow simulations, we used two nonlinear viscoelastic models (Leonov and Phan-Thien/Tanner) to simulate axisymmetric and planar contraction flows and extrudate swell. Their predictions were compared with those obtained using a strictly viscous model (Carreau-Yasuda) and with experimental results. The models are implemented in a modified Elastic Viscous Split Stress (EVSS) mixed finite element formulation. The viscoelastic constitutive equations are calculated using the Lesaint-Raviart method, and the divergence-free Stokes problem is solved applying Uzawa's algorithm. The decoupled iterative scheme is used as a preconditioner for the Generalized Minimal Residual (GMRES) method. Numerical instability was observed starting at quite low elasticity levels. For the converging flows, the predicted flow patterns were in fair agreement with experimental results, but there was a large discrepancy in the entrance pressure drop. In the case of extrudate swell, the agreement with observation was poor, and convergence was impossible except at the lowest flow rate.

After exploring the limits of simulations using viscoelastic models, we conclude that there are serious barriers to progress in the simulation of viscoelastic flows of industrial importance. The ultimate source of the problem is the melt elasticity, and traditional numerical methods and rheological models do not provide a suitable basis for simulating practical flows. A new approach is required, and we propose that a rule-based expert system be used.

À la mémoire de mon père.

RÉSUMÉ

Les polymères fondus présentent généralement un caractère viscoélastique lors des procédés de transformation industriels. L'élasticité devient particulièrement importante dans les géométries comportant une contraction ou une expansion abrupte en direction de l'écoulement. Toutefois, l'incorporation de lois de comportement viscoélastique pour la modélisation des procédés de transformation des polymères s'avère difficile, et de ce fait des modèles inélastiques ont presque exclusivement été utilisés lors des simulations d'écoulements d'importance industrielle.

Afin d'explorer les limites des simulations d'écoulements viscoélastiques, nous avons utilisé deux modèles viscoélastiques non linéaires (Leonov et Phan-Thien/Tanner) afin de simuler les écoulements dans des contractions plane et axisymmétrique ainsi que le gonflement d'extrudat. Les prédictions des deux modèles ont été comparées à celles obtenues à l'aide d'un modèle strictement visqueux (Carreau-Yasuda) et à des mesures expérimentales. Les lois de comportement sont incorporées à une formulation mixte d'éléments finis de type "Elastic Viscous Split Stress" (EVSS) modifiée. La méthode de Lesaint-Raviart sert à la résolution des modèles viscoélastique, et le calcul du problème de Stokes est effectué à l'aide de l'algorithme d'Uzawa. Une approche découplée basée sur l'algorithme "Generalized Minimal Residual" (GMRES) est utilisée pour traiter la non linéarité du problème.

Lors des simulations, des instabilités numériques ont été observées à faible niveaux d'élasticité. Pour les géométries convergentes, les écoulements prédits ont montré un accord satisfaisant avec les données expérimentales, sauf les pertes de pression en entrée qui sont largement sous-estimées. Dans le cas du gonflement d'extrudat, la convergence numérique n'a été possible qu'au plus faible débit et le gonflement prédit est largement sous-estimé.

Suite à l'exploration des limites des simulations à l'aide de lois de comportement viscoélastiques, nous concluons qu'il existe toujours de sérieux obstacles au progrès de la simulation d'écoulements d'importance industrielle. La source ultime du problème réside dans l'élasticité du polymère fondu, et les méthodes numériques traditionnelles de même que les modèles rhéologiques existants ne comportent pas la solution au succès des simulations d'écoulements d'intérêt pratique. Une nouvelle approche est requise, et nous suggérons l'utilisation d'un système expert afin de guider l'évolution des calculs numériques.

REMERCIEMENTS

En premier lieu j'aimerais remercier mes directeurs de thèse, les professeurs John M. Dealy et André Fortin, qui ont toujours su m'encourager et faire preuve d'une patience infinie tout au long de ce projet. Je leur suis aussi fort reconnaissante pour leur générosité et l'ambiance agréable qu'ils ont su établir dans leur groupe de recherche respectif, tant à l'Université McGill qu'à l'École Polytechnique, ce qui a passablement allégé les trois années qu'ont duré mes études doctorales.

J'inclus aussi dans mes remerciements le personnel technique des deux universités qui a rendu possible la mise à terme de ce projet: spécialement MM. Alain Gagnon, Walter Greenland, Charles Dolan et Luciano Cusmish de l'Université McGill, ainsi que Benoît Forest de l'École Polytechnique.

Je suis fort reconnaissante envers Mazen Samara et le Prof. Kamal pour avoir permis l'utilisation de l'appareillage de mesure du gonflement d'extrudat. Aussi un immense merci au personnel du CEMEF à Sophia-Antipolis en France, particulièrement Lucia Gavrus, Erik Brotons, Bruno Vergnes et le Prof. Agassant qui m'ont accueillie au centre de recherche et assistée dans les mesures de l'écoulement plan. Je garde un souvenir impérissable de la Côte d'Azur.

Merci aussi à tous mes collègues de travail pour leur camaderie et entraide, particulièrement Seung Oh Kim, François Koran, Stewart McGlashan et ma grande amie Paula Wood-Adams de l'Université McGill, ainsi que Alain Béliveau, Alain Lioret et Steven Dufour de l'École Polytechnique.

Finalement, je remercie spécialement mes proches dont ma famille et mon compagnon Luc pour leur patience, leur amour et encouragement qui m'ont permis d'aller au bout de cette étape.

TABLE OF CONTENTS

LIST OF TABLES

LIST OF FIGURES

1. Introduction

The broadening of the range of application of plastic parts requires improved final product quality, in terms of both mechanical properties and exterior appearance. Standards for product quality have been raised, while increased competitiveness requires reductions in product development time and unit cost. However, plastic processing continues to involve long product development cycles, high tooling costs, low process yields and product inconsistencies. Numerical simulation can reduce the time required to develop new processes and machines and can aid process optimization by:

1. extrapolation or scale-up of designs,
2. exploration of the effects of individual variables,
3. sensitivity and stability analysis,

all this being achieved at a lower cost than if carried out experimentally.

An important issue in polymer processing is melt rheology, which deals with the relationship between stress and strain in deformable materials. Polymeric liquids are rheologically complex, since they exhibit both viscous resistance to deformation and elasticity. An understanding of their rheological behavior is essential in the development, production and processing of polymeric materials. However, flow phenomena arising from viscoelasticity are very complex, and these cause several problems in the mathematical modeling of certain forming processes. Inelastic models may be adequate to simulate flows in which shear stresses are predominant, but if elongational effects are also important, the viscoelastic nature of polymeric materials can not be ignored.

Plastics can be molded, extruded, formed, machined and joined into various shapes. In several processing operations such as fiber spinning, thermoforming and injection and blow molding, the polymer undergoes both shear and elongation. Viscoelasticity not only affects melt flow but also plays a major role in the development of the microstructure and physical properties of the final plastic part. However, since the incorporation of a viscoelastic constitutive equation into a computer model for polymer processing poses many problems, inelastic models have been used almost exclusively to represent rheological behavior for flow simulation in the plastics industry.

Moreover, all previous attempts to find a general viscoelastic fluid model applicable to all classes of flow and capable of realistic predictions have failed. The motivation for this research was first to determine the limitations of present methods and models for the numerical simulation of the flow of viscoelastic materials. The second objective was to establish the cause of these limitations and suggest methods for overcoming them. To achieve these objectives, two complex flows were subjected to both numerical simulation and experimental observation.

In the next chapter, the state-of-the-art of numerical simulation of the flow of viscoelastic materials is reviewed. In Chapter 3, we present the plan of the research and the constitutive equations selected. Chapter 4 describes the materials used for the experimental study and presents their rheological properties, while Chapter 5 gives the method used to determine the various model parameters. In Chapter 6 we describe the numerical procedure used in the simulations. Experimental methods and results are presented in Chapter 7 for the planar abrupt contraction flow, and in Chapter 8 for the axisymmetric entrance flow and extrudate swell. Chapter 9 presents alternatives to full viscoelastic simulations and proposes a rule-based system for flow simulation. Finally, conclusions, original contributions to knowledge and recommendations for future work are given in Chapter 10.

2. Numerical Simulation of Viscoelastic Flow: State-of-the-Art

2.1 Constitutive Equations for Polymer Melts

Polymer melts behave very differently from purely viscous materials, because in addition to viscous resistance to deformation, they exhibit elasticity. The reason why polymeric liquids are non-Newtonian is related to their molecular structure[1]. Polymer molecules can be represented by long chains with many joints allowing relative rotation of adjacent links, and the presence of this large number of joints allows many different configurations and makes the molecule flexible. At rest, there will be a unique average value of the end-to-end distance, R, for the molecules of a given polymer. When the melt is deformed, this average length is altered, and when the deformation is stopped, Brownian motion will tend to return R to its equilibrium value. This is the molecular origin of the elastic and relaxation phenomena that occur in polymeric liquids, which are said to have a "fading memory".

In this section, we will describe briefly some flow phenomena associated with viscoelasticity and present several constitutive equations that have been developed for polymeric fluids.

2.1.1 Viscoelastic Flow Phenomena

A number of phenomena encountered in the flow of polymers cannot be explained on the basis of purely viscous behavior. We describe a few of these phenomena, and a more thorough discussion on the subject can be found in references 2, 3 and 4.

Weissenberg Effect

This effect, also called rod climbing, was reported by Weissenberg in 1947[5]. It is the tendency of an elastic liquid to rise up around a rotating shaft partially immersed in it. This is very different from the behavior of a Newtonian fluid, which will flow towards the walls due to inertia forces. In the absence of inertial effects, the free surface of a Newtonian fluid would remain flat. Weissenberg deduced that the phenomenon was caused by an elastic normal stress acting along the circular streamlines. This normal stress exists in all shear flows of polymeric liquids except at very low shear rates. Dealy and Vu studied rod climbing in molten polymers[6].

Extrudate Swell

Extrudate swell is defined as the increase in the diameter of a stream as it exits a die. For a Newtonian fluid at low Reynolds number (*Re*), axisymmetric extrudate swell at the exit of a capillary is of the order of 12-13%, and it decreases as *Re* increases, even becoming negative. For a viscoelastic liquid, this extrudate swell can be as high as 200-300%. This phenomenon is related to normal stress differences and increases with increasing flow rate. Due to the fluid's memory, the swell depends on the flow at the entrance to the capillary, but for a sufficiently long capillary, this effect becomes negligible because it is a "fading memory".

Tubeless Siphon

In 1908, Fano[7] reported a remarkable manifestation of fluid elasticity. In an experiment where he immersed the tip of a capillary tube in a beaker filled with a biological macromolecular fluid, he began withdrawing liquid from the beaker through the tube. However, even after the fluid level in the beaker dropped below the tip of the capillary tube, the fluid continued to flow upwards to the tip of the no-longer-submerged capillary. This phenomenon is known as a tubeless siphon and results from the large tensile stress that the fluid can support due to its elasticity[2].

Other flow phenomena such as vortex formation in contraction flows are also related to the elasticity of polymeric fluids.

Simple Flows

For a Newtonian fluid, the viscosity η is independent of shear rate, but for a polymeric fluid η decreases with increasing shear rate; i.e. these fluids are "shear thinning". But shear thinning alone does not imply that a fluid is viscoelastic. A stronger indication of viscoelasticity is the existence of normal stress differences in shearing deformations, which give rise, for example, to the Weissenberg effect.

Another manifestation of viscoelasticity is stress relaxation. Stresses will persist in these materials after deformation has ceased, and the duration of the time during which stresses persist is called the relaxation time of the material. Recoil, the reverse deformation that occurs when the fluid is suddenly relieved of an externally imposed stress, is another manifestation of viscoelasticity. A realistic viscoelastic constitutive equation must be able to predict all the phenomena mentioned above.

2.1.2 Definitions of Tensors and Material Functions

We present here definitions of the tensors and rheological material functions that are used throughout this thesis. The reader is referred to Dealy and Wissbrun[1] for a thorough discussion of these quantities.

Tensors

The strain rate or rate of deformation tensor $\underline{\underline{D}}$ is given by:

Eqn. 2-1 $$\underline{\underline{D}} = \frac{1}{2}\left(\nabla\underline{u} + (\nabla\underline{u})^T\right)$$

where $\underline{u}$ is the velocity vector.

The extra stress or viscous stress tensor $\underline{\underline{\tau}}$ is defined as follows:

Eqn. 2-2 $$\underline{\underline{\tau}} \equiv \underline{\underline{\sigma}} + p\underline{\underline{I}}$$

where p is the pressure, $\underline{\underline{\sigma}}$ is the Cauchy stress tensor and $\underline{\underline{I}}$ is the unit tensor.

Useful measures of strain in polymer rheology are the Cauchy tensor $C_{ij}(t_1,t_2)$ and the Finger tensor $B_{ij}(t_1,t_2)$. The Finger tensor is the inverse of the Cauchy tensor and can also be written $C_{ij}^{-1}(t_1,t_2)$. The first, second and third invariants of the Finger tensor are defined as follows:

Eqn. 2-3 $$I_1 = B_{11} + B_{22} + B_{33}$$

Eqn. 2-4 $$I_2 = C_{11} + C_{22} + C_{33}$$

Eqn. 2-5 $$I_3 = \det(\underline{\underline{B}}) = 1$$

Material Functions

In steady shear, the following material functions (the "viscometric" functions) are defined $(D_{12} \equiv \dot{\gamma})$:

Eqn. 2-6 $$\eta(\dot{\gamma}) \equiv \frac{\tau_{12}}{\dot{\gamma}}$$ (viscosity)

Eqn. 2-7 $$N_1 \equiv \sigma_{11} - \sigma_{22}$$ (first normal stress difference)

Eqn. 2-8 $$N_2 \equiv \sigma_{22} - \sigma_{33}$$ (second normal stress difference)

Sometimes the normal stress coefficients are used:

Eqn. 2-9 $$\Psi_1 \equiv \frac{N_1}{\dot{\gamma}^2}$$ (first normal stress coefficient)

Eqn. 2-10 $$\Psi_2 \equiv \frac{N_2}{\dot{\gamma}^2}$$ (second normal stress coefficient)

Start-up and cessation of shear flow is denoted by a plus or minus sign, respectively:

Eqn. 2-11 $$\eta^+(t,\dot{\gamma}) \equiv \frac{\tau_{12}(t,\dot{\gamma})}{\dot{\gamma}}$$ (start-up flow)

Eqn. 2-12 $$\eta^{-}(t,\dot{\gamma}) \equiv \frac{\tau_{12}(t,\dot{\gamma})}{\dot{\gamma}}$$ (cessation of flow)

In simple uniaxial elongation, we defined a principal stretching stress σ_E:

Eqn. 2-13 $$\sigma_E = \sigma_{11} - \sigma_{22} = \sigma_{11} - \sigma_{33}$$

The elongational viscosity is defined as follows for steady uniaxial elongational flow:

Eqn. 2-14 $$\eta_E(\dot{\varepsilon}) \equiv \frac{\sigma_E}{\dot{\varepsilon}}$$

For start-up of elongational flow, we have the tensile stress growth coefficient:

Eqn. 2-15 $$\eta_E(t,\dot{\varepsilon}) \equiv \frac{\sigma(t,\dot{\varepsilon})}{\dot{\varepsilon}}$$

2.1.3 Generalized Newtonian Fluid Models

The first requirement of a constitutive equation to be used for flow simulation is that it describes adequately the rheological behavior that govern the flow of interest. For certain restricted flows, there are general constitutive equations that relate the stress tensor to the deformation history in terms of a few material parameters or functions. For example, viscometric flows are flows that, from the point of view of a material element, cannot be distinguished from simple shear[2]. Although the shear rate may vary from particle to particle, the deformation history of each fluid element is constant as it flows along a streamline.

The extra stress tensor for viscometric flows is described by the Criminale-Ericksen-Filbey (CEF) equation[4,8]. If it is formulated using the upper-convected derivative of the rate of deformation tensor $\overset{\nabla}{\underline{\underline{D}}}$, it can be written as follows:

Eqn. 2-16 $$\underline{\underline{\tau}} = 2\eta\underline{\underline{D}} - \Psi_1 \overset{\nabla}{\underline{\underline{D}}} + 4\Psi_2 \underline{\underline{D}}^2$$

where the viscosity and first and second normal stress coefficients are functions of II_D, the second invariant of the rate of deformation tensor $\underline{\underline{D}}$:

Eqn. 2-17 $$II_D \equiv 2\underline{\underline{D}}:\underline{\underline{D}}$$

If one is primarily interested in the shearing component of the stress tensor, assuming that normal stresses do not affect the pressure gradient, then Eqn. 2-16 can be simplified to:

Eqn. 2-18 $$\underline{\underline{\tau}} = 2\eta(II_D)\underline{\underline{D}}$$

A material that behaves in this manner is called a "generalized Newtonian fluid".

It is appropriate to use this equation in the conservation of momentum equation to compute the pressure drop and viscous dissipation in a tube or channel with constant cross-section. Eqn. 2-18 has the tensorial character of a Newtonian fluid but can exhibit shear thinning. It is regarded as a purely viscous constitutive equation, since it does not predict normal stress differences, which are manifestations of elasticity.

A popular form for the viscosity as a function of II_D is the Carreau-Yasuda equation[9]:

Eqn. 2-19 $$\eta(II_D) = \eta_0\left(1 + (2\lambda^2 II_D)^{s/2}\right)^{\frac{m-1}{s}}$$

which has Newtonian behavior with viscosity η_0 at low shear rates and power-law behavior at high shear rates. Eqn. 2-18 is often used in complex polymeric flows for which it is not valid for polymeric liquids, but more realistic constitutive equations almost invariably lead to difficult numerical problems[2]. This will be discussed in more detail in section 2.2.1.

2.1.4 Viscoelastic Models

Since the viscometric flow simplification is not always appropriate, a truly viscoelastic model must often be used. Viscoelastic behavior may be linear or nonlinear. Linear viscoelastic behavior is observed only when the deformation is very small or slow, and is therefore not directly relevant to the behavior of molten polymers in processing operations where deformations are always large and rapid. Linear viscoelastic behavior is independent of the kinematics of the deformation and the magnitude of past strains. These simplifications make possible the addition of the effects of successive deformations. The Boltzmann superposition principle (Eqn. 2-20) describes well the linear viscoelastic response of a material to an arbitrary strain history:

Eqn. 2-20
$$\underline{\underline{\tau}}(t) = 2\int_{-\infty}^{t} G(t-t')\underline{\underline{D}}(t')dt'$$

where $\underline{\underline{\tau}}$ is the extra stress tensor, $G(t-t')$ is the relaxation modulus, and $\underline{\underline{D}}(t')$ is the rate of deformation tensor at time t'.

Conversely, in the nonlinear regime the response to an imposed deformation depends on the size, the rate and the kinematics of the deformation. Therefore, it is not possible to measure a response in one type of deformation and use the result to predict the response in another type of deformation, unless the rate, magnitude and kinematics of the deformation are all the same in both cases[1].

Two approaches have been used to formulate nonlinear viscoelastic constitutive equations. The first one is based on the derivation of molecular theories for melts and dilute solutions together with the use of statistical mechanics, but this approach does not always yield closed form constitutive models. Because of the mathematical complexity involved, many simplifying assumptions must be made, and this limits the practical value of the molecular approach. Examples of such theories include the Rouse model for dilute solutions[10], and the Doi-Edwards[11,12,13] without the independent alignment assumption and Curtiss-Bird models[14],[15] for entangled melts, the last two being based on the reptation concept.

The second method is an empirical approach based on continuum mechanics concept[1]. Complications in building the model arise from the involvement of tensor-valued quantities and the fact that the response of the material depends on strains imposed at previous times. These complications make it difficult to establish an acceptable form of nonlinear constitutive equation. Larson[2] has presented an exhaustive review of closed form continuum models.

At the present time, there is no universal theory that describes nonlinear rheological phenomena. Nevertheless, several models have been used in numerical simulations, and these are either differential or integral constitutive equations. These are reviewed in the following sub-sections. Recent numerical approaches called micro-macro formulations are based on kinetic theories rather than closed form constitutive models[16,17,18,19,20,21]. These are described in section 2.5.2.

2.1.4.1 Differential Viscoelastic Models

Many differential models can be written in the following general form:

Eqn. 2-21
$$\underline{\underline{L}} \cdot \underline{\underline{\tau}} + \lambda \overset{\oplus}{\underline{\underline{\tau}}} = 2\eta \underline{\underline{D}}$$

Here, λ is a relaxation time and η=λ*G* is a viscosity. The symbol $\underline{\underline{L}}$ represents a model-dependent tensor function, and the operator ⊕ stands for the convected Gordon-Schowalter derivative[22], which is a combination of the upper ∇ and lower Δ convected derivatives:

Eqn. 2-22
$$\overset{\oplus}{\underline{\underline{\tau}}} = \frac{\xi}{2} \overset{\nabla}{\underline{\underline{\tau}}} + \left(1 - \frac{\xi}{2}\right) \overset{\Delta}{\underline{\underline{\tau}}}$$

Eqn. 2-23
$$\overset{\nabla}{\underline{\underline{\tau}}} = \frac{D\underline{\underline{\tau}}}{Dt} - \nabla \underline{u} \cdot \underline{\underline{\tau}} - \underline{\underline{\tau}} \cdot \nabla \underline{u}^T$$

Eqn. 2-24
$$\overset{\Delta}{\underline{\underline{\tau}}} = \frac{D\underline{\underline{\tau}}}{Dt} + \underline{\underline{\tau}} \cdot \nabla \underline{u} + \nabla \underline{u}^T \cdot \underline{\underline{\tau}}$$

where D/Dt is the material time derivative and ^{T} indicates the transpose.

In order to obtain a more realistic representation of the behavior of polymer liquids, Eqn. 2-21 can be modified to include a discrete spectrum of relaxation times λ_i, where N is the number of modes:

Eqn. 2-25
$$\underline{\underline{\tau}} = \sum_{i=1}^{N} \underline{\underline{\tau_i}}$$

Eqn. 2-26
$$\underline{\underline{L}}(\underline{\underline{\tau_i}}) \cdot \underline{\underline{\tau_i}} + \lambda \overset{\oplus}{\underline{\underline{\tau_i}}} = 2\eta_i \underline{\underline{D}}$$

The simplest differential model is the upper-convected Maxwell model, with $L_{ij}=1$, $\xi=2$ and constant η. The addition of a Newtonian viscosity η_s yields the Oldroyd-B model. However, these constitutive equations do not provide a realistic description of polymeric fluids. More complex models, such as those of Giesekus[23], Leonov[24] and Phan-Thien/Tanner[25] (PTT) have been proposed to give better agreement with data, but identifying the correct model and the suitable parameters remains a difficult task.

2.1.4.2 Integral Viscoelastic Models

For the purpose of expressing integral constitutive equations, deformations are measured relative to the fluid configuration at the present time t. Single integral constitutive equations give the extra stress at a fluid particle as a time integral of the deformation history, as shown by Eqn. 2-27:

Eqn. 2-27
$$\underline{\underline{\tau}}(t) = \int_{-\infty}^{t} m(t-t')\underline{\underline{F}}(\underline{\underline{\tau}})dt'$$

Eqn. 2-28
$$m(t-t') = \frac{dG(t-t')}{dt'} = \sum_{i=1}^{N} \frac{G_i}{\lambda_i} \exp\left(\frac{-(t-t')}{\lambda_i}\right)$$

where we consider a time integral taken along the particle path parameterized by the time t'. The factor $m(t-t')$ is the time dependent memory function that incorporates the concept of fading memory. This means that the deformation experienced by a fluid element in the recent past contributes more to the current stress than earlier deformations[26]. Again, the extra stress can be expressed as a sum of individual contributions (Eqn. 2-25). $\underline{\underline{F}}$ is a model-dependent tensor that describes the deformation of the fluid.

One of the simplest nonlinear integral constitutive equations is the Lodge rubberlike liquid model[27], in which $\underline{\underline{F}}=\underline{\underline{B}}$, where $\underline{\underline{B}}$ is the Finger tensor. This model is equivalent to the upper-convected Maxwell differential model with N=1. Other models of the integral type that have been found to give a better fit to data are of the K-BKZ type[28,29]. In these models, the memory function depends on the strain as well as on time. The strain dependence of the memory function is called the damping function, $h(I_1,I_2)$. In this case, the memory function is said to be "separable" or factorable:

Eqn. 2-29
$$M[(t-t'),I_1,I_2]=m(t-t')h(I_1,I_2)$$

One of the K-BKZ model with a particular form of damping function was proposed by Papanastasiou et al.[30] and fitted well experimental data for simple shear and simple elongational flows.

2.2 Mathematical Treatment of Viscoelastic Flow

2.2.1 Set of Equations to Solve and Inherent Difficulties

The simulation of the flow of viscoelastic materials involves the solution of a set of coupled partial differential (or integral-differential) equations: conservation of mass, conservation of momentum and a rheological equation. If the flow is compressible or non-isothermal, conservation of energy and an equation of state for density are also required. For simplicity, we assume that the flow is isothermal and incompressible. We present the governing equations using a one-mode differential viscoelastic model, since the majority of the numerical methods have been developed for differential models. For incompressible, isothermal flows the conservation equations for mass and momentum are:

Eqn. 2-30 $$\nabla \cdot \underline{u} = 0$$

Eqn. 2-31 $$\rho \frac{D\underline{u}}{Dt} = -\nabla p + \nabla \cdot \underline{\underline{\tau}} + \underline{f}$$

where ρ denotes a constant density, p is the pressure, $\underline{\underline{\tau}}$ is the extra stress tensor and f is a body force. For a Newtonian fluid and in the absence of inertia forces, this set of equations is referred to as the " Stokes problem " (Eqn. 2-30 and Eqn. 2-31).

The extra stress tensor is sometimes split into viscous and viscoelastic contributions, for example in the Oldroyd-B fluid:

Eqn. 2-32 $$\underline{\underline{\tau}} \equiv 2\eta_s \underline{\underline{D}} + \sum_{i=1}^{N} \underline{\underline{\tau_{ve,i}}}$$

where *ve* represents the viscoelastic character, and η_s is a constant viscosity that can be a solvent viscosity for a polymer solution or a fraction of the zero-shear viscosity for a polymer melt:

Eqn. 2-33 $$\eta_0 = \eta_s + \sum_{i=1}^{N} \eta_i$$

This splitting is often arbitrary but it has a strong stabilizing effect on most numerical schemes. The last equation is the rheological model, an example of which is the upper-convected Maxwell model:

Eqn. 2-34 $$\underline{\underline{\tau}} + \lambda \overset{\nabla}{\underline{\underline{\tau}}} - 2\eta \underline{\underline{D}}(\underline{u}) = 0$$

The mathematical type of a system of equations can be described in terms of characteristics[31]. Ellipticity is represented by complex characteristics, while hyperbolicity is represented by real characteristics. Ellipticity and hyperbolicity are the mathematical concepts associated with diffusion and propagation. Ellipticity has a regularizing effect on a singularity while hyperbolicity propagates it. For example, long distance effects controlled by an elliptic set of equations depend only on averaged quantities, whereas phenomena controlled by a hyperbolic system of equations, like shocks or singularities, are transported. The set of equations for a purely viscous fluid is elliptic, but a viscoelastic constitutive equation like Eqn. 2-34 is hyperbolic. The combination of ellipticity and hyperbolicity complicates the simulation of viscoelastic flows. For example, the introduction of a geometrical singularity, such as an abrupt contraction, induces a stress singularity and results in both mathematical and numerical difficulties, since the rheological equation transports the effect of the singularity and pollutes the velocity field[31]. In the next section, we will look at several numerical approaches that have been proposed to overcome these difficulties.

2.2.2 Numerical Approaches to Viscoelastic Simulations

The solution of viscoelastic flow problems presents several numerical challenges in the case of both differential and integral constitutive models. However, certain similarities exist between the two cases, for example the nonlinear character of the governing equations brought about by the constitutive equation for the viscoelastic stresses. Many discretization techniques have been used to solve the conservation and constitutive equations, and these include finite element, boundary element, finite difference and spectral methods. The majority of published simulations have been carried out using finite element methods for both differential and integral constitutive equations. This is due to the advantages of the finite element methods in discretizing arbitrary geometries and imposing simply and accurately a variety of complex boundary conditions[32].

If we assume an Eulerian framework, the upper-convected Maxwell model (Eqn. 2-34) can be expressed as follows:

Eqn. 2-35
$$\lambda\left(\frac{\partial \underline{\underline{\tau}}}{\partial t}+\underline{u}\cdot\nabla\underline{\underline{\tau}}-\nabla\underline{u}\cdot\underline{\underline{\tau}}-\underline{\underline{\tau}}\cdot\nabla\underline{u}^{T}\right)+\underline{\underline{\tau}}-2\eta\underline{\underline{D}}(\underline{u})=0$$

The convective term $\nabla \underline{u} \cdot \underline{\underline{\tau}}$ brings the complication of having to solve a partial differential equation rather than an ordinary differential equation, as would be the case in a Lagrangian framework. Two fundamentally different approaches are used to solve the set of partial differential equations[33]. In the first approach, a mixed formulation is adopted, where the velocity, pressure and extra stress are treated as unknowns, and each of the equations are multiplied independently by a weighting function and transformed into a weighted residual form[34]. In the second approach, the constitutive equation is transformed into an ordinary differential equation either by using a Lagrangian formulation for unsteady flows[35] or by integration along streamlines. Many integral models cannot be expressed in differential form, so either a Lagrangian or streamline formulation must be adopted. Details of these computations have been described by Luo and Tanner[36], Hulsen and van der Zanden[37], Goublomme et al.[38] and Rajagopalan et al.[39]. Luo[40] introduced a control volume approach to solve integral viscoelastic models. Recently, Rasmussen[41] presented a new technique to solve time-dependent three-dimensional viscoelastic flow with integral models, based on a Lagrangian kinematic description of the fluid flow. In this work, we will discuss more thoroughly mixed finite element formulations designed for differential constitutive equations in an Eulerian framework.

2.2.3 Boundary Conditions

In order to complete the mathematical description of a viscoelastic flow, appropriate boundary conditions must be specified. The nature of these boundary conditions is intimately related to the mathematical nature of the governing equations. In the case of elliptic systems with complex characteristics, the problem is well-posed for boundary conditions of the Dirichlet type and for conditions of the Neumann type when the net flux (Green's theorem) is zero, while for hyperbolic systems with real characteristics, it is well-posed for conditions of the Cauchy type on the entrance boundary.

Coupled equations of a mixed elliptic-hyperbolic type have both real and complex characteristics. To date, there is no complete mathematical theory that guides the selection of boundary conditions for the flow of viscoelastic materials[42,43]. The general approach is to use the same boundary conditions as for purely viscous fluids: no-slip at solid walls and specification of the velocity components at the entrance and exit of the flow boundaries. Because of the memory effect, the extra stresses must also be specified at the inflow boundary to reflect the flow history. In practice, conditions that result from a fully developed velocity profile are usually applied at the inlet boundary. However, for extra stress this boundary condition is sometimes as complex as the solution of the flow itself, because of the lack of analytical solutions for the more complex models. It is then common practice to specify inlet extra stresses and known kinematics for the upper-convected Maxwell fluid (Eqn. 2-34). These approximate boundary conditions result in a rearrangement of the velocity and stresses at the inflow and outflow, and this rearrangement is sometimes important enough to restrain numerical convergence in simulations. It is then highly desirable to improve the quality of the boundary conditions.

In summary, the issue of appropriate boundary conditions for viscoelastic computations is still an open question[42]. The approach adopted may make it possible to proceed numerically but not be completely supported by either mathematical or experimental results. For example, it is known that the no-slip boundary condition does not apply in all situations for polymeric fluids. Also, the imposition of proper boundary conditions at geometric singularities, such as capillary exit, is still a subject of discussion.

2.3 Algorithm Development

2.3.1 Failure of Traditional Numerical Methods

Numerical analysts have been interested in simulating viscoelastic flows for many years. As mentioned above, the numerical computation of viscoelastic flows involves strongly nonlinear, coupled equations of a mixed elliptic-hyperbolic type. The use of conventional numerical techniques has proven unsuccessful due to a loss of convergence, even at low levels of melt elasticity. It took almost ten years to identify what is called the “ high Deborah number problem ”. The Deborah number (*De*) is a dimensionless group that indicates the degree of elasticity of the flow. Classical finite element techniques based on the application of the Galerkin method to the mixed formulation failed at relatively low *De*, and it was unknown at the time if these limits were intrinsically related to the continuous problem or to inadequate numerical schemes. It is now understood and accepted that the computational difficulties are numerical in nature and are due to the hyperbolic nature of the constitutive equations, the existence of stress singularities, and the method of resolution of the coupled equations. Debbaut and Crochet[44] were able to increase the *De* limit for an abrupt 4:1 contraction by imposing more strongly the incompressibility constraint. For the same problem Keunings[45] concluded, after a critical examination of the numerical solutions and an intensive mesh refinement study, that the limiting values of *De* were numerical artifacts caused by excessive approximation errors. From then on, it was suggested[45] that efforts be focused on complex flows with singularities or boundary layers in order to test algorithms robustness, since strong gradients have a tendency to increase numerical imprecision.

2.3.2 First Successful Approach

Most of the early work on viscoelastic flow analysis was based on the three-field mixed finite element formulation[46,47,48]. The momentum, continuity and constitutive equations are expressed in a weighted residual form, and this leads to an approximation of the Stokes problem (Eqn. 2-30 and Eqn. 2-31) when applied to a Newtonian flow. For an Oldroyd-B fluid with one-mode, and neglecting body forces, the equations in the weak formulation are:

Find $(\underline{u}, p, \underline{\underline{\tau}}) \in V \times Q \times S$ such that:

Eqn. 2-36 $$\left((\nabla \underline{v})^T, 2\eta_S \underline{\underline{D}} + \underline{\underline{\tau}}\right) - \left(\nabla \cdot \underline{v}, p\right) = 0 \qquad \forall \underline{v} \in V$$

Eqn. 2-37 $$\left(q, \nabla \cdot \underline{u}\right) = 0 \qquad \forall q \in Q$$

Eqn. 2-38 $$\left(\underline{\underline{s}}, \lambda \overset{\nabla}{\underline{\underline{\tau}}} + \underline{\underline{\tau}} - 2\eta \underline{\underline{D}}\right) = 0 \qquad \forall \underline{\underline{s}} \in S$$

where $\underline{\underline{s}}$, $\underline{v}$ and q are weighting functions, and $(\ldots,\ldots)$ is the appropriate inner product.

In 1987, based on this formulation, Marchal and Crochet[49] proposed a new method that showed good numerical behavior. First, they introduced a new computational element for the stress components composed of 16 sub-elements (4 x 4), in order to have a discrete representation of the extra stresses that would satisfy the equivalence compatibility condition. The polynomial approximations of the three variables need to be carefully selected with respect to each other to satisfy the so-called generalized inf-sup (Brezzi-Babuska) compatibility condition[50]. When this condition is satisfied, the mixed formulation including extra stresses provides a convergent approximation for the different variables. The velocity is approximated by biquadratic polynomials, while the pressure is bilinear and continuous. Since the approximation for the stress is also continuous, the inf-sup condition is satisfied by using a sufficient number of interior nodes in each element, such as the 4 x 4 sub-elements used by Marchal and Crochet[49], as proven later by Fortin and Pierre[51].

Once the compatibility of spatial discretization was settled, Marchal and Crochet[49] used two methods to account for the convective term in the constitutive equation: the Streamline Upwind Petrov Galerkin (SUPG) method, and the Streamline Upwind (SU) method:

Eqn. 2-39 SUPG: $$\left(\underline{\underline{s}} + \alpha \underline{u} \cdot \nabla \underline{\underline{s}}, \lambda \overset{\nabla}{\underline{\underline{\tau}}} + \underline{\underline{\tau}} - 2\eta \underline{\underline{D}}\right) = 0$$

Eqn. 2-40 SU: $$\left(\underline{\underline{s}}, \lambda \overset{\nabla}{\underline{\underline{\tau}}} + \underline{\underline{\tau}} - 2\eta \underline{\underline{D}}\right) + \left(\alpha \underline{u} \cdot \nabla \underline{\underline{s}}, \underline{u} \cdot \nabla \underline{\underline{\tau}}\right) = 0$$

Those are examples of finite element methods in which the weighting functions differ from the basis functions. In both methods, artificial diffusion is introduced in the flow direction by the upwind term $\alpha \underline{u} \cdot \nabla \underline{\underline{s}}$ in order to stabilize the convection-dominated transport. Over the years, several variations of the parameter α have been proposed, but are all of the form[33]:

Eqn. 2-41 $$\alpha = \frac{h}{U}$$

where h is a characteristic length of the geometry and U a characteristic velocity of the flow.

The SU method, where the upwind term is applied only to the convective term of the constitutive equation, showed an increased robustness compared to SUPG, which produced oscillatory stress fields at steep stress boundary layers or near singularities. However, the SU formulation is an inconsistent substitution of the exact solution, since the second term of Eqn. 2-40 remains as a residual, and even if it converges well it is not always toward the correct solution[52, 53].

The relative success of this approach showed that a combination of compatible discretization spaces with a discretization technique adapted to the rheological equation could eliminate the loss of convergence at high *De*. Unfortunately, the new element was rapidly shown to be too costly in memory space for practical use.

2.3.3 Economical Storage Techniques

Marchal and Crochet's element could only be used for single mode simulations, considering the large memory space needed to solve viscoelastic flow problems, but it became possible to do multimode calculations when Fortin and Fortin[54] introduced their economical storage technique. Fortin and Fortin[54] presented a discontinuous Galerkin (DG) method to handle the constitutive equation, based on ideas of Lesaint and Raviart[55]. Upwinding is introduced in this method by the jump of discontinuous variables at the interfaces of elements:

Eqn. 2-42 GD: $$\left(\underline{\underline{s}}, \lambda \overset{\nabla}{\underline{\underline{\tau}}} + \underline{\underline{\tau}} - 2\eta \underline{\underline{D}}\right) - \sum_{e=1}^{M} \int_{\Gamma_e^{in}} \underline{\underline{s}} : \underline{u} \cdot \underline{n} \left(\underline{\underline{\tau}} - \underline{\underline{\tau}}^{nup}\right) d\Gamma = 0$$

where $\underline{n}$ is the outward unit normal on the boundary of element e, Γ^{in}_{e} is the part of element e boundary where $\underline{u} \cdot \underline{n} < 0$, and $\underline{\underline{\tau}}^{nup}$ the extra stress tensor in the neighboring upwind element[33].

The equivalence compatibility condition was also satisfied in their method by the respective discretizations, but this time the solution was decoupled; velocity, pressure and extra stresses were not solved simultaneously. By use of the DG technique, the solution for the stresses did not imply the inversion of large linear systems but only local calculations on elementary systems. However, the method was found to be insufficiently robust because of the fixed-point algorithm used to couple the Stokes problem and the viscoelastic equation. Later, Fortin and Fortin[56] used a quasi-Newton iterative solver (GMRES, for " Generalized Minimal Residual ") for the solution of the linear system. This increased the algorithm robustness but did not achieve the performance of Marchal and Crochet's method[49] due to oscillatory behavior produced by the DG formulation near singularities. However, the economical storage technique was a major contribution to the simulation of viscoelastic flows; the only large system to store is the one related to the Stokes problem, for which a LU factorization is done. The DG method allows the solution of the constitutive equation on an element by element basis, resulting in very efficient solvers and greatly reducing the memory space needed to solve flow problems using differential multimode models. Later, the robustness of GMRES was tested with more success by Guénette and Fortin[57].

2.3.4 Projection Technique

The major contribution of Rajagopalan et al.[58] was the introduction of a fourth field in the mixed finite element formulation of viscoelastic flow, opening the door to all the projection techniques that are now used to introduce compatibility of discretized spaces. Rajagopalan et al. implemented the EVSS method (Elastic Viscous Split Stress) which is a projection technique based on the splitting of the extra-stress tensor into viscous and elastic parts as shown in Eqn. 2-43:

Eqn. 2-43 $$\underline{\underline{E}} = \underline{\underline{\tau}} - 2\eta \underline{\underline{D}}$$

A change of variable is performed in the momentum and the constitutive equations yielding a set of equations involving the velocity $\underline{u}$, the pressure p and the new variable $\underline{\underline{E}}$. Moreover, the rate of deformation tensor $\underline{\underline{D}}$ is introduced as an additional unknown, $\underline{\underline{d}}$, leading to a four-field $(\underline{u}, p, \underline{\underline{E}}, \underline{\underline{d}})$ problem. In summary, the EVSS method based on the four-field formulation can be formulated as follows:

Find $(\underline{u}, p, \underline{\underline{E}}, \underline{\underline{d}}) \in V \times Q \times S \times C$ such that:

Eqn. 2-44 $$\left((\nabla \underline{v})^T, 2(\eta_S + \eta)\underline{\underline{D}}(\underline{u}) + \underline{\underline{\tau}}\right) - (\nabla \cdot \underline{v}, p) = 0 \qquad \forall \underline{v} \in V$$

Eqn. 2-45 $$(q, \nabla \cdot \underline{u}) = 0 \qquad \forall q \in Q$$

Eqn. 2-46 $$\left(\underline{\underline{s}}, \lambda \overset{\nabla}{\underline{\underline{E}}} + \underline{\underline{E}} + 2\eta\lambda \overset{\nabla}{\underline{\underline{D}}}(\underline{u})\right) = 0 \qquad \forall \underline{\underline{s}} \in S$$

Eqn. 2-47 $$\left(\underline{\underline{c}}, \underline{\underline{d}} - \underline{\underline{D}} = 0\right) \qquad \forall \underline{\underline{c}} \in C$$

where $\underline{\underline{c}}$ is a suitable weighting function.

This method is remarkably stable. However, it requires the convected derivative of the rate of deformation tensor (in Eqn. 2-46), and the change of variable of Eqn. 2-43 does not yield a closed expression for all constitutive equations.

These disadvantages were corrected by Guénette and Fortin[57] who recently proposed a modification of the EVSS formulation, in which the main difference lies in the introduction of a stabilizing elliptic operator in the discrete version of the momentum equation:

Eqn. 2-48 $$\left((\nabla \underline{v})^T, 2(\eta_s + \alpha)\underline{\underline{D}}(\underline{u}) - \alpha \underline{\underline{d}} + \underline{\underline{\tau}}\right) - (\nabla \cdot \underline{v}, p) = 0$$

The parameter α is positive and *a priori* arbitrary, but if properly chosen it improves the overall convergence of the algorithm. In the discrete approximation (Eqn. 2-48), the difference in the discretization of the α terms combined with the inf-sup condition has a stabilization effect on the discretization. Their method is not restricted to a particular class of constitutive equations and is easier to implement than the original EVSS method. It was tested in conjunction with the non-consistent (SU) streamline upwind method on the 4:1 contraction and stick-slip problems. The algorithm seems robust, and no limiting *De* number was reached when using the one-mode PTT model for the stick-slip problem[57].

Recently, Fan et al.[59] introduced another stabilized formulation, based on the incompressibility residual of the finite element discretization and the SUPG technique. They claim that the new method has the same level of stability and robustness of the modified EVSS method[57] and is superior to the EVSS technique[58], since it does not require the solution of the convected derivative of the rate of deformation tensor.

2.3.5 Influence of Theoretical Work

Fortin and Pierre[51] made a mathematical analysis of the Stokes problem for the three-field formulation used by Marchal and Crochet[49]. They confirmed that the success of the method was dependent, among others, on the compatibility between discretized spaces. They showed that in the absence of a purely viscous contribution (η_s=0) and using a regular Lagrangian interpolation, three conditions must hold[33].

1. The velocity-pressure interpolation in the Stokes problem must satisfy the Brezzi-Babuska condition to prevent spurious oscillation phenomena.
2. If a discontinuous interpolation of the viscoelastic stress $\underline{\underline{\tau}}$ is used (as in the DG technique), the space of the strain rate tensor $\underline{\underline{D}}(\underline{u})$ obtained after differentiation of the velocity field $\underline{u}$ must be in the same discretization space as $\underline{\underline{\tau}}$.
3. If a continuous interpolation of the extra stress $\underline{\underline{\tau}}$ is used (as in the SUPG or SU techniques), the number of internal nodes must be larger than the number of nodes on the side of the element used for the velocity interpolation.

The compatibility between discretized spaces also contributes to the success of the four-field modified EVSS technique[57], as later proven by Fortin et al.[60] based on a generalized theory of mixed problems. However, the influence of the discretization of the constitutive equation near a singularity remains unexplained.

2.4 Comparisons with Experiments

With the improved performance of numerical methods for viscoelastic flow simulations, direct comparison of the numerical results with the experimental data became increasingly feasible and necessary. Actual comparison may be based on global flow features such as die swell or pressure drop measurements or on local flow kinematics measured by streakline photography, laser Doppler velocimetry (LDV) or birefringence.

2.4.1 First Comparisons: Boger Fluids

The first comparisons between numerical simulations and experimental data were made using the upper-convected Maxwell (UCM) and Oldroyd-B models, which can not capture the full nonlinear behavior of polymer fluids. To narrow the gap between experimental observation and prediction, the so-called Boger fluids were developed[61]. These elastic fluids are specially prepared solutions of high molecular weight polymers in viscous solvents and are thought to be nearly free of shear thinning[2]. They are also characterized by a first normal stress difference proportional to the square of the shear rate, a zero second normal stress difference and an elongational viscosity that increases with elongation rate. Boger fluids are reasonably well described up to high frequency in dynamic shear experiments by a two-mode version of the UCM equation[62]. At low and moderate frequencies, the faster of these modes can be collapsed into a retardation term, and a single-mode Oldroyd-B equation is then a sufficient rheological description[2]. Experimental elongational data for Boger fluids have compared favorably with numerical simulations using the Oldroyd-B equation[63]. Debbaut et al.[64], Luo and Tanner[65] and Coates et al. [66] also tried to reproduce numerically the flow kinematics measured by streakline photography of a Boger fluid in abrupt 4:1 and 8:1 contractions[67]. Most of the results were in qualitative but not quantitative agreement with the measurements. Recent sources of disagreement between experiments and simulations appear to indicate that Boger fluids are not accurately represented by the Oldroyd-B model and that improved agreement is obtained by using a single-mode finitely extensible nonlinear elastic (FENE-P) dumbbell model[15,68,69].

However, Boger fluids do not reflect the viscoelastic behavior of polymer melts. With the development of new and more realistic constitutive models, further investigation of Boger fluids is now of less interest. In the following sections, we present a short review on studies that compare experimental data for polymer melts to simulations of complex flows with more realistic rheological models.

2.4.2 Rheological Models Frequently Used in Simulations

Simulations of flows of molten polymers under typical processing conditions require the use of suitable rheological constitutive equations. Before looking at complex viscoelastic flow phenomena like rod-climbing, extrudate swell and vortex formation in contraction flows, the constitutive equation must be able to describe the simplest "rheometric" flows, i.e. flows used to establish rheological parameters. The model should predict shear thinning, normal stress differences in shear, stress relaxation, recoil and sensitivity to kinematics. Some of the models that have been proposed for polymers have been mentioned earlier: these include the Giesekus, Leonov, Phan-Thien/Tanner (PTT) and K-BKZ models. Their superiority has also been shown in providing numerical solutions for viscoelastic flows with geometric singularities, such as occur at sharp corners in contraction or expansion flows. These flows are notoriously difficult to simulate, in particular for the UCM and Oldroyd-B models.

A significant portion of the work on the numerical analysis of viscoelastic flow of polymer melts is based on streamline integration methods, employing K-BKZ type constitutive models and the damping functions proposed by Papanastasiou et al.[30] (PSM) or Wagner[70]. The popularity of the PSM damping function arises from the possibility of fitting shear and elongational data independently. Of the differential type models, PTT and Giesekus are the ones most often used, which is surprising considering that the simple Leonov model gives more realistic values of limiting extensional viscosities than Giesekus[2] and contains no nonlinear parameters. The Giesekus model has one parameter that controls nonlinearity, whereas the PTT model has two. The latter has the ability to fit shear and extensional properties independently. However it gives spurious oscillations during start-up of shear flow[71]. Therefore, none of the existing constitutive models are entirely suitable for the simulation of complex flows.

2.4.3 Determination of Model Parameters

It was pointed above that the use of a viscoelastic constitutive equation in simulations requires the determination of several parameters. Linear viscoelastic data, usually the storage and loss moduli (G', G"), which are easy to measure, are used to determine a discrete relaxation spectrum [G_i, λ_i]. Very long, entangled polymer chains have many modes of motion and thus of relaxation, and these can not be described in terms of a single relaxation time. Usually, between five and ten modes are necessary to provide a good fit of the relaxation modulus[1].

However, such a fit may not be adequate for properties that depend in detail on molecular weight distribution (MWD). For example, the compliance and other manifestations of melt elasticity, such as normal stress difference and extrudate swell are very sensitive to MWD[1]. While the rheological behavior depends strongly on molecular structure, rheological data have been used to provide information about molecular structure: this has been called the "inverse problem". A number of researchers have had significant success in the calculation of the viscosity MWD of linear polymers[72,73,74] by using linear viscoelastic data. Obviously, important information about the MWD is lost when using a discrete spectrum of relaxation times, and this might affect the predictions in flow simulations of phenomena that depend strongly on MWD, i.e. on the spectrum.

The experimental determination of the nonlinear parameters in the various models is a more difficult task. Some parameters are related to shear behavior and can be easily obtained by measuring viscosity, but for parameters related to extensional behavior or normal stresses, the available experimental data are quite limited. In particular, we lack reliable data for normal stresses at high shear rates and the response to large, rapid extensional flows. As a result, important parameters in a viscoelastic constitutive equation are often determined by fitting the viscosity curve and the few available data for first normal stress difference in shear or extensional data at low strain rates. Inadequate parameter evaluation can result in poor predictions if we try to simulate typical processing conditions, where deformations tend to be complex, large and rapid. In any event, it appears that no existing model is able to fit the available data for typical commercial thermoplastics.

In addition, there is no straightforward way to evaluate model parameters for complex flows where both shear and extensional modes of deformation occur simultaneously, for example in converging and diverging flows. Nouatin et al.[75] presented preliminary work using a numerical procedure to identify rheological parameters of Oldroyd-B and PTT models by finite element simulation and inverse problem solving. They reported encouraging results and will carry out future work to identify parameters by use of actual experimental data.

2.4.4 Planar Abrupt Contraction Flow

Contraction flow has received more attention than any other complex flow. This can be explained by the simplicity of the geometry and the fact that it has features that arise in polymer processing. Accelerating flows from a large cross-section via an abrupt or angular entry into a smaller cross-section, i.e. entry flows, arise in polymer processing applications such as extrusion and injection molding. Planar contraction flow has also been chosen as a benchmark problem to evaluate numerical methods and constitutive equations by comparing numerical predictions with experimental results[76]. A detailed review of comparisons of experiment and simulation for planar abrupt contraction flow has been presented by Schoonen[77]. In Table 2-1 we summarize numerical simulations of planar abrupt contraction flows that have been compared with experiments, including the number of modes used in the calculations.

Table 2-1 Numerical Simulations of Planar Abrupt Contraction Flow

Author(s)	Type of Model	Model	Number of Modes	Numerical Method	Material
White et al. (1988)[78,79]	Differential	PTT	1	Penalty FEM	PS, LDPE
Park et al. (1992)[80]	Integral	K-BKZ	8	Streamline FEM[36]	HDPE
Maders (1992)[81]	Differential	White-Metzner[82]	1	Decoupled FEM	LLDPE
Kiriakidis et al. (1993)[83]	Integral	K-BKZ	8	Streamline FEM[36]	LLDPE
Ahmed et al. (1995)[84]	Integral	K-BKZ	8	FEM (Polyflow)[85]	HDPE, LDPE
Fiegl and Öttinger (1996)[86]	Integral	Rivlin-Sawyers[87]	14	FEM	LDPE
Beraudo et al. (1998)[88]	Differential	PTT	7, 8	DG FEM	LLDPE, LDPE
Schoonen (1998)[77]	Differential	PTT, Giesekus	4, 8	FEM EVSS DG	LDPE

FEM: Finite Element Method
DG: Discontinuous Galerkin
EVSS: Elastic Viscous Split Stress

It is obvious from Table 2-1 that the use of integral models makes it possible to use more relaxation times. This is because in integral models, the contribution from each mode gets summed up in a single integral, while for differential models the number of equations to solve for the extra stress is multiplied by the number of modes considered.

Authors of papers frequently fail to mention numerical convergence problems near the singularities, although White et al.[78,79] and Schoonen[77] did explain how they circumvented the problem. The loss of convergence was delayed by White et al. assuming Newtonian behavior in the elements that were in contact with the re-entrant corner, while Schoonen had to use a parameter set for the PTT model that was inconsistent with uniaxial extensional flow behavior.

Interestingly, two simulations using different constitutive equations for the same material and same flow gave conflicting results. Comparing their results with the data of Beaufils[89], Maders et al.[81] used a one-mode White-Metzner model and reported that the predicted stresses along the centerline showed a slower decay than the experiments. Comparing with the same experimental data, the simulations of Kiriakidis et al.[83] underestimated the stresses in the downstream channel using a multimode K-BKZ model.

Finally, Ahmed et al.[84] and Fiegl and Öttinger[86] explained some of the discrepancies between experimental results and simulations in terms of the 2D nature of the simulation and a 3D component of the experimental flow. Most authors refer to the study of Wales[90] who empirically found the effects of confining walls to be negligible for an aspect ratio exceeding 10 for fully developed shear flow. However, this ratio is mostly used in the channel (downstream section), whereas quantitative comparisons are also made in the upstream section where the ratio is rarely larger than 10[77].

2.4.5 Axisymmetric Abrupt Contraction Flow

Most of the simulations of axisymmetric abrupt contraction flow have been done using integral models. In Table 2-2, we present a summary of numerical simulations of this flow that were compared with experimental results.

When comparison was made with experimental entrance pressure drop in these studies, poor agreement with the simulations was obtained. Fiegl and Öttinger[91] reported reasonable quantitative agreement in terms of vortex growth, but computed values of the entrance pressure loss were underestimated. Barakos and Mitsoulis[92] also reported the underestimation of entrance pressure loss, measured by Meissner[93], by their finite element simulations.

Table 2-2 Numerical Simulations of Axisymmetric Abrupt Contraction Flow

Author(s)	Type of Model	Model	Number of Modes	Numerical Method	Material
Dupont and Crochet (1988)[94]	Integral	K-BKZ	8	Streamline FEM	LDPE
Luo and Mitsoulis (1990)[95]	Integral	K-BKZ	8	Streamline FEM[36]	LDPE
Hulsen and van der Zanden (1991)[37]	Differential	Giesekus	8	Streamline FEM	LDPE
Fiegl and Öttinger (1994)[91]	Integral	Rivlin-Sawyers	9	FEM	LDPE
Barakos and Mitsoulis (1995)[92]	Integral	K-BKZ	8	Streamline FEM[36]	LDPE
Luo (1996)[40]	Integral	K-BKZ	8	Control volume SIMPLE	LDPE

FEM: Finite Element Method
SIMPLE: Semi-Implicit Method for Pressure Linked Equations

2.4.6 Axisymmetric Converging Flow

The prediction of entrance pressure loss in converging axisymmetric flow has been the subject of several recent studies using both integral and differential models. These are summarized in Table 2-3.

Most studies report that numerical predictions of entrance pressure drop were substantially underestimated when compared to experimental data. Mitsoulis et al.[96] claimed that the entrance pressure loss was insensitive to extensional rheology.

Beraudo[97] and Fiegl and Öttinger[91] tried to explain these discrepancies. According to the authors, the experimental values include die exit effects, and the degree to which these effects contribute to the experimentally determined entrance pressure loss is unknown.

However, exit pressure drop is known to be very small[98] and would not compensate for the large difference between experimental and predicted entrance pressure drop.

Table 2-3 Numerical Simulations of Axisymmetric Converging Flow

Author(s)	Type of Model	Model	Number of Modes	Numerical Method	Material
Beraudo (1995)[97]	Differential	PTT	7	DG FEM	LLDPE
Guillet et al. (1996)[99]	Integral	Wagner[100]	7, 8	Stream-tube mapping	LLDPE, LDPE
Hatzikiriakos and Mitsoulis (1996)[101]	Integral	K-BKZ	6	Streamline FEM	LLDPE
Mitsoulis et al. (1998)[96]	Integral, differential, viscous	K-BKZ, PTT, Carreau[102]	6, 8	Streamline FEM, EVSS-SUPG	LLDPE

FEM: Finite Element Method
DG: Discontinuous Galerkin
EVSS: Elastic Viscous Split Stress
SUPG: Streamline Upwind Petrov Galerkin

2.4.7 Extrudate Swell

2.4.7.1 Annular Swell

Many attempts have been made to simulate extrudate swell. In Table 2-4, we present a summary of simulations of annular extrudate swell that were compared with experimental data. Two independent swell ratios are required to describe annular swell: the diameter swell and the thickness swell. Two studies comparing numerical simulations with annular extrudate swell measurements (Luo and Mitsoulis[103] and Tanoue et al.[104]) used the experimental data of Orbey and Dealy[105] for three HDPE melts.

Convergence problems were reported for the tapered geometries by Luo and Mitsoulis[103] and Garcia-Rejon et al.[106]. Some of the results presented were not fully converged solutions (Luo and Mitsoulis[103]), and computations failed to converge for diverging angles beyond +30° and for converging angles beyond -30° (Garcia-Rejon et al.[106]).

Table 2-4 Numerical Simulations of Annular Extrudate Swell

Author(s)	Type of Model	Model	Number of Modes	Numerical Method	Material
Luo and Mitsoulis (1989)[103]	Integral	K-BKZ	8	Streamline FEM[36]	HDPE
Garcia-Rejon et al. (1995)[106]	Integral	K-BKZ	6	FEM (Polyflow)[85]	HDPE
Otsuki et al. (1997)[107]	Integral	K-BKZ	6	Streamline FEM	HDPE
Tanoue et al. (1998)[104]	Differential	Giesekus	1	Under relaxation mixed FEM	HDPE

FEM: Finite Element Method

For the straight annular die, results from Luo and Mitsoulis[103] showed reasonable agreement of prediction and experiment for the diameter swell, but the thickness swell was not close to the experimental data. Garcia-Rejon[106] et al. reported opposite results: predictions of thickness swell were in reasonably good agreement with experimental data, but the agreement was poor for diameter swell.

Tanoue et al.[104] reported deviations as high as 34 % between simulation and experiment. According to the authors, the use of a discrete spectrum of relaxation times would improve the predictions.

2.4.7.2 Capillary Swell

Axisymmetric swell was also the subject of numerous studies. Table 2-5 presents numerical simulations of axisymmetric extrudate swell that were compared with experimental results.

Again, most of the studies were done using integral models. Many studies used the data of Meissner[93] to compare with their simulations. The temperature was kept constant in these swell experiments by extruding into silicone oil at 150°C. The comparisons between simulations and measured values for a long and a short die are presented in

Tables 2-6 and 2-7. Model parameters were fitted to shear and elongational rheological data. The number of modes used in the simulations is given in Table 2-5.

Table 2-5 Numerical Simulations of Axisymmetric Extrudate Swell

Author(s)	Type of Model	Model	Number of Modes	Numerical Method	Material
Luo and Tanner (1986)[108]	Integral	K-BKZ	8	Streamline FEM[36]	LDPE
Bush (1989)[109]	Differential	Leonov	7	BEM	LDPE
Goublomme and Crochet (1992)[38]	Integral	K-BKZ	6	FEM	HDPE
Goublomme and Crochet (1993)[110]	Integral	Wagner	6	FEM	HDPE
Barakos and Mitsoulis (1995)[92]	Integral	K-BKZ	8	Streamline FEM[36]	LDPE
Sun et al. (1996)[111]	Integral	K-BKZ	8	Streamline FEM	LDPE
Beraudo et al. (1998)[88]	Differential	PTT	7	DG FEM	LLDPE

FEM: Finite Element Method
BEM: Boundary Element Method
DG: Discontinuous Galerkin

In general, moderate agreement is obtained for the low and medium apparent shear rates, while swell is largely overestimated at the highest shear rate. We also see that predictions differ considerably from one study to another.

Comparing with their own measurements, Beraudo et al.[88] reported good agreement for a long die but poor agreement for a short die. The computation largely underpredicted the experimental value for the short die, and the underestimation was larger at high shear rates. It is worth mentioning that in their swell experiments, the polymer was extruded directly into air[97], thus involving sagging due to gravity and non-isothermal effects that could result in an underestimation of the ultimate swell.

Finally, Goublomme and Crochet[38,110] simulated the extrudate swell of an HDPE melt that had been measured by Koopmans[112]. Extrusion was into a silicone oil bath at 190°C. Inclusion of a converging upstream conical section in the simulation to match the experimental set-up resulted in a very high calculated swelling ratio (~ 9 calculated vs. 2.38-2.61 measured)[38]. With a different Wagner damping function modified to give a non-zero second normal stress difference, quantitative agreement with experimental results was obtained. However, the required ratio of second to first normal stress difference ($N_2/N_1 = -0.3$)[110] was larger than typical reported values.

In conclusion, the simulation of extrudate swell has produced contradictory results, underestimating or overestimating swell, usually differing considerably from measured values.

Table 2-6 Comparisons between Predicted and Measured Extrudate Swell (long die)

Reference	Model	Swell (0.1 s^{-1})	Swell (1.0 s^{-1})	Swell (10.0 s^{-1})
Luo and Tanner[108]	K-BKZ	31 %	51 %	82 %
Barakos and Mitsoulis[92] *	K-BKZ	30 %	69 %	84 %
Sun[111] **	K-BKZ	30 %	62 %	94 %
Bush[109] ***	Leonov	37 %	53 %	77 %
Meissner[93] ****	Experiments	34 %	52 %	56 %

* Mesh M2
** Mesh M3
*** Special form of Leonov model, results taken from figure
**** Extrapolated values for an infinite long die

Table 2-7 Comparisons between Predicted and Measured Extrudate Swell (orifice)

Reference	Model	Swell (0.1 s^{-1})	Swell (1.0 s^{-1})	Swell (10.0 s^{-1})
Barakos and Mitsoulis[92] *	K-BKZ	54 %	133 %	195 %
Sun[111] **	K-BKZ	49 %	163 %	223 %
Meissner[93]	Experiments	58 %	125 %	195 %

* Mesh M2
** Mesh M3

2.4.8 Other Complex Flows

We provide here a brief summary of other complex polymer flows such as planar flow around a cylinder and cross-slot flow. The planar flow around a cylinder has been proposed as a benchmark problem for numerical techniques[113], but it has received only limited attention up to now. This flow is of interest because along the centerline, a material element undergoes various types of deformation: it will be compressed when approaching the cylinder, then sheared along the cylinder's surface and finally stretched in the wake of the cylinder. In cross-slot flow, or planar stagnation, two liquids impinge to create a steady extensional deformation. At the stagnation point a material element experiences a very large extensional strain rate, which will produce a high level of orientation.

Table 2-8 presents recent numerical simulations of planar flow around a cylinder where predictions were compared with experiments.

Table 2-8 Numerical Simulations of Planar Flow around a Cylinder

Author(s)	Type of Model	Model	Number of Modes	Numerical Method	Material
Hartt and Baird (1996)[114]	Differential, integral	PTT, Rivlin-Sawyers	1 (PTT), 7 (RS)	FEM (Polyflow)[85]	LLDPE, LDPE
Baaijens et al. (1997)[115]	Differential	PTT, Giesekus	4, 8	FEM EVSS DG	LDPE
Schoonen (1998)[77]	Differential	PTT, Giesekus	4, 8	FEM EVSS DG	LDPE

FEM: Finite Element Method
EVSS: Elastic Viscous Split Stress
DG: Discontinuous Galerkin

Baaijens et al.[115] tested two differential constitutive equations, PTT and Giesekus, with model parameters fitted to shear data including viscosity and first normal stress difference. For the PTT model, no unique set of parameters could be identified without the use of elongational data. Three parameter sets were tried, all giving equally good fits of the shear data. However, comparison with experimentally obtained birefringence patterns revealed that neither of the models could predict quantitatively the observed stress patterns. These results were consistent with those reported by Hartt and Baird[114] for the same flow of polyethylene melts.

Schoonen[77] did an experimental/numerical study of an LDPE melt in both planar flow around a cylinder and cross-slot flow. He compared the predictions of the multimode Giesekus and PTT models with velocities measured using particle tracking velocimetry and stresses measured by fieldwise flow induced birefringence. Where the PTT model gave better agreement than the Giesekus model with both velocity and stress data in planar abrupt contraction flow (section 2.4.4), the Giesekus model performed better for the cylinder and cross-slot flow. The PTT model, which described rheological properties best, gave convergence problems. Schoonen had to use a parameter set for the PTT model that was consistent with shear data but not uniaxial extensional behavior in order to obtain numerical convergence.

2.5 Conclusions

Major difficulties persist in the simulation of polymer flows, both on the experimental and the numerical side, and these are summarized below.

2.5.1 Limitations of Numerical Simulations of Viscoelastic Flows

Over the past decade, significant progress has been made in the numerical and experimental analysis of viscoelastic flows. Within the category of numerical mixed methods, the modified EVSS technique first introduced by Guénette and Fortin[57], appears to provide the most robust formulation currently available. To achieve accurate results, the modified EVSS method should be combined with an upwind scheme like the SUPG formulation or the discontinuous Galerkin (Lesaint-Raviart) method.

However, despite the improved performance of numerical methods for viscoelastic flow simulations, serious convergence problems remain. For flow geometries with a singularity, such as sharp corners for enclosed flows and discontinuities in boundary conditions for free-surface flows, a numerical breakdown occurs above a modest elasticity level or *De* number. Simulations of these flows are still limited, in general, to low Deborah numbers, i.e., either to low flow rates or materials with short relaxation times.

Apart from purely numerical issues, such as convergence problems, the predictive capability of any numerical analysis is only as good as the input data; i.e., the constitutive model, material parameters and boundary conditions. Attempts to find a general viscoelastic fluid model that would be applicable to all classes of flow problems and be able to give reliable results have so far failed. If good success is obtained in comparison with experimental data for a particular class of flow problem, poor agreement is usually observed with another class of flows. Even when convergence is possible, confrontation with experimental results increasingly reveals the inability of existing constitutive equations to predict the complicated stress fields of industrial forming operations. This holds in particular for flow regions with strong elongational components. At the present time, it is not clear if the poor agreement between simulations and experiments is due to the inadequacy of the models or to the poor evaluation of the model parameters. We lack, in particular, reliable data for normal stresses at high shear rates and response to large, rapid extensional flows to fit the model parameters. And as was mentioned previously, there is no straightforward way to evaluate model parameters for complex flows where both shear and extensional modes of deformation are occurring simultaneously, for example in converging and diverging flows.

2.5.2 Kinetic Theory Models: A Promising Approach?

A relatively recent approach that does not require closed form constitutive models is the so-called micro-macro formulation based on kinetic theories[16-21]. Hua and Schieber[16] recently presented calculations of viscoelastic flow through fibrous media using kinetic theory models and a combined finite element and Brownian dynamics technique. Comparisons were made using the same numerical technique with analogous models that lead to closed-form constitutive equations, specifically the FENE-P dumbbell, which is an approximate FENE model, and the Doi-Edwards reptation model with and without the independent alignment assumption. They reported significant quantitative differences between the predictions of the approximate and the more realistic models. For example, the FENE-P dumbbell underestimated the magnitude of the normal stress by as much as 25% compared to FENE model, and reptation with independent alignment underestimated it by 22% compared to the more realistic reptation model. The use of kinetic theory models improves considerably the quality of the prediction, but although no constitutive equation is solved explicitly, problems still arise that prevent convergence of the flow field at high *De* number. According to Hua and Schieber[16], a way to avoid the numerical instability problem might be the use of more accurate finite element methods, such as the modified EVSS formulation or a higher order technique[116]. Using their current method, they had to modify the momentum equation by adding a relaxation parameter to make the equation more elliptic in order to obtain numerical convergence.

It seems that using more realistic constitutive equations such as kinetic theory models does not eliminate numerical convergence problems while requiring much larger computational resources.

REFERENCES

[1] Dealy J.M., Wissbrun K.F., "Melt Rheology and its Role in Plastics Processing", *Van Nostrand Reinhold*, New York (1990)
[2] Larson R., "Constitutive Equations for Polymer Melts and Solutions", *Butterworths*, Boston (1988)
[3] Agassant J.F., Avenas P., Sergent J.-Ph., Carreau P.J., « Polymer processing. Principles and Modeling », *Hanser Publishers*, New York (1991)
[4] Bird R.B., Curtiss C.F., Armstrong R.C., Hassager O., "Dynamics of Polymeric Liquids, Vol. 1: Fluid Mechanics", Second Edition, *John Wiley & Sons*, New York (1987)
[5] Weissenberg K., *Nature*, 159, p. 310 (1947)
[6] Dealy J.M., Vu T.K.P., "The Weissenberg Effect in Molten Polymers", *J. Non-Newt. Fl. Mech.*, 3, p. 127 (1977)
[7] Fano G., *Arch. Fisiol.*, 5, p. 365 (1908)
[8] Criminale W.O. Jr., Ericksen J.L., Filbey G.L. Jr., *Arch. Ratl. Mech. Anal.*, 1, p. 410 (1958)
[9] Yasuda K.Y., Armstrong R.C., Cohen R.E., *Rheol. Acta*, 20, p. 163 (1981)
[10] Rouse P.E. Jr., "A Theory of the Linear Viscoelastic Properties of Dilute Solutions of Coiling Polymers", *J. Chem. Phys.*, 21, p. 1272 (1953)
[11] Doi M., Edwards S.F., "Dynamics of Concentrated Polymer Systems. Part 1.- Brownian Motion in the Equilibrium State", *J. Chem. Soc., Faraday Trans. II*, 74, p. 1789 (1978)
[12] Doi M., Edwards S.F., " Dynamics of Concentrated Polymer Systems. Part 4.- Rheological Properties ", *J. Chem. Soc., Faraday Trans. II*, 75, p. 38 (1979)
[13] Doi M., Edwards S.F., "The Theory of Polymer Dynamics", *Oxford University Press*, Oxford (1983)
[14] Curtiss C.F., Bird R.B., "A Kinetic Theory for Polymer Melts. II. The Stress Tensor and the Rheological Equations of State", *J. Chem. Phys.*, 74, p. 2016 (1982)
[15] Bird R.B., Curtiss C.F., Armstrong R.C., Hassager O., "Dynamics of Polymeric Liquids, Vol. 2", Second Edition, *John Wiley & Sons*, New York (1987)
[16] Hua C.C., Schieber J.D., "Viscoelastic Flow through Fibrous Media Using the CONNFFESSIT Approach", *J. Rheol.*, 42(3), p. 477-491 (1998)
[17] Halin P., Lielens G, Keunings R., Legat V., "The Lagrangian Particle Method for Macroscopic and Micro-Macro Viscoelastic Flow Computations", *J. Non-Newt. Fl. Mech.*, 79, p.387-403 (1998)
[18] Öttinger H.C., van den Brule B.H.A.A., Hulsen M.A., "Brownian Configuration Fields and Variance Reduced Connffessit", *J. Non-Newt. Fl. Mech.*, 70, p. 255-261 (1997)
[19] Hulsen M.A., van Heel A.P.G., van den Brule B.H.A.A., "Simulation of Viscoelastic Flows Using Brownian Configuration Fields", *J. Non-Newt. Fl. Mech.*, 70, p. 79-101 (1997)
[20] Picasso M., Laso M., Öttinger H.C., "Two-Dimensional, Time-Dependent Viscoelastic Flow Calculations Using Connffessit", *AIChE J.*, 43, p. 877-892 (1997)
[21] Bell T.W., Nyland G.H., Graham M.D., de Pablo J.J., "Combined Brownian Dynamics and Spectral Method Simulations of the Recovery of Polymeric Fluids after Shear Flow", *Macromolecules*, 30, p. 1806-1812 (1997)
[22] Gordon R.J., Schowalter W.R., *Trans. Soc. Rheol.*, 16, p. 79 (1972)
[23] Giesekus H., "A Simple Constitutive Equation for Polymer Fluids Based on the Concept of Deformation Dependent Tensorial Mobility", *J. Non-Newt. Fl. Mech.*, 11, p.69-109 (1982)
[24] Leonov A.I., "Nonequilibrium Thermodynamics and Rheology of Viscoelastic Polymer Media", *Rheol. Acta*, 15, p. 85-98 (1976)
[25] Phan-Thien N., Tanner R.I., "A New Constitutive Equation Derived from Network Theory", *J. Non-Newt. Fl. Mech.*, 2, p. 353-365 (1977)

[26] Legat V., "Computer Modeling of Viscoelastic Flow", in "Rheological Fundamentals of Polymer Processing", J.A. Covas et al. (eds.), *Kluwer Academic Publishers,* The Netherlands, p. 209-229 (1995)

[27] Lodge A.S., "Elastic Liquids", *Academic Press,* London (1969)

[28] Bernstein B., Kearsley E.A., Zapas L.J., *Trans. Soc. Rheol.,* 7, p. 391-410 (1963)

[29] Kaye A., "Non-Newtonian Flow in Incompressible Fluids", *College of Aeronautics,* Cranfield, Note No. 134 (1962)

[30] Papanastasiou A.C., Scriven L.E., Macosko C.W., "An Integral Constitutive Equation for Mixed Flows: Viscoelastic Characterization", *J. Rheol.,* 27(4), p. 387 (1983)

[31] Demay Y., "Computation of 2D Viscoelastic Flows for a Differential Constitutive Equation", in "Rheology of Polymer Melt Processing", J.M. Piau and J.-F. Agassant (eds.), *Elsevier Science,* Amsterdam (1996)

[32] Mitsoulis E., Vlachopoulos J., "The Finite Element for Flow and Heat Transfer Analysis", *Adv. Polym. Techn.,* 4, p. 107 (1984)

[33] Baaijens, F.P.T., "Mixed Finite Element Methods for Viscoelastic Flow Analysis: a Review", *J. Non-Newt. Fl. Mech.,* 79, p. 361-385 (1998)

[34] Crochet M.J., Davies A.R., Walters K., "Numerical Simulation of Non-Newtonian Flow", *Elsevier,* Amsterdam (1984)

[35] Rasmussen H.K., Hassager O., "Simulation of Transient Viscoelastic Flow", *J. Non-Newt. Fl. Mech.,* 46, p. 298-305 (1993)

[36] Luo X.L., Tanner R.I., *J. Non-Newt. Fl. Mech.,* 21, p. 179-199 (1986)

[37] Hulsen M.A., van der Zanden J., "Numerical Simulations of Contraction Flows using a Multi-Mode Giesekus Model", *J. Non-Newt. Fl. Mech.,* 38, p. 183-221 (1991)

[38] Goublomme A., Draily B., Crochet M.J., "Numerical Prediction of Extrudate Swell of a High-Density Polyethylene", *J. Non-Newt. Fl. Mech.,* 44, p. 171-195 (1992)

[39] Rajagopalan D., Armstrong R.C., Brown R.A., "Comparison of Computational Efficiency of Flow Simulations with Multimode Constitutive Equations: Integral and Differential Models", *J. Non-Newt. Fl. Mech.,* 46, p. 243-273 (1993)

[40] Luo X.L., "A Control Volume Approach for Integral Viscoelastic Models and its Application to Contraction Flow of Polymer Melts", *J. Non-Newt. Fl. Mech.,* 64, p. 173-189 (1996)

[41] Rasmussen H.K., "Time-Dependent Finite-Element Method for the Simulation of Three-Dimensional Viscoelastic Flow with Integral Models", *J. Non-Newt. Fl. Mech.,* 84, p. 217-232 (1999)

[42] Mitsoulis E., "Numerical Simulation of Viscoelastic Fluids", in "Polymer Flow Engineering", p. 649-704

[43] Renardy M., "Recent Advances in the Mathematical Theory of Steady Flow of Viscoelastic Fluids", *J. Non-Newt. Fl. Mech.,* 29, p. 11 (1988)

[44] Debbaut B., Crochet M.J., "Further Results on the Flow of a Viscoelastic Fluid Through an Abrupt Contraction", *J. Non-Newt. Fl. Mech.,* 20, p. 173-185 (1986)

[45] Keunings R., "On the High Weissenberg Number", *J. Non-Newt. Fl. Mech.,* 20, p. 209-226 (1986)

[46] Crochet M.J., Keunings R., "Die Swell of a Maxwell Fluid: Numerical Predictions", *J. Non-Newt. Fl. Mech.,* 7, p. 199-212 (1980)

[47] Crochet M.J., Keunings R., " On Numerical Die Swell Calculations", *J. Non-Newt. Fl. Mech.,* 10, p. 85-94 (1982)

[48] Crochet M.J., Keunings R., " Finite Element Analysis of Die Swell of Highly Elastic Fluids", *J. Non-Newt. Fl. Mech.,* 10, p. 339-356 (1982)

[49] Marchal J.M., Crochet M.J., "A New Element for Calculating Viscoelastic Flows", *J. Non-Newt. Fl. Mech.,* 26, p. 77-114 (1987)

[50] Brezzi F., Fortin M., "Mixed and Hybrid Finite Element Methods: Series in Computational Mechanics", *Springer*, New York (1991)
[51] Fortin M., Pierre R., "On the Convergence of the Mixed Method of Crochet and Marchal for Viscoelastic Flows", *Int. J. Numer. Methods Fl.*, 7, p. 1035-1052 (1987)
[52] Lunsmann W.J., Genieser L., Armstrong R.C., Brown R.A., "Finite Element Analysis of Steady Viscoelastic Flow Around a Sphere in a Tube: Calculations with Constant Viscosity Models", *J. Non-Newt. Fl. Mech.*, 48, p. 63-99 (1993)
[53] Szady M.J., Salamon T.R., Liu A.W., Bornside D.E., Armstrong R.C., Brown R.A., "A New Mixed Finite Element Method for Viscoelastic Flows Governed by Differential Constitutive Equations", *J. Non-Newt. Fl. Mech.*, 59, p. 215-243 (1995)
[54] Fortin M., Fortin A., "A New Approach for the FEM simulation of Viscoelastic Flows", *J. Non-Newt. Fl. Mech.*, 32, p. 295-310 (1989)
[55] Lesaint P. Raviart P.A., "On a Finite Element Method for Solving the Neutron Transport Equations", in "Mathematical Aspects of Finite Elements in Partial Differential Equations", C. de Boor (ed.), *Academic Press*, New York, p. 89-123 (1974)
[56] Fortin A., Fortin M., "A Preconditioned Generalized Minimal Residual Algorithm for the Numerical Solution of Viscoelastic Fluid Flows", *J. Non-Newt. Fl. Mech.*, 36, p. 277-288 (1990)
[57] Guénette R., Fortin M., "A New Mixed Finite Element Method for Computing Viscoelastic Flows", *J. Non-Newt. Fl. Mech.*, 60, p.27-52 (1995)
[58] Rajagopalan D., Armstrong R.C., Brown R.A., "Finite Element Methods for Calculation of Steady, Viscoelastic Flow Using a Constitutive with a Newtonian Viscosity", *J. Non-Newt. Fl. Mech.*, 36, p.159-192 (1990)
[59] Fan Y., Tanner R.I., Phan-Thien N., "Galerkin/Least-Square Finite-Element Methods for Steady Viscoelastic Flows", *J. Non-Newt. Fl. Mech.*, 84, p. 233-256 (1999)
[60] Fortin M., Guénette R., Pierre R., "Numerical Analysis of the Modified EVSS", *Comp. Meth. Appl. Mech., Eng.*, 143(1), p. 79-96 (1997)
[61] Boger D.V., " Model Polymer Fluid Systems ", *Pure Appl. Chem.*, 57, p. 921 (1985)
[62] Mackay M.E., Boger D.V., *J. Non-Newt. Fl. Mech.*, 22, p. 235 (1987)
[63] Sridhar T., Gupta R.K., Boger D.V., Binnington R., *J. Non-Newt. Fl. Mech.*, 21, p. 115 (1986)
[64] Debbaut B., Marchal J.M., Crochet M.J., *J. Non-Newt. Fl. Mech.*, 29, p. 119 (1988)
[65] Luo X.-L., Tanner R.I., *J. Non-Newt. Fl. Mech.*, 31, p. 143 (1989)
[66] Coates P.J., Armstrong R.C., Brown R.A., *J. Non-Newt. Fl. Mech.*, 42, p. 141 (1992)
[67] Boger D.V., " Viscoelastic Flows through Contractions ", *Ann. Rev. Fluid Mech.*, 19, 157-182 (1987)
[68] Caswell B., " Report on the IX th International Workshop on Numerical Methods in Non-Newtonian Flows ", *J. Non-Newt. Fl. Mech.*, 62, p. 99-110 (1996)
[69] Mackay M.E., Petrie C.J.S., "Estimates of Apparent Elongational Viscosity Using the Fibre Spinning and "Pure" Methods", *Rheol. Acta*, 28, p. 281-293 (1989)
[70] Wagner M., "Analysis of Time-Dependent Nonlinear Stress-Growth Data for Shear and Elongational Flow of a Low Density Branched Polyethylene Melt ", *Rheol. Acta*, 15, p. 136-142 (1976)
[71] Carrot C., Guillet J., Revenu P., Arsac A., " Experimental Validation of Non Linear Network Models ", in "Rheology of Polymer Melt Processing", J.M. Piau and J.-F. Agassant (eds.), *Elsevier Science*, Amsterdam (1996)
[72] Shaw M.T., Tuminello W.H., "A Closer Look at the MWD-Viscosity Transform", *Polym. Eng. Sci.*, 34(2), p. 159-165 (1994)
[73] Liu Y., Shaw M.T., Tuminello W.H., "Optimized Data Collection for Determination of the MWD from the Viscosity Data of Polymer Melts", *Polym. Eng. Sci.*, 38(1), p. 169-176 (1998)

[74] Wood-Adams P.M., "Determination of Molecular Weight Distribution from Rheological Measurements", Master's Thesis, McGill University, Montreal, Canada (1995)
[75] Nouatin O.H., Coupez T., Agassant J.F., " Identification of Viscoelastic Rheological Parameters by Inverse Analysis ", Proceedings of *EURORHEO '98*, p. 112-113 (1998)
[76] Gotsis A.D., Baird D.G., Reddy J.N., " Comparison of Experimental Data with the Numerical Simulation of Planar Entry Flow: Role of the Constitutive Equation ", *Int. J. Num. Meth. Fl.*, 10, p. 373-400 (1990)
[77] Schoonen J.F.M., " Determination of Rheological Constitutive Equations using Complex Flows ", Ph.D. thesis, Technische Universiteit Eindhoven, Eindhoven, The Netherlands (1998)
[78] White S.A., Baird D.G., " Numerical Simulation Studies of the Planar Entry Flow of Polymer Melts ", *J. Non-Newt. Fl. Mech.*, 30, p. 47-71 (1988)
[79] White S.A., Baird D.G., " Flow Visualization and Birefringence Studies on Planar Entry Flow Behavior of Polymer Melts ", *J. Non-Newt. Fl. Mech.*, 29, p. 245-267 (1988)
[80] Park H.J., Kiriakidis D.G., Mitsoulis E., Lee K.J., " Birefringence Studies in Die Flows of an HDPE Melt ", *J. Rheol.*, 36(8), p. 1563-1583 (1992)
[81] Maders H., Vergnes B., Demay Y., Agassant J.F., " Steady Flow of a White-Metzner Fluid in a 2-D Abrupt Contraction: Computation and Experiments ", *J. Non-Newt. Fl. Mech.*, 45, p. 63-80 (1992)
[82] White J.L., Metzner A.B., *J. Appl. Polym. Sci.*, 8, p. 1367 (1963)
[83] Kiriakidis D.G., Park H.J., Mitsoulis E., Vergnes B., Agassant J.F., " A Study of Stress distribution in Contraction Flows of an LLPDE Melt ", *J. Non-Newt. Fl. Mech.*, 47, p. 339-356 (1993)
[84] Ahmed R., Liang R.F., Mackley M.R., " The Experimental Observation and Numerical Prediction of Planar Entry Flow and Die Swell for Molten Polyethylenes ", *J. Non-Newt. Fl. Mech.*, 59, p. 129-153 (1995)
[85] Polyflow, v. 3.2.0, Louvain-La-Neuve, Belgium (1992)
[86] Fiegl K., Öttinger H.C., " A Numerical Study of the Flow of a Low-Density-Polyethylene Melt in Planar Contraction and Comparison to Experiments ", *J. Rheol.*, 40(1), p. 21-35 (1996)
[87] Wagner M.H., Demarmels A., " A Constitutive Analysis of Extensional Flows of Polyisobutylene ", *J. Rheol.*, 34, p. 943-958 (1990)
[88] Beraudo C., Fortin A., Coupez T., Demay Y., Vergnes B., Agassant J.F., " A Finite Element Method for Computing the Flow of Multi-Mode Viscoelastic Fluids: Comparison with Experiments ", *J. Non-Newt. Fl. Mech.*, 75, p. 1-23 (1998)
[89] Beaufils P., Vergnes B., Agassant J.F., " Characterization of the Sharkskin Defect and its Development with the Flow Conditions ", *Int. Polym. Process.*, IV(2), p. 78-84 (1989)
[90] Wales J.L.S., " The Application of Flow Birefringence to Rheological Studies of Polymer Melts ", Ph.D. thesis, Delft University of Technology, The Netherlands (1976)
[91] Fiegl K., Öttinger H.C., " The Flow of a LDPE Melt through an Axisymmetric Contraction: A Numerical Study and Comparison to Experimental Results ", *J. Rheol.*, 38(4), p. 847-874 (1994)
[92] Barakos G., Mitsoulis E., "Numerical Simulation of Extrusion through Orifice Dies and Prediction of Bagley Correction for an IUPAC-LDP Melt", *J. Rheol.*, 39(1), p. 193-209 (1995)
[93] Meissner J., "Basic Parameters, Melt Rheology, Processing and End-Use Properties of Three Similar Low Density Polyethylene Samples", *Pure Appl. Chem.*, 42, p. 551-612 (1975)
[94] Dupont S., Crochet M.J., "The Vortex Growth of a K.B.K.Z. Fluid in an Abrupt Contraction", *J. Non-Newt. Fl. Mech.*, 29, p. 81-91 (1988)
[95] Luo X.-L., Mitsoulis E., "A Numerical Study of the Effect of Elongational Viscosity on Vortex Growth in Contraction Flows of Polyethylene Melts", *J. Rheol.*, 34(3), p. 309-342 (1990)
[96] Mitsoulis E., Hatzikiriakos S.G., Christodoulou K., Vlassopoulos D., "Sensitivity Analysis of the Bagley Correction to Shear and Extensional Rheology", *Rheol. Acta*, 37, p. 438-448 (1998)

---

[97] Beraudo C., "Méthodes éléments finis pour la simulation numérique d'écoulements de fluides viscoelastiques de type différentiel dans des géométries convergentes", Ph.D. thesis, École Nationale Supérieure des Mines de Paris, Sophia Antipolis, France (1995)
[98] Laun H.M., "Polymer Melt Rheology with a Slit die", *Rheol. Acta,* 22, p. 171-185 (1983)
[99] Guillet J., Revenu P., Béreaux Y., Clermont J.-R., "Experimental and Numerical Study of Entry Flow of Low-Density Polyethylene Melts", *Rheol. Acta,* 35, p. 494-507 (1996)
[100] Soskey P.L., Winter H.H., " Large Step Shear Strain Experiments with Parallel Disk Rotational Rheometers ", *J. Rheol.,* 28(5), p. 625-645 (1984)
[101] Hatzikiriakos S.G., Mitsoulis E., "Excess Pressure Losses in the Capillary Flow of Molten Polymers", *Rheol. Acta,* 35, p. 545-555 (1996)
[102] Carreau P.J., Ph.D. Thesis, Univ. of Wisconsin, Madison (1969)
[103] Luo X.-L., Mitsoulis E., " Memory Phenomena in Extrudate Swell Simulations for Annular Dies ", *J. Rheol.,* 33(8), p. 1307-1327 (1989)
[104] Tanoue S., Kajiwara T., Iemoto Y., Funatsu K., " High Weissenberg Number Simulation of an Annular Extrudate Swell Using the Differential Type Constitutive Equation ", *Polym. Eng. Sci.,* 38(3), p. 409-419 (1998)
[105] Orbey N., Dealy J.M., *Polym. Eng. Sci.,* 24, p. 511 (1984)
[106] Garcia-Rejon A., DiRaddo R.W., Ryan M.E., " Effect of Die Geometry and Flow Characteristics on Viscoelastic Annular Swell ", *J. Non-Newt. Fl. Mech.,* 60, p. 107-128 (1995)
[107] Otsuki Y., Kajiwara T., Funatsu K., " Numerical Simulations of Annular Extrudate Swell of Polymer Melts ", *Polym. Eng. Sci.,* 37(7), p. 1171-1181 (1997)
[108] Luo X.-L., Tanner R.I., " A Streamline Element Scheme for Solving Viscoelastic Flow Problems. Part II: Integral Constitutive Models ", *J. Non-Newt. Fl. Mech.,* 22, p. 71-89 (1986)
[109] Bush M.B., " Prediction of Polymer Melt Extrudate Swell Using a Differential Constitutive Model ", *J. Non-Newt. Fl. Mech.,* 31, p. 179-191 (1989)
[110] Goublomme A., Crochet M.J., " Numerical Prediction of Extrudate Swell of a High-Density Polyethylene: Further Results ", ", *J. Non-Newt. Fl. Mech.,* 47, p. 281-287 (1993)
[111] Sun J., Phan-Thien N., Tanner R.I., " Extrudate Swell Through an Orifice Die ", *Rheol. Acta,* 35, p. 1-12 (1996)
[112] Koopmans R.J., " Extrudate Swell of High Density Polyethylene. Part I: Aspects of Molecular Structure and Rheological Characterization Methods, Part II: Time Dependency and Effects of Cooling and Sagging ", *Polym. Eng. Sci.,* 32(23), p. 1741-1754 (1993)
[113] Hassager O., " Working Group on Numerical Techniques ", *J. Non-Newt. Fl. Mech.,* 29, p. 2-5 (1988)
[114] Hartt W.H., Baird D.G., " The Confined Flow of Polyethylene Melts Past a Cylinder in a Planar Channel ", *J. Non-Newt. Fl. Mech.,* 65, p. 247-268 (1996)
[115] Baaijens F.P.T., Selen S.H.A., Baaijens H.P.W., Peters G.W.M., Meijer H.E.H., " Viscoelastic Flow Past a Confined Cylinder of a LDPE Melt ", *J. Non-Newt. Fl. Mech.,* 68, p.173-203 (1997)
[116] Talwar K.K., Khomani B., " Applications of Higher Order Finite Element Method to Viscoelastic Flow in Porous Media ", *J. Rheol.,* 36, p. 1377-1416 (1992)

3. Plan of the Research

3.1 Objectives

The objectives of this work were as follows:

1. To determine the limitations of present methods for the numerical simulation of the flow of viscoelastic materials.
2. To establish the cause of the limitations and suggest methods for overcoming them.

In order to achieve these objectives, we carried out viscoelastic flow simulations using a numerical procedure described in Chapter 6. For these simulations, we used two differential viscoelastic constitutive equations and compared their predictions with those of a strictly viscous model. The models selected are presented in the next section.

We also conducted an experimental study of two complex flows: a planar abrupt 8:1 contraction flow and an axisymmetric entrance flow and extrudate swell. The materials used for these experiments are described in Chapter 4.

3.2 Models Selected for this Research

3.2.1 Carreau-Yasuda Model

In order to appreciate the added value of using a viscoelastic constitutive equation in flow simulations, we carried out calculations using a strictly viscous model. We chose the Carreau-Yasuda[1] model, a generalized Newtonian model that describes fairly well the shear dependence of the viscosity of polymer melts. This model was previously introduced in Chapter 2:

Eqn. 3-1a $$\underline{\underline{\tau}}(t) = \eta\left[II_D(t)\right]\underline{\underline{D}}(t)$$

where

Eqn. 3-1b $$\eta[II_D(t)] = \eta_0\left(1 + (2\lambda^2 II_D(t))^{s/2}\right)^{\frac{m-1}{s}}$$

The scalar viscosity is a function of II_D, the second invariant of the rate of deformation tensor. As stated before, normal stress differences in shear and transient stresses in start-up flows are not predicted by this purely viscous model.

Four parameters must be specified in order to use the model: the zero-shear viscosity (η_0), which can be estimated using the discrete relaxation spectrum, a characteristic time (λ), a power-law index (m), which is related to the slope of the viscosity curve at high shear rates, and a second power-law index (s), which controls the transition between the plateau and the power-law regions. The Carreau-Yasuda model parameters for the two materials studied are presented in sections 5.1.1 and 5.2.1.

3.2.2 Leonov Model

The first viscoelastic constitutive equation we selected is a modified Leonov model[2]. This model was initially chosen because it is the only one that satisfies basic stability criteria[3], Hadamard (thermodynamic) and dissipative stability criteria, while describing well the material functions usually measured[2]. The original model proposed by Leonov[4,5], which is derived from irreversible thermodynamic principles, is an extension of the theory of rubber elasticity to viscoelastic liquids. The simple Leonov model, which uses only the parameters of the discretized linear viscoelastic spectrum, has been found to provide a good representation of data for shear flows and to be easy to use[6]. However, it provided a poor fit to extensional flow data. Recently, a new formulation of the general class of differential constitutive equations proposed by Leonov was presented[2]. This latest version eliminates some of the recognized deficiencies of the original "simple" model by adding only one or two nonlinear parameters. This modification makes possible a fairly accurate description of simple flows for polymers such as low and high density polyethylenes (LDPE and HDPE), polystyrene (PS) and polyisobutylene (PIB)[2].

For the sake of simplicity, we present here the modified Leonov model for a single relaxation time and an incompressible fluid. However, the model can easily be extended to cover the multimode case and compressibility. Derivation of the compressible case for the simple model is presented in references 7, 8 and 9. A multimode incompressible version was used in our simulations.

The evolution equations for the Finger tensor B_{ij} and the associated dissipation function D are[4]:

Eqn. 3-2 $$\overset{\nabla}{B}_{ij} + 2B_{ik} \bullet \mathrm{e}_{kj_p} = 0$$

Eqn. 3-3 $$D = \mathrm{tr}(\tau_{ij} \bullet \mathrm{e}_{ij_p}) \qquad (\mathrm{tr}(\mathrm{e}_{ij_p}) = 0)$$

Here, $\overset{\nabla}{B}_{ij}$ is the upper-convected time derivative of the Finger tensor, $\mathrm{e}_{ij_p} = \mathrm{e}_{ij_p}(B_{ij})$ is the irreversible strain rate tensor, and τ_{ij} is the extra stress tensor. For incompressible liquids, the invariants of the Finger tensor are as follows:

Eqn. 3-4 $$\mathrm{I}_1 = \mathrm{tr}B_{ij}, \quad \mathrm{I}_2 = \mathrm{tr}C_{ij}, \quad \mathrm{I}_3 = \det B_{ij} = 1.$$

The irreversible rate of deformation tensor, e_{ij_p}, has the following general form:

Eqn. 3-5 $$\mathrm{e}_{ij_p} = \frac{b}{4\lambda}\left[B_{ij} - B_{ij}^{-1} + \left(\frac{\mathrm{I}_2 - \mathrm{I}_1}{3}\right)\delta_{ij}\right]$$

Here δ_{ij} is the unit tensor, λ is the relaxation time in the linear Maxwell limit, and $b=b(\mathrm{I}_1,\mathrm{I}_2)$ can be thought of as a deformation-history-dependent scaling factor for the linear relaxation times and is an adjustable parameter. The simplest choice is to let $b=1$, which is known as the standard Leonov model. It is sufficient that $b(\mathrm{I}_1,\mathrm{I}_2)$ be positive for the dissipation function to be positive definite, which is required by the Second Law of thermodynamics. The form of the evolution equation (Eqn. 3-2) becomes:

Eqn. 3-6
$$2\lambda \overset{\nabla}{B}_{ij} + b(I_1, I_2)\left[B_{ik}B_{kj} + B_{ij}\frac{(I_2 - I_1)}{3} - \delta_{ij}\right] = 0$$

In order to relate the extra stress tensor to the elastic Finger tensor during the deformation history, a functional form for the elastic potential $W(I_1, I_2, T) \equiv \rho_o f$ must be provided. Here, ρ_o is the density, and f is the specific Helmholtz free energy. The following general elastic potential has been suggested[2]:

Eqn. 3-7
$$W(I_1, I_2) = \frac{3G}{2(n+1)}\left\{(1-\beta)\left[\left(\frac{I_1}{3}\right)^{n+1} - 1\right] + \beta\left[\left(\frac{I_2}{3}\right)^{n+1} - 1\right]\right\}$$

where G is the linear Hookean elastic modulus, and β and n are numerical parameters. Eqn. 3-7 yields the Mooney potential for n=0, and the neo-Hookean potential for $n=\beta=0$, which is the case for HDPE and PS[2]. A constitutive equation with b=1 and the neo-Hookean potential ($n=\beta=0$) gives back the simple Leonov model in its original form. Finally, the extra stress tensor can be written in the Finger form as:

Eqn. 3-8
$$\tau_{ij} = 2\left(B_{ij}\frac{\partial W}{\partial I_1} - B_{ij}^{-1}\frac{\partial W}{\partial I_2}\right) - G\delta_{ij}$$

The functional form of the b function is determined from extensional flow data, and we present in sections 5.1.2 and 5.2.2 the results for our LLDPE and HDPE. We also compare the predictions of the modified Leonov model with those obtained using the simple model.

3.2.3 Phan-Thien Tanner Model

Calculations using the simple Leonov model in numerical flow simulations indicated serious convergence problems. While a major effort was directed at achieving satisfactory simulations, it was found that the use of this equation exacerbated the convergence problems of the numerical analysis and made it impossible to obtain solutions for most cases.

In order to achieve the objectives of the research, therefore, a second viscoelastic constitutive equation was selected for use. A differential model was chosen so that the existing numerical code could be used. The Phan-Thien/Tanner model[10,11] (Eqn. 3-9) had shown itself to behave well in numerical simulations, although it did not give as good a fit of measurable material functions. Fortin[12] reported having successful results in terms of numerical convergence with that model. However, even this equation gave convergence problems, as will be seen in Chapter 8.

Like the Leonov model, the PTT model does not predict a separable relaxation modulus, although it is derived from network theory. Separability refers to the possibility of separating time and strain effects in the nonlinear relaxation modulus, as discussed in section 2.1.4 (Eqn. 2-29).

The PTT model is expressed as follows:

Eqn. 3-9 $$\lambda \overset{\oplus}{\underline{\underline{\tau}}} + Y\left(tr\underline{\underline{\tau}}\right)\underline{\underline{\tau}} = 2\eta\underline{\underline{D}}$$

where $\oplus$ stands for the convected Gordon-Schowalter derivative[13], which is a combination of the upper ∇ and lower Δ convected derivatives:

Eqn. 3-10 $$\overset{\oplus}{\underline{\underline{\tau}}} = \frac{\xi}{2}\overset{\nabla}{\underline{\underline{\tau}}} + \left(1 - \frac{\xi}{2}\right)\overset{\Delta}{\underline{\underline{\tau}}}$$

where ξ=2 represents the upper-convected derivative

ξ=0, the lower-convected derivative

ξ=1, it is the corotional derivative.

Phan-Thien and Tanner suggested two possibilities for the function $Y\left(tr\underline{\underline{\tau}}\right)$:

Eqn. 3-11 $$Y\left(tr\underline{\underline{\tau}}\right) = 1 + \frac{\lambda\varepsilon}{\eta}tr\underline{\underline{\tau}}$$

Eqn. 3-12 $$Y\left(tr\underline{\underline{\tau}}\right)=\exp\left(\frac{\lambda\varepsilon}{\eta}tr\underline{\underline{\tau}}\right)$$

With either choice, the PTT model has two nonlinear parameters (ξ and ε) to be determined for each material in addition to the discrete spectrum. Nonlinear shear and extensional data are needed to determine the nonlinear parameters of the model. The parameter ξ controls the level of shear thinning, while ε has little influence on shear properties and serves mainly to blunt the extensional singularity that would otherwise be present[6,10,11].

Larson[6] pointed out that there are disadvantages to using the Gordon-Schowalter derivative for melts. These disadvantages are inherited by the PTT model if $\xi \neq 2$. Primary among these are unphysical oscillations in the shear stress and first normal stress during start-up of steady shear at large shear rates. Other problems have also been reported when $\xi \neq 2$; for example a maximum in the flow curve, which is physically unrealistic[14], and the violation of Lodge-Meissner relationship[15]. Using $\xi = 2$ avoids these problems, but then the model predicts N_2=0, which is also unrealistic. Despite these problems, the PTT model is known to give a moderate to good fit[6] of shear and extensional rheological properties of polymer melts using Eqn. 3-12 for $Y\left(tr\underline{\underline{\tau}}\right)$ and of polymer solutions with Eqn. 3-11. Eqn. 3-12 is suitable for polymer melts, since the exponential term results in a maximum in the steady-state elongational viscosity and is thus in better agreement with experimental data. The linear equation for Y (Eqn. 3-11) predicts a plateau value of the elongational viscosity at high strain rates, which is more suitable for polymer solutions. The PTT model parameters we used for our materials are presented in sections 5.1.3 and 5.2.3.

REFERENCES

[1] Yasuda K.Y., Armstrong R.C., Cohen R.E., *Rheol. Acta,* 20, p. 163 (1981)

[2] Simhambhatla M., Leonov A.I., "On the Rheological Modeling of Viscoelastic Polymer Liquids with Stable Constitutive Equations", *Rheol. Acta,* 34, p. 259-273 (1995)

[3] Leonov A.I., "Viscoelastic Constitutive Equations and Rheology for High Speed Polymer Processing", *Polym. Intern.,* 36(2), p. 187-193 (1995)

[4] Leonov A.I., "Nonequilibrium Thermodynamics and Rheology of Viscoelastic Polymer Media", *Rheol. Acta,* 15, p. 85-98 (1976)

[5] Leonov A.I., Lipkina E.H., Paskhin E.D., Prokunin A.N., "Theoretical and Experimental Investigation of Shearing in Elastic Polymer Liquids", *Rheol. Acta,* 15, p. 411-426 (1976)

[6] Larson R.G., "Constitutive Equations for Polymer Melts and Solutions", *Butterworths Series in Chem. Eng.,* Boston (1988)

[7] Baaijens F.P.T., "Calculation of Residual Stresses in Injection Molded Products", *Rheol. Acta,* 30, p. 284 (1991)

[8] Flaman A.A.M., "Buildup and Relaxation of Molecular Orientation in Injection Molding. Part I: Formulation", *Polym. Eng. Sci.,* 33(4), p. 193 (1993)

[9] Flaman A.A.M., "Buildup and Relaxation of Molecular Orientation in Injection Molding. Part II: Experimental Verification", *Polym. Eng. Sci.,* 33(4), p. 202 (1993)

[10] Phan Thien N., Tanner R.I., "A New Constitutive Equation Derived from Network Theory", *J. Non-Newt. Fl. Mech.,* 2, p. 353-365 (1977)

[11] Phan Thien N., "A Nonlinear Network Viscoelastic Model", *J. Rheol.,* 22, p. 259-283 (1978)

[12] Fortin A., Beliveau A., "Injection Molding for Charged Viscoelastic Fluid Flow Problems", *PPS-14,* p. 327-328, Yokohama, Japan (1998)

[13] Gordon R.J., Schowalter W.R., *Trans. Soc. Rheol.,* 16, p. 79 (1972)

[14] Beraudo C., "Méthodes éléments finis pour la simulation numérique d'écoulements de fluides viscoelastiques de type différentiel dans des géométries convergentes", Ph.D. thesis, École Nationale Supérieure des Mines de Paris, Sophia Antipolis, France (1995)

[15] Carrot C., Guillet J., Revenu P., Arsac A., " Experimental Validation of Non Linear Network Models ", in "Rheology of Polymer Melt Processing", J.M. Piau and J.-F. Agassant (eds.), *Elsevier Science,* Amsterdam (1996)

4. Rheological Characterization

4.1 Materials Used

In the original research plan, a single polymer was to be studied in two types of complex flow. This was intended to make possible the performance evaluation of the constitutive equations of interest in different flow situations. However, the linear low-density polyethylene (LLDPE) that was studied in the axisymmetric extrudate swell experiments proved to be unstable in the extruder used for the planar abrupt contraction flow. It was not possible to obtain a steady flow rate, and it was necessary to use another material for these experiments, a high-density polyethylene (HDPE). The LLDPE was Dowlex™ (Dow Chemical Company) 2049A, which is a commercial high stability copolymer made using a Ziegler-Natta catalyst. It is used primarily in packaging and is processed by extrusion and film blowing. The HDPE X1010 was an experimental DSM material polymerized using a catalyst different from the one used to make DSM commercial blow molding resins and sold as Stamylan™ HD. Some characteristics of the two resins are presented in Table 4-1.

Table 4-1 Experimental Materials

Resin	Density (g/cm^3)	Melt Index (g/10 min.)	Molecular Weight (M_w) (g/mol)	Polydispersity (M_w/M_n)
LLDPE	0.926	1.0 *	119 600	3.82
HDPE	0.957	1.15 **	195 000	35.0

* 2.16 kg, 190°C (ASTM D1238, Method E)
** Test I5

4.2 Experimental Methods

4.2.1 Small Amplitude Oscillatory Shear

The experiment most widely used to determine the linear viscoelastic properties of polymer melts is small amplitude oscillatory shear. The storage and loss moduli were measured using a Rheometrics Dynamic Analyzer II (RDA II), a controlled strain rheometer. The instrument was operated in a parallel plate configuration (plate diameter=25 mm), under a nitrogen atmosphere to prevent thermal degradation. Thermal stability tests were performed to ensure that the resins did not degrade under test conditions, and strain sweeps were performed to verify that the measurements were within the linear viscoelastic regime at all frequencies. The nominal frequency range of the RDA II is from 0.001 to 500 rad/s, but the useful frequency range is resin dependent and must be determined experimentally.

Samples for dynamic measurements were compression molded. The molding temperature and pressure cycle was optimized to produce homogeneous samples without residual stresses or voids and to minimize thermal degradation. The samples were prepared at 180°C according to the sequence of times and applied pressures presented in Table 4.2.

Table 4-2 Compression Molding Procedure at 180°C

Cycle	melting	compression	compression	compression	Cooling *
Pressure (MPa)	0	1.2	2.4	3.6	3.6
Time (min.)	5	5	5	5	~10

* pressure released when T < 40°C

4.2.2 Steady Shear

Capillary Rheometer

The viscosity of the LLDPE was measured on an Instron, piston-driven, constant speed capillary rheometer. In this instrument, the apparent wall shear rate is calculated from the piston speed, and the wall shear stress is calculated from the force measured by the load cell. Accurate control of the temperature in the barrel (±1°C) is achieved through three independent heating zones with PID controllers and J-type thermocouples[1]. Circular dies of 1.4 mm diameter and L/D ratios of 4.75, 9.5 and 19.0 were used to obtain accurate values of the Bagley corrections which agreed with values obtained using an orifice die[2] (L/D < 0.5).

Sliding Plate Rheometer

The sliding plate rheometer shears a melt between two stainless steel plates. The moving plate, which can produce shear rates up to 500 s^{-1}, is driven by a servo-hydraulic linear actuator. The shear stress is measured at the center of the sample by a shear stress transducer developed at McGill University. All measurements take place in a temperature-controlled oven. A detailed description can be found in reference 3. Measurements were made at 200°C for the HDPE resin.

4.2.3 Extensional Flow

Transient elongational experiments were performed using a Meissner[4] type apparatus, the Rheometrics Melt Elongational rheometer (RME), by Plastech Engineering AG laboratory in Zurich. The sample, clamps and leaf springs are installed in a temperature-controlled oven, which is heated by electrical heater wires embedded in the walls. The sample is supported by a cushion of inert gas (nitrogen) and stretched homogeneously between two sets of conveyor belt clamps at a constant Hencky strain rate defined as follows:

Eqn. 4-1 $$\dot{\varepsilon} = \frac{d(\ln(L))}{dt}$$

where L is the actual sample length.

The strain rate range of the instrument is 0.001 to 3 s^{-1}, but the attainable strain rate range is resin dependent and must be determined experimentally. Measurements were performed at 150°C for the LLDPE and at 200°C for the HDPE.

4.3 Linear-Low Density Polyethylene

All rheological measurements for the LLDPE were performed at 150°C, which is the temperature at which the extrudate swell measurements were conducted. In order to make sure that the polymer was fully molten at that temperature, we consulted data previously collected for this material[5]. Heat capacity measurements carried out in a differential scanning calorimeter showed a melting peak temperature of 126°C. Pressure-volume-temperature (PVT) data obtained in cooling gave the following crystallization temperature, T_c, as a function of pressure:

Eqn. 4-2

$$T_c = 113.52 + (0.281)P$$

with P the pressure in MPa. The highest pressure reached in the capillary rheometer was 42 MPa, which gives a crystallization temperature of 125°C. We are therefore confident that all measurements were performed in the molten state.

4.3.1 Storage and Loss Moduli

The storage (G') and loss (G") moduli were measured for three samples, with a maximum between-sample variation of 3 %. Measurements were made over a frequency range of 0.02 to 500 rad/s. Results are presented in Fig. 4-1.

The discrete spectrum of relaxation times was determined from the oscillatory shear data by linear regression as described in reference 6. In that technique we specify N values of λ_i distributed around a center time and with a specified distance between times, within the range of experimental frequencies. The values of G_i are then determined by a least-squares procedure, using M sets of data:

Eqn. 4-3

$$\underset{G_i}{MIN}\left|\sum_{j=1}^{M}\left[\left(\sum_{i=1}^{N}\frac{1}{G'(\omega_j)}G_i\frac{(\omega_j\lambda_i)^2}{1+(\omega_j\lambda_i)^2}-1\right)^2+\left(\sum_{i=1}^{N}\frac{1}{G''(\omega_j)}G_i\frac{(\omega_j\lambda_i)}{1+(\omega_j\lambda_i)^2}-1\right)^2\right]\right.$$

A minimum of six modes was necessary to obtain a good fit of the experimental moduli. We determined two discrete spectra: one for all the experimental data available and one for a truncated set of data where we removed the measurements at the lowest frequencies. This was done to obtain a smaller longest relaxation time in order to improve the numerical convergence of the simulations. Both fits are shown in Fig. 4-2. The parameter sets [G_i, λ_i] are presented in Table 4-3.

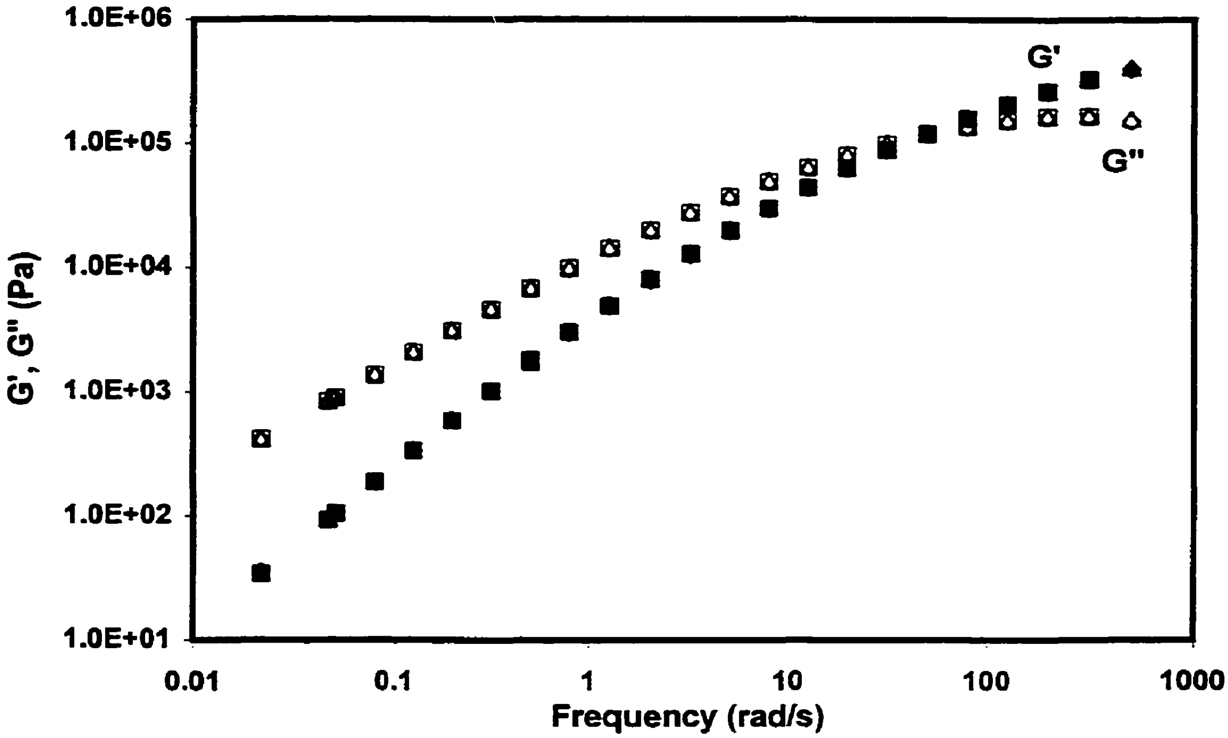

Figure 4-1 Dynamic Moduli of the LLDPE at 150°C.

Table 4-3 Discrete Relaxation Spectra for the LLDPE at 150°C

	All Data		Truncated Data	
Mode	***G* (Pa)**	**λ (s)**	***G* (Pa)**	**λ (s)**
1	2.51×10^5	1.43×10^{-3}	2.38×10^5	2.00×10^{-3}
2	2.09×10^5	1.00×10^{-2}	1.77×10^5	1.00×10^{-2}
3	6.38×10^4	7.00×10^{-2}	6.25×10^4	5.00×10^{-2}
4	1.17×10^4	4.90×10^{-1}	2.16×10^4	2.50×10^{-1}
5	1.11×10^3	3.43×10^0	2.00×10^3	1.25×10^0
6	1.10×10^2	24.0×10^0	8.36×10^2	6.25×10^0

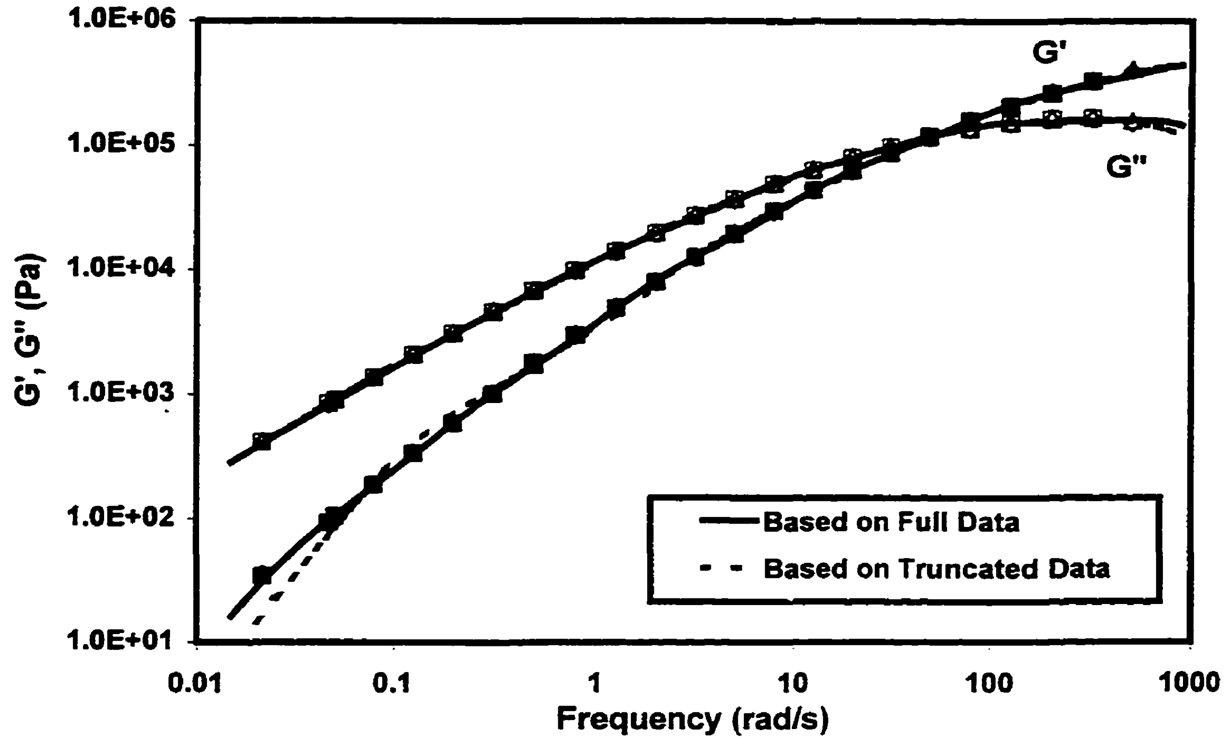

Figure 4-2 Fits of the Discrete Spectra for the LLDPE at 150°C.

4.3.2 Viscosity

Measurements were made at 150°C, and the results were compared with others[5] obtained at 160°, 200° and 240°C using a master curve at 200°C and an activation energy (E_a) of 26.1 kJ/mol. The Bagley corrections were in reasonable agreement with values obtained by Kim[2] using an orifice die (L/D < 0.5) (Figure 4-3). With all corrections applied (Bagley and Rabinowitch), the flow curve compared well with data obtained from the sliding plate rheometer at the same temperature by Koran[7]. The flow curve is presented in Fig. 4-4. Finally, in Fig. 4-5 the viscosity is plotted along with the complex viscosity, showing that the empirical Cox-Merz rule (Eqn. 4-4) does not apply for this material at high shear rates, which is unusual for a linear material.

Eqn. 4-4 $$\eta(\dot{\gamma}) = |\eta^*(\omega)| \qquad (\omega = \dot{\gamma})$$

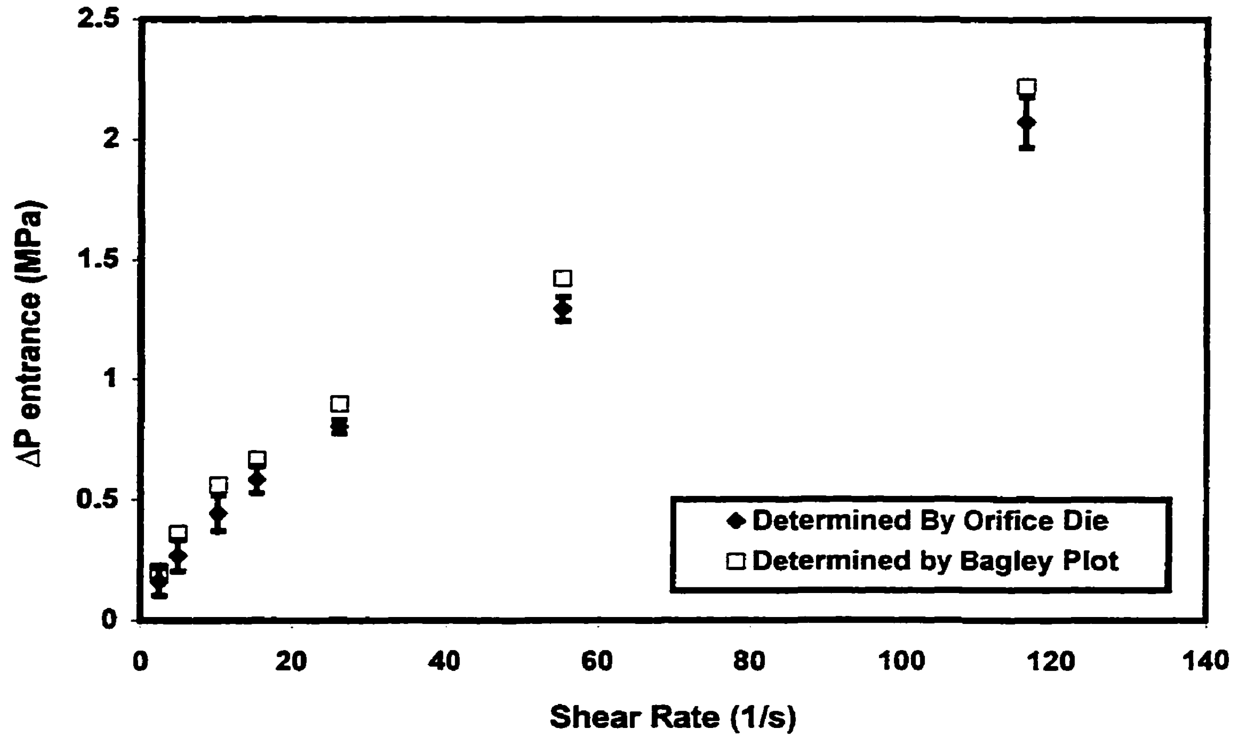

Figure 4-3 Entrance Pressure Drop by Two Methods for the LLDPE at 150°C.

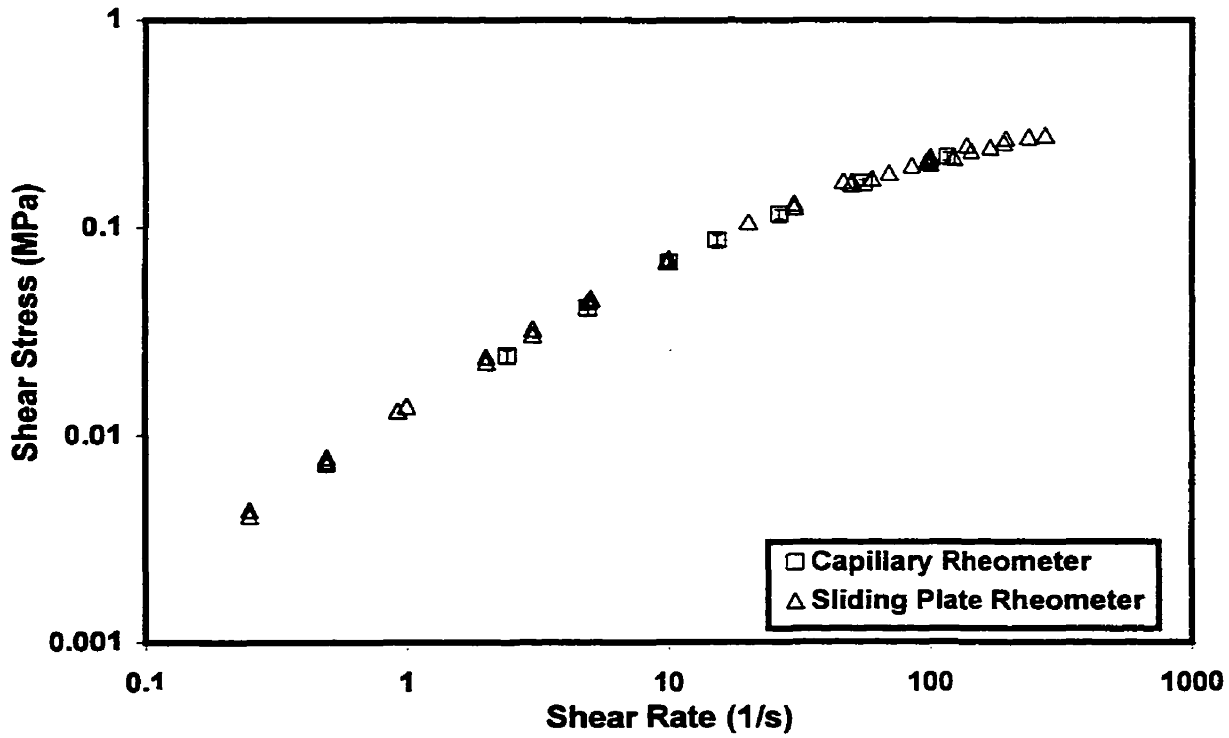

Figure 4-4 Flow Curve by Two Rheometers for the LLDPE at 150°C.

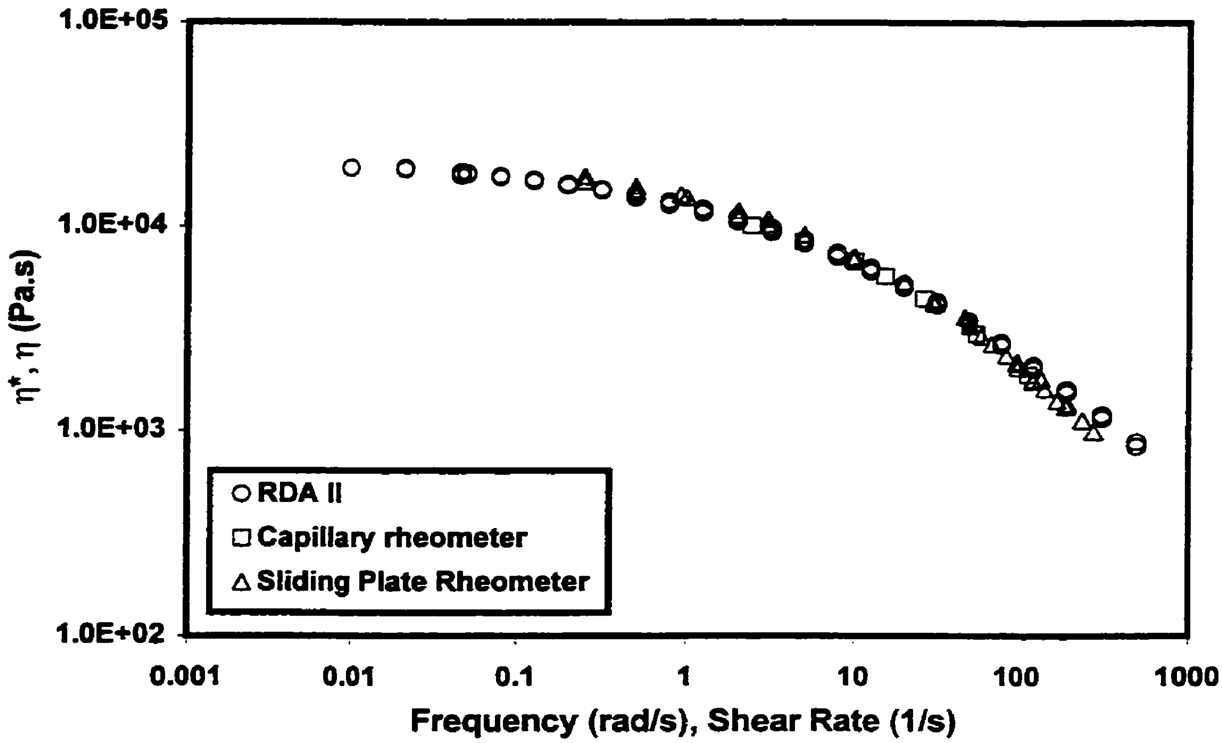

Figure 4-5 Complex Viscosity and Viscosity of the LLDPE at 150°C.

4.3.3 Tensile Stress Growth Coefficient

Transient elongational experiments were performed at 150°C for nominal strain rates of 0.01, 0.1 and 1.0 s^{-1}. Using particle tracking and video images of three zones in the sample, it was possible to obtain an accurate value of the strain rate. The true strain rates were found to be 0.01024, 0.09460 and 1.004 s^{-1}. Even if we eliminate the uncertainty in the strain rate, an important source of error that remains is the uncertainty in the force measurement. According to the instrument manufacturer, this uncertainty is 0.001 N. The error on the stress can be determined by performing an error propagation analysis[8]. The stress is calculated by the following equation:

Eqn. 4-5
$$\sigma_E(t) = \frac{F(t)}{A(t)} = \frac{F(t)}{A_o \exp(-\dot{\varepsilon}t)}$$

where F(t) is the force as a function of time and A(t) is the cross sectional area as a function of time. A_o is the cross sectional area of the sample just before the deformation begins:

Eqn. 4-6
$$A_o = H_{RT} W_{RT} \left(\frac{\rho_{RT}}{\rho_{TT}} \right)^{2/3}$$

The subscripts RT and TT refer to the room and test temperatures, and H and W are the initial height and width of the sample. The LLDPE melt density at test temperature (150°C) is 0.785 g/cm^3. Neglecting the uncertainty in the cross-sectional area, the error propagation analysis gives:

Eqn. 4-7
$$\left. \frac{\Delta \sigma_E}{\sigma_E} \right| = \frac{\Delta F}{F} = \frac{0.001}{F}$$

In Fig. 4-6, we have included the error bars calculated with Eqn. 4-7. We can see that at low strain rates, the uncertainty in the force leads to a very large uncertainty in the rheological properties of interest.

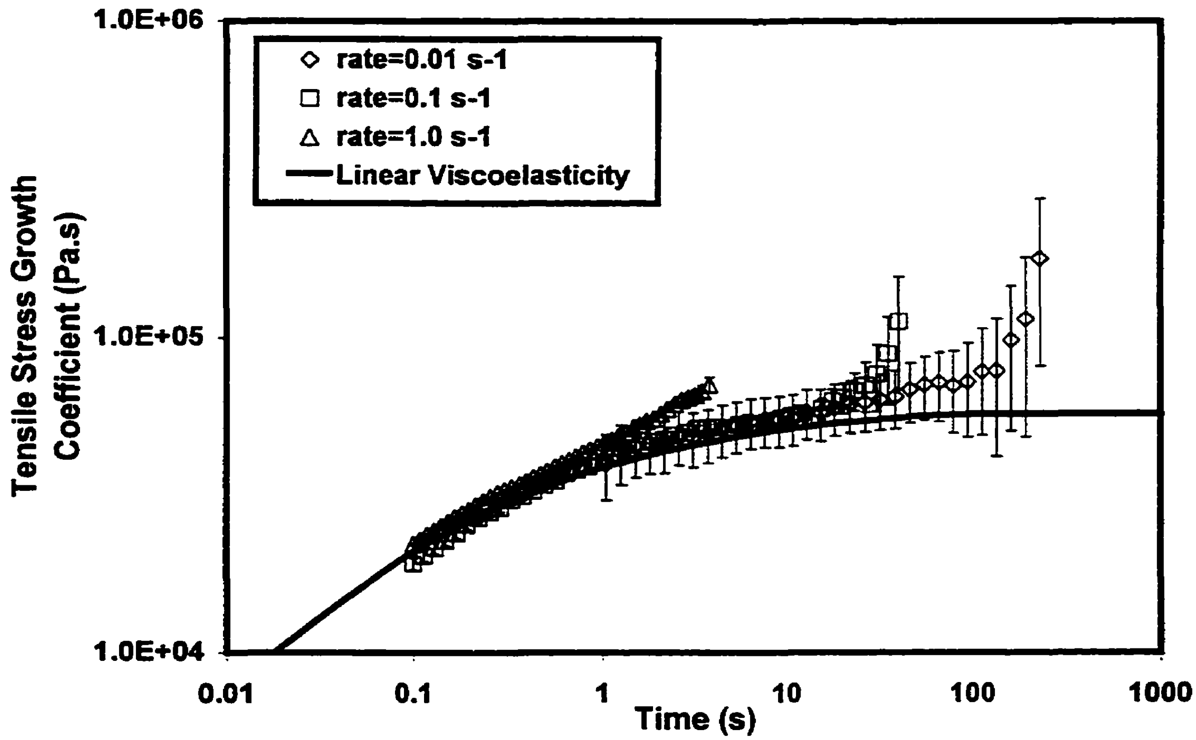

Figure 4-6 Transient Elongational Stress for the LLDPE at 150°C.

4.4 High Density Polyethylene

4.4.1 Storage and Loss Moduli

The storage (G') and loss (G") moduli were measured on five samples, with a maximum between-sample variation of 4 %. Measurements were made over a frequency range of 0.02 to 500 rad/s. Average values of G' and G" for the five samples are presented in Figure 4-7. We determined also for this material two discrete spectra: one for all the experimental data available, and one for a truncated set of data, where we removed the data at the lowest frequencies. Again, a minimum of six modes was necessary to obtain a good fit of the experimental moduli. Both fits are presented in Fig. 4-8. The parameter sets [G_i, λ_i] are presented in Table 4-4.

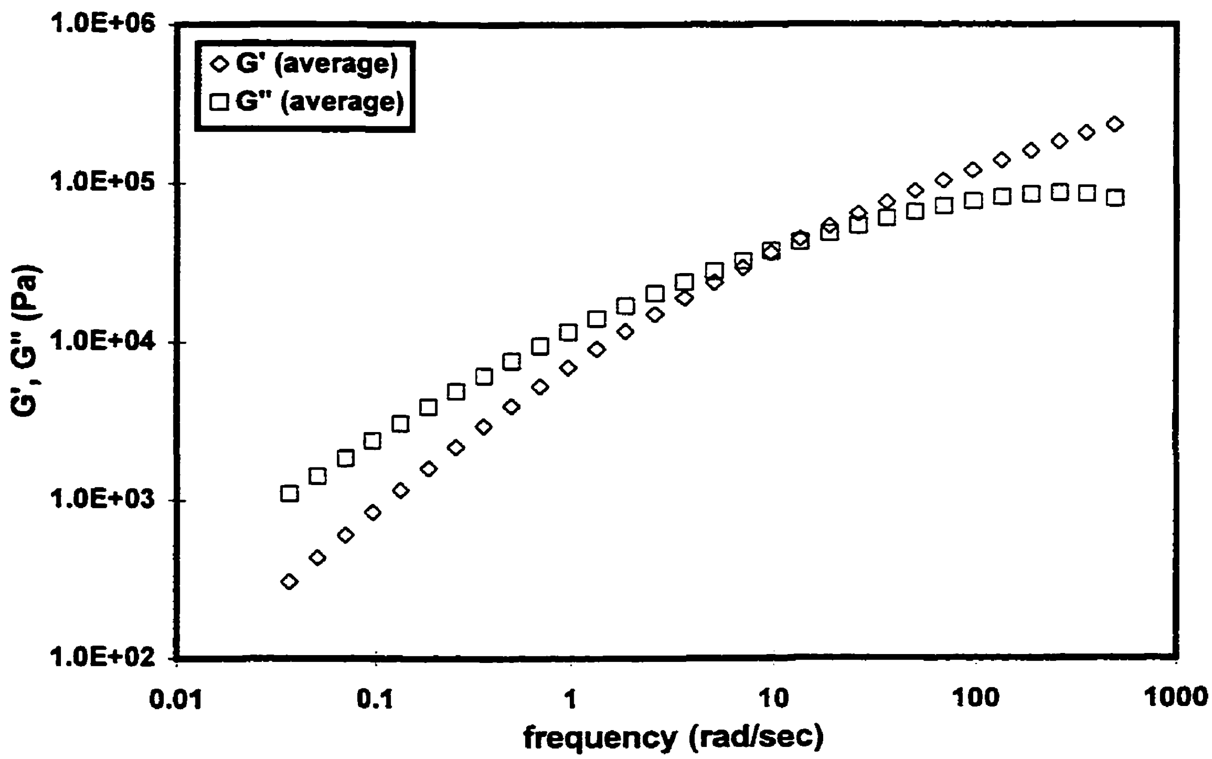

Figure 4-7 Dynamic Moduli of the HDPE at 200°C.

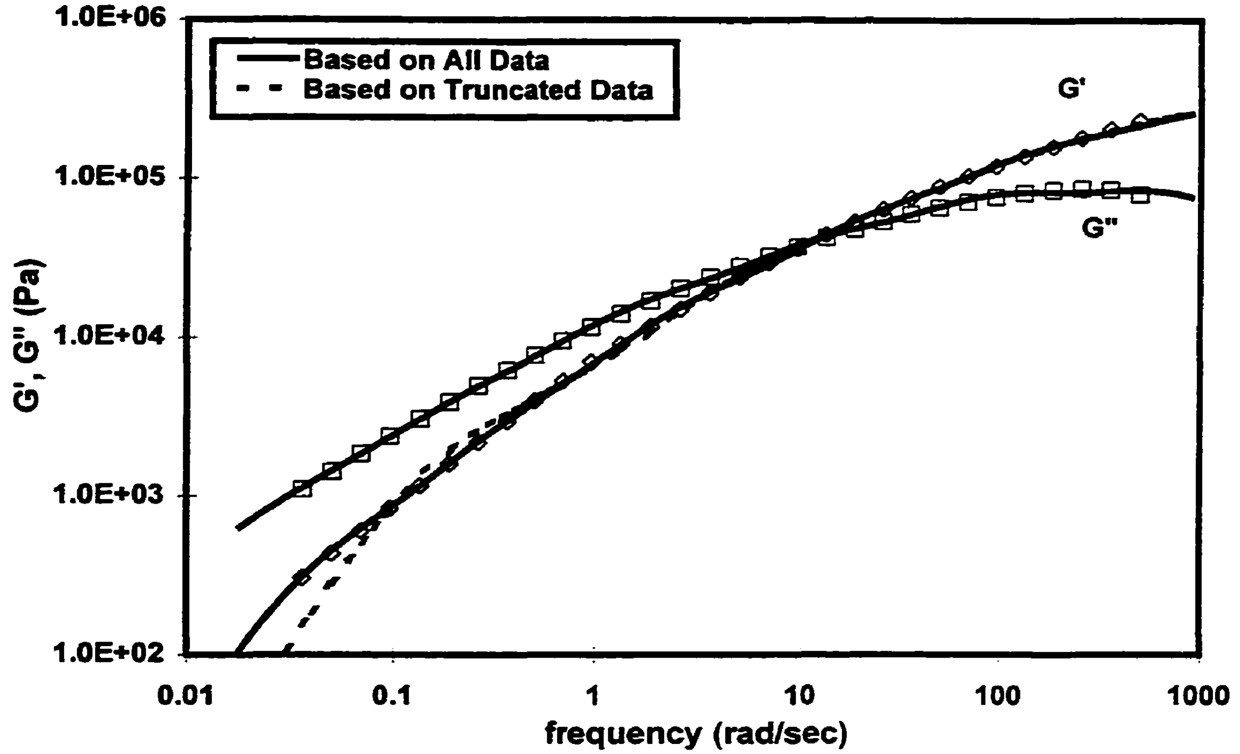

Figure 4-8 Fits of the Discrete Spectra for the HDPE at 200°C.

Table 4-4 Discrete Relaxation Spectra for the HDPE at 200°C

	All Data		Truncated Data	
Mode	***G* (Pa)**	**λ (s)**	***G* (Pa)**	**λ (s)**
1	1.31×10^5	1.43×10^{-3}	1.23×10^5	2.00×10^{-3}
2	1.09×10^5	1.00×10^{-2}	9.29×10^4	1.00×10^{-2}
3	4.81×10^4	7.00×10^{-2}	4.21×10^4	5.00×10^{-2}
4	1.66×10^4	4.90×10^{-1}	2.51×10^4	2.50×10^{-1}
5	3.08×10^3	3.43×10^0	3.54×10^3	1.25×10^0
6	5.98×10^2	24.0×10^0	2.95×10^3	6.25×10^0

4.4.2 Viscosity and First Normal Stress Difference

The viscosity of the HDPE was measured using the sliding plate rheometer at 200°C. Our results were compared with data obtained at DSM using capillary and cone and plate rheometers at 190°C and shifted to 200°C using an activation energy E_a of 27.6 kJ/mol which was determined by DSM. Good agreement was found between the three sets of data (Fig. 4-9). In Fig. 4-10, the viscosity is plotted along with the complex viscosity. The cone and plate data do not follow the same trend as the measurements in small amplitude oscillatory flow, which is incorrect since both the complex viscosity and the viscosity should reach the same plateau-value, η_0. If we disregard the cone and plate data, since it is not possible to evaluate the error involved in these measurements, we conclude that the empirical Cox-Merz rule is valid for this material.

The first normal stress difference was also measured using the cone and plate rheometer at 190°C. We present these data, shifted to 200°C, in Fig. 4-11, using the same shift factor as previously. These data were not used to fit the model parameters.

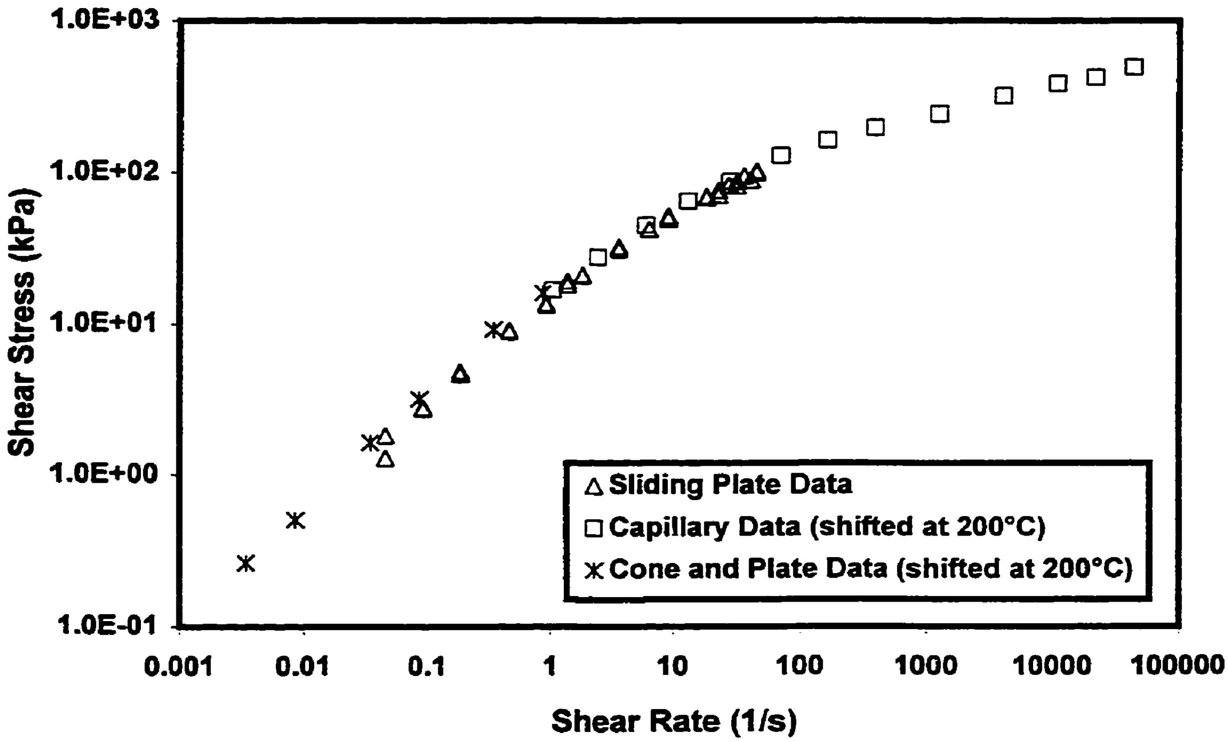

Figure 4-9 Flow Curve by Three Rheometers for the HDPE at 200°C.

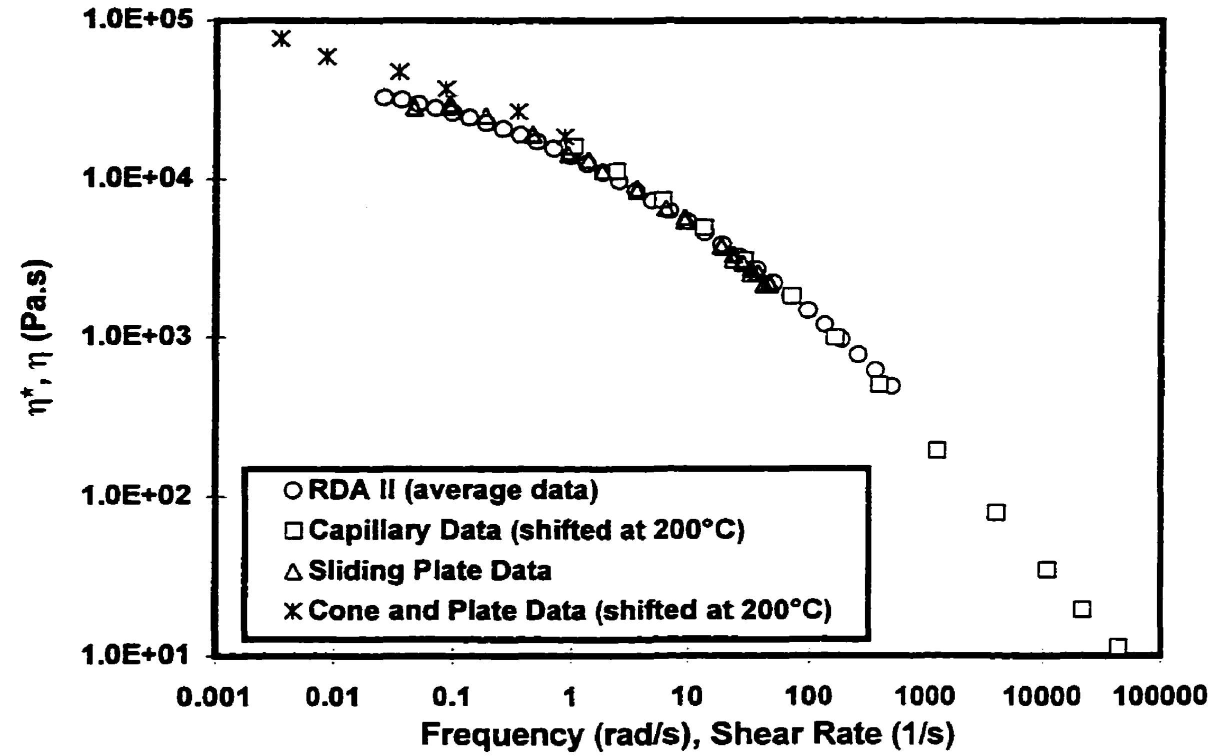

Figure 4-10 Complex Viscosity and Viscosity of the HDPE at 200°C.

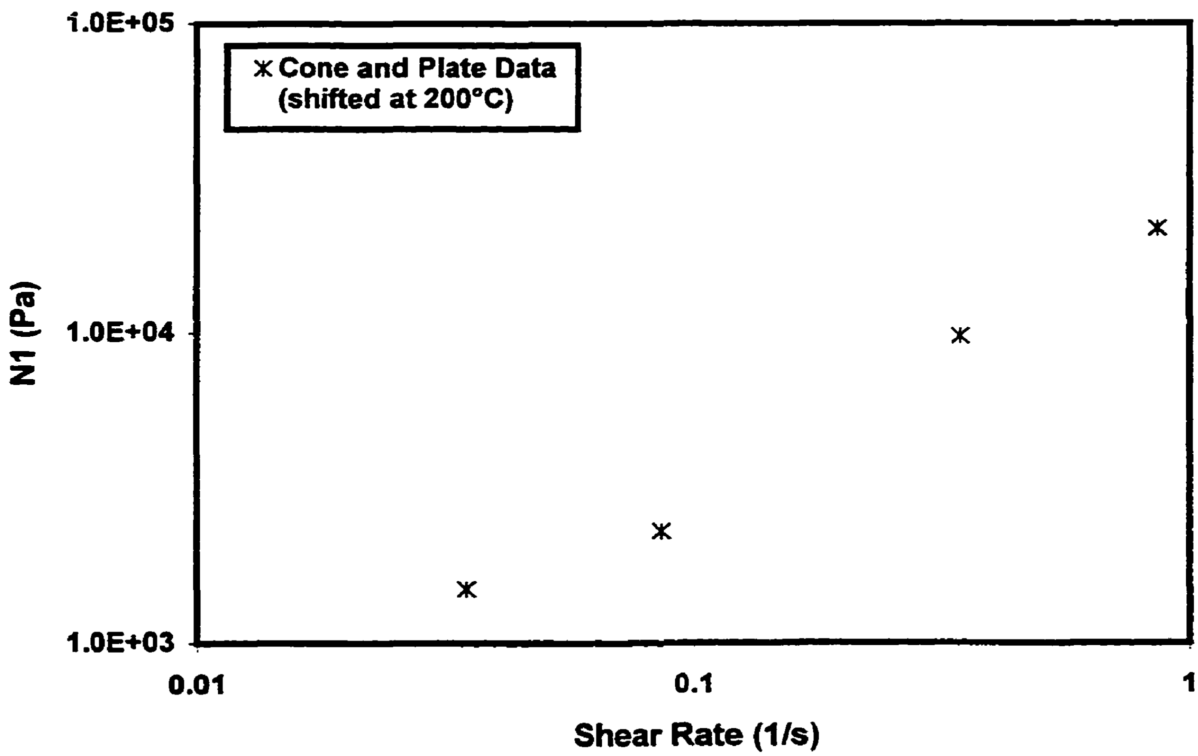

Figure 4-11 First Normal Stress Difference of the HDPE Shifted from 190° to 200°C.

4.4.3 Tensile Stress Growth Coefficient

We saw in section 4.3.3 (Fig. 4.6) that a large error is present in the stress at low extensional rates due to the low forces. On the other hand, artificial strain hardening is often observed at high rates with the RME rheometer for non-strain hardening materials[9]. For the HDPE, we chose a medium rate and had two replicates done in order to verify reproducibility. Three measurements were done at a rate of 0.5 s^{-1} at 200°C. Using particle tracking and video images of three zones, it was possible to obtain an accurate value of the strain rate. The true strain rates were 0.4845, 0.4959 and 0.4946 s^{-1}. (The HDPE melt density at test temperature is 0.742g/cm^3). Excellent agreement was found between the three sets of data (Fig. 4.12). The error bars are smaller than the size of the symbols.

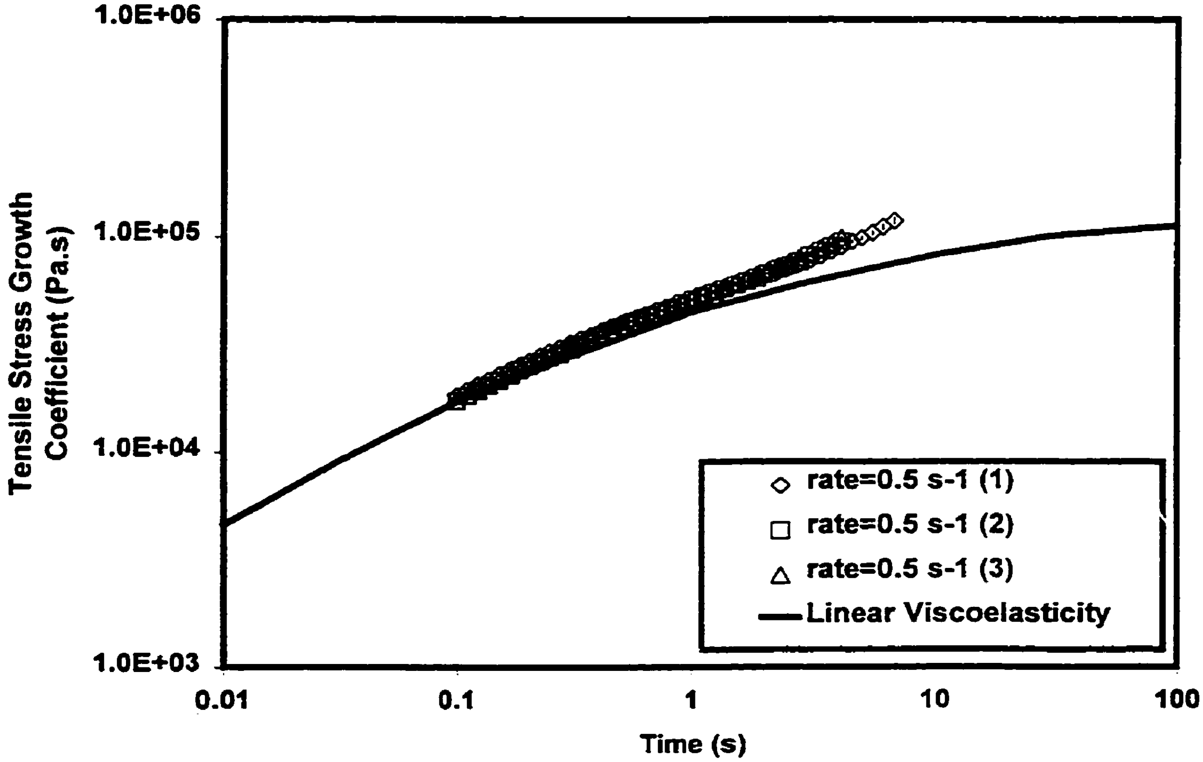

Figure 4-12 Transient Elongational Stress for the HDPE at 200°C.

REFERENCES

[1] Sentmanat M.L., Dealy J.M., "Some Factors Affecting Capillary Rheometer Performance", *ANTEC '95, Society of Plastic Engineers*, p. 1068-1072 (1995)
[2] Kim S.O., unpublished work, McGill University, Montreal, Canada (1999)
[3] Giacomin A.J., Samurkas T., Dealy J.M., " A Novel Sliding Plate Rheometer for Molten Plastics ", *Polym. Eng. Sci.*, 29(8), p. 499 (1989)
[4] Meissner, J., Hostettler J., " A New Elongational Rheometer for Polymer Melts and Other Highly Viscoelastic Liquids ", *Rheol. Acta,* 33, p. 1-21 (1994)
[5] Heuzey M.C., " The Occurrence of Flow Marks during Injection Molding of Linear Polyethylene ", Master's Thesis, McGill University, Montreal, Canada (1996)
[6] Orbey N., Dealy J.M., " Determination of the Relaxation Spectrum from Oscillatory Shear Data ", *J. Rheol.,* 35(6), p. 1035-1049 (1991)
[7] Koran F., "The effect of Pressure on the Rheology and Wall Slip of Polymer Melts", Ph.D. Thesis, McGill University, Montreal, Canada (1998)
[8] Wood-Adams P., "The Effect of Long Chain Branching on the Rheological Behavior of Polyethylenes Synthesized using Single Site Catalysts", Ph.D. Thesis, McGill University, Montreal, Canada (1998)
[9] Hepperle, J., Saito T., unpublished work, Institute of Polymer Materials, University of Erlangen-Nuremberg, Erlangen, Germany (1998)

5. Determination of Model Parameters

5.1 Linear Low-Density Polyethylene

5.1.1 Viscous Model

The Carreau-Yasuda generalized Newtonian model (Eqn. 5-1) contains four parameters: the zero-shear viscosity η_0, a characteristic time λ, and two power-law indexes, *m* and *s*.

Eqn. 5-1
$$\eta(II_D) = \eta_0\left(1 + (2\lambda^2 II_D)^{s/2}\right)^{\frac{m-1}{s}}$$

The zero-shear viscosity was calculated from the discrete spectrum based on all the data presented in Table 4-3, as follows:

Eqn. 5-2
$$\eta_0 = \sum_{i=1}^{N} G_i \lambda_i = 19079\ Pa.s$$

The other three parameters were determined by a least-squares procedure, using *M* sets of data:

Eqn. 5-3
$$MIN \sum_{j=1}^{M} \left(\frac{\eta_{meas_j} - \eta_{calc_j}}{\eta_{meas_j}} \right)^2$$

where η_{meas} represents the experimental viscosity, and η_{calc} the viscosity calculated using Eqn. 5-1. The parameters determined for the LLDPE are presented in Table 5-1, and the corresponding fit of the viscosity is shown in Fig. 5-1.

Table 5-1 Carreau-Yasuda Model Parameters for the LLDPE at 150°C

Parameter	Value
η_0 [Pa.s]	19079
λ [s]	0.39
m	0.41
s	0.76

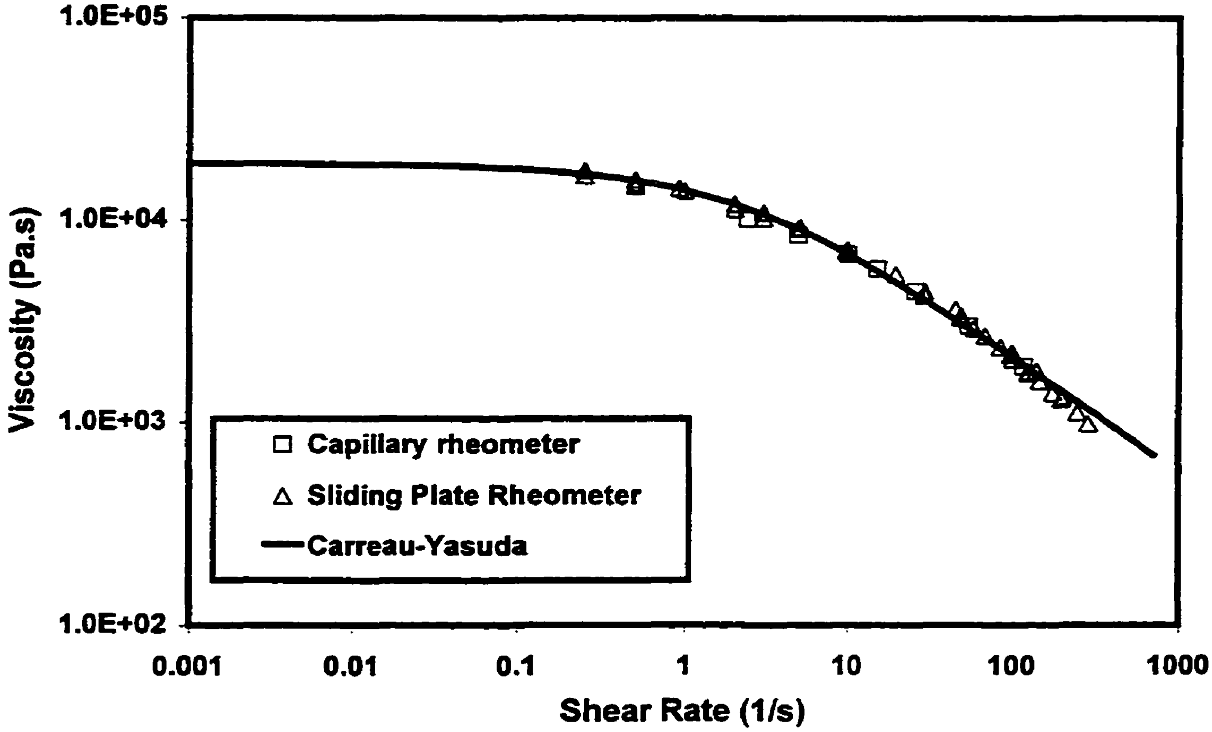

Figure 5-1 Viscosity Fit of Carreau-Yasuda Equation for the LLDPE at 150°C.

5.1.2 Leonov Model Parameters

Specification of both $b(I_1,I_2)$ in the evolution equation (Eqn. 5-4) and the elastic potential (Eqn. 5-5) are required in order to use the modified Leonov model[1], which we write as follows:

Eqn. 5-4

$$2\lambda \overset{\nabla}{B}_{ij} + b(I_1,I_2)\left[B_{ik}B_{kj} + B_{ij}\frac{(I_2 - I_1)}{3} - \delta_{ij}\right] = 0$$

Eqn. 5-5

$$W(I_1,I_2) = \frac{3G}{2(n+1)}\left\{(1-\beta)\left[\left(\frac{I_1}{3}\right)^{n+1} - 1\right] + \beta\left[\left(\frac{I_2}{3}\right)^{n+1} - 1\right]\right\}$$

For polyethylene, Simhambhatla and Leonov[1] suggested using a Neo-Hookean elastic potential ($n=\beta=0$ in Eqn. 5-5). The procedure recommended by the authors[1] for the choice of $b(I_1,I_2)$ is as follows. First, perform preliminary calculations for various flows using the simple model (b=1). Then, if there is disagreement with experimental data, a functional form of b that brings the calculations into qualitative agreement with the data can be systematically developed. To model the viscoelastic behavior of various polymers (LDPE, HDPE, PS, and PIB), simple power-law or exponential functions of the invariants of the Finger tensor with one or two adjustable parameters are usually sufficient.

We found that the best result for non-strain hardening materials was obtained with an exponential function of I_1, the first invariant of the Finger tensor:

Eqn. 5-6

$$b(I_1) = \exp\left[m\left(\frac{I_1}{3} - 1\right)\right]$$

To fit the m parameter, we used the transient elongational data, since this form of the b function has very little influence on the prediction of viscosity. The best value of the parameter was determined using an IMSL/Fortran™ subroutine (DUVMIF)[2]. This routine is based on a quadratic interpolation method to find the least value of a function specified by the user. The value obtained was m=0.02. The complete set of parameters is presented in Table 5-2.

Table 5-2 Leonov Model Parameters for the LLDPE at 150°C

Parameter	Value
n	0
β	0
m	0.02

5.1.3 Phan-Thien/Tanner Model Parameters

The PTT model[3,4] can be expressed as follows for polymer melts.

Eqn. 5-7
$$\lambda\left(\frac{\xi}{2}\overset{\nabla}{\underline{\underline{\tau}}}+\left(1-\frac{\xi}{2}\right)\overset{\Delta}{\underline{\underline{\tau}}}\right)+\underline{\underline{\tau}}\exp\left(\frac{\lambda\varepsilon}{\eta}tr\underline{\underline{\tau}}\right)=2\eta\underline{\underline{D}}$$

It has two nonlinear parameters (ξ and ε) to be determined in addition to the discrete spectrum. The parameter ξ controls the level of shear thinning in shear flows and ε the extensional behavior. We used the IMSL/Fortran™ subroutine described earlier to determine the parameters. The value of ξ was determined by fitting the viscosity curve and that of ε by fitting the transient elongational data. The resulting parameters are presented in Table 5-3.

Table 5-3 PTT Model Parameters for the LLDPE at 150°C

Parameter	Value
ξ	1.79
ε	0.16

5.1.4 Viscosity

We already mentioned that the simple and modified Leonov models do not differ in their shear predictions if Eqn. 5-6 is used, so we show only the results for the modified model. In Fig. 5-2, we show the fit of the Leonov and PTT models for the viscosity. With one parameter fitted exclusively to shear data (ξ), the PTT model reproduces more realistically the observed behavior. The Leonov model predicts the Cox-Merz rule, which is not valid for this material at high shear rates (Chapter 4).

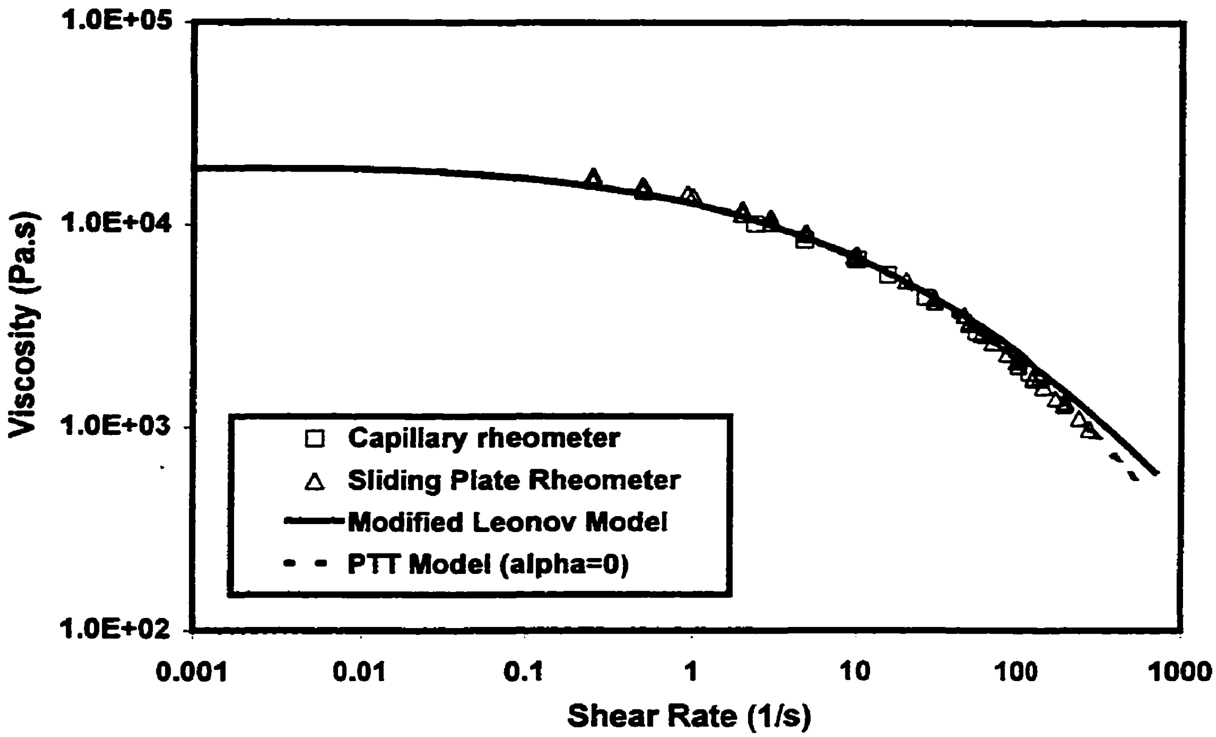

Figure 5-2 Fit of Viscosity with Leonov and PTT models for the LLDPE at 150°C.

It was mentioned in Chapter 3 that one of the problems with the PTT model when $\xi \neq 2$ is the presence of a maximum in the flow curve, which is physically unrealistic[5]. Crochet et al.[6] showed that it is possible to avoid this problem by using a non-zero viscous component ($\eta_s \neq 0$). This way, the shear stress becomes a strictly increasing function of the shear rate if the viscosity ratio fulfills the following condition:

Eqn. 5-8 $$\frac{\eta_s}{\eta} \geq \frac{1}{8}$$

with

Eqn. 5-9 $$\eta_s + \eta = \eta_0$$

However, when a spectrum of relaxation times is used instead of a single mode, this condition can be relaxed. The use of a multimode spectrum for polymer melts is always strongly recommended since a single mode can not fit data properly and leads to numerical problems.

Beraudo[5] used a viscosity ratio (η_s/η_0) of 1/8 in her simulations, although she used a spectrum of relaxation times. We verified the effect of that ratio on the prediction of the viscosity for our material, and the result is presented in Fig. 5-3. We found that this criterion could not be applied blindly in simulations. Instead, we fitted an additional parameter, α, that governs the viscosity ratio based on shear data.

Eqn. 5-10

$$\alpha = \frac{\eta_s}{\eta_0}$$

We obtained $\alpha=10^{-5}$ for the LLDPE, which shows that the condition given by Eqn. 5-8 can be ignored when using a spectrum of relaxation times. Fig. 5-4 shows the flow curve with $\alpha=0$, and we can see that there is no maximum in the curve over the range of experimental data, even without a viscous contribution.

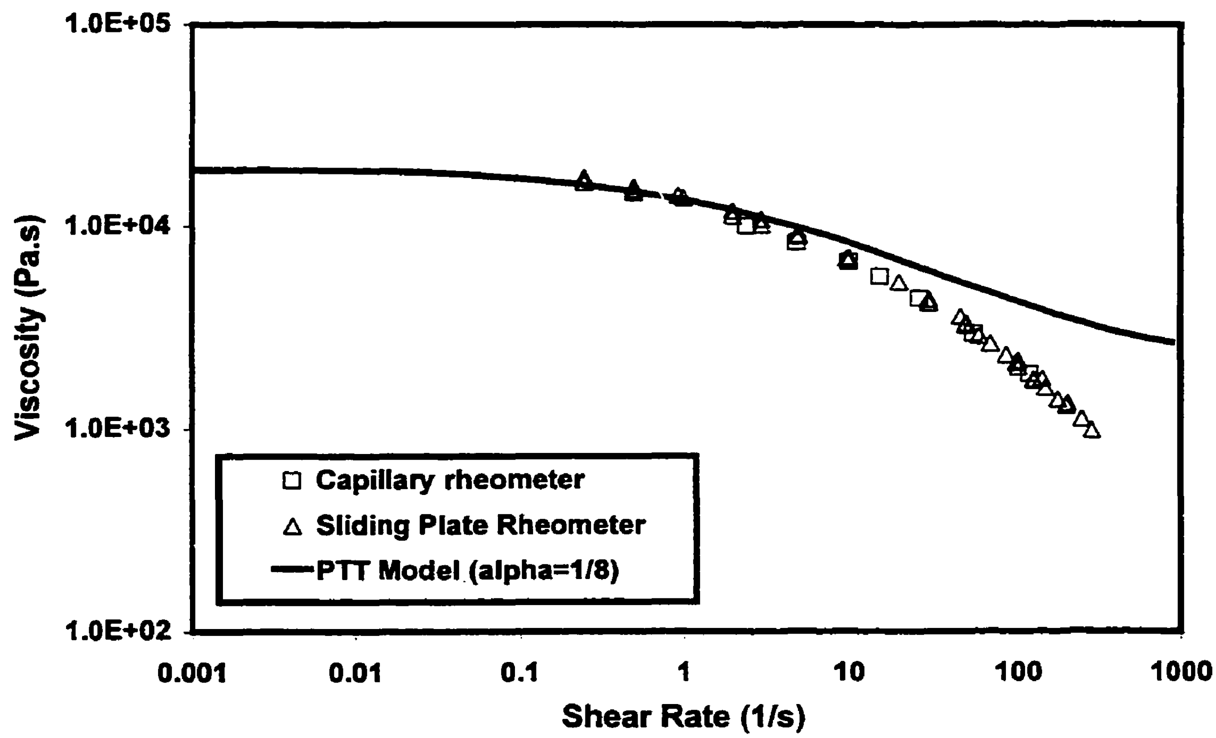

Figure 5-3 Viscosity Curve of PTT Model with α=1/8 for the LLDPE at 150°C.

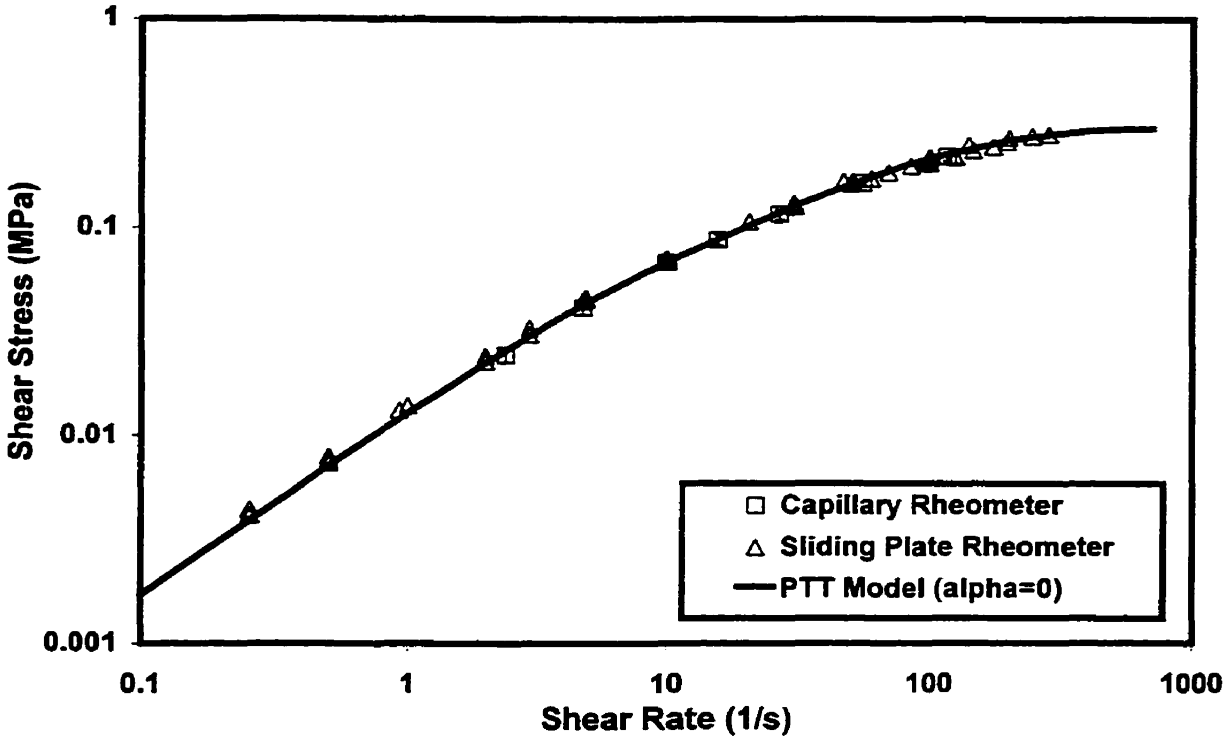

Figure 5-4 Flow Curve Predicted by the PTT Model with α=0.

5.1.5 Tensile Stress Growth Coefficient

In Fig. 5-5, we show the fit of the tensile stress growth coefficient provided by the Leonov and PTT models. The resulting curves are very similar for the two models. Good agreement is obtained for the highest strain rate (1.0 s^{-1}), but at the lowest rates less strain hardening is predicted than is seen experimentally. However, considering the large error involved in the measurements at these rates, we suspect that these data are not reliable.

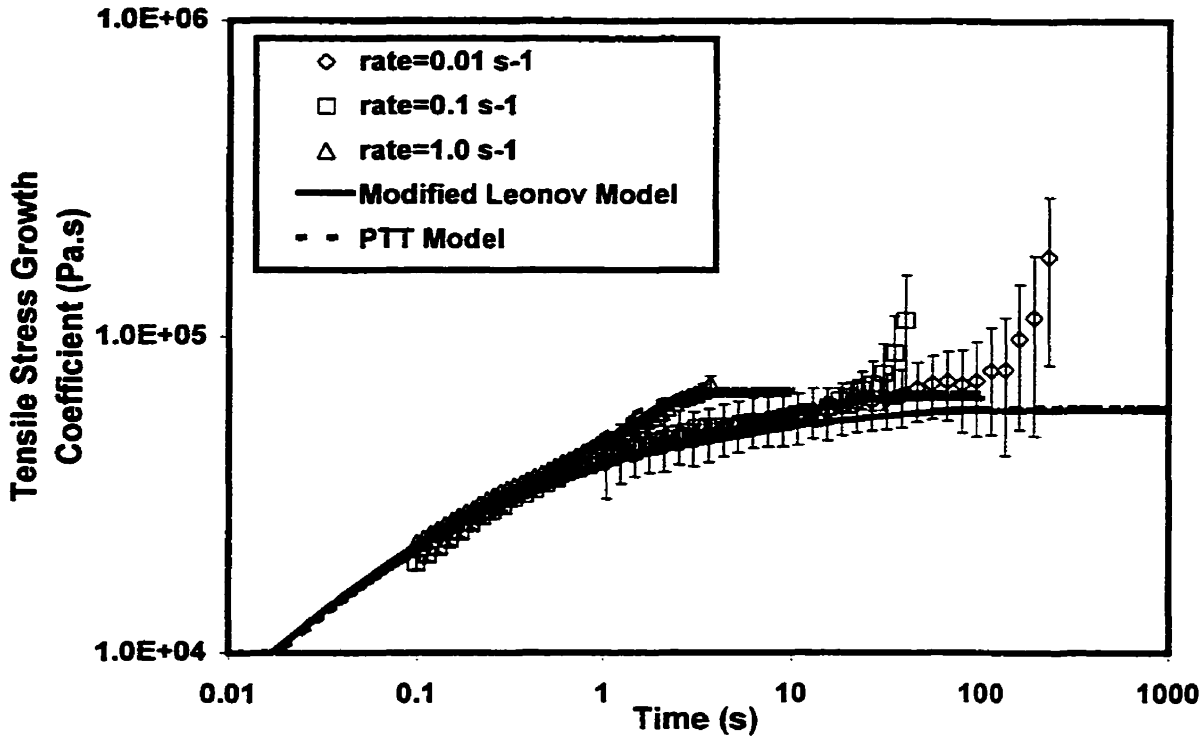

Figure 5-5 Fit of Tensile Stress Growth Coefficient for the LLDPE at 150°C.

5.1.6 Prediction of Normal Stress Differences

We had no data for the LLDPE to compare with the predicted first normal stress difference, so we used Laun's[7] empirical relation for Ψ_1:

Eqn. 5-11
$$\Psi_1(\dot{\gamma}) = 2\frac{G'}{\omega^2}\left[1+\left(\frac{G'}{G''}\right)^2\right]^{0.7}$$

This relationship was verified by Laun[7] for low and high-density polyethylenes, polypropylene and polystyrene. The comparison for N_1 is presented in Fig. 5-6 for the Leonov and PTT models. The agreement is good with both models at low and moderate shear rates, but the Leonov model follows more closely Laun's empirical relation at high shear rates.

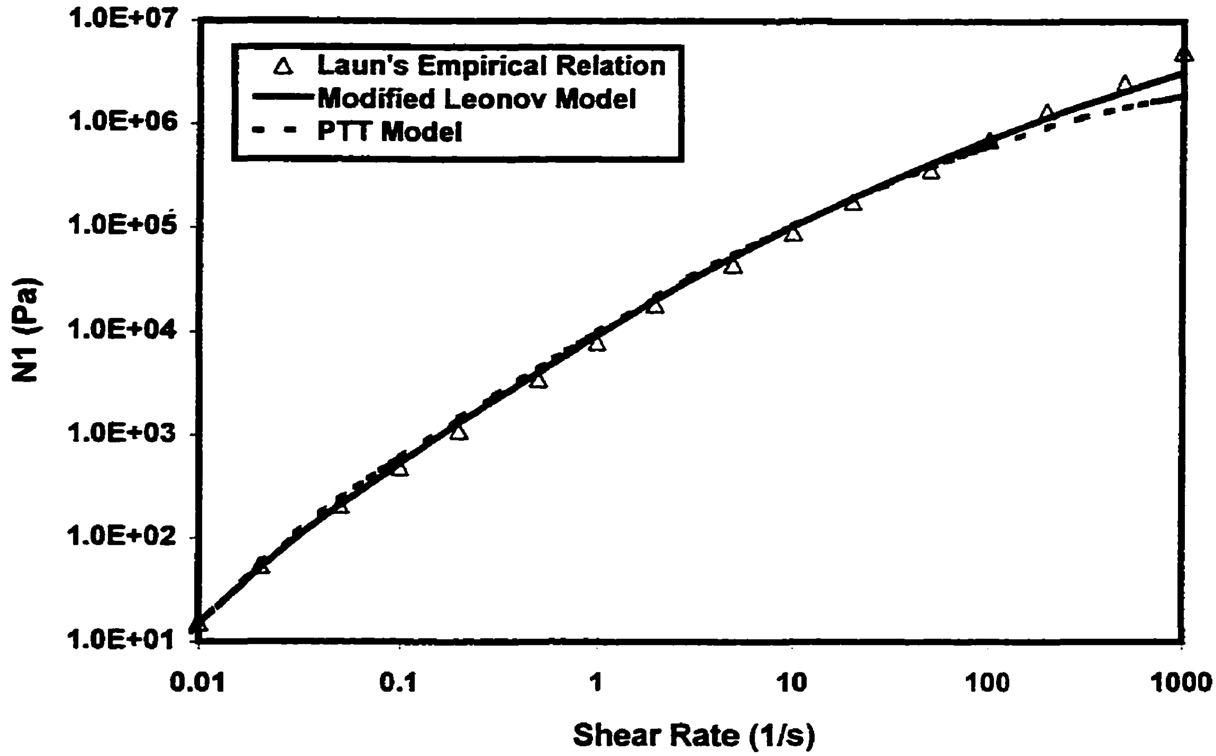

Figure 5-6 Prediction of First Normal Stress Difference for the LLDPE at 150°C.

For N_2/N_1, the ratio of the second to first normal stress difference, the Leonov model predicts a value that varies with shear rate. At low shear rates, N_2/N_1 = -0.25 and approaches zero at high shear rates (Fig. 5-7). Experimental data for steady simple shear of a number of materials indicate that N_2 is negative and has a magnitude about 10 to 30% that of N_1[8]. For N_2/N_1, PTT gives a constant ratio of –0.105 according to Eqn. 5-12.

Eqn. 5-12
$$\frac{N_2}{N_1} = \frac{2-\xi}{2}$$

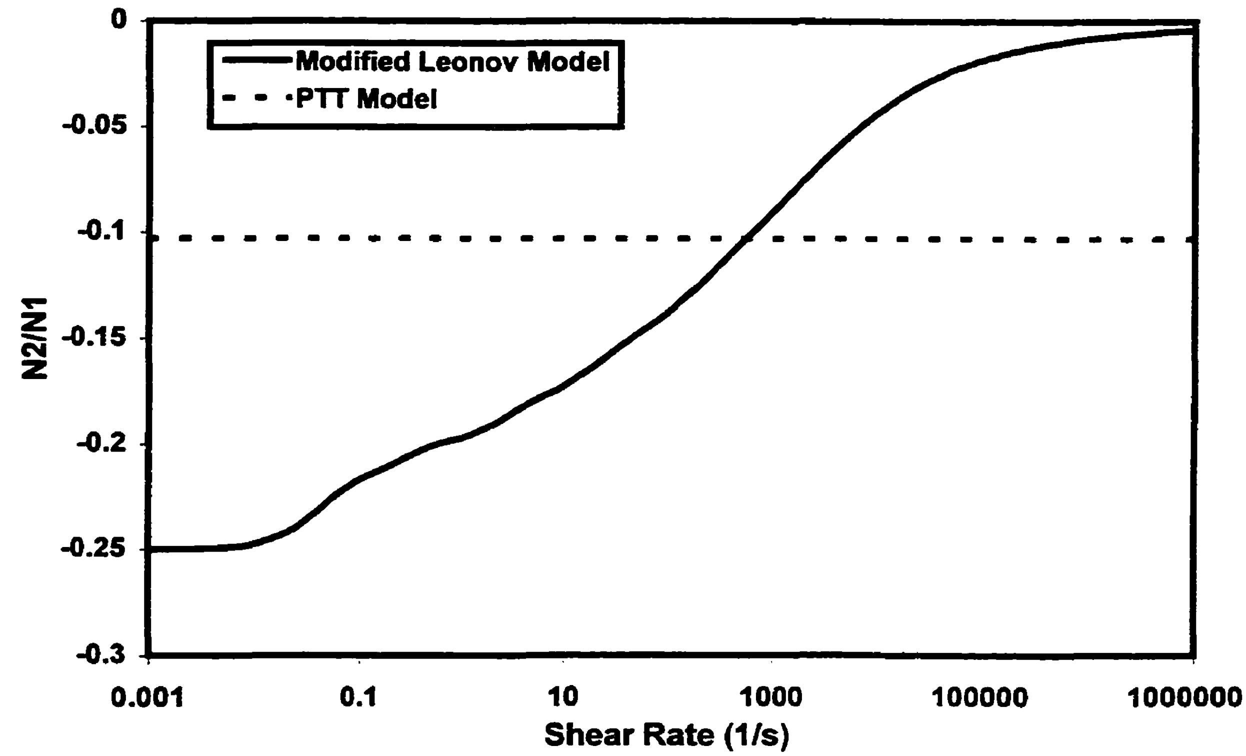

Figure 5-7 Ratio of Second to First Normal Stress Difference for the LLDPE at 150°C.

5.1.7 Prediction of Elongational Viscosity

We present in Fig. 5-8 the elongational viscosity predicted by both versions of the Leonov model and by the PTT model. The modified Leonov and PTT models both predict a maximum in the elongational viscosity curve, which is more realistic for polymer melts. We observe that both models agree over the range of strain rates where the respective parameters were fitted. However, the predictions differ considerably at higher elongational rates. The simple Leonov model predicts a plateau value of the elongational viscosity of six times the zero-shear viscosity at high strain rates. The inaccurate elongational flow behavior is the main deficiency of the simple model since linear polymers usually exhibit little strain hardening.

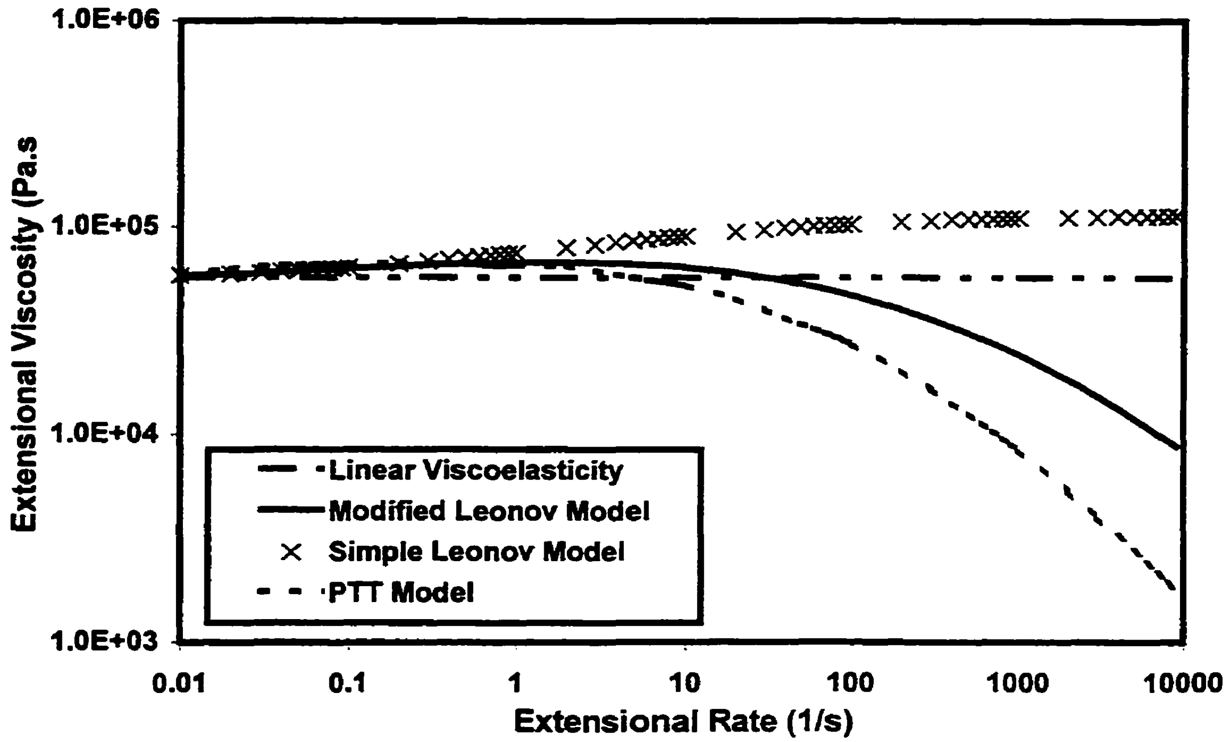

Figure 5-8 Prediction of Elongational Viscosity for the LLDPE at 150°C.

5.2 High-Density Polyethylene

5.2.1 Viscous Model

Using the procedure described in section 5.1.1, we determined the parameters for the Carreau-Yasuda equation for the HDPE. The zero-shear viscosity is calculated from the discrete spectrum based on all the data given in Table 4-4. The resulting parameters are presented in Table 5-4, and the corresponding fit of the viscosity is shown in Fig. 5-9. As discussed previously in Chapter 4, we see a disagreement with the cone and plate data.

Table 5-4 Carreau-Yasuda Model Parameters for the HDPE at 200°C

Parameter	Value
η_0 [Pa.s]	37694
λ [s]	0.48
m	0.20
s	0.45

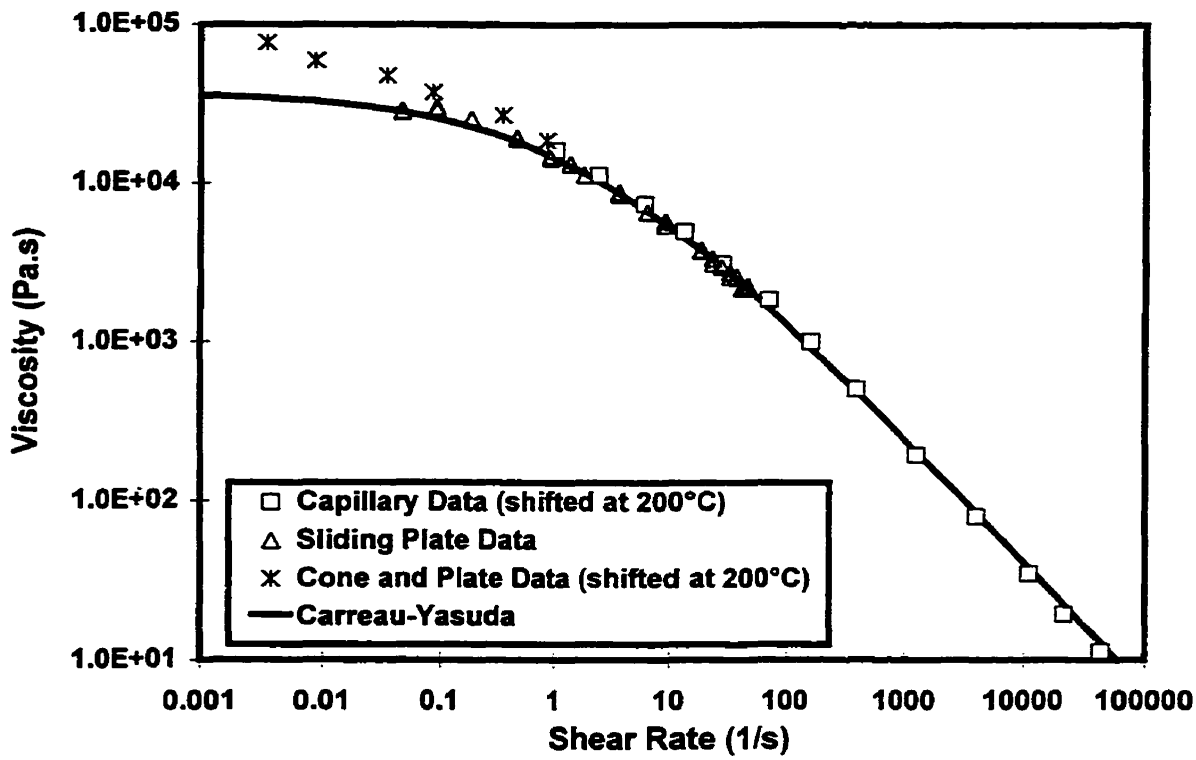

Figure 5-9 Viscosity Fit by Carreau-Yasuda Equation for the HDPE at 200°C.

5.2.2 Leonov Model Parameters

The functional form of $b(I_1,I_2)$ given by Eqn. 5-6 was used for the HDPE. The parameters m, n and β (Eqn. 5-5), determined using the IMSL/Fortran™ subroutine, are shown in Table 5-5.

Table 5-5 Leonov Model Parameters for the HDPE at 200°C

Parameter	Value
n	0
β	0
m	0.3

5.2.3 Phan-Thien/Tanner Model Parameters

The parameters of the PTT model (Eqn. 5-7) for the HDPE are presented in Table 5-6. Again, ξ was fitted to the viscosity curve and ε to the transient elongational data.

Table 5-6 PTT Model Parameters for the HDPE at 200°C

Parameter	Value
ξ	1.82
ε	0.32

5.2.4 Viscosity

In Fig. 5-10, we show the fit of the modified Leonov and PTT models for the viscosity. We see that none of the models reproduce well the viscosity at high shear rates. However, at these high rates, flow instabilities can become important, so the reliability of these data points can be questioned. With the PTT model, we had to use a small viscous contribution to avoid a maximum in the flow curve (Fig. 5-11). We used $\alpha=3.6\text{x}10^{-4}$, which is still much smaller than the recommended value of $\eta_s/\eta_0=1/8$. In Fig. 5-12, we show what the viscosity curve looks like if $\alpha=1/8$ is used. This emphasizes that one should be careful in using the rule suggested by Crochet et al.[6] (Eqn. 5-8) along with a spectrum of relaxation times.

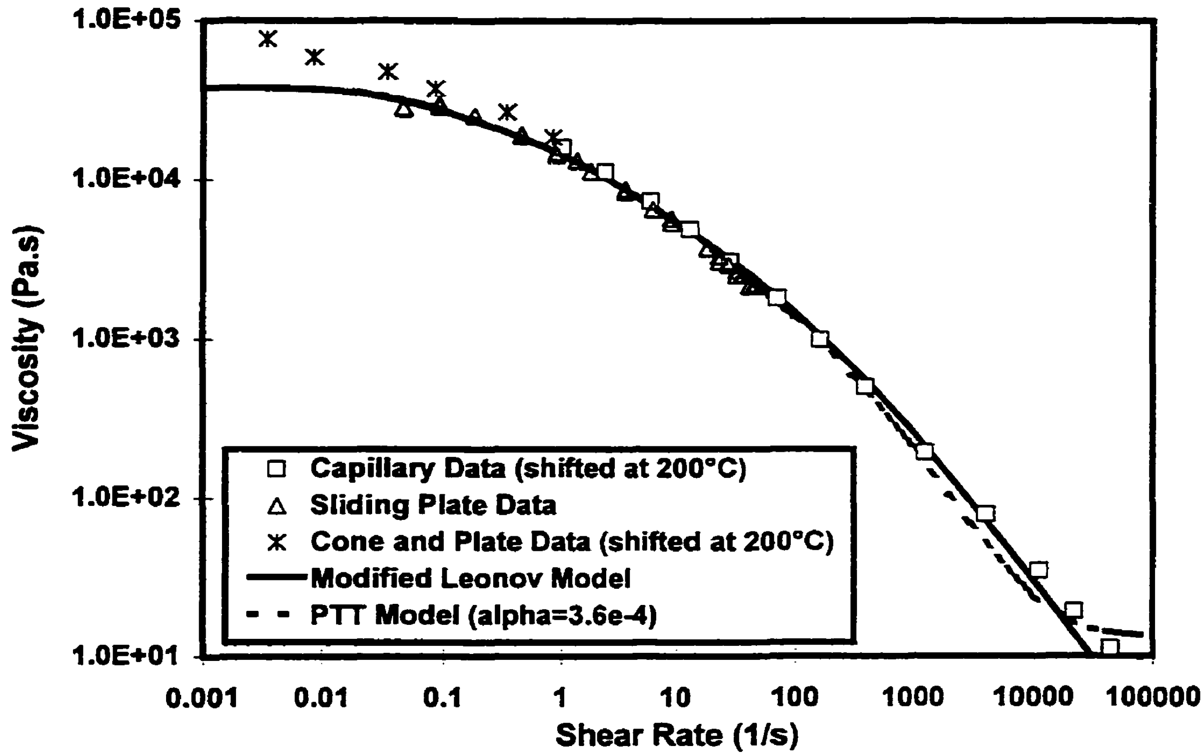

Figure 5-10 Fit of Viscosity by Leonov and PTT Models for the HDPE at 200°C.

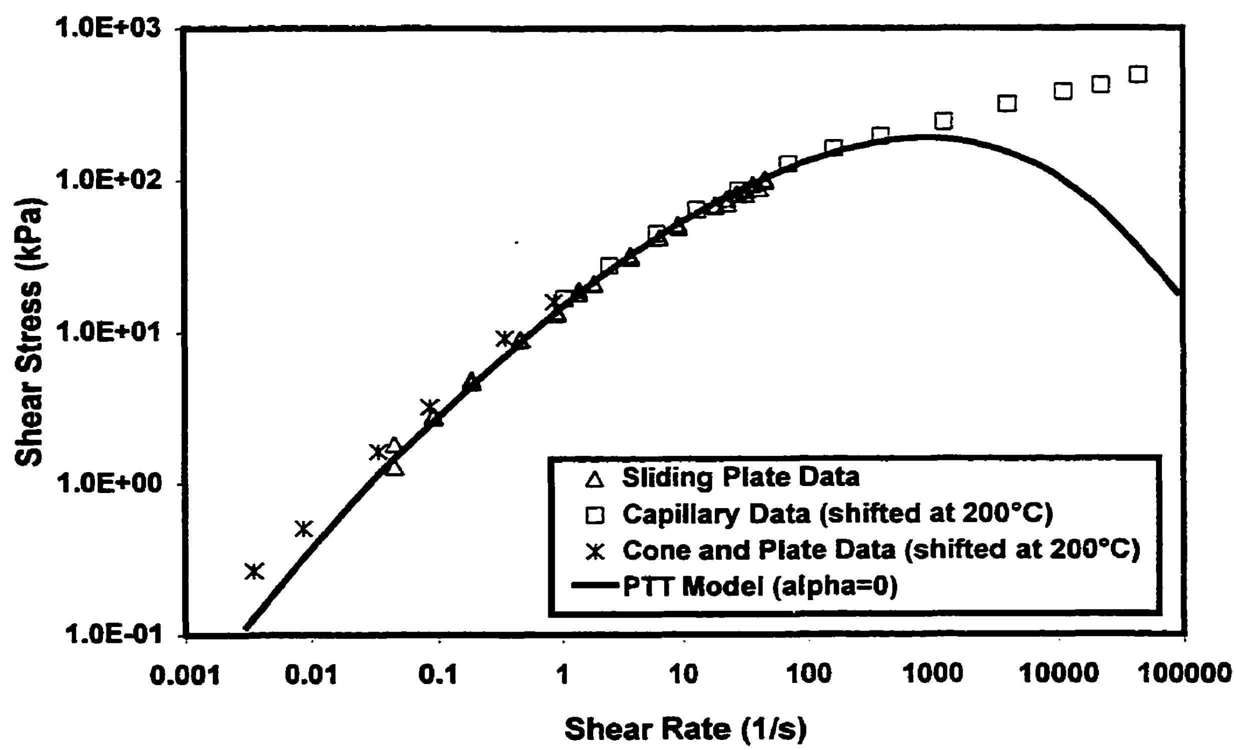

Figure 5-11 Flow Curve for the HDPE at 200°C Predicted by the PTT Model without the Viscous Contribution.

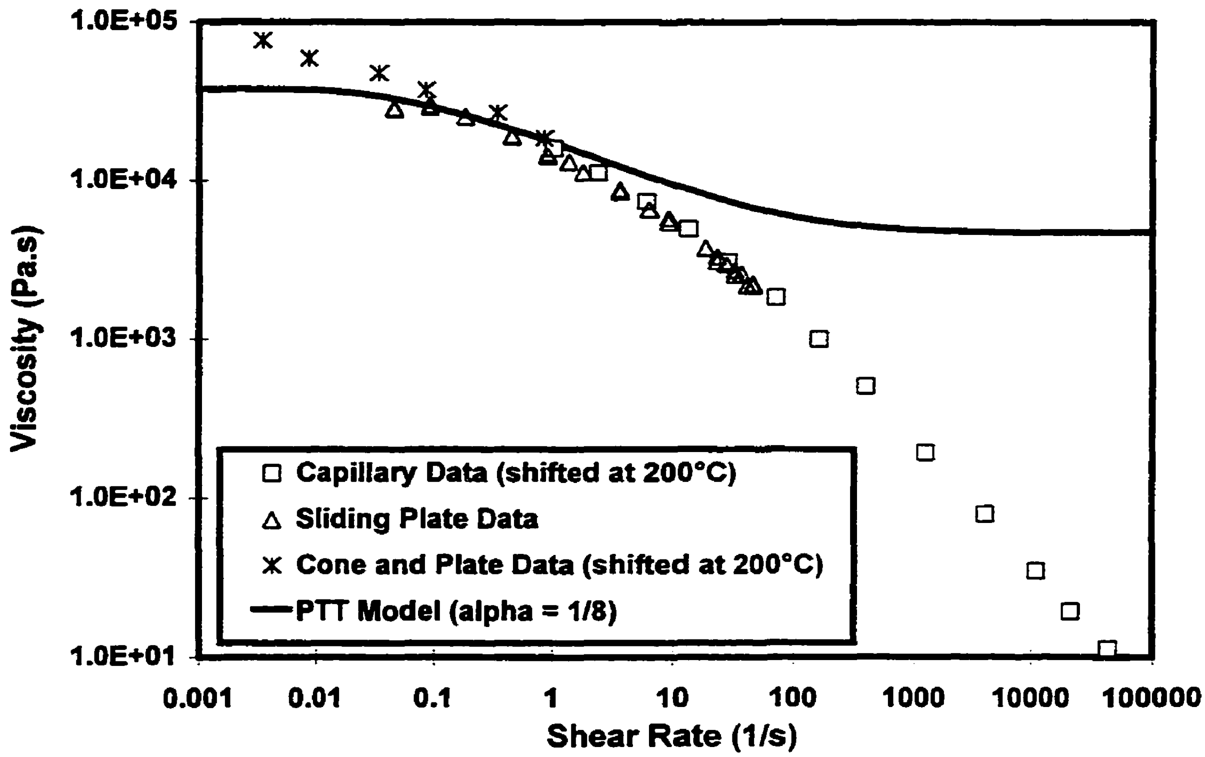

Figure 5-12 Viscosity Curve of PTT Model with α=1/8 for the HDPE at 200°C.

5.2.5 Tensile Stress Growth Coefficient

In Fig. 5-13, we show the fit of the tensile stress growth coefficient. Both models give equally good fits, except for data at rate 1, which shows a higher level than the predicted steady state.

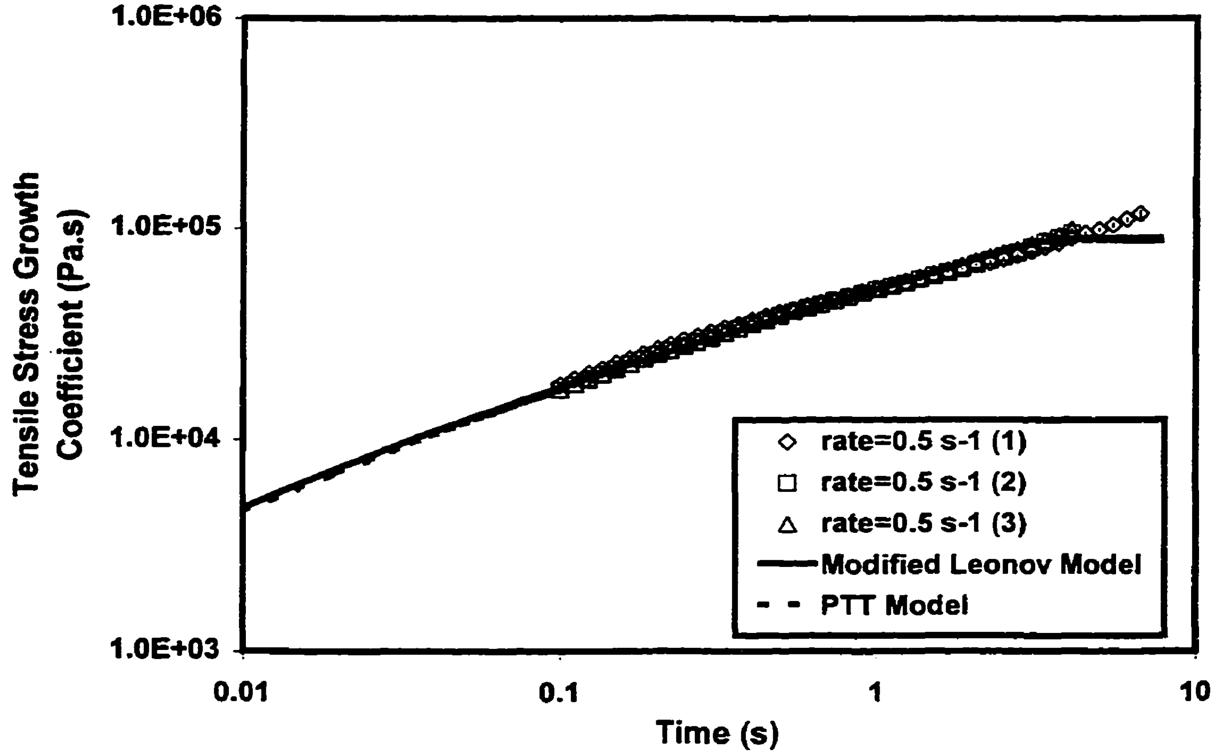

Figure 5-13 Fit of Tensile Stress Growth Coefficient for the HDPE at 200°C.

5.2.6 Prediction of Normal Stress Differences

We had only a few cone and plate data for the first normal stress difference, so we again used Laun's empirical relation to verify the predictions. The comparison for N_1 is presented in Fig. 5-14. The agreement is good with both models at low and moderate shear rates, and again for this material, the Leonov model is closer to Laun's empirical relation at high shear rates. The cone and plate data are in fair agreement with the predictions, except at the lowest shear rate. This is similar to what is seen in the viscosity curve.

For the ratio of the second to first normal stress difference, the Leonov model predicts N_2/N_1 = -0.25 at low values of the shear rate. This ratio decreases toward zero with increasing shear rate (Fig. 5-15). The PTT model gives a constant ratio of –0.09.

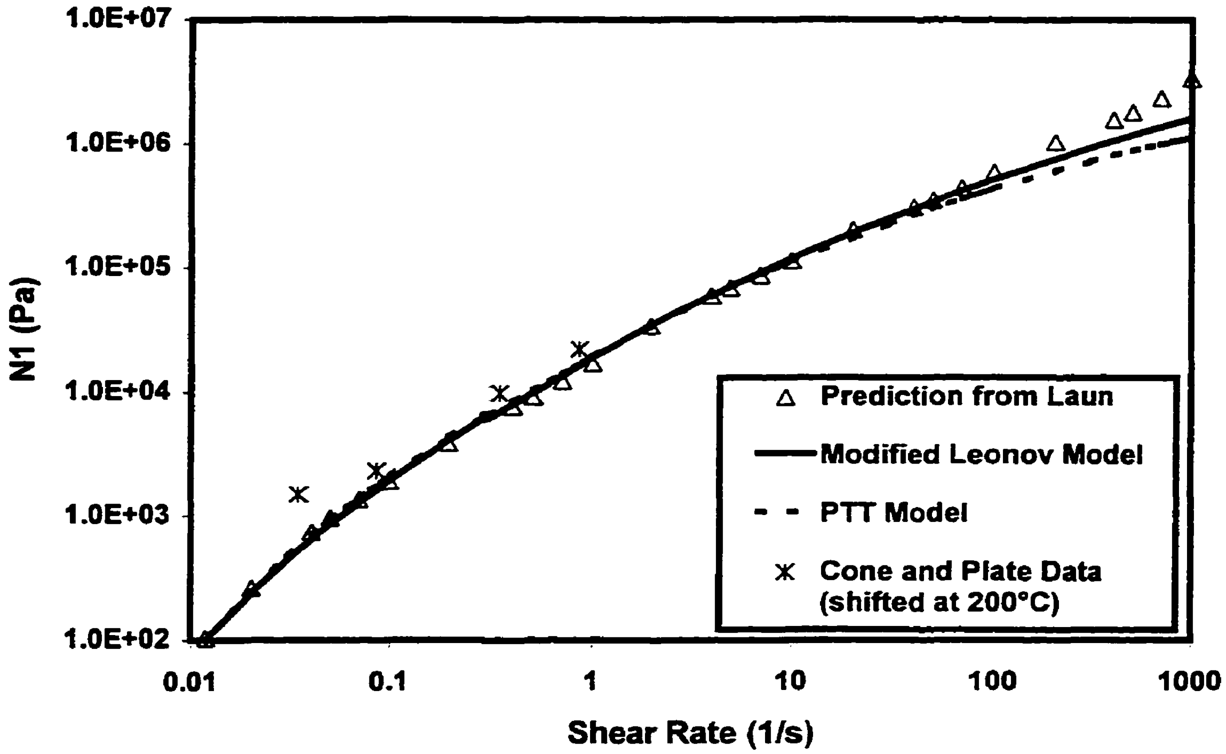

Figure 5-14 Prediction of First Normal Stress Difference for the HDPE at 200°C.

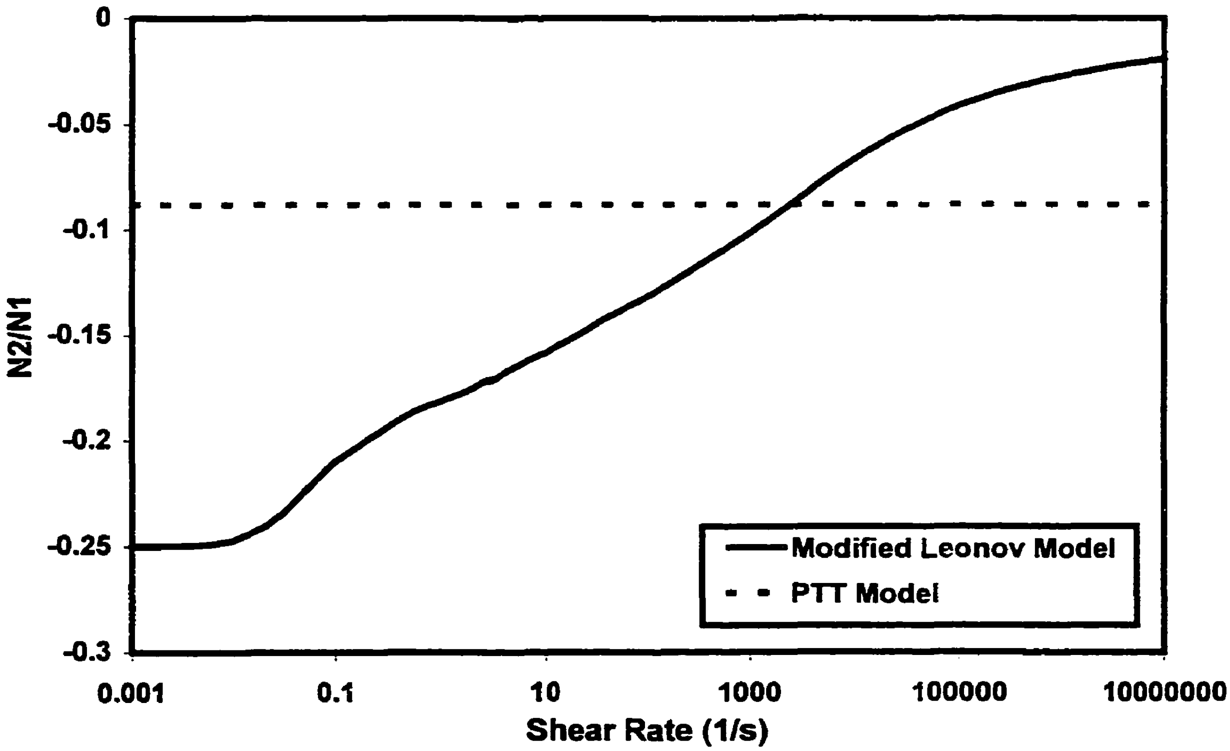

Figure 5-15 Ratio of Second to First Normal Stress Difference for the HDPE at 200°C.

5.2.7 Prediction of Elongational Viscosity

We present in Fig. 5-16 the elongational viscosity predicted by both versions of the Leonov model and by the PTT model. Again, the modified Leonov and PTT models predict a maximum in the elongational viscosity curve. We see that both models agree over a range around the strain rate at which the parameters were fitted (0.5 s^{-1}) and at higher rates. The simple Leonov model always predicts a plateau value of the elongational viscosity that is six times the zero-shear viscosity at high strain rates.

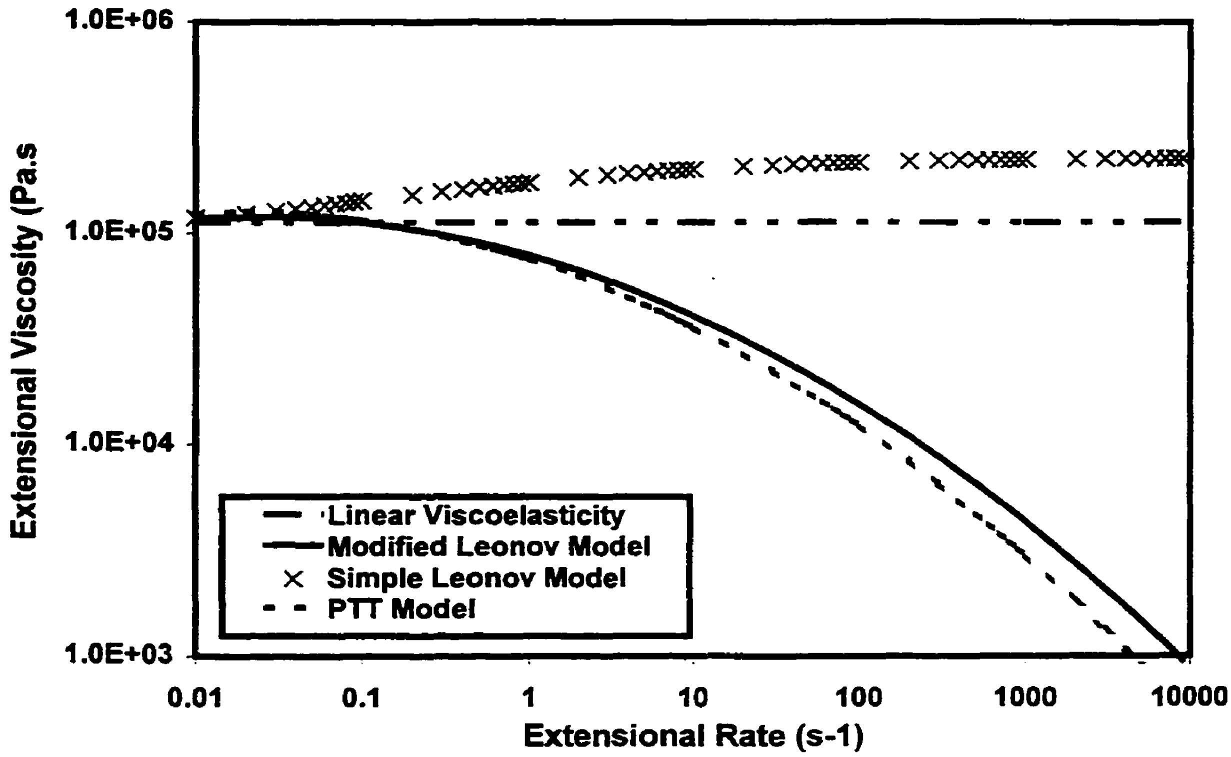

Figure 5-16 Prediction of Elongational Viscosity for the HDPE at 200°C.

In conclusion, we can say that both viscoelastic models give similar fits and predictions of the rheological properties. Also, our results showed that for the PTT model the addition of a viscous contribution to avoid the maximum in the flow curve should be done with caution.

REFERENCES

[1] Simhambhatla M., Leonov A.I., "On the Rheological Modeling of Viscoelastic Polymer Liquids with Stable Constitutive Equations", *Rheol. Acta*, 34, p. 259-273 (1995)
[2] IMSL Math/Library, Version 2.0, p. 972 (1991)
[3] Phan Thien N., Tanner R.I., "A New Constitutive Equation Derived from Network Theory", *J. Non-Newt. Fl. Mech.*, 2, p. 353-365 (1977)
[4] Phan Thien N., "A Nonlinear Network Viscoelastic Model", *J. Rheol.*, 22, p. 259-283 (1978)
[5] Beraudo C., "Méthodes éléments finis pour la simulation numérique d'écoulements de fluides viscoelastiques de type différentiel dans des géométries convergentes", Ph.D. thesis, École Nationale Supérieure des Mines de Paris, Sophia Antipolis, France (1995)
[6] Crochet M.J., Davies A.R., Walters K., "Numerical Simulation of Non-Newtonian Flows", *Ed. Elsevier*, Amsterdam (1984)
[7] Laun H.M., *Rheol. Acta*, 30, p. 459 (1986)
[8] Dealy J.M., Wissbrun K.F., "Melt Rheology and its Role in Plastics Processing", *Van Nostrand Reinhold*, New York (1990)

6. Numerical Method

6.1 Description of the Problem

6.1.1 Four-Field Mixed Formulation

In Chapter 2, we presented the system of equations that must be solved to simulate the flow of viscoelastic materials. We recall here that for isothermal flows, neglecting compressibility and body forces, the conservation equations for mass and momentum can be written as follows:

Eqn. 6-1 $$\nabla \cdot \underline{u} = 0$$

Eqn. 6-2 $$\rho \frac{D\underline{u}}{Dt} + \nabla p - \nabla \cdot \underline{\underline{\tau}} = 0$$

where ρ denotes a constant density, p is the pressure, and $\underline{\underline{\tau}}$ is the extra stress tensor. For a Newtonian fluid and neglecting inertia forces, this set of equations constitutes the " Stokes problem ". In the absence of a viscous contribution, and for a multimode representation, the extra stress tensor is expressed as follows:

Eqn. 6-3 $$\underline{\underline{\tau}} = \sum_{i=1}^{N} \underline{\underline{\tau_i}}$$

where N represents the number of modes.

The last equation required to close the above system is the rheological model, which in our work is the Leonov or the Phan-Thien/Tanner model:

Eqn. 6-4 $$\lambda \underline{\underline{A}}\left(\underline{\underline{\tau_i}}\right) + \underline{\underline{B}}\left(\underline{\underline{\tau_i}}\right) = 2\eta_i \underline{\underline{D}}(\underline{u})$$

where $\eta_i = \lambda_i G_i$.

For the Leonov model:

Eqn. 6-5 $$\underline{\underline{A}}\left(\underline{\underline{\tau_i}}\right)=\lambda_i \overset{\nabla}{\underline{\underline{\tau_i}}}$$

Eqn. 6-6 $$\underline{\underline{B}}\left(\underline{\underline{\tau_i}}\right)=\frac{b}{2G_i}\left\{\underline{\underline{\tau_i}}\cdot\underline{\underline{\tau_i}}-\frac{\left(\underline{\underline{\tau_i}}+G_i\underline{\underline{\delta}}\right)}{3}\left[tr\left(\underline{\underline{\tau_i}}+G_i\underline{\underline{\delta}}\right)-G_i^2 tr\left[\left(\underline{\underline{\tau_i}}+G_i\underline{\underline{\delta}}\right)^{-1}\right]\right]\right\}$$

For the PTT model:

Eqn. 6-7 $$\underline{\underline{A}}\left(\underline{\underline{\tau_i}}\right)=\lambda_i\left(\frac{\xi}{2}\overset{\nabla}{\underline{\underline{\tau_i}}}+\left(1-\frac{\xi}{2}\right)\overset{\Delta}{\underline{\underline{\tau_i}}}\right)$$

Eqn. 6-8 $$\underline{\underline{B}}\left(\underline{\underline{\tau_i}}\right)=\underline{\underline{\tau_i}}\exp\left(\frac{\lambda_i\varepsilon}{\eta_i}tr\underline{\underline{\tau_i}}\right)$$

A modified elastic-viscous stress splitting (EVSS) method[1] is introduced to facilitate the choice of the discretization spaces. This requires the explicit introduction and discretization of a tensor variable, $\underline{\underline{d}}$, which is the gradient of the velocity $\underline{u}$:

Eqn. 6-9 $$\underline{\underline{d}}=\nabla\underline{u}$$

Thus, the rate of deformation tensor $\underline{\underline{D}}(\underline{u})$ can be expressed as:

Eqn. 6-10 $$\underline{\underline{D}}=\frac{\left(\underline{\underline{d}}+\underline{\underline{d}}^T\right)}{2}$$

The conservation equation for momentum (Eqn. 6-2) becomes:

Eqn. 6-11 $$-\nabla\cdot\left(2\alpha\underline{\underline{D}}\right)+\nabla p-\nabla\cdot\underline{\underline{\tau}}=-\nabla\cdot\left(2\alpha\left(\frac{\underline{\underline{d}}+\underline{\underline{d}}^T}{2}\right)\right)$$

The parameter α can take any value, but $\alpha=\eta_0$ has been reported to be an optimal choice[1].

6.1.2 Free Surface

In the presence of a free surface, as in extrudate swell, a pseudo-concentration method is used[2], requiring the solution of the additional equation:

Eqn. 6-12
$$\frac{\partial F}{\partial t} + \underline{u} \cdot \nabla F = 0$$

where the function F represents the pseudo-concentration that describes the interface between the polymer and another fluid, in this case air:

Eqn. 6-13
$$F = \begin{cases} 0 & \text{in air} & \text{(fluid 0)} \\ 1 & \text{in the polymer melt} & \text{(fluid 1)} \end{cases}$$

This function specifies the material properties appropriate for each region of the computational domain. For example, the relaxation time λ as a function of the pseudo-concentration is defined as follows:

Eqn. 6-14
$$\lambda(F) = \lambda_0 + (\lambda_1 - \lambda_0)F$$

Since air is not viscoelastic, $\lambda_0=0$, and Eqn. 6-14 simplifies to:

Eqn. 6-15
$$\lambda(F) = \lambda_1 F$$

All the material properties are evaluated using equations similar to Eqn. 6-14.

Preliminary calculations were done using a fictitious fluid instead of air with a viscosity equal to 10^{-3} times the polymer viscosity. Later, the viscosity of this fluid was set equal to zero, using the same value of α (Eqn. 6-11) in the entire flow domain, based on melt properties, without changing the results of the simulations.

In summary, the global system of equations to solve is shown below.

Eqn. 6-16

$$\begin{cases} \nabla \cdot \underline{u} = 0 \\ -\nabla \cdot \left(2\alpha \underline{\underline{D}}\right) + \nabla p - \nabla \cdot \underline{\underline{\tau}} = -\nabla \cdot \left(2\alpha\left(\dfrac{\underline{\underline{d}} + \underline{\underline{d}}^T}{2}\right)\right) \\ \underline{\underline{d}} = \nabla \underline{u} \\ \lambda \underline{\underline{A}}\left(\underline{\underline{\tau}}_i\right) + \underline{\underline{B}}\left(\underline{\underline{\tau}}_i\right) = 2\eta_i \underline{\underline{D}}(u) \\ \dfrac{\partial F}{\partial t} + \underline{u} \cdot \nabla F = 0 \end{cases}$$

6.1.3 Weak Formulation

In order to obtain the weak formulation corresponding to this system, each equation is multiplied by an associated weighting function and integrated over a domain Ω. After applying the divergence theorem to the Stokes problem, we have the following weighted residual problem:

Find $(u,p,\tau, d) \in V \times Q \times \Sigma \times \Sigma$ such that:

Eqn. 6-17

$$\int_\Omega q \nabla \cdot \underline{u}\, d\underline{x} = 0 \qquad \forall q \in Q$$

$$2\alpha \int_\Omega \underline{\underline{D}}(u) : \underline{\underline{D}}(v)\, d\underline{x} - \int_\Omega p \nabla \cdot \underline{v}\, d\underline{x} = -\int_\Omega (\underline{\underline{\tau}} - 2\alpha \underline{\underline{d}}) : \underline{\underline{D}}(\underline{v})\, d\underline{x} \qquad \forall \underline{v} \in V$$

$$\int_\Omega \left[\lambda \underline{\underline{A}}\left(\underline{\underline{\tau}}_i\right) + \underline{\underline{B}}\left(\underline{\underline{\tau}}_i\right)\right] : \underline{\underline{\phi}}\, d\underline{x} = 2\eta_i \int_\Omega \underline{\underline{D}}(u) : \underline{\underline{\phi}}\, d\underline{x} \qquad \forall \underline{\underline{\phi}} \in \Sigma$$

$$\int_\Omega \underline{\underline{d}} : \underline{\underline{\psi}}\, d\underline{x} = \int_\Omega \underline{\underline{D}}(u) : \underline{\underline{\psi}}\, d\underline{x} \qquad \forall \underline{\underline{\psi}} \in \Sigma$$

where q, $\underline{v}$, $\underline{\underline{\phi}}$ and $\underline{\underline{\psi}}$ are suitable weighting functions. The additional equation associated with the pseudo-concentration has the following weak formulation:

Eqn. 6-18
$$\int_{\Omega}\left(\frac{\partial F}{\partial t}+\underline{u}\cdot\nabla F\right)G\,d\underline{x}=0 \qquad \forall G\in\zeta$$

6.2 Discretization

Only triangular elements are considered in this work. In order to solve the weighted residual problem by the finite element method, we need to discretize the variables. This is a difficult task, since compatibility conditions exist in the four-field Stokes problem for the discretized variables $\underline{u}_h$, p_h, $\underline{\underline{\tau}}_h$ and $\underline{\underline{d}}_h$. Their respective discretization must therefore satisfy a generalization of Brezzi's condition[3] (the inf-sup condition) valid for the usual velocity-pressure formulation of the Stokes problem, presented in Chapter 2. The chosen discrete subspaces are V_h, Q_h, Σ_h and ζ_h and the chosen discretization is illustrated in Fig. 6-1. P_2^+ is the quadratic polynomial set defined on element K, to which a cubic "bubble" function associated with the centroid node is added, and P_1 is the discontinuous linear polynomial set defined on element K. We chose identical discretization spaces for the variables $\underline{\underline{\tau}}$ and $\underline{\underline{d}}$, but it is possible to select another discretization space for $\underline{\underline{d}}$. The discretized variable F_h is approximated by piecewise linear polynomials, as for $\underline{\underline{\tau}}_h$ and $\underline{\underline{d}}_h$.

By replacing the spaces V, Q and Σ by their respective subspaces V_h, Q_h and Σ_h in the continuous weighted residual problem (Eqn. 6-17), we obtain the following discrete weak formulation:

Find $(\underline{u}_h, p_h, \underline{\underline{\tau}}_h, \underline{\underline{d}}_h) \in V_h \times Q_h \times \Sigma_h \times \Sigma_h$ such that:

$$\int_\Omega q_h \nabla \cdot \underline{u}_h \, d\underline{x} = 0 \qquad \forall q_h \in Q_h$$

$$2\alpha \int_\Omega \underline{\underline{D}}(\underline{u}_h) : \underline{\underline{D}}(\underline{v}_h)\, d\underline{x} - \int_\Omega p_h \nabla \cdot \underline{v}_h \, d\underline{x} = -\int_\Omega (\underline{\underline{\tau}}_h - 2\alpha \underline{\underline{d}}_h) : \underline{\underline{D}}(\underline{v}_h)\, d\underline{x}$$

Eqn. 6-19 $\qquad \forall \underline{v}_h \in V_h$

$$\int_\Omega \left[\lambda \underline{\underline{A}}\left(\underline{\underline{\tau}}_{i_h}\right) + \underline{\underline{B}}\left(\underline{\underline{\tau}}_{i_h}\right)\right] : \underline{\underline{\phi}}_h \, d\underline{x} = 2\eta_i \int_\Omega \underline{\underline{D}}(\underline{u}_h) : \underline{\underline{\phi}}_h \, d\underline{x} \qquad \forall \underline{\underline{\phi}}_h \in \Sigma_h$$

$$\int_\Omega \underline{\underline{d}}_h : \underline{\underline{\psi}}_h \, d\underline{x} = \int_\Omega \underline{\underline{D}}(\underline{u}_h) : \underline{\underline{\psi}}_h \, d\underline{x} \qquad \forall \underline{\underline{\psi}}_h \in \Sigma_h$$

where q_h, $\underline{v}_h$, $\underline{\underline{\phi}}_h$ and $\underline{\underline{\psi}}_h$ are suitable discretized weighting functions. For the pseudo-concentration, we have the following additional equation:

Eqn. 6-20 $$\int_\Omega \left(\frac{\partial F_h}{\partial t} + \underline{u}_h \cdot \nabla F_h \right) G_h \, d\underline{x} = 0 \qquad \forall G_h \in \zeta_h$$

We can see that the variable $\underline{\underline{d}}_h$ is a projection of $\underline{\underline{D}}(\underline{u}_h)$ in the discrete subspace Σ_h, and as was mentioned in Chapter 2, there is no equality between $\underline{\underline{d}}_h$ and $\underline{\underline{D}}(\underline{u}_h)$ in the discrete problem.

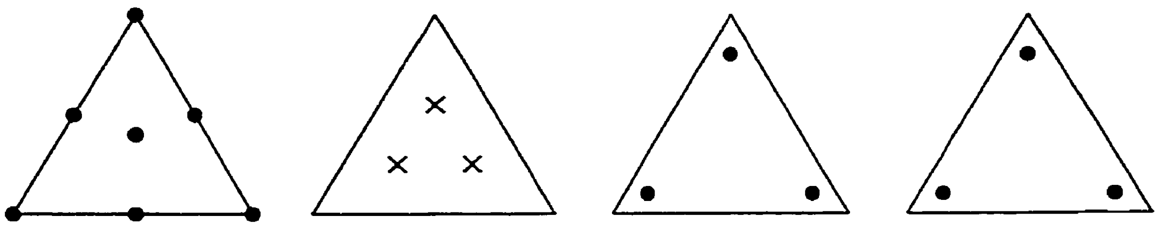

Figure 6-1 The P_2^+ - P_1 - P_1 - P_1 elements for variables $\underline{u}_h$, p_h, $\underline{\underline{\tau}}_h$ and $\underline{\underline{d}}_h$ (and F_h)[4].

We also note the similarity between the constitutive equation (Eqn. 6-4) and the pseudo-concentration equation (Eqn. 6-12). Indeed, the upper and lower convected derivatives in the constitutive equation are defined as follows:

Eqn. 6-21 $$\overset{\nabla}{\underline{\underline{\tau}}} = \frac{\partial \underline{\underline{\tau}}}{\partial t} + \underline{u} \cdot \nabla \underline{\underline{\tau}} - \nabla \underline{u} \cdot \underline{\underline{\tau}} - \underline{\underline{\tau}} \cdot (\nabla \underline{u})^T$$

Eqn. 6-22 $$\overset{\Delta}{\underline{\underline{\tau}}} = \frac{\partial \underline{\underline{\tau}}}{\partial t} + \underline{u} \cdot \nabla \underline{\underline{\tau}} + (\nabla \underline{u})^T \cdot \underline{\underline{\tau}} + \underline{\underline{\tau}} \cdot \nabla \underline{u}$$

Both the constitutive equation and the pseudo-concentration equation are suitable for the discontinuous Galerkin method, which is described in section 6.3.2.

6.3 Numerical Solution

The global system presented in Eqn. 6-19 and Eqn. 6-20 can be quite large, especially when a multimode representation of the extra stress tensor is employed. A coupled approach to solve this problem would require too much memory space, so we use instead a decoupled approach. We solve separately the following sub-systems:

- the Stokes problem for fixed $\underline{\underline{\tau}}_h$ and $\underline{\underline{d}}_h$
- the constitutive equation for fixed $\underline{u}_h$
- the projection $\underline{\underline{d}}_h = \underline{\underline{D}}(\underline{u}_h)$ for fixed $\underline{u}_h$.

The coupling of these sub-systems, along with the treatment of nonlinearity, is done through GMRES (for " Generalized Minimal Residual ")[5] a Newton-Krylov iterative solver. When a free surface is present, the discretized pseudo-concentration F_h is updated for fixed $\underline{u}_h$ outside GMRES, by a fixed-point algorithm. In the following sections, we describe the solution of each decoupled sub-system and the solution of the global four-field system by GMRES.

6.3.1 Stokes Problem

For fixed $\underline{\underline{\tau}}_h$ and $\underline{\underline{d}}_h$, the discretized Stokes problem is as follows:

Find $(\underline{u}_h, p_h) \in V_h \times Q_h$ such that:

Eqn. 6-23 $$\int_\Omega q_h \nabla \cdot \underline{u}_h \, d\underline{x} = 0 \qquad \forall q_h \in Q_h$$

$$2\alpha \int_\Omega \underline{\underline{D}}(\underline{u}_h) : \underline{\underline{D}}(\underline{v}_h) \, d\underline{x} - \int_\Omega p_h \nabla \cdot \underline{v}_h \, d\underline{x} = -\int_\Omega (\underline{\underline{\tau}}_h - 2\alpha \underline{\underline{d}}_h) : \underline{\underline{D}}(\underline{v}_h) \, d\underline{x}$$

$$\forall \underline{v}_h \in V_h$$

This discrete problem can be represented by the following matrix problem:

Eqn. 6-24 $$\begin{cases} B\underline{u}_h = 0 \\ A\underline{u}_h + B^T p_h = \underline{C}\left(\underline{\underline{\tau}}_h, \underline{\underline{d}}_h\right. \end{cases}$$

We use Uzawa's algorithm[6] to solve this system, allowing a reduction in the size of the global matrix. Furthermore, four degrees of freedom per element, two in velocity and two in pressure, are removed according to the condensation technique of Fortin and Fortin[7]. The system is finally solved through a direct method by a *LU* factorization.

6.3.2 Discontinuous Galerkin Method

We will only describe the method for the constitutive equation (Eqn. 6-4), but a similar treatment is applied to the pseudo-concentration (Eqn. 6-12). In the more general time-dependent case, a fully implicit second order Gear scheme is used for the time derivative. For stationary problems, like those studied in this work, the time derivative is simply dropped.

The discrete weighted residual formulation of the constitutive equation is defined as follows in the traditional Galerkin method:

Eqn. 6-25 $$\int_\Omega \left[\lambda \underline{\underline{A}}\left(\underline{\underline{\tau}}_{i_h}\right) + \underline{\underline{B}}\left(\underline{\underline{\tau}}_{i_h}\right)\right] : \underline{\underline{\phi}}_h \, d\underline{x} = 2\eta_i \int_\Omega \underline{\underline{D}}(\underline{u}_h) : \underline{\underline{\phi}}_h \, d\underline{x} \qquad \forall \underline{\underline{\phi}}_h \in \Sigma_h$$

If we decompose this formulation into elementary sub-systems, we obtain the following weak formulation on each element K:

Eqn. 6-26

$$\int_K \left[\lambda \left(\underline{u}_h \cdot \nabla \underline{\underline{\tau}}_{i_h} - \nabla \underline{u} \cdot \underline{\underline{\tau}}_{i_h} - \underline{\underline{\tau}}_{i_h} \cdot (\nabla \underline{u}_h)^T \right) + \underline{\underline{B}}\left(\underline{\underline{\tau}}_{i_h} \right) \right] : \underline{\underline{\phi}}_h \, d\underline{x} = 2\eta_i \int_K \underline{\underline{D}}(\underline{u}_h) : \underline{\underline{\phi}}_h \, d\underline{x}$$

$$\forall \underline{\underline{\phi}}_h \in P_1(K)$$

We use the upper-convected derivative for $\underline{\underline{A}}(\underline{\underline{\tau}}_{i,h})$ to simplify the last formulation, but a similar treatment can be applied to the Gordon-Schowalter derivative of Eqn. 6-7.

A discontinuous polynomial approximation (P_1) for each variable $\underline{\underline{\tau}}_i$ of mode i is used on each element K. The velocity field $\underline{u}_h$ is known from the previous iteration. The discontinuous approximation gives rise to a discontinuity jump at the element interface in the derivative of $\underline{\underline{\tau}}_{i,h}$, as illustrated in Fig. 6-2. The convective term in Eqn. 6-26 becomes:

Eqn. 6-27 $$\int_K \underline{u}_h \cdot \nabla \underline{\underline{\tau}}_{i_h} : \underline{\underline{\varphi}}_h \, d\underline{x} \rightarrow \int_K \underline{u}_h \cdot \nabla \underline{\underline{\tau}}_{i_h} : \underline{\underline{\varphi}}_h \, d\underline{x} + \int_{\partial K^-} (\underline{u}_h \cdot \underline{n}) \left[\underline{\underline{\tau}}_{i_h} \right] : \underline{\underline{\varphi}}_h \, ds$$

where $\underline{n}_K$ is the unit normal vector to the boundary ∂K pointing outside K (Fig. 6-2). The inflow boundary ∂K^- with respect to the velocity field is defined as:

Eqn. 6-28 $$\partial K^- = \left\{ \underline{x} \in \partial K \middle| \underline{u} \cdot \underline{n}_K < 0 \right\}$$

$[\underline{\underline{\tau}}_{i,h}]$ is the jump in the variable $\underline{\underline{\tau}}_{i,h}$ and is expressed as:

Eqn. 6-29 $$\left[\underline{\underline{\tau}}_{i_h} \right](\underline{x}) \equiv \underline{\underline{\tau}}_{i_h}^{-}(\underline{x}) - \underline{\underline{\tau}}_{i_h}^{+}(\underline{x}) \equiv \lim_{\varepsilon \to 0^-} \underline{\underline{\tau}}_{i_h}(\underline{x} + \varepsilon \underline{u}) - \lim_{\varepsilon \to 0^+} \underline{\underline{\tau}}_{i_h}(\underline{x} + \varepsilon \underline{u})$$

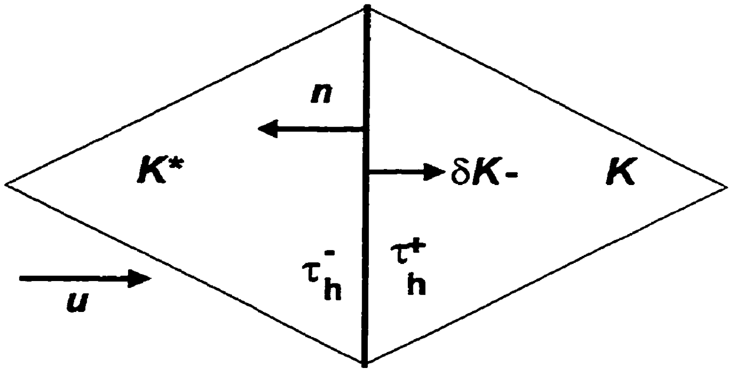

Figure 6-2 Discontinuity Jump at the Interface of Two Elements[8].

When we replace Eqn. 6-27 in the weighted residual formulation of Eqn. 6-26, and assume that $\underline{\underline{\tau}}_{i,h}^{+} = \underline{\underline{\tau}}_{i,h}$, we obtain a new formulation:

Eqn. 6-30
$$\int_K \left[\lambda\left(\underline{u}_h \cdot \nabla \underline{\underline{\tau_i}}_h - \nabla\underline{u}\cdot\underline{\underline{\tau_i}}_h - \underline{\underline{\tau_i}}_h \cdot (\nabla \underline{u}_h)^T\right) + \underline{\underline{B}}\left(\underline{\underline{\tau_i}}_h\right)\right] : \underline{\underline{\phi}}_h \, d\underline{x}$$
$$- \int_{\partial K^-} \underline{u}_h \cdot \underline{n}\left(\underline{\underline{\tau_i}}_h\right) : \underline{\underline{\phi}}_h \, ds = 2\eta_i \int_K \underline{\underline{D}}(\underline{u}_h) : \underline{\underline{\phi}}_h \, d\underline{x} - \int_{\partial K^-} \underline{u}_h \cdot \underline{n}\left(\underline{\underline{\tau_i}}_h^{-}\right) : \underline{\underline{\phi}}_h \, ds$$
$$\forall \underline{\underline{\phi}}_h \in P_1(K)$$

This is the discrete formulation proposed by Lesaint and Raviart[9]. It results in a small nonlinear system on each element K, which is linearized by a Newton method:

Eqn. 6-31
$$M_K\left(\underline{u}_K, \underline{\underline{\tau_i}}_K\right)\underline{\underline{\tau_i}}_K = E_K(\underline{u}_K) + H_K \underline{\underline{\tau_i}}_K^{-} \quad (\mathrm{i} = 1, \mathrm{N\ equations})$$

However, the resolution of this system requires knowledge of the quantity $\underline{\underline{\tau}}_{i,h}^{-}$ on elements adjacent to ∂K^- so that a particular numbering of the elements is necessary. A perfect numbering is not always possible. In the presence of recirculation zones, for example, the best possible numbering is provided and the elements are swept many times so that the resolution can be seen as a block relaxation (Gauss-Seidel type) method.

In conclusion, we have to solve for each i mode the nonlinear system given by Eqn. 6-30 of size 9 x 9 for 2D problems and 12 x 12 for axisymmetric problems, on each element. For the pseudo-concentration, we have to solve a 3 x 3 linear system given by the following equation:

Eqn. 6-32 $$\int_K (\underline{u}_h \cdot \nabla F_h) G_h \, d\underline{x} - \int_{\partial K^-} (\underline{u}_h \cdot \underline{n}) F_h G_h \, ds = -\int_{\partial K^-} (\underline{u}_h \cdot \underline{n}) F_h^- G_h \, ds$$

or in matrix form:

Eqn. 6-33 $$S_K(\underline{u}_K, F_K) F_K = L_K F_K^-$$

2.3.3 Gradient Tensor of Velocity

The projection of $\underline{\underline{D}}(\underline{u}_h)$ in the discrete subspace Σ_h can be calculated by considering the following problem for a fixed $\underline{u}_h$:

Eqn. 6-34 $$\int_\Omega \underline{\underline{d}}_h : \underline{\underline{\psi}}_h \, d\underline{x} = \int_\Omega \underline{\underline{D}}(\underline{u}_h) : \underline{\underline{\psi}}_h \, d\underline{x} \qquad \forall \underline{\underline{\psi}}_h \in \Sigma_h$$

The projection is achieved on an elementary basis since no continuity is required at the elements interface for variables $\underline{\underline{d}}_h$ and $\underline{\underline{\psi}}_h$. Therefore, we have to consider only these elementary systems:

Eqn. 6-35 $$\int_K \underline{\underline{d}}_h : \underline{\underline{\psi}}_h \, d\underline{x} = \int_K \underline{\underline{D}}(\underline{u}_h) : \underline{\underline{\psi}}_h \, d\underline{x} \qquad \forall \underline{\underline{\psi_{ij}}}_h \in P_1(K)$$

The last equation can be expressed in matrix form:

Eqn. 6-36 $$O_K \underline{\underline{d}}_K = W(\underline{u}_K)$$

The small elementary systems are solved by a direct method with a LU factorization.

6.3.4 Resolution of the Global System

Following the presentation of the various sub-systems, the global system, composed of Eqn. 6-19 and Eqn. 6-20 if a free surface is present, can now be expressed in the following way.

Eqn. 6-37
$$\begin{cases} B\underline{u}_h = 0 \\ A\underline{u}_h + B^T p_h = \underline{C}\left(\underline{\underline{\tau}}_h, \underline{\underline{d}}_h\right) \\ M_K\left(\underline{u}_K, \underline{\underline{\tau_i}}_K\right)\underline{\underline{\tau_i}}_K = E_K(\underline{u}_K) + H_K \underline{\underline{\tau_i}}_K^- \quad (\mathrm{i} = 1, \mathrm{N\ equations}) \\ O_K \underline{\underline{d}}_K = W(\underline{u}_K) \end{cases}$$

Eqn. 6-38
$$S_K(\underline{u}_K, F_K)F_K = L_K F_K^-$$

Eqn. 6-37 is a nonlinear system, so we need to use an iterative method to solve it. A fixed-point method is not applicable, since it results in a loss of numerical convergence as viscoelasticity becomes more important. The Newton method is more suitable for this problem. It generally applies to problems of the form:

<u>Find x such that R(x)=0.</u>

The algorithm of the Newton method is as follows:

1. Given $\underline{X}_0$, an initial guess;
2. For $n \geq 0$:

Eqn. 6-39
$$J_n \delta X = -R(\underline{X}_n)$$

where J_n is the Jacobian matrix of $R(\underline{X}_n)$ evaluated in $\underline{X}_n$;

3. $\underline{X}_{n+1} = \underline{X}_n + \delta X$;
4. If $\|\delta X\| < \varepsilon$ and $\|R(\underline{X}_n)\| < \varepsilon$, stop.

   Otherwise, go back to step 2.

Our specific problem can be expressed as follows:

Find $(\underline{u}_h, \underline{p}_h, \underline{\underline{\tau}}_h, \underline{\underline{d}}_h)$ such that $R(\underline{u}_h, \underline{p}_h, \underline{\underline{\tau}}_h, \underline{\underline{d}}_h)=0$

where $R(u_h, p_h, \tau_h, d_h)$ is given by:

$$R\left(\underline{u}_h, p_h, \underline{\underline{\tau}}_h, \underline{\underline{d}}_h\right)=\begin{cases} B\underline{u}_h \\ A\underline{u}_h + B^T p_h - \underline{C}\left(\underline{\underline{\tau}}_h, \underline{\underline{d}}_h\right) \\ \sum_K M_K\left(\underline{u}_K, \underline{\underline{\tau_i}}_K\right)\underline{\underline{\tau_i}}_K - E_K(\underline{u}_K) - H_K \underline{\underline{\tau_i}}_K^- & (\mathrm{i}=1,\mathrm{N\ equations}) \\ \sum_K O_K \underline{\underline{d}}_K - W(\underline{u}_K) \end{cases}$$

The difficulty for this large system is to solve the problem without calculating explicitly the Jacobian matrix of Eqn. 6-39, which would require too much memory space. To avoid building this large global matrix at every iteration, we use an approximation based on a finite central difference:

Eqn. 6-40
$$J\underline{d} \approx \frac{R(\underline{X}+h\underline{d}) - R(\underline{X}-h\underline{d})}{2h}$$

where $\underline{X}=(u_h, p_h, \tau_h, d_h)^T$ and h is small (usually of the order of 10^{-6}).

The system to solve is highly nonlinear, and this causes convergence problems. In order to obtain a better conditioning of the system, we use instead a preconditioned residual $\widetilde{R}\left(\underline{u}_h, p_h, \underline{\underline{\tau}}_h, \underline{\underline{d}}_h\right)$ [1,10], defined as $\widetilde{R}\left(\underline{u}_h, p_h, \underline{\underline{\tau}}_h, \underline{\underline{d}}_h\right)=\left(\delta\underline{u}, \delta p, \delta\underline{\underline{\tau}}, \delta\underline{\underline{d}}\right)^T$, where $\delta\underline{u}$, δp, $\delta\underline{\underline{\tau}}$ and $\delta\underline{\underline{d}}$ are determined as follows:

1. Solve the following Stokes problem:

$$B\delta\underline{u} = -B\underline{u}_h$$
$$A\delta\underline{u} + B^T\delta p = -A\underline{u}_h - B^T p_h + \underline{C}(\underline{\underline{\tau}}_h, \underline{\underline{d}}_h)$$

   and obtain a solution corrected in velocity, $\underline{u} = \underline{u}_h + \delta\underline{u}$.

2. Solve the constitutive equation by a Newton method for fixed $\underline{u}_K$, for all K elements:

$$J_K\left(\underline{u}_K, \underline{\underline{\tau_i}}_K\right)\delta\underline{\underline{\tau_i}}_K = -M_K\left(\underline{u}_K, \underline{\underline{\tau_i}}_K\right)\underline{\underline{\tau_i}}_K + E_K\left(\underline{u}_K\right) + H_K\underline{\underline{\tau_i}}_K^- + H_K\delta\underline{\underline{\tau_i}}_K^-$$

(i = 1, N equations)

where J_K is the Jacobian matrix obtained by the linearization due to the Newton method, $\underline{u}_h$ being fixed. The residual $\delta\underline{\underline{\tau}}$ is made up of all the elementary residuals $\delta\underline{\underline{\tau}}_K$. Note that it is possible to ignore the last term of the previous equation and to perform only one sweep, which accelerates the calculations.

3. Compute the local projections of tensor $\underline{\underline{D}}(\underline{u}_h)$ on all K elements:

$$O_K \delta \underline{\underline{d}}_K = -O_K \underline{\underline{d}}_K + W(\underline{u}_K)$$

The residual $\delta\underline{\underline{d}}$ is also made of all the elementary residuals $\delta\underline{\underline{d}}_K$.

The definition of this new residual $\widetilde{R}$ is simply the preconditioning of the residual R with the inverse of a matrix $\widetilde{J}$, which is a block-diagonal matrix built with the respective Jacobian matrix of the decoupled sub-systems. For the resolution of the coupled system of Eqn. 6-39, we used the GMRES iterative method. This method has been designed to solve non-symmetrical linear systems. In the GMRES algorithm, the Jacobian matrix is only present in matrix-vector products. It is then not necessary to explicitly build the large global Jacobian matrix. Instead we use the approximation given by Eqn. 6-40, which reduces considerably the memory space needed.

We tried to incorporate the calculation of the pseudo-concentration (Eqn. 6-38) in the GMRES method for the calculation of the free surface, but it caused convergence problems. Instead, the free surface was updated outside GMRES, using a fixed-point algorithm for fixed $\underline{u}_K$. The other variables, solved in GMRES, were calculated for a fixed position of the free surface. More details on the discontinuous Galerkin method applied to the pseudo-concentration can be found in reference 2.

Finally, for some simulations at low Deborah number it was found useful to do one to three fixed point iterations as a preconditioner to GMRES. However, this caused convergence problems at high levels of elasticity and had to be avoided for these flow conditions.

REFERENCES

1 Guénette R., Fortin M., "A New Mixed Finite Element Method for Computing Viscoelastic Flows", *J. Non-Newt. Fl. Mech.*, 60, p.27-52 (1995)

2 Béliveau A., « Méthodes de Lesaint-Raviart Modifiées : Applications au Calcul des Surfaces Libres », Ph.D. Thesis, École Polytechnique de Montréal, Montréal, Canada (1997)

3 Brezzi F., Fortin M., "Mixed and Hybrid Finite Element Methods: Series in Computational Mechanics", *Springer*, New York (1991)

4 Fortin A., Béliveau A., Heuzey M.C., Lioret A., « Ten Years Using Discontinuous Galerkin Methods for Polymer Processing », to be published in the Proceedings of *Int. Symp. on Discontinuous Galerkin Methods : Theory, Computations and Applications*, Salve Regina College, Newport, RI, USA (1999)

5 Fortin A., Fortin M., "A Preconditioned Generalized Minimal Residual Algorithm for the Numerical Solution of Viscoelastic Fluid Flows", *J. Non-Newt. Fl. Mech.*, 36, p. 277-288 (1990)

6 Fortin M., Fortin A., "A Generalization of Uzawa's Algorithm for the Solution of Navier-Stokes Equations", *Comm. Appl. Num. Meth.*, 1, p. 205-208 (1985)

7 Fortin M., Fortin A., "Experiments with Several Elements for Viscous Incompressible Flows", *Int. J. Num. Meth. Fl.*, 5, p. 911-928 (1985)

8 Lioret A., « Méthodes d'Éléments Finis Adaptative pour les Écoulements de Fluides Viscoélastiques », Master's Thesis, École Polytechnique de Montréal, Montréal, Canada (1998)

9 Lesaint P. Raviart P.A., "On a Finite Element Method for Solving the Neutron Transport Equations", in "Mathematical Aspects of Finite Elements in Partial Differential Equations", C. de Boor (ed.), *Academic Press*, New York, p. 89-123 (1974)

10 Fortin A., Zine A., Agassant J.F., "Computing Viscoelastic Fluid Flow at Low Cost", *J. Non-Newt. Fl. Mech.*, 45, p. 209-229 (1992)

7. Planar Abrupt Contraction Flow of High-Density Polyethylene

7.1 Experimental Methods

7.1.1 Die Geometry

Extrusion experiments were carried out using a slit die with transparent walls made of Pyrex™. The die is continuously fed by a Kaufmann PK 25 single screw extruder. It consists of a large reservoir, in which the pressure and the temperature are measured, and a die land, which can be adjusted to vary the local geometry. Details of the die design are given in reference 1. We used only one configuration consisting of an abrupt 8:1 contraction. The geometry of the slit die is shown in Fig. 7-1, and the dimensions are given in Table 7-1. With regard to the aspect ratios W/H of the reservoir and channel we note that these are smaller than the minimum value[2] of 10 recommended to ensure 2D flow, especially in the case of the reservoir. This issue will be discussed when comparing data with the results of numerical simulations. All the experiments were carried out at 200 ± 2°C and at mass flow rates varying between 0.21 and 2.6 kg/h, which correspond to apparent shear rates in the channel in the range of 4.6 to 56 s^{-1}. The transparent glass walls permit the use of laser-Doppler velocimetry and the measurement of flow-induced birefringence.

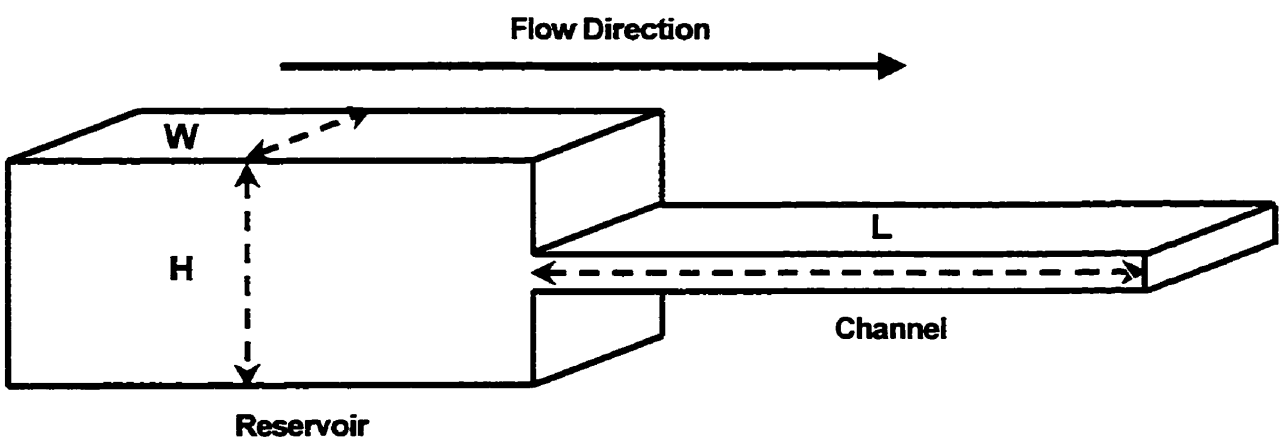

Figure 7-1 Geometry of the Planar 8:1 Abrupt Contraction.

Table 7-1 Geometrical Characteristics of the Die

H (reservoir)	H (channel)	L (channel)	W	W/H (reservoir)	W/H (channel)
20 mm	2.5 mm	20 mm	16 mm	0.8	6.4

7.1.2 Laser-Doppler Velocimetry

Due to its high spatial and temporal resolution, laser-Doppler velocimetry (LDV) is a useful technique for local velocity measurement in translucent fluids, as it does not disturb the flow. LDV is based on the frequency shift of light that is scattered by small moving particles. The technique is as follows: a measuring volume is created by the intersection of two light beams of equal intensity, and the frequency of one beam is shifted with respect to the other. The frequency shift (Doppler shift) of the scattered light with respect to the reference dual beams is directly proportional to the velocity of a moving particle in the fluid passing through the measuring volume. Details of the LDV method can be found in reference 3.

We used the Flowlite™ dual-beam system of Dantec, controlled by the Flow Velocity Analyzer™ and operated from a personal computer with the Burstware™ software (Fig. 7-2). A 10 mW He-Ne laser generates the incident light beam (red light: λ=632.8 nm). The beam is divided in two by a prism, and one beam has its frequency shifted (40 MHz) with respect to the other by a Bragg cell. The two beams are transmitted by optical fibers to a probe or optical head, where a lens (f = 160 mm) focuses the beams into the measuring volume. The dimensions of this ellipsoidal measuring volume are $\delta x = \delta y$ = 108 μm and δz = 913 μm[4]. The scattered light is received by the same probe and transmitted to the Doppler analyzer, which can perform fast-Fourier transform (FFT) analysis. The probe is placed on a XY translation table (Dantec Lightweight Traverse) that is controlled by Burstware™. Displacement along the z-axis is done manually with a micrometric positioning screw. The x component of the velocity (u_x) was measured at six fixed x positions (three in the reservoir and three in the channel) as a function of y. In Table 7-2 and Fig. 7-3 we present the fixed x positions where the velocity profiles were measured. Only one half of the geometry is shown, since it is symmetric with respect to the y axis.

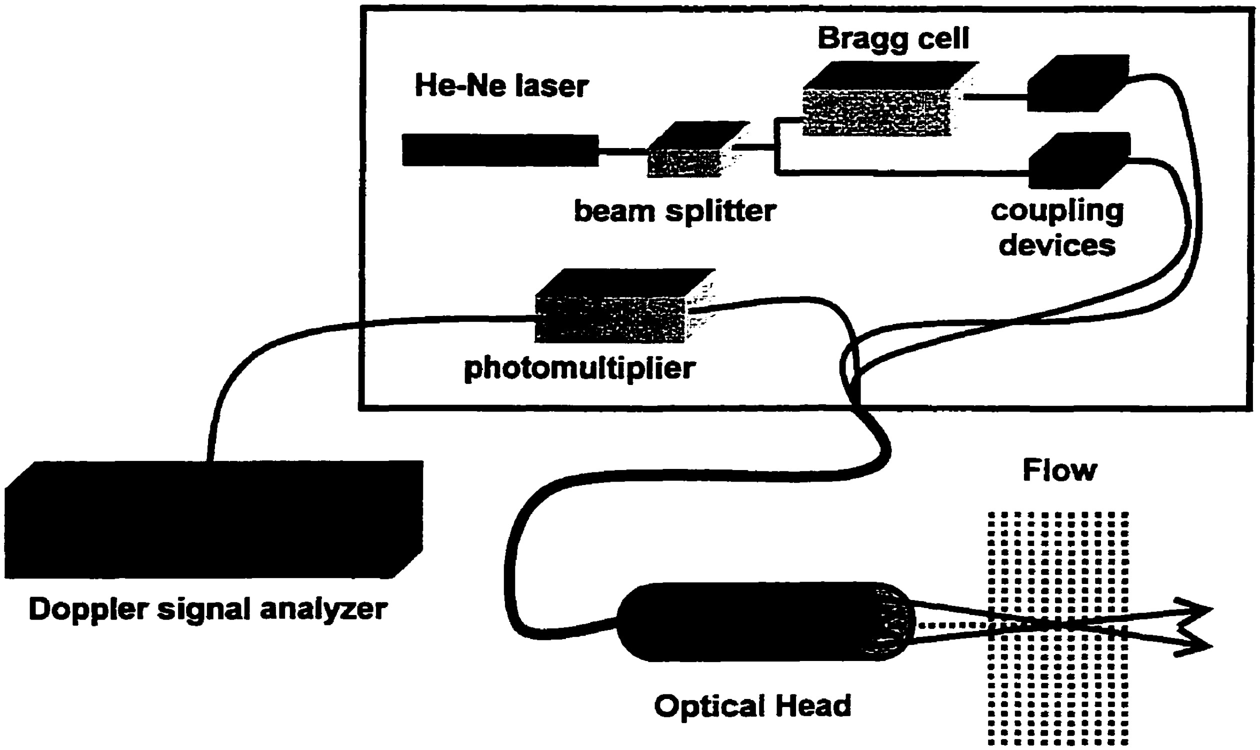

Figure 7-2 Experimental Set-Up of LDV Measurements.

Table 7-2 Velocimetry Measurements Locations

Position	Reservoir	Channel
1	- 14 mm	+ 2.0 mm
2	- 6.5 mm	+ 10 mm
3	- 3.0 mm	+ 17 mm

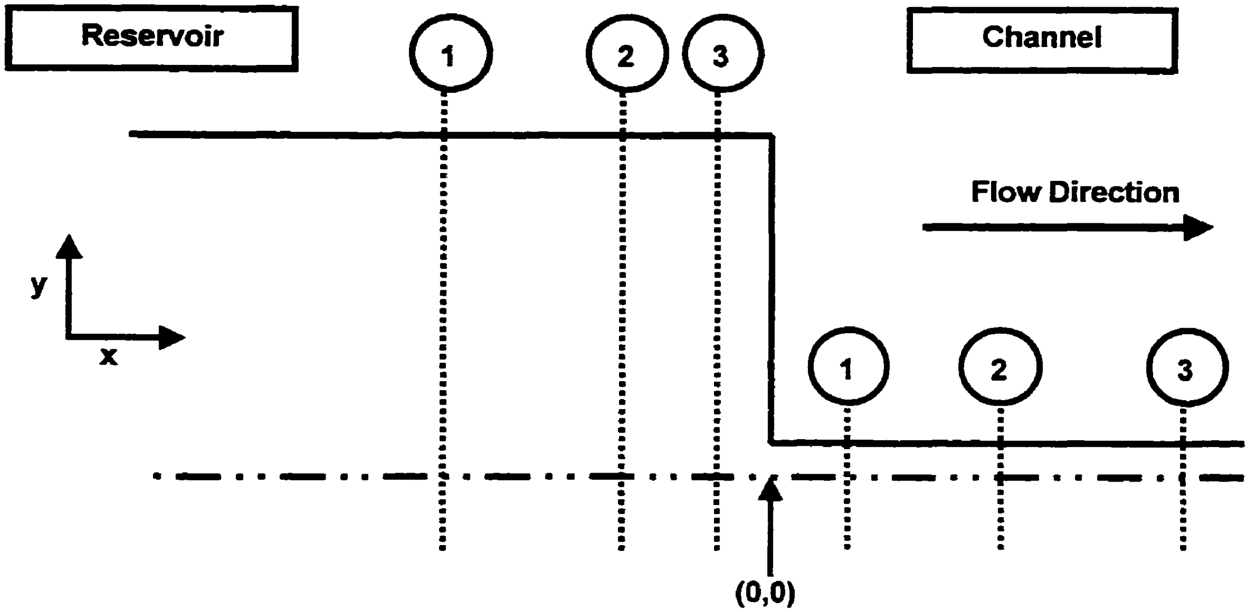

Figure 7-3 Positions of the Velocity Profile Measurements.

7.1.3 Flow-Induced Birefringence

Birefringence occurs in an optically anisotropic material in which there are different velocities of light for different directions of propagation. Anisotropy is a result of the material structure and can appear in some materials at rest, such as calcite crystals. It can also be induced in materials that are isotropic at rest, for example by flow in polymer melts or elastic deformation of solid polymers. In the last two examples, birefringence is a result of the difference in polarizability of a polymer chain along its backbone and perpendicular to it. Polarizability is a measure of the strength of the response of the electrons in a bond between the atoms of the polymer molecule.

The use of birefringence to infer the components of the stress tensor in a flowing or deformed polymer depends upon the existence and validity of a "stress-optical relation"[5]. This relation is given by the semi-empirical stress optical law as a proportionality between the components of the refractive index and stress tensors:

Eqn. 7-1 $$n_{ij} = C\tau_{ij}$$

where C is the stress optical coefficient. For a flexible polymer, this coefficient is proportional to the polarizabilities parallel and transverse to the polymer backbone. For a given polymer, C is essentially independent of the molecular weight and its distribution and is relatively insensitive to temperature[5].

The experimental set-up to measure flow-induced birefringence in polymer melts is shown in Fig. 7-4. A beam of polarized monochromatic light is directed at the melt flowing through the transparent slit die and then passes through an analyzer. We used a diffuse monochromatic light source of sodium (yellow light: λ=589.8 nm). The optical anisotropy of the flowing polymer produces an interference pattern consisting of isochromatic and isoclinic fringes. The measurement of the isoclinic fringes is generally inaccurate and tedious[6], so we added two quarter-waves plates on each side of the die to obtain only the isochromatic fringe pattern.

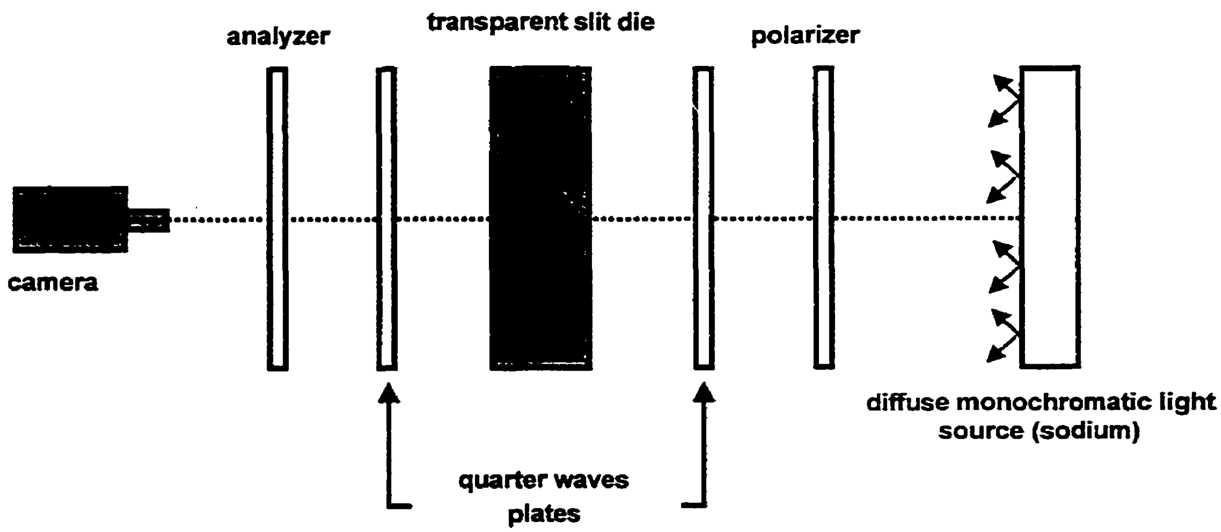

Figure 7-4 Experimental Set-Up for the Measurement of Flow-Induced Birefringence.

7.1.4 Flow Rate-Pressure Curve

Extrusion experiments were carried out at twelve flow rates. In Fig. 7-5, we present the characteristic curve of flow rate vs. pressure for the extruder and die used, using pressure transducer data. If we neglect the correction for the entrance pressure drop, we can convert these data to shear rate vs. viscosity by applying the Rabinowitch correction. These results are presented in Fig. 7-6, along with rheological data, and they are in agreement with the viscosity curve measured in the laboratory.

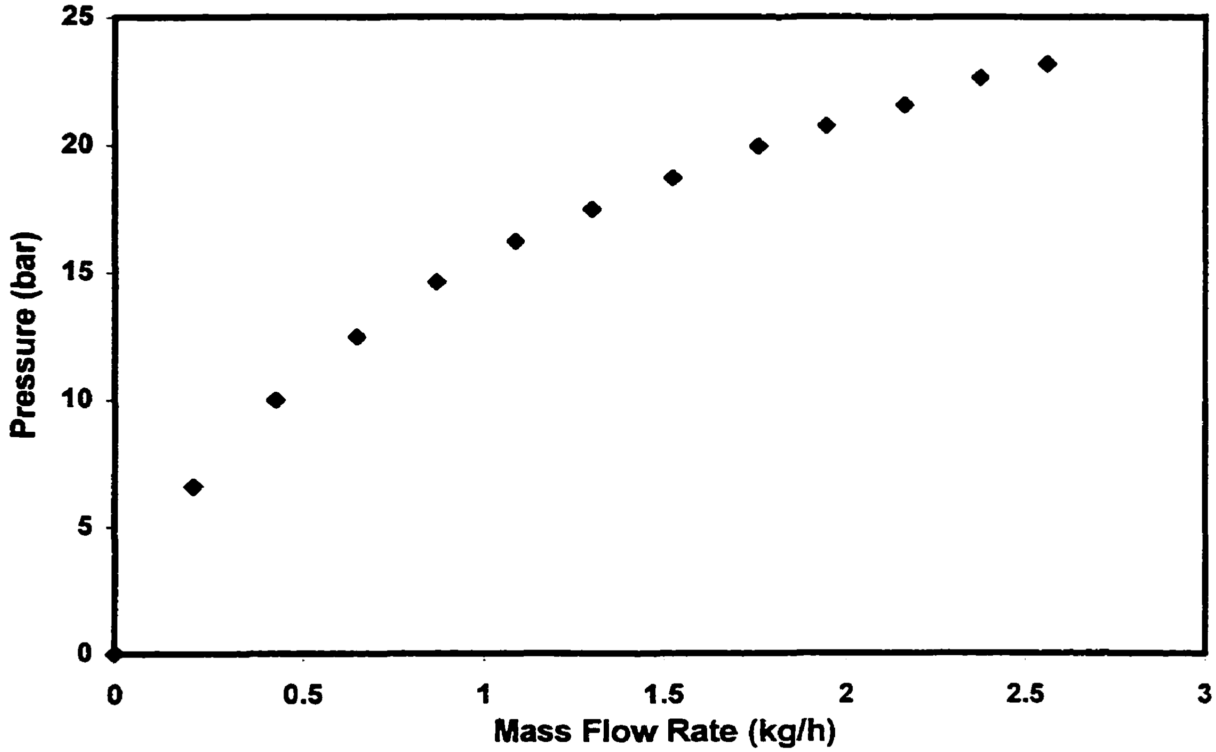

Figure 7-5 Characteristic Curve of Die-Extruder at 200°C.

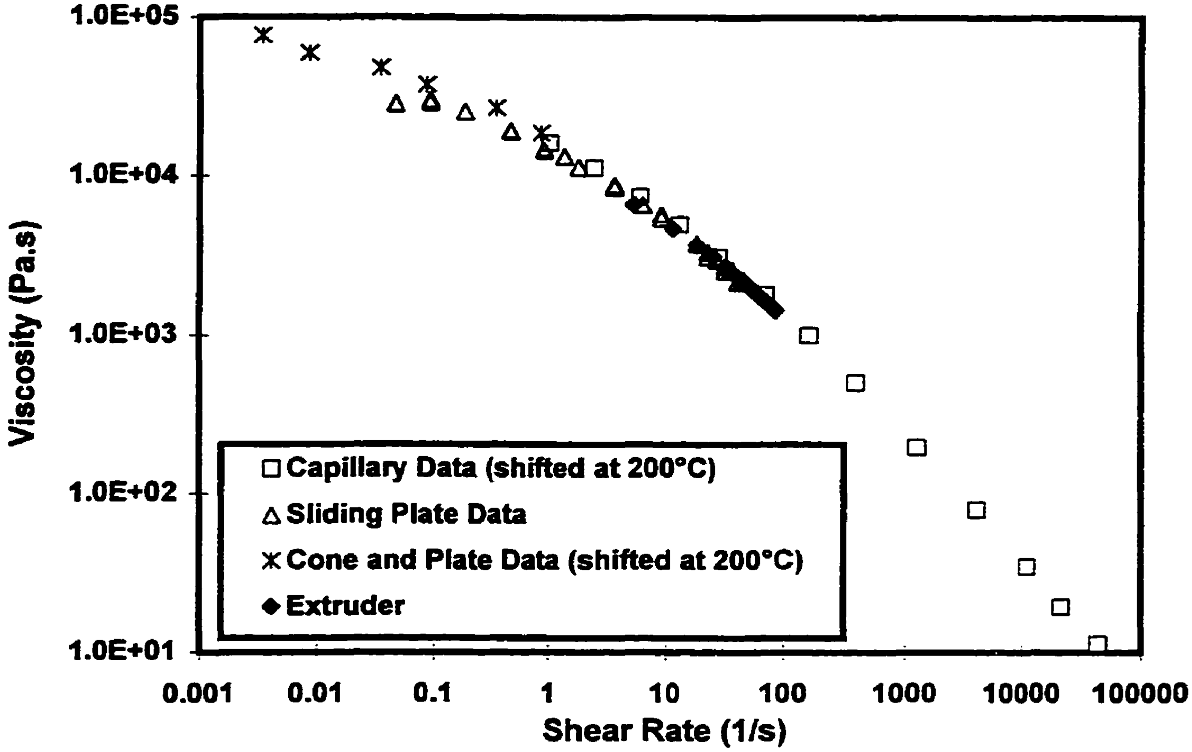

Figure 7-6 Comparison of Extruder Data with Viscosity Curve of HDPE at 200°C.

7.2 Numerical Procedure

7.2.1 Meshes

Two meshes were used for the 2D simulations in order to verify the mesh independence of the solutions. Both meshes are composed of triangular elements. One is an unstructured mesh, while the other is structured. The number of elements for each mesh is presented in Table 7-3, and the meshes are shown in Figs. 7-7 and 7-8 in the region near the contraction. The numerical procedure used was described in Chapter 6.

Table 7-3 Mesh Characteristics for 2D Flow Simulations

Mesh	Planar_1	Planar_2
	Unstructured	Structured
Number of Elements	1277	2976

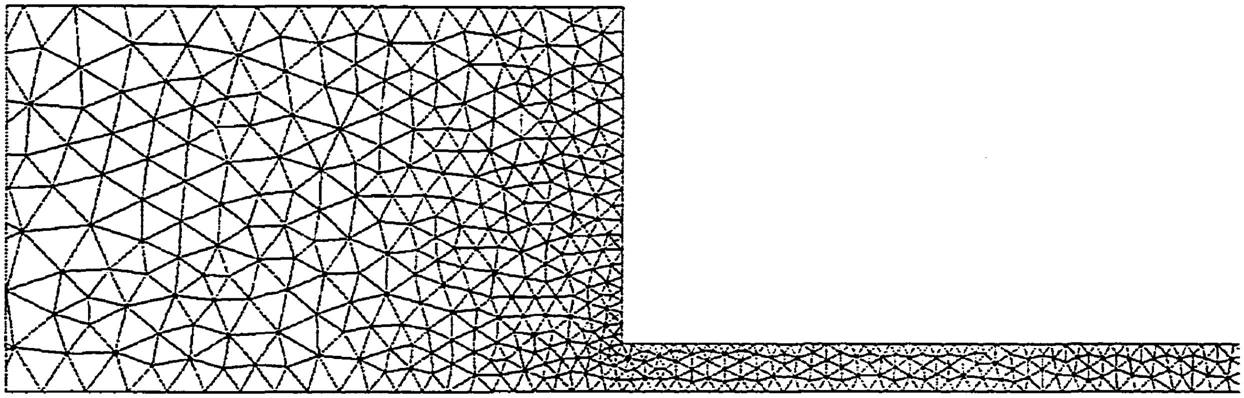

Figure 7-7 Mesh Planar_1.

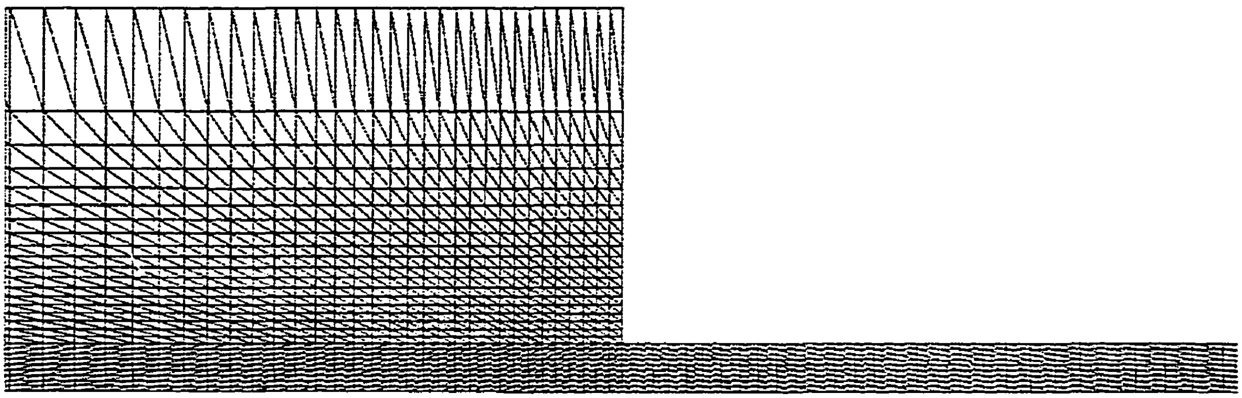

Figure 7-8 Mesh Planar_2.

7.2.2 Viscoelastic Converged Solutions

Numerical convergence is always limited in viscoelastic simulations of fields that contain flow singularities. The maximum flow rate for convergence depends on the mesh, the longest relaxation time of the discrete spectrum, and the constitutive equation. As the mesh is more refined near the flow singularity or reentrant corner, convergence becomes more difficult as in the case of mesh Planar_2. Convergence was also more difficult when using the discrete spectrum based on all data as compared to the spectrum based on truncated data (Table 4-4), since the longest relaxation time is longer in the former case (24.0 sec. vs. 6.25 sec.). We will refer to these spectra as the "full" and "truncated" spectra. We also found that the simple Leonov model gave more convergence problems than the PTT model, possibly because of stronger nonlinearity in the extra stress. It was not possible to determine exactly why this occurred. We did not try simulations with the modified Leonov model, considering the difficulties encountered using the simple model. We present a map of the converged solutions for the various cases (Tables 7-4 and 7-5). Convergence is expressed in terms of the number of flow rates converged, where the maximum is twelve (12). Note that for the PTT model, the same nonlinear parameters (ξ, ε) were used with the full and the truncated spectra, these parameters giving equally good fits of the rheological data.

Table 7-4 Converged Solutions with the PTT Model (max=12)

Spectrum	**Mesh**	
	Planar_1	Planar_2
Full	6	0
Truncated	12	12

Table 7-5 Converged Solutions with the Simple Leonov Model (max=12)

Spectrum	**Mesh**	
	Planar_1	Planar_2
Full	1	0
Truncated	3*	1

* third solution not fully converged

7.3 Total Pressure Drop

For each flow rate we compared the predicted total pressure drop with the one indicated by the pressure transducer in the reservoir. The predicted pressure drop was evaluated as follows:

Eqn. 7-2 $$\Delta P_{calc} = P_{reservoir} - P_{L=20mm}$$

where $P_{reservoir}$ is the pressure in the reservoir at the position of the pressure transducer, and $P_{L=20mm}$ is the pressure in the slit die at L=20mm which corresponds to the die exit. In Fig. 7-9 the results of both viscoelastic models and the viscous model are compared to the measured values. Note that only three points were obtained with the simple Leonov model. The calculated pressures are slightly overestimated by the viscoelastic models, while they are underestimated at high shear rates by the viscous model, but in general the agreement is good. Since the melt is predominantly in shear flow, even the viscous model can give a good approximation of the total pressure drop. In Fig. 7-10, we compare the predictions of the PTT model with the full and truncated spectra and we see that they agree very well. This shows that there is no advantage in using the full spectrum, which usually gives more convergence problems. Finally, mesh independence is demonstrated in Fig. 7-11.

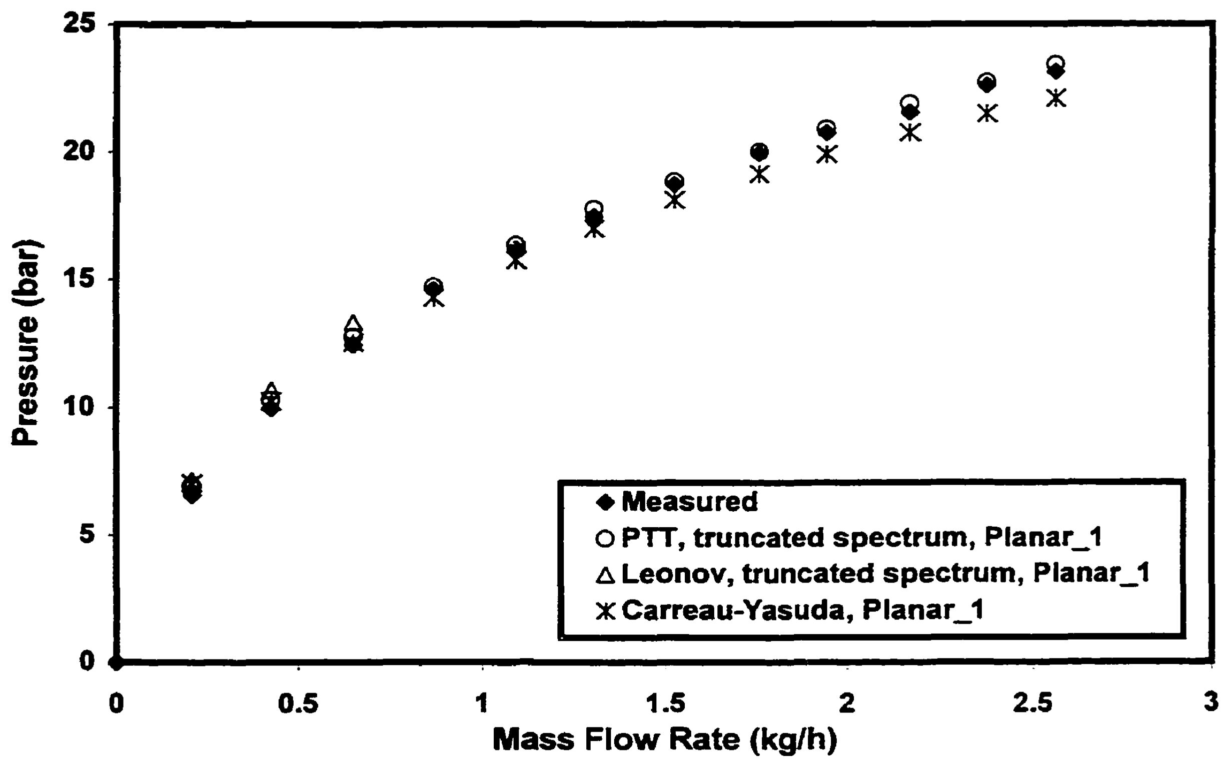

Figure 7-9 Comparison of Predicted Total Pressure Drop with Experimental Values.

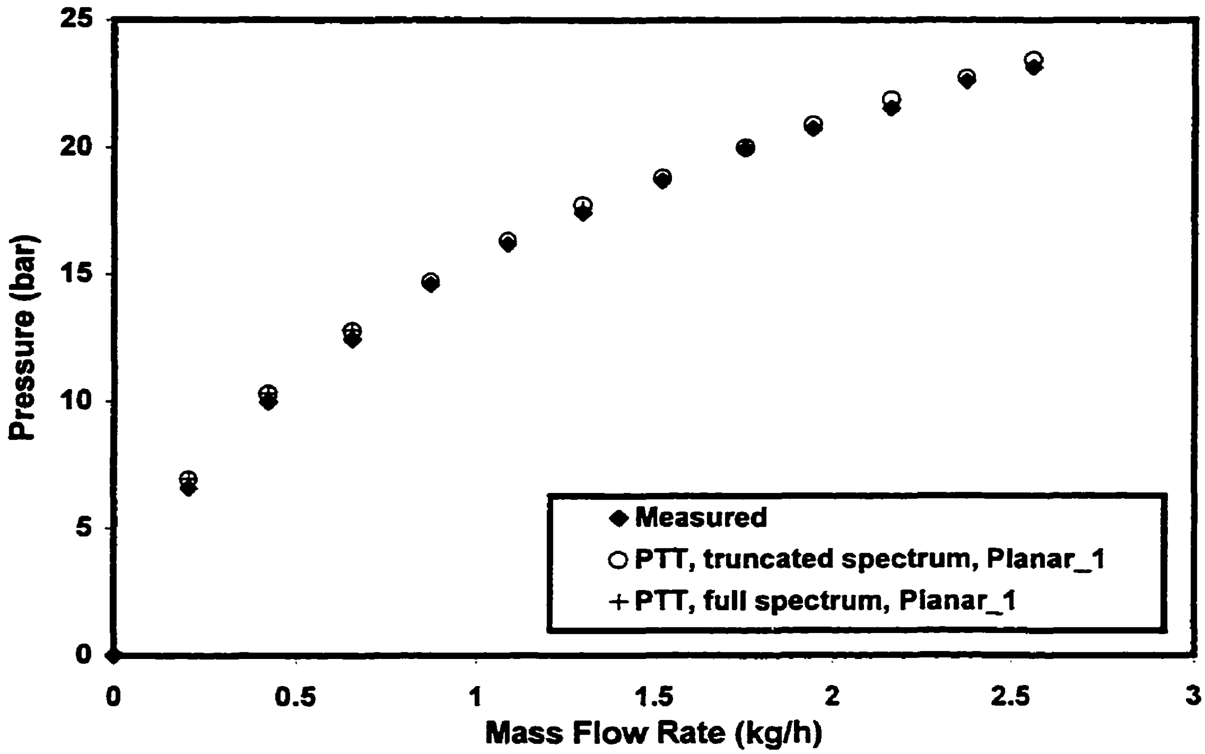

Figure 7-10 Influence of Discrete Spectrum on Prediction of Total Pressure Drop.

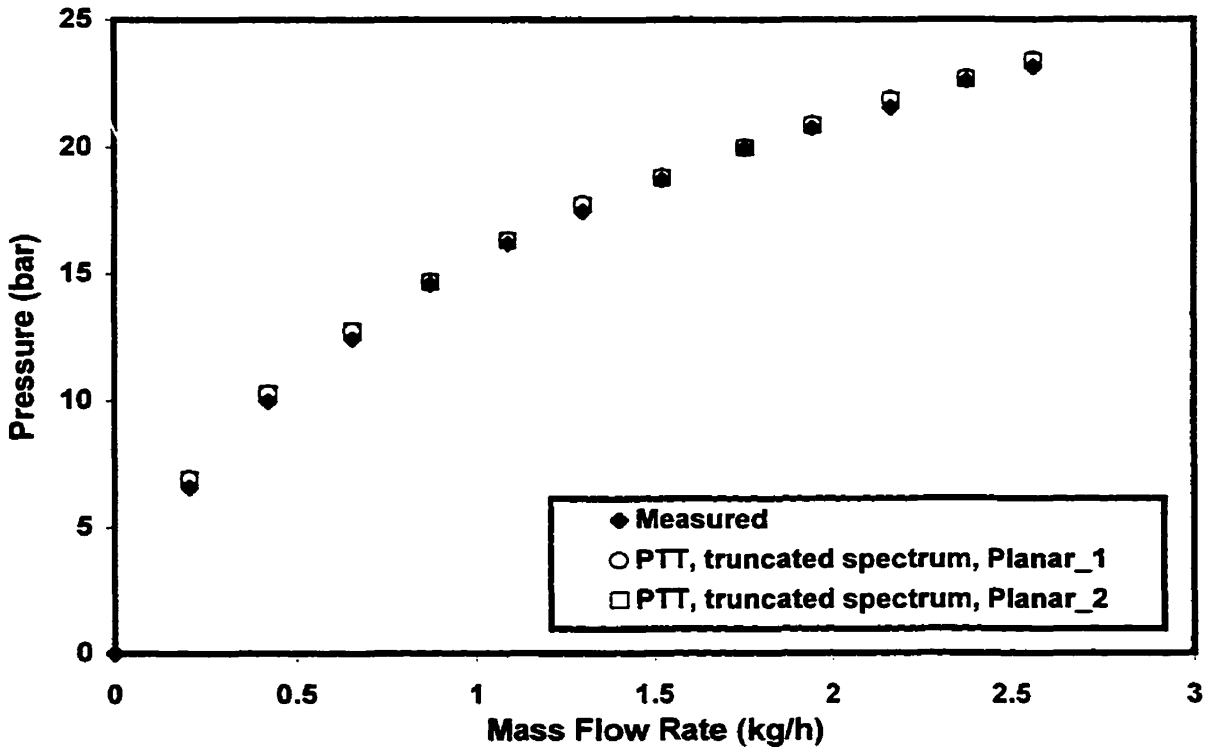

Figure 7-11 Mesh Independence for the Prediction of Total Pressure Drop.

7.4 Velocity

The velocity profiles were measured for the three lowest flow rates, and the results are shown in Figs. 7-12 to 7-17 for the six measurement positions shown in Fig. 7-3 and Table 7-2. The predicted velocity profiles were computed on mesh Planar_1 for all models using the truncated spectrum for the viscoelastic models. Note that both viscoelastic models predict the same velocity profiles.

Where the flow is dominated by shear (position 1 in the reservoir and all three positions in the channel) all models including the viscous model give good predictions of the velocity profiles. However, where the extensional component of the flow becomes important, as we get closer to the contraction (positions 2 and 3 in the reservoir), we start seeing disagreement between the predictions and the measurements. There is also more dispersion in the experimental results at these positions, since a small difference in Δx or Δy results in a large difference in velocity. The viscous model most underestimates the velocity as the extension becomes more important, but the viscoelastic models are also unable to capture well the behavior of the flow. In Fig. 7-15 the viscous model is seen to be in better agreement with experimental data where the flow is dominated by shear. It appears that the flow becomes fully developed faster than predicted by the viscoelastic models.

Again mesh independence was verified by comparing the results with mesh Planar_2. This is shown in Fig. 7-18 using the truncated spectrum for the third flow rate of position 3 in the reservoir. We also verified for the same flow conditions that the use of the full spectrum did not improve the velocity profile predictions (Fig. 7-19).

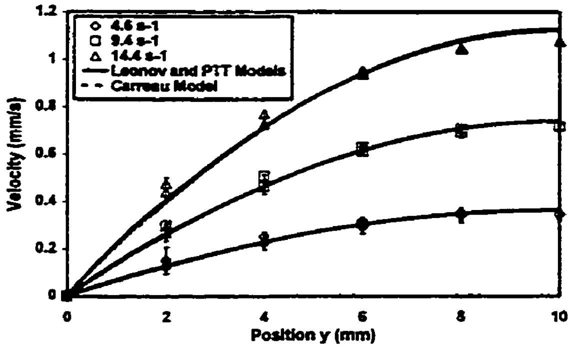

Figure 7-12 Velocity Profile (Reservoir, position 1).

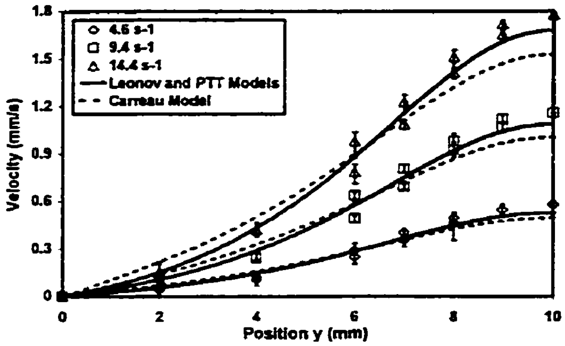

Figure 7-13 Velocity Profile (Reservoir, Position 2).

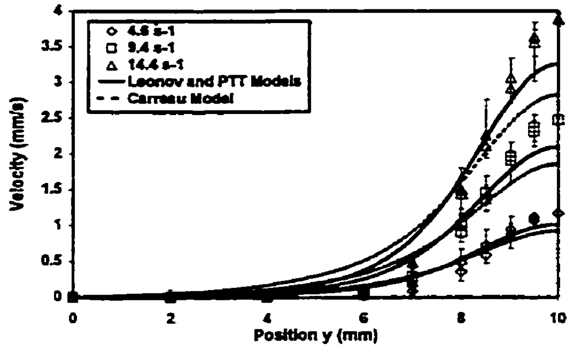

Figure 7-14 Velocity Profile (Reservoir, Position 3).

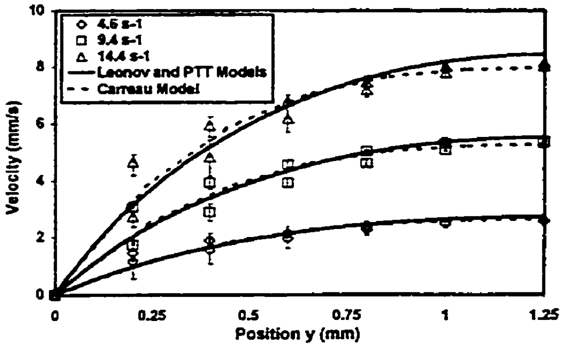

Figure 7-15 Velocity Profile (Channel, Position 1).

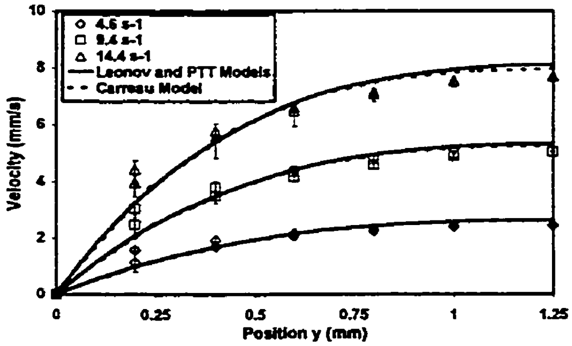

Figure 7-16 Velocity Profile (Channel, Position 2).

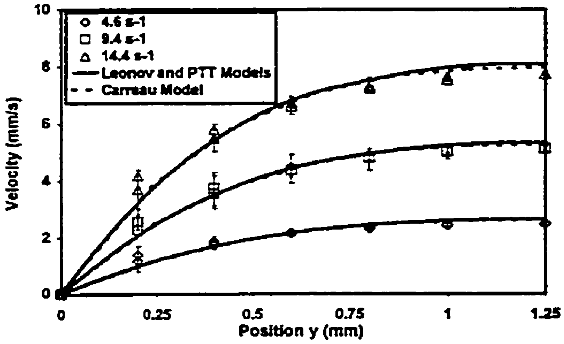

Figure 7-17 Velocity Profile (Channel, Position 3).

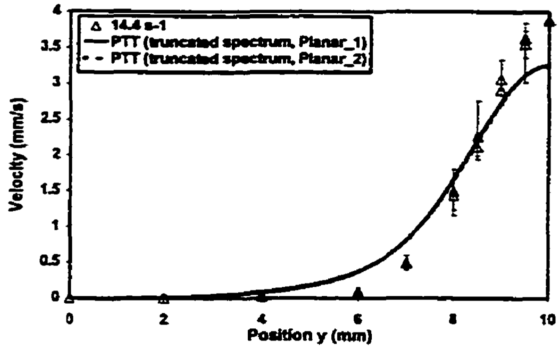

Figure 7-18 Mesh Independence (Reservoir, Position 3).

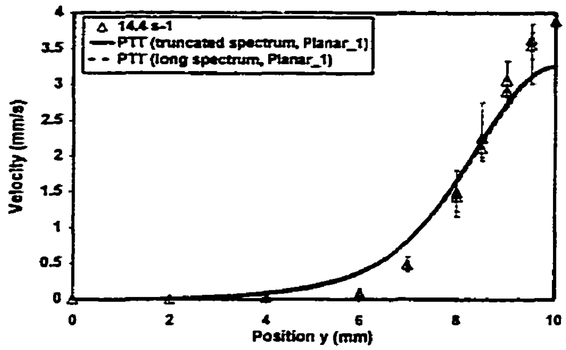

Figure 7-19 Influence of Spectrum (Reservoir, Position 3).

7.5 Birefringence

It was mentioned that the use of birefringence data to infer the components of the stress tensor in a flowing polymer depends upon the validity of the stress-optical relation:

$$n_{ij} = C\tau_{ij}$$

where C is the stress optical coefficient. In order to compare the experimental birefringence with the calculated one, we need to know the value of this coefficient. An approximate value can be obtained by comparing the maximum values of the first principal stress difference ($(\sigma_1 - \sigma_2)_{calc}$) calculated by the finite element simulations with the corresponding maximum birefringence (Δ_{max}) measured on the axis of symmetry for all flow rates. The maximum birefringence (Δ_{max}) is obtained by fitting a cubic spline to the data at each flow rate and finding the maximum from the spline (Fig. 7-20). We obtained a linear relation between $(\sigma_1 - \sigma_2)_{calc}$ and Δ_{max} (Fig. 7-21), which implies the validity of the stress-optical relation. By measuring the slope, we can evaluate the stress optical coefficient. We obtained a value of 1.47 x 10^{-9} m^2/N, which is lower than the value reported by Beraudo[7] for a LLDPE (2.1 x 10^{-9} m^2/N) but equal to that reported by Schoonen[8] (C = 1.47 x 10^{-9} m^2/N) for a low-density polyethylene.

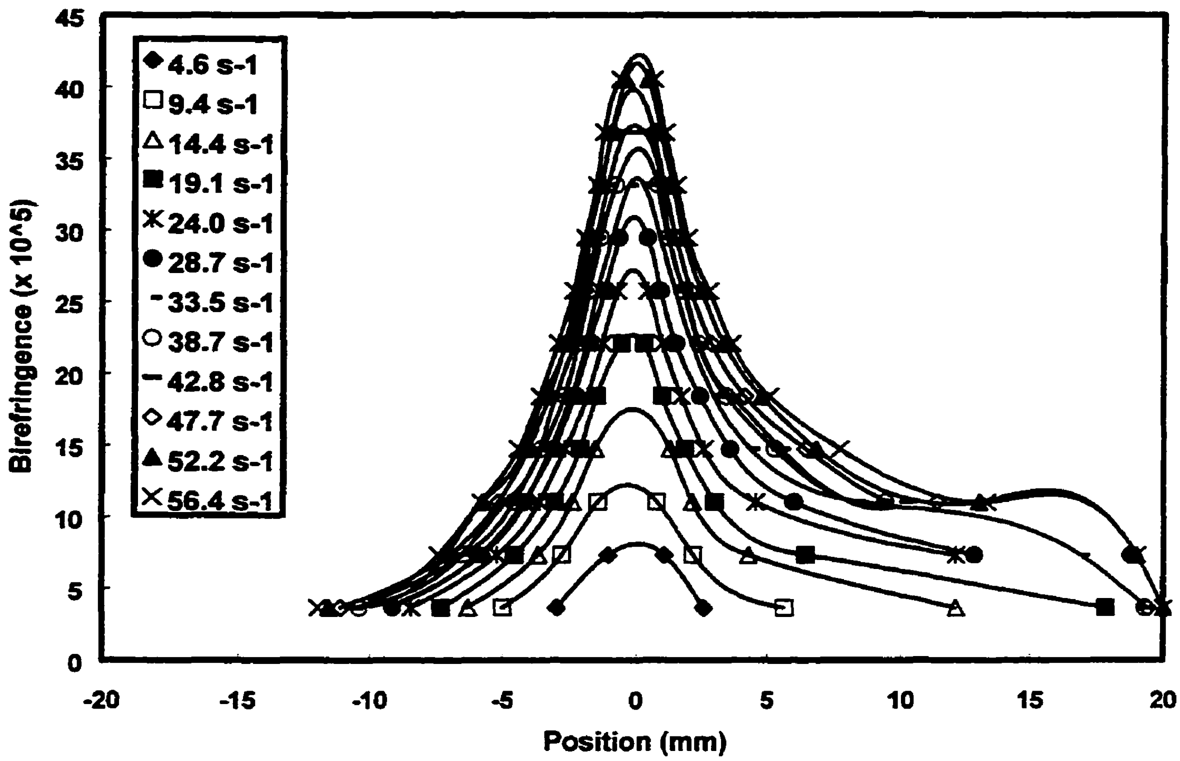

Figure 7-20 Evaluation of Δ_{max} on the Axis of Symmetry.

We can make two types of comparison between the measured and the calculated birefringence, one qualitative and the other more quantitative. In the qualitative case, we look at the entire flow domain and compare the shapes of the calculated birefringence fringes and their relative positions with experimental data. In the quantitative case, we compare the birefringence predicted by the various models with the measured birefringence on the axis of symmetry. In a 2D planar flow domain, the first principal stress difference, which is used to calculate birefringence, is given by the following equation:

Eqn. 7-3 $$\sigma_1 - \sigma_2 = \sqrt{N_1^2 - 4\tau_{12}^2}$$

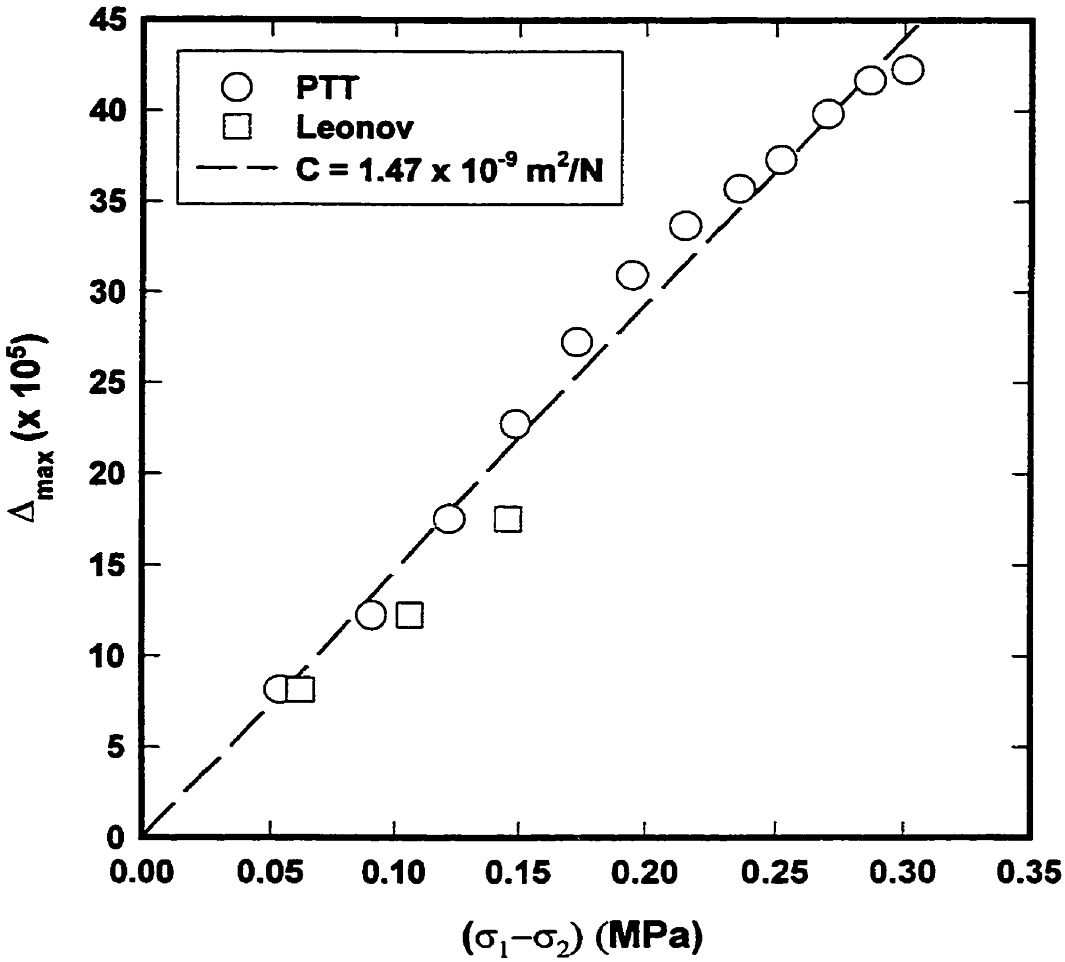

Figure 7-21 Calculation of the Stress Optical Coefficient.

In Figs. 7-22 and 7-23 we present the qualitative comparison on the entire flow domain for the third apparent shear rate (14.4 s^{-1}), which is the highest rate for which we obtained a converged solution with the Leonov model. Fig. 7-22 shows the solution obtained for the Leonov model, while Fig. 7-23 was obtained for the PTT model. Both models represent well the measured birefringence in terms of the shape and position of the fringes in the reservoir, but the Leonov model is closer to the data in the channel. In Fig. 7-24 we show the calculated birefringence for the highest apparent shear rate (56.4 s^{-1}) for the PTT model. Again, good qualitative agreement is obtained.

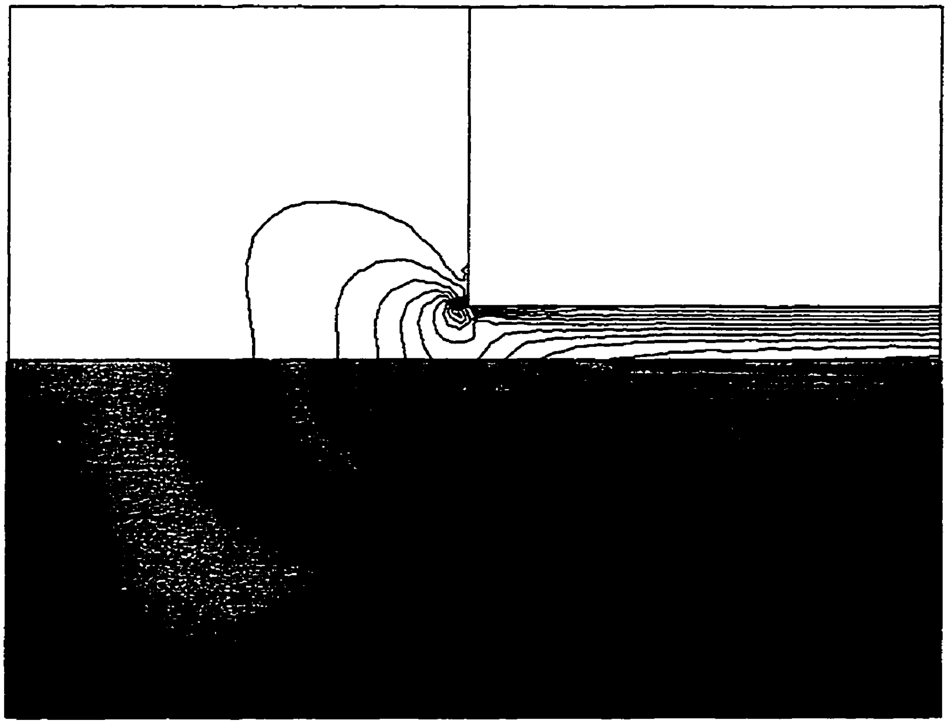

Figure 7-22 Comparison of Measured and Calculated Birefringence (Leonov Model, $\dot{\gamma}_a = 14.4\,\mathrm{s}^{-1}$).

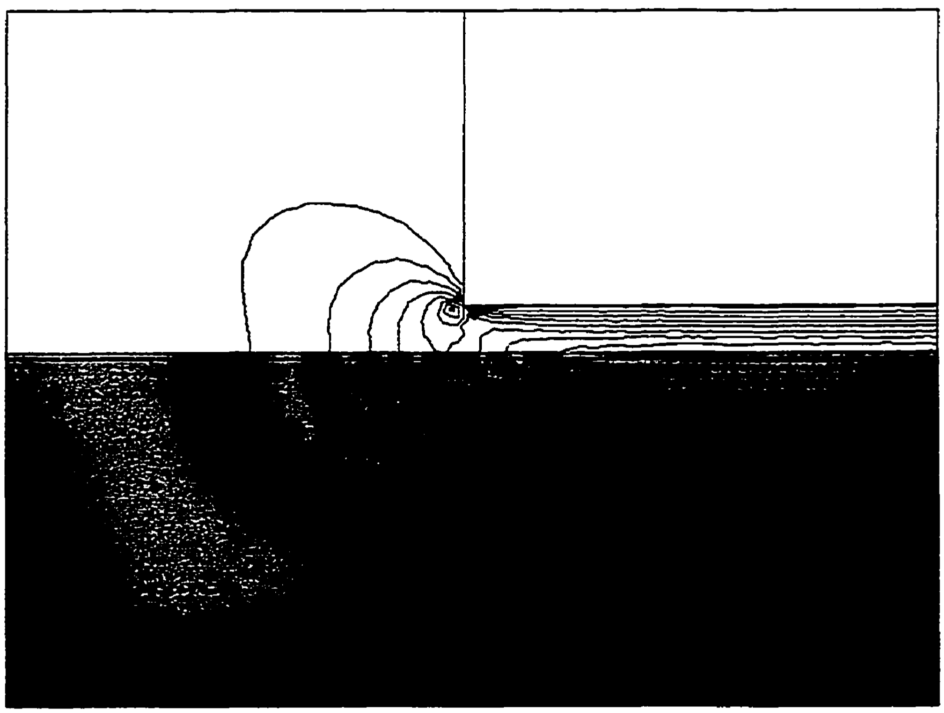

Figure 7-23 Comparison of Measured and Calculated Birefringence (PTT Model, $\dot{\gamma}_a = 14.4\,\mathrm{s}^{-1}$).

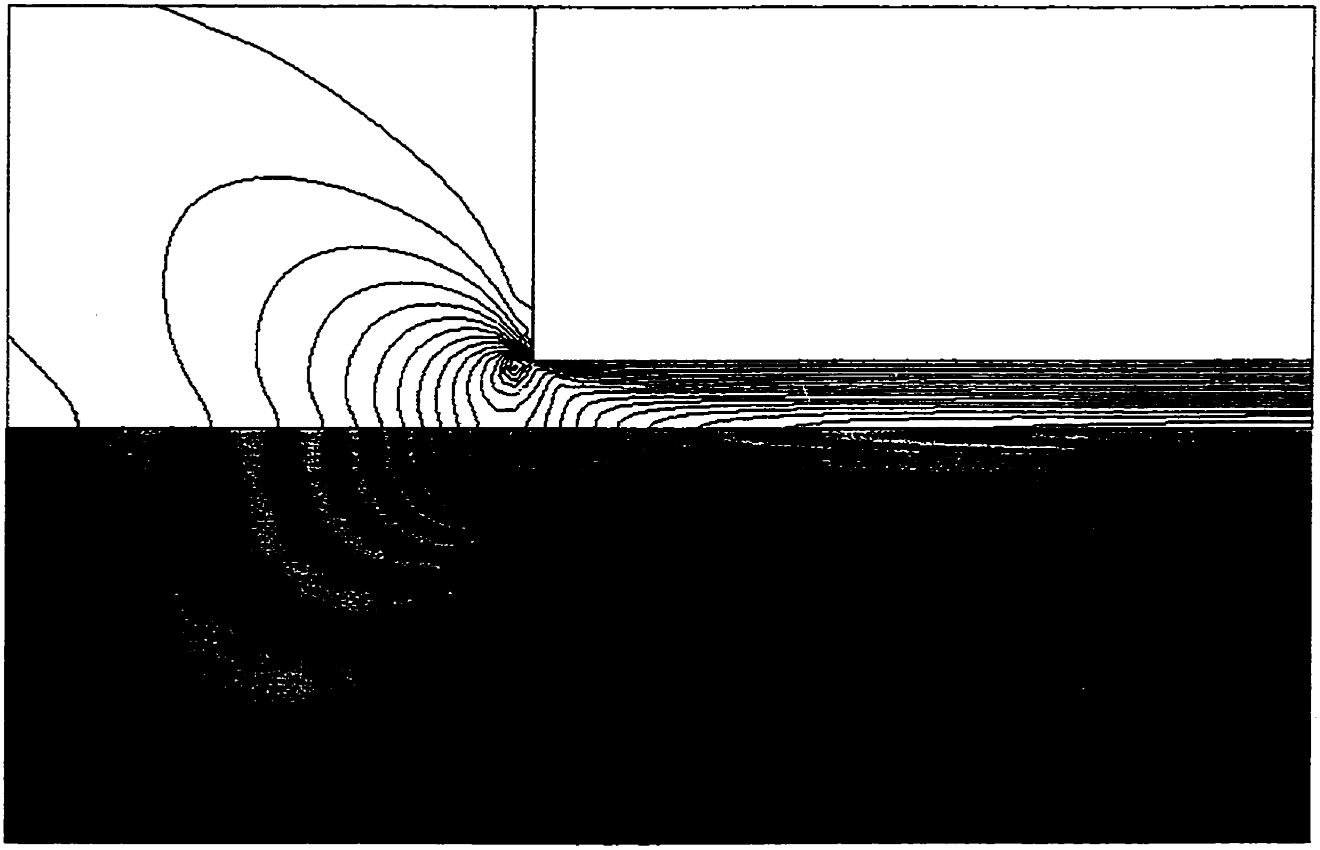

Figure 7-24 Comparison of Measured and Calculated Birefringence (PTT Model, $\dot{\gamma}_a = 56.4\ s^{-1}$).

To evaluate more quantitatively the performance of the models, we compare the calculated and measured birefringence on the axis of symmetry. In Figs. 7-25 to 7-27, we show the results of the three models for the three lowest apparent shear rates. The Carreau-Yasuda model gives clearly the poorest prediction; the normal stresses relax immediately, going to zero as soon as the streamlines become parallel in the channel. While the predictions of the velocity profiles were similar for the two viscoelastic models, they now differ considerably; the Leonov model gives a much better representation of the experimental birefringence, with the PTT model relaxing too fast in the channel, as was seen in the quantitative comparison on the entire flow domain. This fast relaxation is shown again for the highest apparent shear rate where we compare the predictions of the PTT and Carreau-Yasuda models.

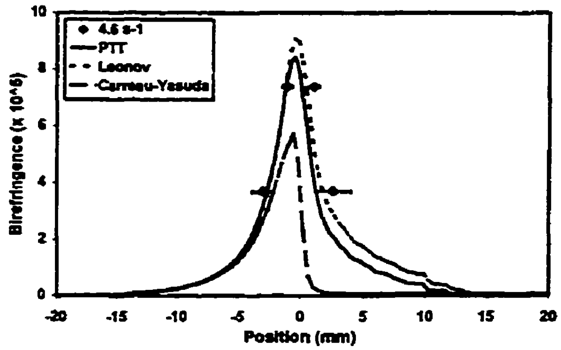

Figure 7-25 Predicted and Measured Birefringence on the Axis of Symmetry ($\dot{\gamma}_a = 4.6\,s^{-1}$).

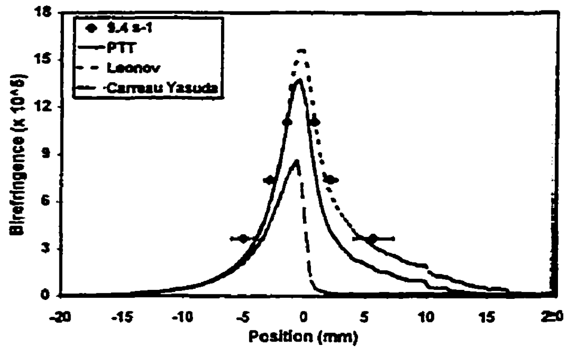

Figure 7-26 Predicted and Measured Birefringence on the Axis of Symmetry ($\dot{\gamma}_a = 9.4\,s^{-1}$).

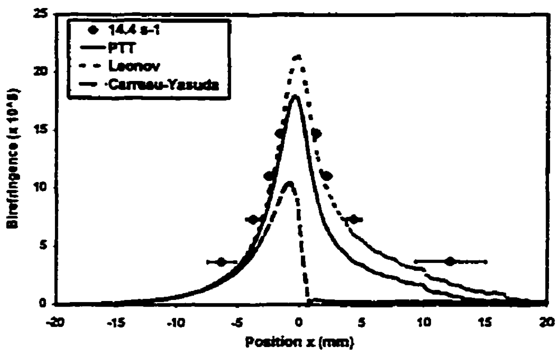

Figure 7-27 Predicted and Measured Birefringence on the Axis of Symmetry ($\dot{\gamma}_a = 14.4\,s^{-1}$).

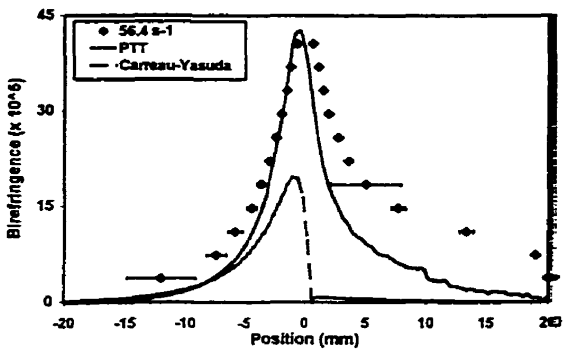

Figure 7-28 Predicted and Measured Birefringence on the Axis of Symmetry ($\dot{\gamma}_a = 56.4\,s^{-1}$).

We saw previously that there was no difference in the predictions of the pressure drop or the velocity when using the full spectrum vs. the truncated one. For the birefringence on the axis of symmetry, there is a small difference in the maximum birefringence if we use the full spectrum (Fig. 7-29). This difference amounts to 1.2 % at an apparent shear rate of 28.7 s^{-1}. Similarly, there is a small difference in the maximum birefringence between the predictions with the two meshes (Fig. 7-30) of 2.4 %. What is remarkable with the structured mesh is the smoothness of the curve and the absence of oscillations in the stresses.

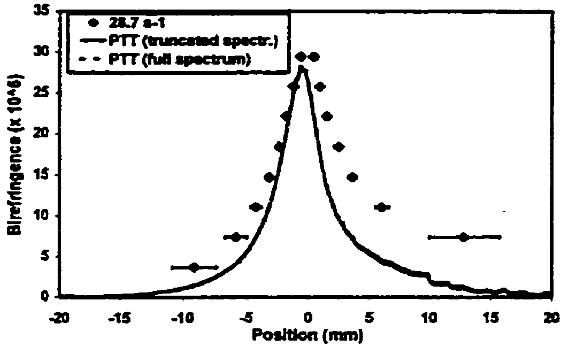

Figure 7-29 Influence of Spectrum on Birefringence ($\dot{\gamma}_a = 28.7\,\mathrm{s}^{-1}$).

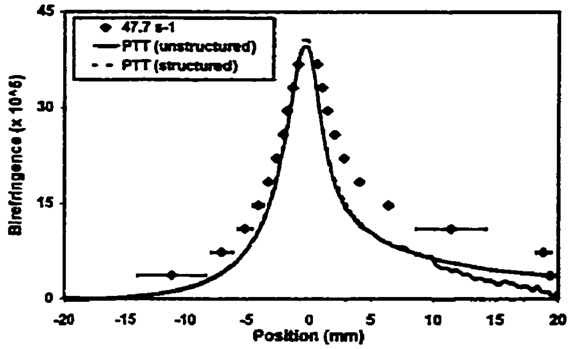

Figure 7-30 Influence of Mesh on Birefringence ($\dot{\gamma}_a = 47.7\,\mathrm{s}^{-1}$).

7.6 Discussion

In general, the results of simulations of planar abrupt contraction flow are disappointing. The model giving the most realistic representation of the experimental stresses, the simple Leonov model, is also the one posing the most serious numerical convergence problems. The predictions of total pressure drop by the viscoelastic models are good, but so are those of the strictly viscous Carreau-Yasuda model. The viscous model is also able to give an excellent prediction of the velocity field when there is no strong elongational component. However, when this component becomes important, even the viscoelastic models have difficulty in capturing all aspects of the behavior of the melt.

Noting the rapid change in the flow field near the contraction, we did a sensibility study in this region to evaluate the effect of a small error in Δx on the velocity profile. We looked at the predicted velocity fields assuming the position of the measurement was in error by $\pm$ 0.5 mm in x at positions 2 and 3 in the reservoir. The results of the study are shown in Figs. 7-31 and 7-32. Surprisingly, the predicted velocity profiles are now in perfect agreement with the measurements. This shows that results of the simulations in terms of velocity might be better than originally thought, and that a small error in the measurement position where the flow is changing rapidly can result in a large error in velocity.

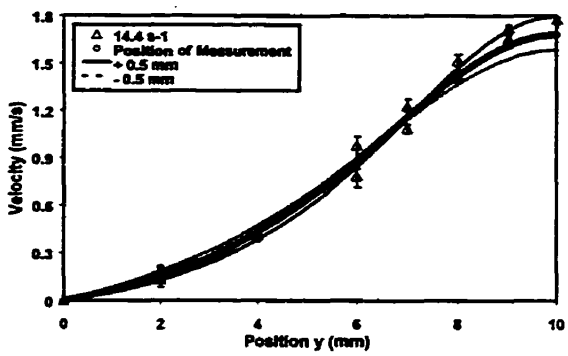

Figure 7-31 Influence of Δx on Velocity Profile (reservoir, position 2).

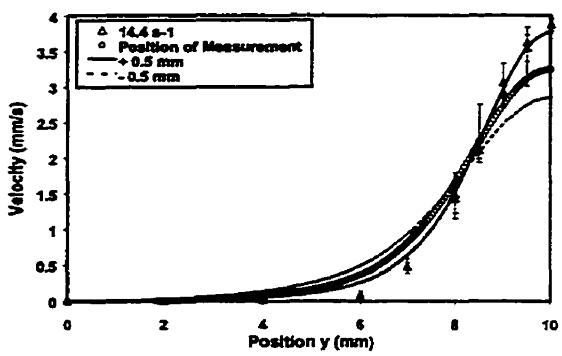

Figure 7-32 Influence of Δx on Velocity Profile (reservoir, position 3).

It was also concluded that there is little advantage in working with the full spectrum vs. the truncated spectrum. Of course, there is a limitation on the amount of truncation that can be done before starting to loose information about the material. Our truncation was sufficient to facilitate numerical convergence without affecting the predictions of the variables studied.

The faster relaxation of the stresses in the channel predicted by the PTT model in comparison with the experiments was also observed by Beraudo[7] and Schoonen[8]. It is hard to say why the model behaves in this way. For one thing, the parameter that controls elongation, ε, was determined from uniaxial elongation experiments, while we applied it to a flow where the elongation is planar. Furthermore, this parameter was determined at low extension rates, while this rate can become quite large in the actual flow situations. For example, at the highest apparent shear rate (56.4 s^{-1}) the extension rate on the axis of symmetry reaches a value of 8 s^{-1} near the contraction (x=0), as seen in Fig. 7-33.

Finally, the fact that we had a ratio of W/H < 10 neither in the reservoir nor in the channel may invalidate the assumption of 2D flow. This could explain the difference between the shape of the predicted fringes in the reservoir ("butterfly" shape) and the experimental ones, which are rounder[9].

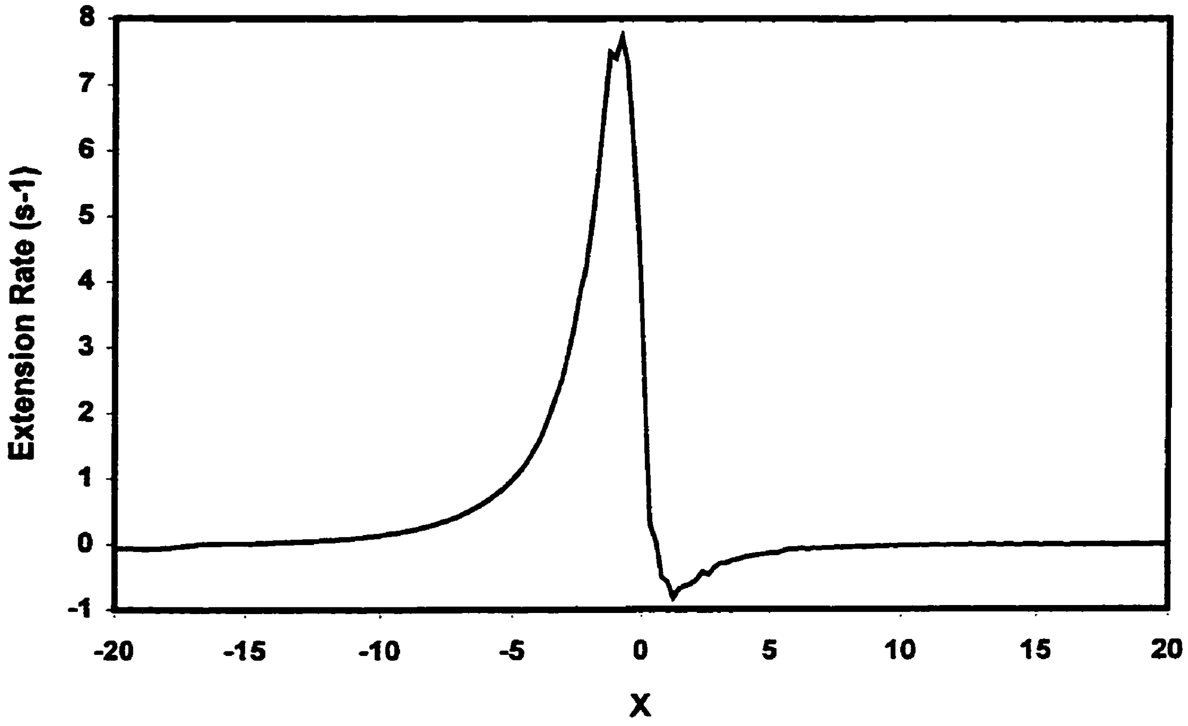

Figure 7-33 Extension Rate on the Axis of Symmetry ($\dot{\gamma}_a = 56.4\ s^{-1}$).

REFERENCES

[1] Beaufils P., Vergnes B., Agassant J.F., " Characterization of the Sharkskin Defect and its Development with the Flow Conditions ", *Int. Polym. Process.*, IV(2), p. 78-84 (1989)
[2] Wales J.L.S., " The Application of Flow Birefringence to Rheological Studies of Polymer Melts ", Ph.D. Thesis, Delft University of Technology, The Netherlands (1976)
[3] Durst F., Melling A., Whitelaw J.H., " Principles and Practice of laser-Doppler Anemometry ", *Academic Press*, 2nd edition (1981)
[4] Gavrus L., "Étude du comportement des polyéthylenes: Biréfringence d'écoulement et anémometrie laser", rapport d'étape, École Nationale Supérieure des Mines de Paris, Sophia Antipolis, France (1995)
[5] Dealy J.M., Wissbrun K.F., "Melt Rheology and its Role in Plastics Processing", *Van Nostrand Reinhold*, New York (1990)
[6] McHugh A.J., Mackay M.E., Khomani B., " Measurements of Birefringence by the Method of Isoclinics ", *J. Rheol.*, 31(7), p. 619-634 (1987)
[7] Beraudo, C., "Méthodes éléments finis pour la simulation numérique d'écoulements de fluides viscoelastiques de type différentiel dans des géométries convergentes", Ph.D. thesis, École Nationale Supérieure des Mines de Paris, Sophia Antipolis, France (1995)
[8] Schoonen J.F.M., " Determination of Rheological Constitutive Equations using Complex Flows ", Ph.D. thesis, Technische Universiteit Eindhoven, Eindhoven, The Netherlands (1998)
[9] Baaijens F.P.T., private communication (1999)

8. Axisymmetric Entrance Flow and Extrudate Swell of Linear Low-Density Polyethylene

8.1 Experimental Methods

8.1.1 Capillary Extrusion

Extrusion experiments were carried out in a constant speed, piston-driven capillary rheometer, as described in section 4.2.2. Circular dies with a 90° tapered entrance angle of 1.4 mm diameter and three L/D ratios were used (4.75, 9.5, 19.0). We also included in the study a longer die (L/D=38.0) for the extrudate swell experiments, in order to ensure fully developed flow at the exit. A schematic view of the rheometer is shown in Fig. 8-1. In this instrument, the apparent wall shear rate is related to the flow rate, and the wall shear stress to the force measured by the load cell. All the experiments were carried out at 150 ± 1°C and at apparent shear rates between 2.22 and 88.8 s^{-1}. The quantities measured are the total pressure drop given by the load cell, the entrance pressure drop, inferred from a Bagley plot or measured directly for an orifice die (see Fig. 4-3), and the extrudate swell. The experimental set-up for the extrudate swell measurement is described in the next section.

8.1.2 Extrudate Swell Measurement

The die swell experiments were also performed at 150°C and apparent shear rates from 2.22 to 88.8 s^{-1}. The ratio measured is the time-dependent extrudate swell $B(t)$, defined as:

Eqn. 8-1 $$B(t) = D_e(t) / D_c$$

where D_c is the capillary diameter and $D_e(t)$ is the diameter of the extrudate, which is a function of time. In addition to the capillary rheometer, the experimental apparatus to measure die swell consists of a thermostating chamber, an optical detection system and a data acquisition system. For the accurate measurement of the diameter of a soft, delicate, hot, and moving object, a non-contacting sensor must be used. In this work an optical system was used, consisting of a photodiode array and a 2 mW He-Ne laser beam. This system was designed by Samara[1].

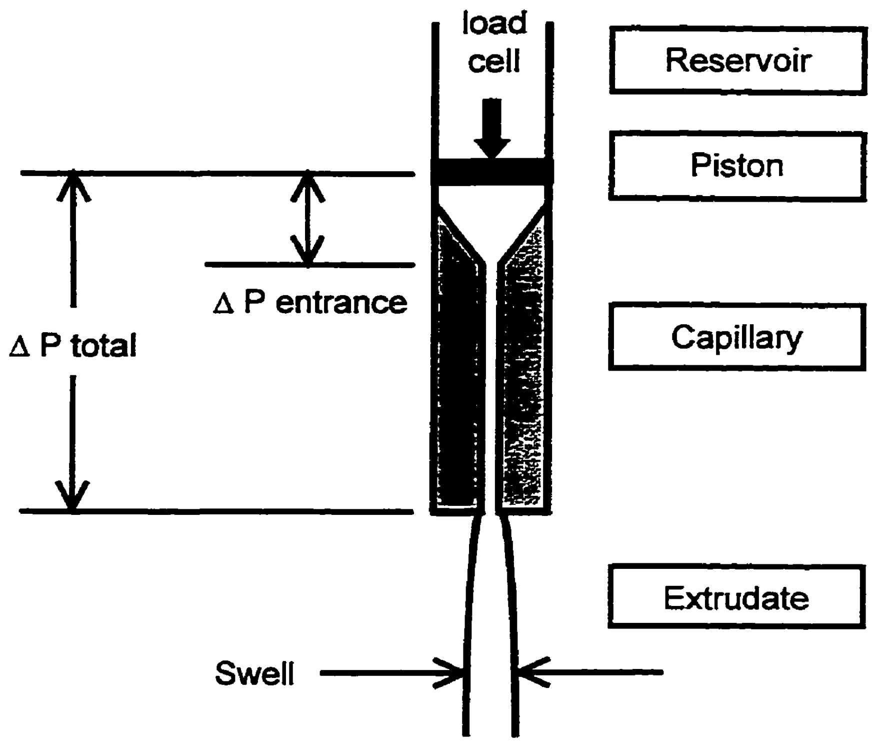

Figure 8-1 Capillary Rheometer.

A schematic view of the experimental apparatus is shown in Fig. 8-2. To measure die swell, the resin is extruded from the die into a thermostating chamber. An expanded and collimated laser beam is used as a back-light source to cast a shadow of the polymeric extrudate onto a linear photodiode array. An achromatic lens magnifies this shadow. The electrical signal from the photodiode array is then processed using a specially designed circuit. The data logger we used was designed to enable real time acquisition of data using a microcomputer.

Two problems can arise during extrusion of polymer directly into air. First, extrusion into ambient air leads to premature freezing and the development of frozen-in stresses. Second, if the polymer is extruded into a heated oven, it will sag under its own weight. The use of an oil-filled thermostating chamber eliminates both of these problems. The thermostating chamber is composed of a stainless steel container, an outer compartment, and two rectangular stainless steel inner compartments. The inner compartments were equipped with two quartz windows each to allow the laser beam to pass through. The chamber was equipped with two plug-screw 300 watt immersion heaters. A temperature controller, operating in conjunction with a thermocouple, was used to control and monitor the temperature in the inner compartments.

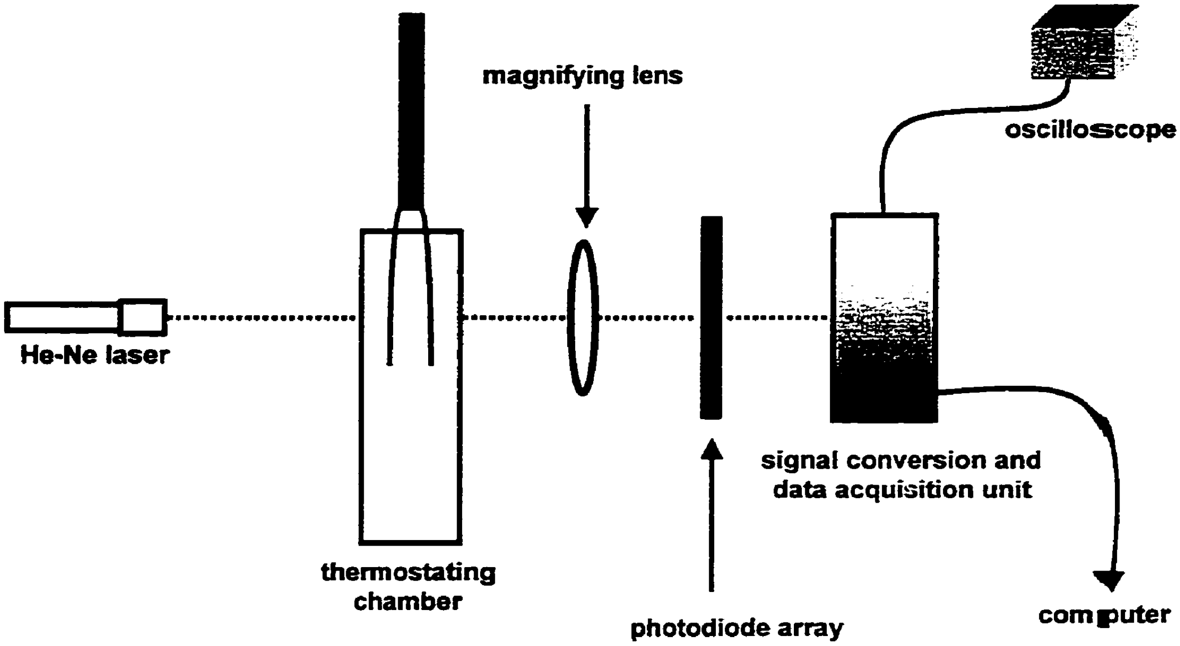

Figure 8-2 Experimental Setup for Extrudate Swell Measurements.

The outer compartment was filled with 200 centistokes (cS) silicone oil (200® Fluid from Dow Corning). The inner compartments contained a mixture of silicone oils, mainly 2 cS and 5 cS Dow Corning 200® Fluid. The oils were mixed in proportions found by trial-and-error to achieve a density slightly lower than that of the melt at the test temperature. We found that a 52 % - 48 % by volume mixture of 2 cS - 5 cS gave the best results. We also determined the small amount of swell due to the oil and subtracted it from the measured swell. This procedure is discussed in section 8.5.1. Note that the maximum temperature to which the oils could be heated was 150°C, which explains the selection of the operating temperature for the experiments. A complete description of the experimental apparatus and procedure can be found in reference 1.

8.2 Numerical Procedure

8.2.1 Meshes

Simulations of entrance pressure drop and extrudate swell were performed separately. The boundary conditions of fully developed flow were used for the extrudate swell simulation so that it could be decoupled from the flow in the reservoir.

Two meshes were used for the axisymmetric entrance flow simulations in order to verify mesh independence of the solutions. Both meshes are composed of triangular elements and are unstructured. Several meshes were tested for extrudate swell, but it was possible to obtain numerical convergence at our test conditions on only one of them. This mesh is also unstructured and made of triangular elements. The number of elements for each mesh is presented in Table 8-1, and the meshes are shown in Figs. 8-3, 8-4 and 8-5.

Table 8-1 Mesh Characteristics for Axisymmetric Flow Simulations

Mesh	Axi_1	Axi_2	Swell_1
Number of Elements	Unstructured 1611	Unstructured 3402	Unstructured 1822

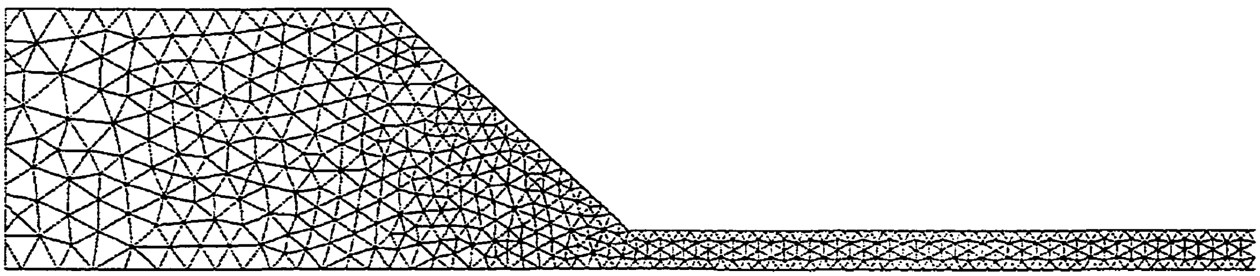

Figure 8-3 Mesh Axi_1.

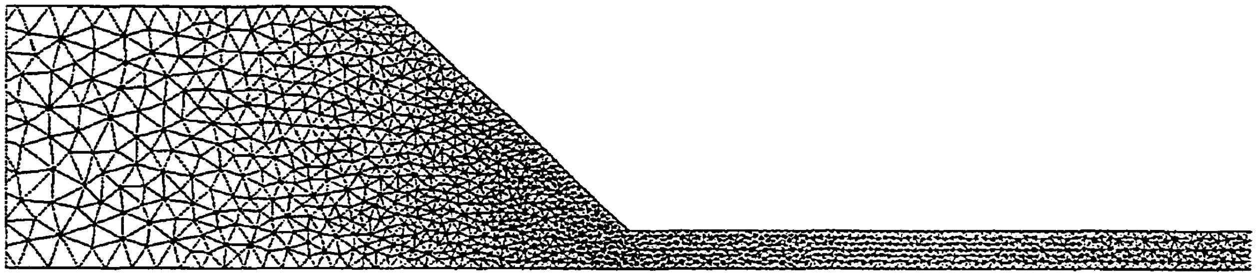

Figure 8-4 Mesh Axi_2.

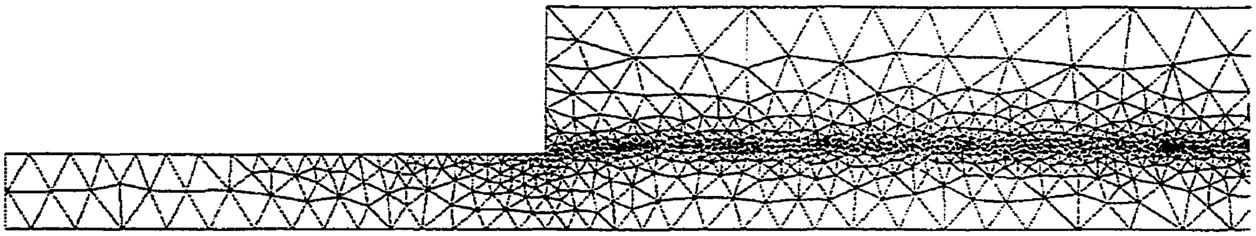

Figure 8-5 Mesh Swell_1.

8.2.2 Viscoelastic Converged Solutions

Numerical convergence can be easily summarized for the axisymmetric entrance flow simulations. The PTT model gave converged solutions for all seven experimental flow rates, on both meshes and with both the full and truncated spectra shown in Table 4-3. On the other hand, it was impossible to obtain a converged solution with the simple Leonov model for any of these conditions at one of the experimental flow rates.

For extrudate swell simulations, a peculiar behavior was observed with the simple Leonov model. As we slowly increased the flow rate from Newtonian behavior to viscoelastic, the ultimate swell ($t \rightarrow \infty$) started to decrease from its Newtonian value of 13 %. This behavior is shown in Fig. 8-6 (mesh Swell_1, truncated spectrum). A similar observation has been reported by Rekers[2]. However, we lost convergence at a very low shear rate, and it was not possible to verify if this trend was continuing at higher shear rates. We present below a map of the converged solutions for the various cases of entrance flow and extrudate swell. It is expressed in terms of the number of flow rates converged, where the maximum is seven.

Table 8-2 Converged Solutions with the PTT Model (max=7)

Spectrum	Mesh		
	Axi_1	Axi_2	Swell_1
Full	7	7	0
Truncated	7	7	1

Table 8-3 Converged Solutions with the Simple Leonov Model (max=7)

Spectrum	Mesh		
	Axi_1	Axi_2	Swell_1
Full	0	0	0
Truncated	0	0	0

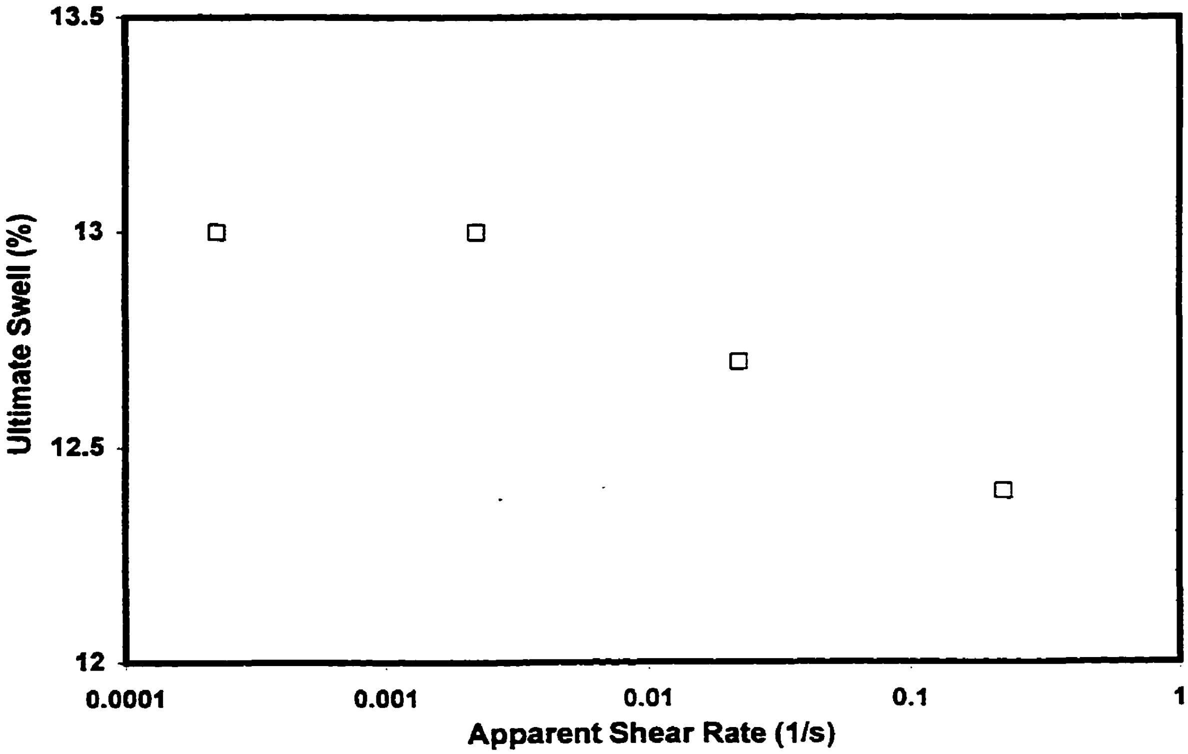

Figure 8-6 Ultimate Swell Predicted by the Simple Leonov Model.

8.3 Total Pressure Drop

The numerical results presented here were obtained with the PTT and Carreau-Yasuda models. We compare the calculated and experimental total pressure drop for an L/D of

19.0, since the viscosity was thought to be affected by the pressure with the L/D of 38.0, and pressure effects are not included in the finite element model. The predicted total pressure drop was evaluated as follows:

Eqn. 8-2
$$\Delta P_{calc} = P_{reservoir} - P_{L/D=19}$$

In Fig. 8-7, the results of both models are compared to measured values. The calculated pressures are slightly underestimated at high shear rates, especially by the Carreau-Yasuda model, but in general the agreement is good. Since the melt is predominantly in shear flow, even the strictly viscous model can give a good approximation of the total pressure drop. In Fig. 8-8, we compare the predictions of the PTT model with the full and the truncated spectra, and we see that they agree very well. Finally, mesh independence is demonstrated in Fig. 8-9.

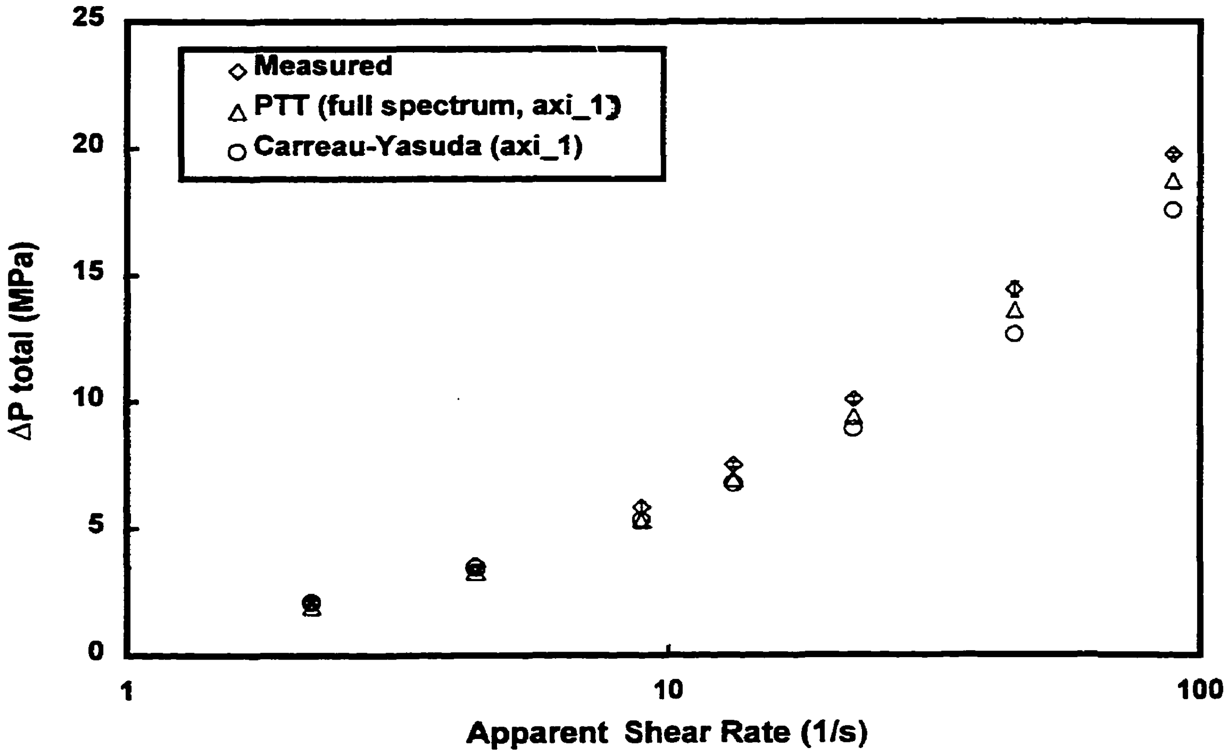

Figure 8-7 Comparison of Predicted Total Pressure Drop with Experimental Values.

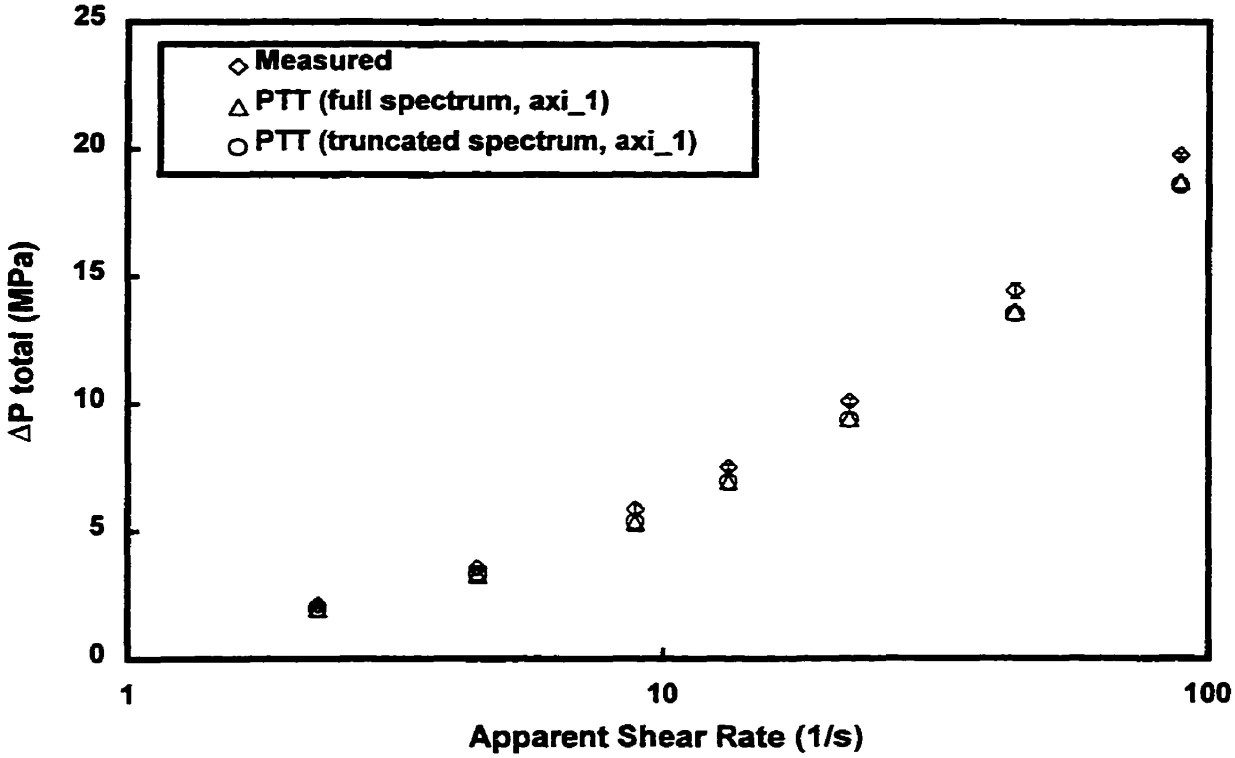

Figure 8-8 Influence of Discrete Spectra on Prediction of Total Pressure Drop.

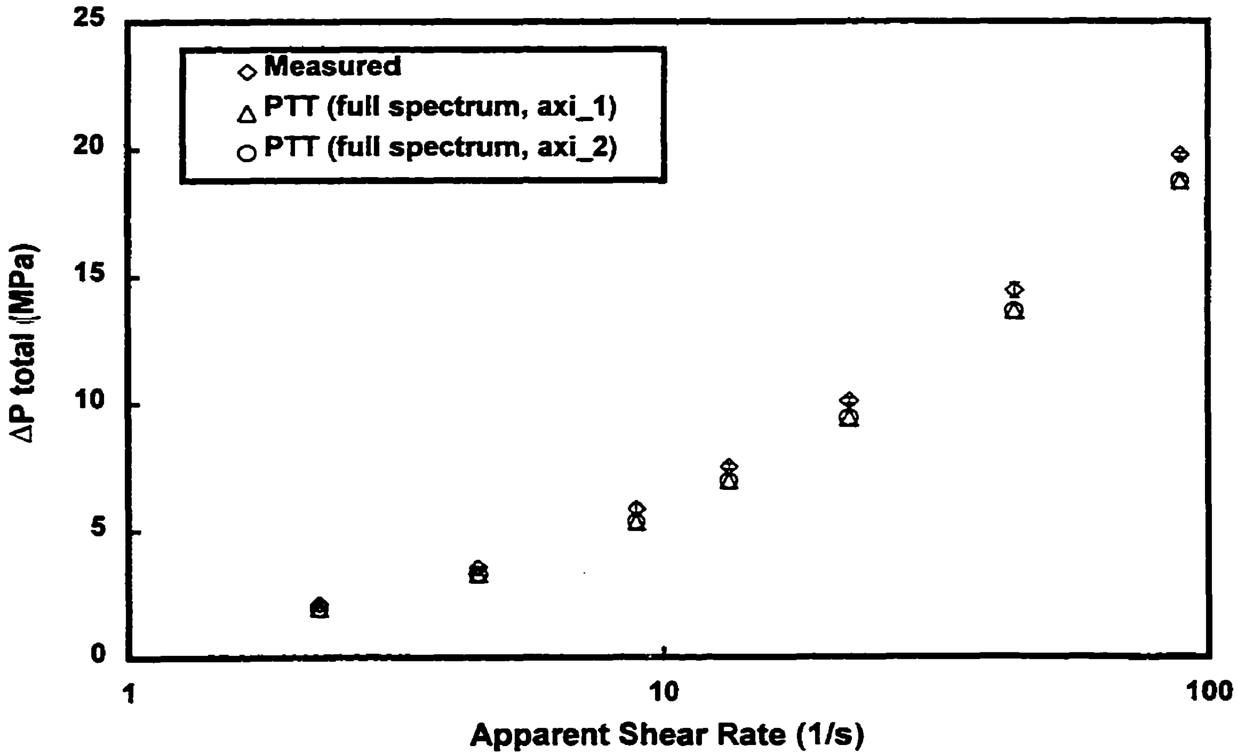

Figure 8-9 Mesh Independence on Prediction of Total Pressure Drop.

8.4 Entrance Pressure Drop

In the entrance region the melt undergoes both shear and elongation, so we expect to see a difference between the predictions of the viscoelastic and the viscous models. Fig. 8-10 shows the measured values of the entrance pressure drop along with the predictions of both models. The predicted entrance pressure drop was evaluated as follows:

Eqn. 8-3
$$\Delta P_{calc} = P_{reservoir} - P_{L/R=0.5}$$

The Carreau-Yasuda model underestimates the entrance pressure drop, as expected because of the strong elongational component of the flow. For example, at the highest apparent shear rate (88.8 s^{-1}) the extension rate on the axis of symmetry reaches a value of 22 s^{-1} near the contraction (x=0), as seen in Fig. 8-11. The oscillations in $\dot{\varepsilon}$ after the contraction are typical of results obtained on unstructured meshes when using the discontinuous Galerkin method[3]. However, the PTT model also underestimates the entrance pressure drop by about 50%. Earlier simulations of entrance flow have also produced entrance pressure drops well below those observed experimentally[4,5,6,7,8]. In Fig. 8-12, we compare the predictions of the PTT model with the full and truncated spectra, and we see again that they agree well. Finally, mesh independence is demonstrated in Fig. 8-13.

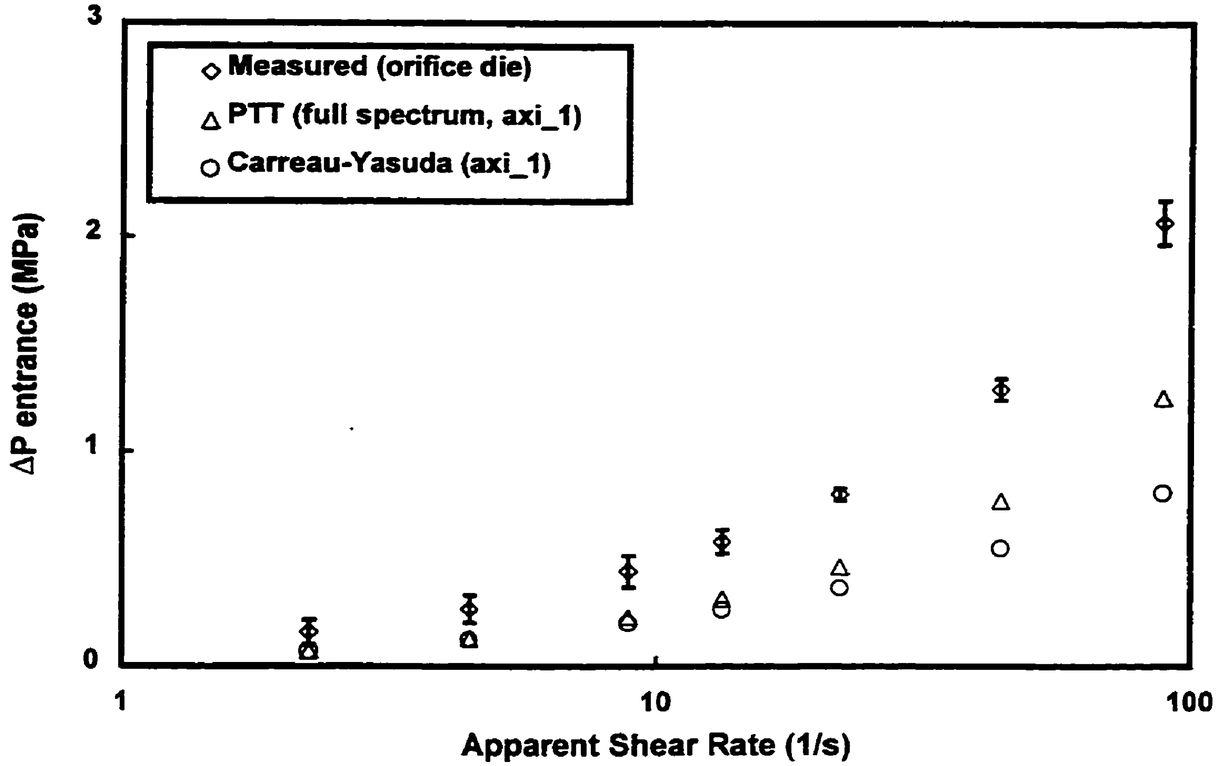

Figure 8-10 Comparison of Predicted Entrance Pressure Drop with Experiments.

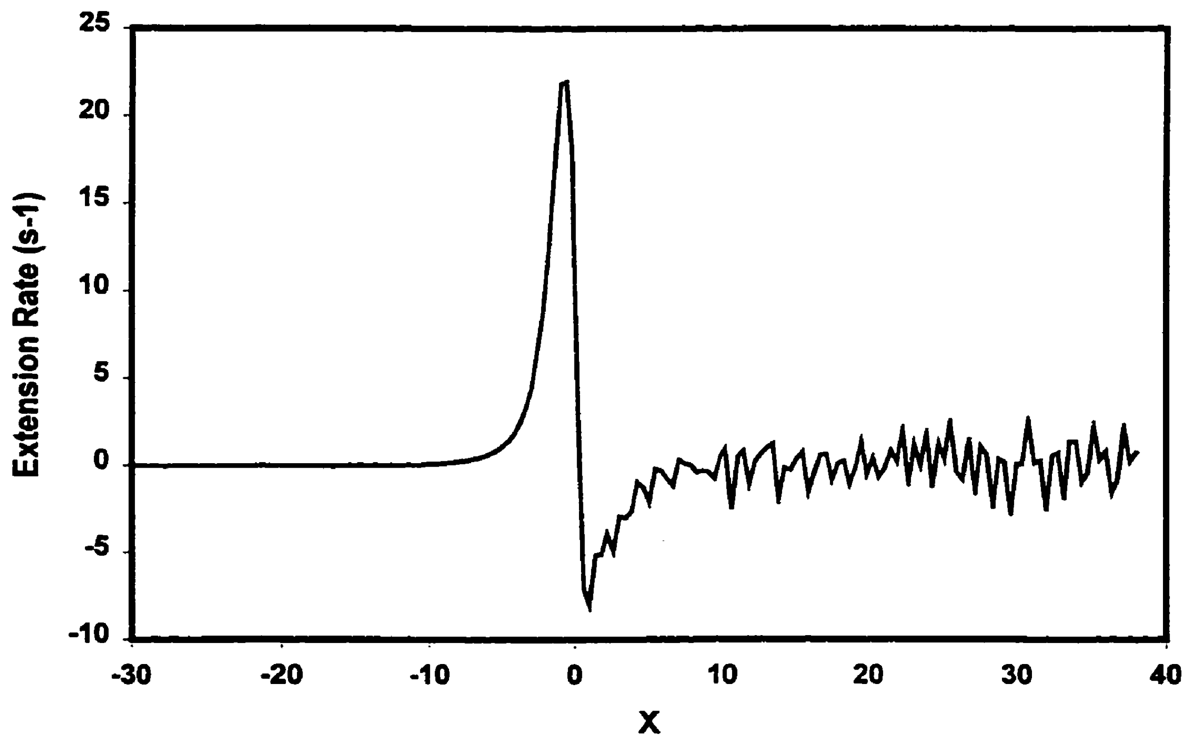

Figure 8-11 Extension Rate on the Axis of Symmetry ($\dot{\gamma}_a = 88.8\,s^{-1}$).

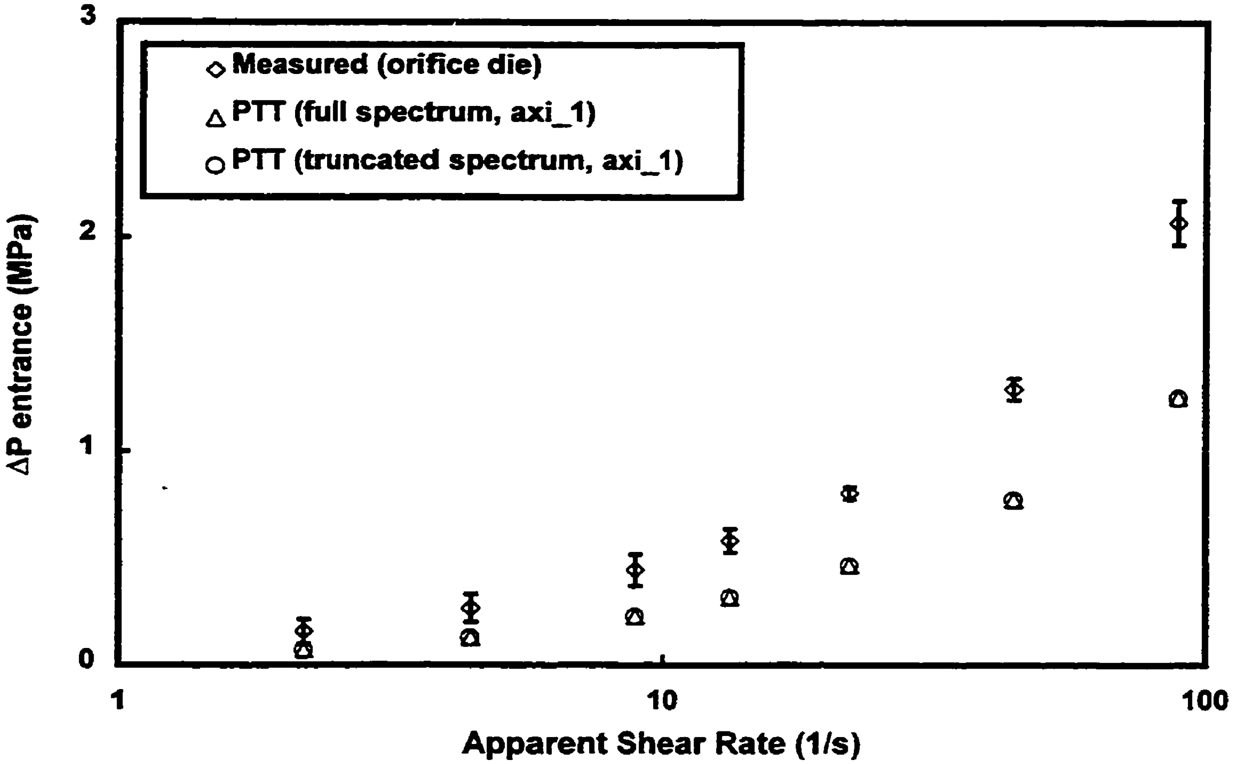

Figure 8-12 Influence of Discrete Spectrum on Prediction of Entrance Pressure Drop.

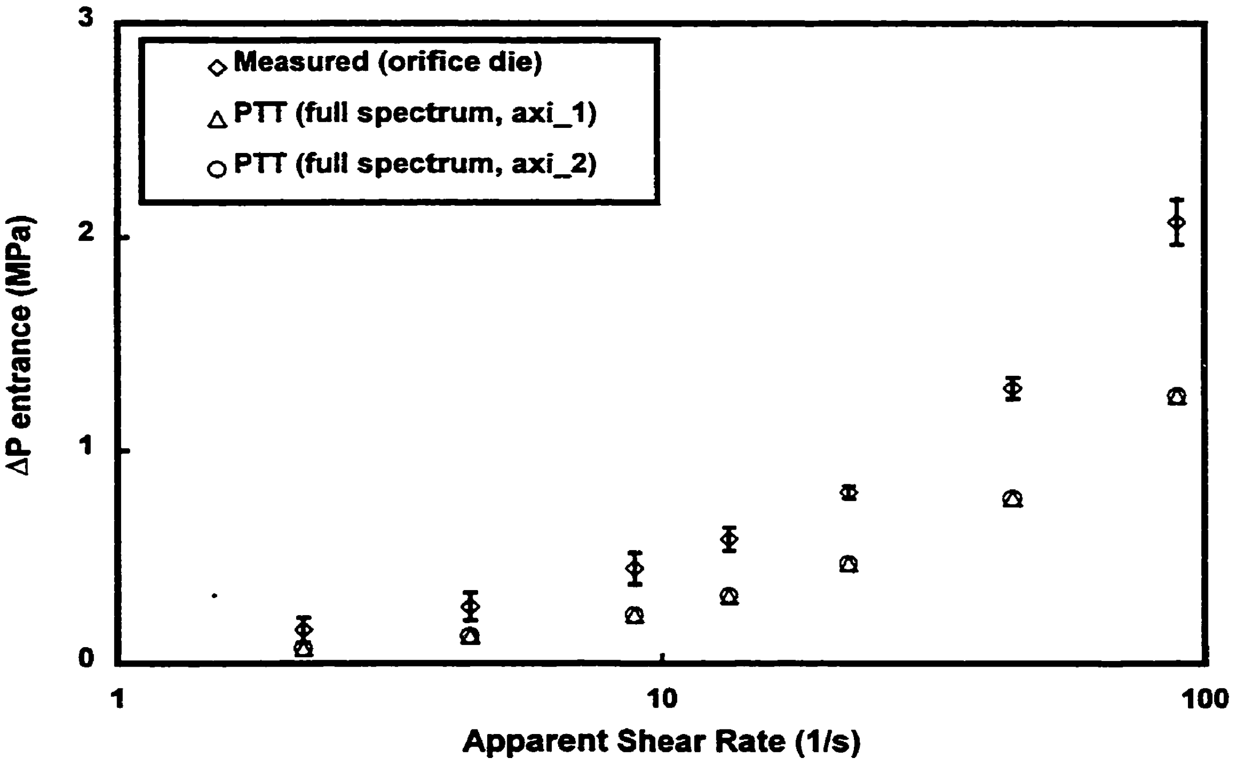

Figure 8-13 Mesh Independence on Prediction of Entrance Pressure Drop.

8.5 Extrudate Swell

8.5.1 Experimental Results

The measurements were made with an L/D of 38.0 to ensure fully developed flow at the die exit. Comparisons with swell data for L/D = 19.0 showed that fully developed flow was not reached in the shorter die since swell was larger. Fig. 8-14 shows the measured swell as a function of time for the seven apparent shear rates.

Utracki et al.[9,10] have found that Dow Corning 200® fluid silicone oils do not swell polyethylene if medium viscosity grades (50 cS and 100 cS) are used. However, some interaction between the oil and polymer occurs when low viscosity grades are used with polyethylene. In the present study, a mixture of low viscosity grades of silicone oil was used (2 cS and 5 cS) in order to provide an oil density slightly lower than the polymer melt density. The swell due to the oil was measured so that it could be subtracted from the measured swell using a method similar to that of reference 1. The resin was extruded directly into air at an apparent wall shear rate of 13.3 s^{-1}. Cut extrudate strips were annealed for 30 minutes in an oven at 150°C in a bath of 500 cS silicone oil. We verified that the high viscosity oil was not absorbed by the polymer by weighing the sample before and after annealing. The annealed samples were placed in the thermostated chamber, and extrudate swell was measured at 150°C using the apparatus. It seems reasonable to assume that after annealing, all the stresses are relaxed and the equilibrium swell is reached. Consequently, any additional swell would be due to interaction with the oil. The oil swell curve is shown at the bottom of Fig. 8-14. This swell was subtracted from all the extrudate swell measured values. This is shown in Fig. 8-15 for the apparent shear rate of 88.8 s^{-1}. In this way the net swell without the effect of oil was obtained. We assumed that the oil absorption effect was the same at all shear rates.

No data are available at short times for the lowest apparent shear rates in Fig. 8-14. The method used does not allow an accurate capture of the instantaneous swell that occurs in the first seconds of extrusion for these rates, because a significant time is required for the sample to reach the viewing chamber at these shear rates. Finally, the ultimate net swell, obtained at long times, is shown in Fig. 8-17 as a function of apparent shear rate.

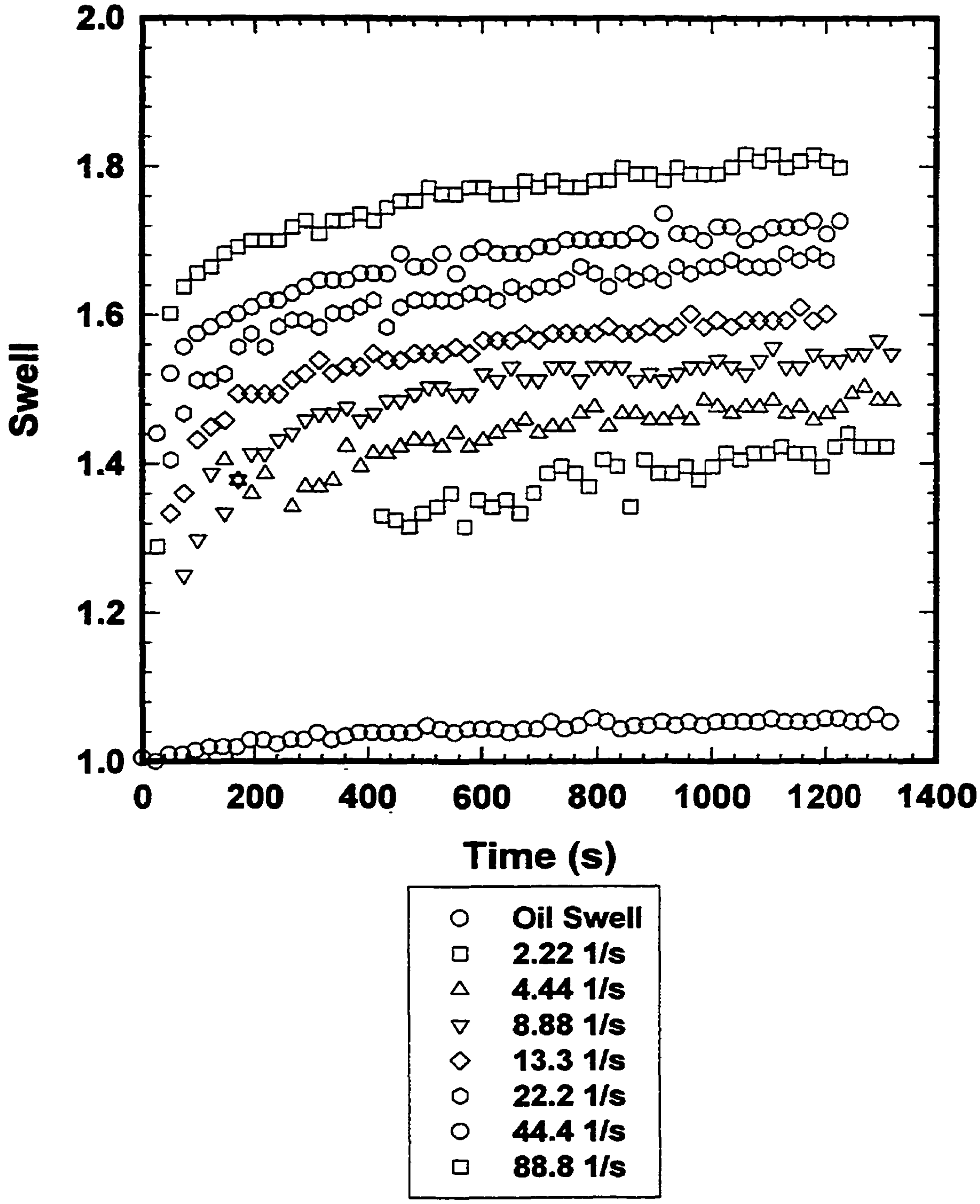

Figure 8-14 Total Swell and Oil Swell as a Function of Time.

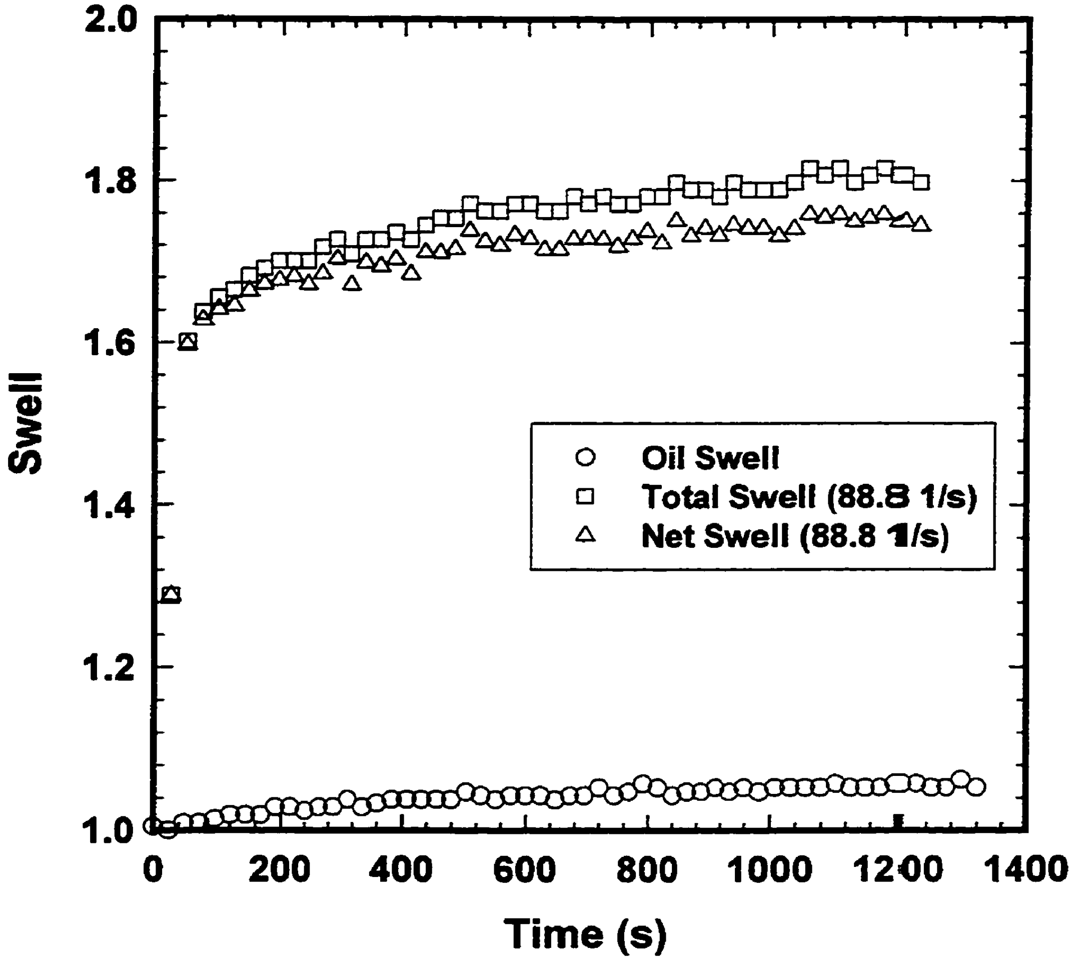

Figure 8-15 Net Swell as a Function of Time after Oil Swell Subtraction.

8.5.2 Comparison with Simulations

As was mentioned in section 8.2.2, it was not possible to calculate the viscoelastic swell for most conditions, although the Newtonian swell (13 %) was easily calculated on several meshes. The Leonov model was discarded early, first because of its pathological prediction of decreasing swell, and second because of numerical convergence problems. With the PTT model, which showed almost no convergence problems in other situations, we were able to obtain a converged solution only for the lowest apparent shear rate (2.22 s^{-1}) and only on one mesh. In Fig. 8-16, we show the predicted interface calculated on mesh Swell_1 with the truncated spectrum. The ultimate swell (20 %), shown in Fig. 8-17 along with experimental values, is almost half of the measured swell for that flow condition (37 %). The experimental ultimate swell data is presented in the appendix. Since we could not obtain a converged solution using the full spectrum, it is not possible to know at this time if the low calculated swell is related to the use of the truncated spectrum. As mentioned previously in section 2.4.3, extrudate swell depends strongly on molecular weight distribution, i.e. on the detailed spectrum.

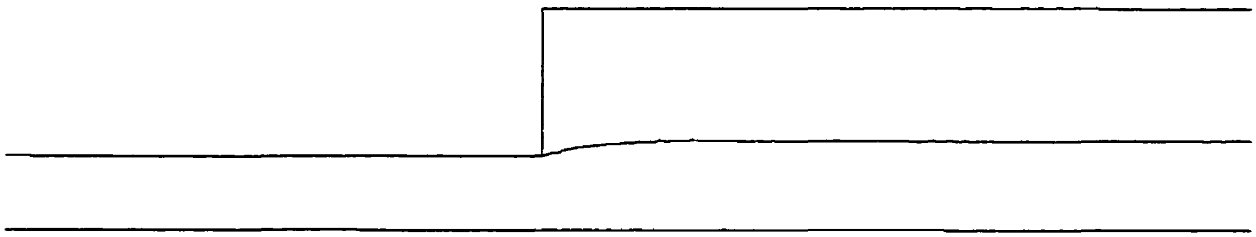

Figure 8-16 Calculated Interface with PTT Model (truncated spectrum, mesh Swell_1).

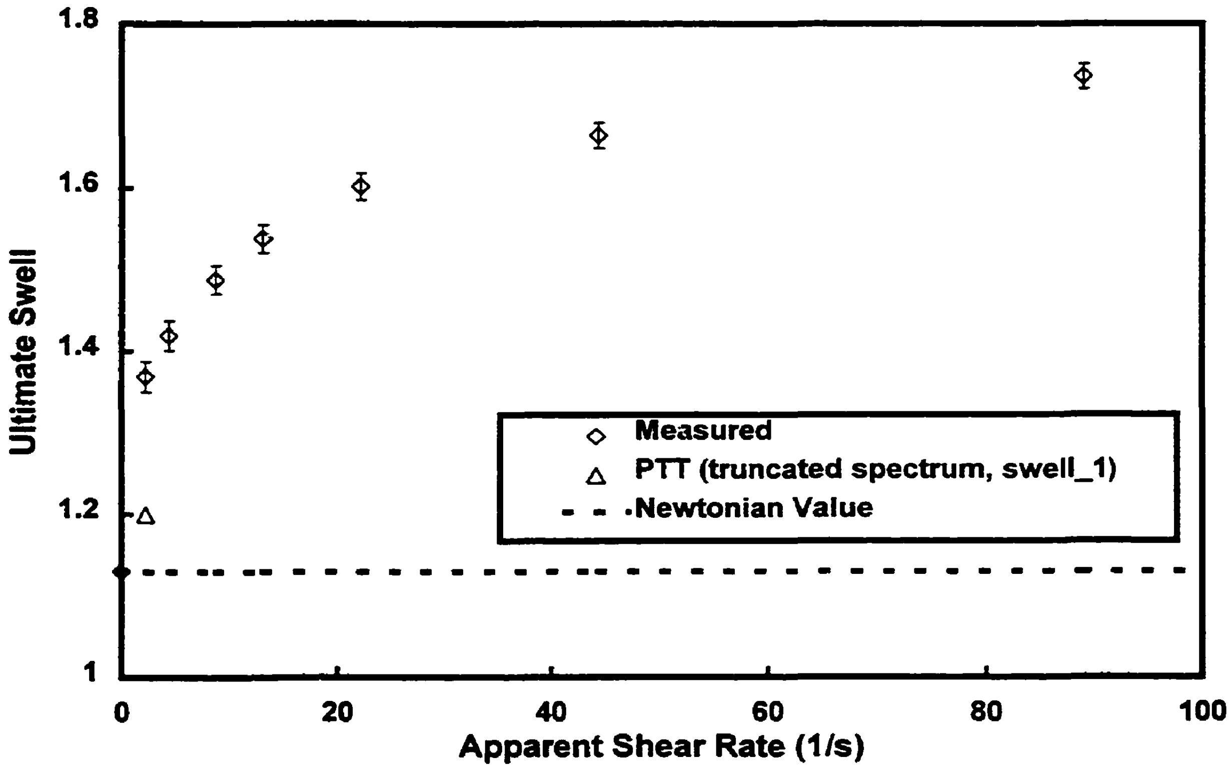

Figure 8-17 Measured and Predicted Ultimate Swell.

8.6 Discussion

In general, the results of simulations of axisymmetric entrance flow and extrudate swell are disappointing. The performance of the simple Leonov model is much worse than in the planar case, in terms of numerical convergence problems and the prediction of decreasing swell. The Leonov model gave realistic predictions for planar contraction flow (see Chapter 7) but was not useful for axisymmetric extrudate swell.

The PTT model was much easier to work with in terms of numerical convergence for the prediction of entrance flow but not for the free surface flow. The predictions of total pressure drop are good, but so are those of the strictly viscous Carreau-Yasuda model. Predictions of entrance pressure drop are largely underestimated, even with the viscoelastic PTT model. We also tried using ε=0 in the simulations, which gives the strongest strain-hardening behavior in elongation, but this only increased the prediction of the entrance pressure drop by 6 %. This poor performance is similar to what is seen in planar flow for velocity fields with a strong elongational component (section 7.4). At this time, it is difficult to say why this is so. There are two possibilities: either the models are inappropriate, or the parameters determined in simple flows can not reproduce the features of complex flows. However, the models must also be correct for the simple flows. We also note that the elongation rate in the flow simulated can be much larger than the range of extension rates for which it was possible to fit the viscoelastic model parameters.

Beraudo[7] suggested that the most appropriate quantity to be compared with the measured pressure is the *rr* component of the Cauchy stress tensor, evaluated at the wall. Using this suggestion for the orifice die, we have:

Eqn. 8-4

$$\Delta P_{calc} = -\sigma_{rr\,reservoir} + \sigma_{rr\,L/R=0.5} = P_{reservoir} - P_{L/R=0.5} + \Delta\tau_{rr}$$

where $\Delta\tau_{rr} = \tau_{rr\,L/R=0.5} - \tau_{rr\,reservoir}$

The contribution of the extra stress difference, $\Delta\tau_{rr}$, is negative and decreases the computed entrance pressure drop by 3-4 %, thus increasing the discrepancy with the measured values.

Finally, for the free surface prediction, the difficulty was not with the calculation of the free surface position itself but in trying to converge the extra stresses for a fixed position of the interface. We also tried an alternative to the use of the pseudo-concentration, where the interface is modeled by a function h (for height) calculated from the velocity profile.

Eqn. 8-5
$$\frac{\partial h}{\partial t} + u_1 \frac{\partial h}{\partial x} = u_2$$

But this did not facilitate the convergence of the extra stresses and failed to give a converged solution for any of our experimental conditions.

REFERENCES

[1] Samara M.K., " Design and Construction of Computerized Die Swell Apparatus ", Master's Thesis, McGill University, Montreal, Canada (1985)
[2] Rekers G., " Numerical Simulation of Unsteady Viscoelastic Flow of Polymers ", Ph.D. Thesis, University of Twente, Twente, The Netherlands (1995)
[3] Lioret A., " Méthodes d'Éléments Finis Adaptative pour les Écoulements de Fluides Viscoélastiques », Master's Thesis, École Polytechnique de Montréal, Montréal, Canada (1998)
[4] Guillet J., Revenu P., Béreaux Y., Clermont J.-R., "Experimental and Numerical Study of Entry Flow of Low-Density Polyethylene Melts", *Rheol. Acta,* 35, p. 494-507 (1996)
[5] Fiegl K., Öttinger H.C., " The Flow of a LDPE Melt through an Axisymmetric Contraction: A Numerical Study and Comparison to Experimental Results ", *J. Rheol.,* 38(4), p. 847-874 (1994)
[6] Mitsoulis E., Hatzikiriakos S.G., Christodoulou K., Vlassopoulos D., "Sensitivity Analysis of the Bagley Correction to Shear and Extensional Rheology", *Rheol. Acta,* 37, p. 438-448 (1998)
[7] Beraudo C., "Méthodes éléments finis pour la simulation numérique d'écoulements de fluides viscoelastiques de type différentiel dans des géométries convergentes", Ph.D. thesis, École Nationale Supérieure des Mines de Paris, Sophia Antipolis, France (1995)
[8] Hatzikiriakos S.G., Mitsoulis E., "Excess Pressure Losses in the Capillary Flow of Molten Polymers", *Rheol. Acta,* 35, p. 545-555 (1996)
[9] Utracki L.A., Catani A., Lara J., Kamal M.R., "Polymer Processing and Properties", G. Astarita and L. Nicolais, eds., Capri, Italy, p. 79 (1983)
[10] Utracki L.A., Lara J., Intern. Workshop on *Extensional Flows,* Mulhouse-La Bress, France (1983)

9. Alternative Approaches

In order to optimize the design of plastics processing equipment and the processability of plastics resins other than by trial and error, it is necessary to have a reasonably accurate model of the process of interest. However, the numerous difficulties involved in viscoelastic flow simulation have led to the development of alternative approaches that avoid the explicit modeling of fluid elasticity. These make use of specific material functions, particularly viscosity, normal stress differences and elongational viscosity. Highly simplified constitutive models are used, which are strictly valid only in steady simple shear or elongational flows and employ empirical equations fitted to experimental data.

In this chapter, we describe several of these simplified approaches and propose the use of a rule-based expert system as an alternative to full viscoelastic flow simulations.

9.1 Viscometric Flow

The viscometric flow approximation has been used successfully by Vlachopoulos et al.[1,2,3,4]. This is based on the observation that most polymer processing operations involve flow in channels where there is a main flow direction such that the streamlines are almost parallel, therefore justifying the treatment of the flow as locally viscometric. This approach is based on the Criminale-Ericksen-Filbey (CEF) equation (Eqn. 2-16) and requires a minimum amount of experimental information, i.e. the viscosity and normal stress differences. It takes into account the effect of normal stresses, which is a manifestation of viscoelasticity, but avoids explicit reference to the fluid memory.

In the field of numerical simulation, one often talks about the "high Weissenberg number problem". However, this reveals an error in terminology. The reference should be to the "high Deborah number problem", the term introduced in Chapter 2. The Weissenberg number (*We*) indicates the degree of nonlinearity or anisotropy that is manifested in a given flow, while the Deborah number (De) indicates the relative importance of elasticity.

Eqn. 9-1 $$We \equiv \lambda \dot{\gamma}$$

Eqn. 9-2 $$De \equiv \frac{\lambda_{fluid}}{\lambda_{flow}}$$

The Weissenberg number is the product of a characteristic relaxation time of the material and a typical strain rate, while the Deborah number is the characteristic relaxation time of the fluid λ_{fluid} divided by the characteristic time of the flow λ_{flow}. The characteristic time of the flow λ_{flow} is a time reflecting the variation of the strain history.

The confusion between the two arises from the fact that in many flows of practical importance they are directly related to each other. The distinction is particularly important in flow stability analyses, and those working in this field have been very careful not to confuse the two expressions. For example, Larson[5] has properly distinguished between De and We. Moreover, McKinley[6] has explained in detail how the two are related in converging flows and has introduced a "scaling factor" that expresses this relationship quantitatively.

Fully developed flow in a channel of constant cross section, which is a viscometric flow, is a flow in which De is zero because of constant-stretch history but in which We increases with the flow rate. Vlachopoulos et al., among others, have had considerable success in the modeling of melt flows in which De is small but We can be quite large. Examples of forming processes simulated using the viscometric flow approach include extrusion[7], film blowing[8], thermoforming[9] and calendering[10] for polymer melts and elastomers[11]. However, we have to keep in mind that the viscometric approach remains an approximation, which is similar to the lubrication approximation used to simplify the momentum equation in certain polymer processes, such as injection molding.

9.2 Power-Law Models for Elongational Viscosity

Gupta[12] has also adopted a simplified approach, but this time to simulate the axisymmetric entrance flow of polymers. Generalized Newtonian models, which have been successfully used in shear-dominated flows, do not provide an accurate simulation of applications involving an elongational flow, such as flow at the entrance of an extrusion die. On the other hand, viscoelastic constitutive equations have not produced simulations that are in good quantitative agreement with experimental data and are subject to convergence problems at high Deborah number. Gupta has developed software for the simulation of axisymmetric polymeric flow that requires only knowledge of the viscosity and the strain-rate dependence of the elongational viscosity of the polymer (which is not easy to measure). According to the author, his software can accurately predict the velocity and pressure field in applications involving a significant elongational flow component. However, the constitutive equations employed in the software do not predict normal stresses in shear flow. Apparently, the incorporation of a first normal stress difference prediction in the software gives convergence problems[13], and the incorporation of a second normal stress difference has not been tried yet. Viscosity and elongational viscosity are modeled using the following equations:

Eqn. 9-3 $$\eta_s = A\sqrt{II_D}^{\,n-1} \text{ for } II_D > II_{D_0}, \qquad \eta_s = \eta_0 \text{ for } II_D \le II_{D_0}$$

Eqn. 9-4 $$\eta_e = B\sqrt{II_D}^{\,m-1} \text{ for } II_D > II_{D_1}, \qquad \eta_e = 3\eta_0 \text{ for } II_D \le II_{D_1}$$

The strain rate for transition from Newtonian to power-law behavior can be different for the shear and elongational viscosities.

A more elaborate four-parameter model for the elongational viscosity has also been used, but the author has not revealed its form[13]. The parameters are determined by inverse problem solving; for a given shear rate, the viscosity and the entrance pressure drop are measured, and the parameters ruling the elongational viscosity are found by trial-and-error fitting. Gupta[12] reported that the (elongational viscosity)/(shear viscosity) ratio was important in determining the recirculating vortex and the extra pressure loss in axisymmetric entrance flow. Obviously, the predictive capabilities and the versatility of this approach are limited. Two more references, Gotsis and Odriozola[14] and Schunk and Scriven[15], explain how elongational viscosity can be incorporated in simulations without using a viscoelastic constitutive equation.

9.3 Approximate Prediction of Extrudate Swell

Seriai et al.[16] derived a semi empirical equation to predict the extrudate swell of linear polymers. The model is based on the rubber-like elasticity theory and on the calculation of the elongational strain recovery of a Lodge fluid[17,18]. The theoretical extrudate swell ratio mainly depends on the relaxation modulus, the extension ratio, and the recoverable shear strain. The main advantage of this model is that it provides good accuracy for short dies over a wide range of shear rates, where other available semi-empirical theories assume fully developed flow in a long die[19]. In extrusion processes, relatively short dies are generally used, and transient flow dominates. The strain history of the melt is thus of central importance and can not be neglected.

Bush[20] has also made a simplified simulation of extrudate swell. He models extrudate swell as the stratified flow of two, Newtonian, isothermal fluids with different viscosities. By suitable selection of the viscosity ratio, the model can take into account nonisothermal, shear-thinning and elastic effects. The model provides a means of simulating complex geometrical effects in profile extrusion without the burden of a full viscoelastic model and provides a practical aid for die design. The application to three-dimensional flow problems is also feasible using this method.

9.4 Rule-Based Flow Simulations

The simplified approaches described above have been helpful in certain applications, such as the design of certain types of die, extruders and injection molds. However, the predictive capabilities and versatility of these approaches remain limited. On the other hand, no practical method has been developed for dealing with viscoelastic flow situations in which there is a strong convergence or divergence of streamlines or a singularity in the boundary conditions.

While there is no question that the rheological models used to date in the numerical simulation of the flow of polymeric liquids are quite inadequate, the computational problems encountered in viscoelastic flow simulations occur even when the inaccuracy of the model is unlikely to be the cause. These problems arise under conditions where the models are thought to be reasonably reliable, i.e., at low *De* and when slip or fracture is not anticipated.

Therefore, it is concluded that the source of the problem is the viscoelasticity of the fluid, i.e., the dependence of its state of stress on the past history of the deformation. In particular, the notorious convergence problems mentioned above do not occur in the simulation of flow at small *De*. This conclusion is strengthened by the observation that it has not been possible by elaboration or variation of the numerical method used in the simulation to eliminate the convergence problem. Neither has it been possible to eliminate the problem by the use of molecular dynamic models of rheological behavior.

It is very unlikely that any single, closed form constitutive equation will ever be developed that can describe accurately all aspects of the rheological behavior of highly entangled molten polymers. Furthermore there are phenomena, such as slip and fracture, that can not be predicted by a continuum mechanics model but that must be taken into account in the modeling of many industrial forming operations.

Obviously, a new approach is needed to deal with such flows. The most likely approach appears to be a rule-based expert system that is able to select, from a repertoire of possible models of rheological and slip behavior, the one that is most appropriate in each region of the flow field. A major challenge in the development of such a system is a method for matching the solutions at the boundaries of neighboring regions. In this last section, we provide background information on rule-based expert systems and an overview of how such a system might be used in the simulation of viscoelastic flows.

9.4.1 Fundamentals of Knowledge-Based Expert Systems

Expert systems, based on techniques developed from artificial intelligence research, are currently used in a number of engineering applications, especially in the manufacturing and process control domains[21]. An excellent review of knowledge-based expert systems for materials processing has been presented by Lu[22].

An expert system can be distinguished from a conventional computer program in terms of its three basic components[22], which are shown in Fig. 9-1 and listed below.

1. A knowledge base - which contains domain knowledge such as rules, facts, and other information that may be useful in formulating a solution.
2. An inference engine - which applies proper domain knowledge and controls the order and strategies of problem solving.
3. A blackboard - which records the intermediate hypotheses and results that the expert system manipulates.

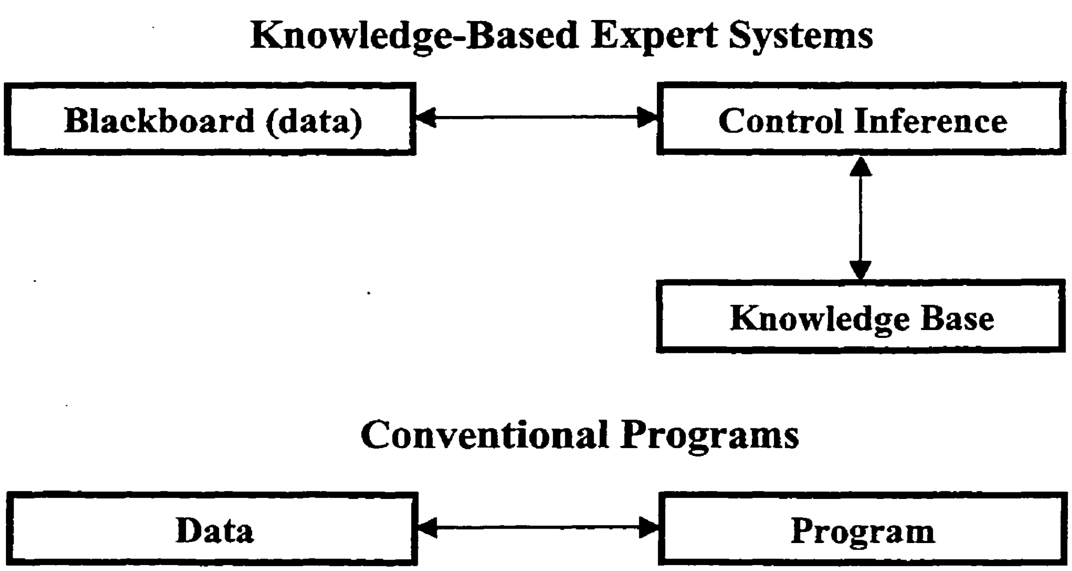

Figure 9-1 Expert Systems vs. Conventional Programs[22].

A conventional program contains only two parts, the program and the data, as shown in Fig. 9-1, and all the required control and domain knowledge is coded into the program that manipulates data in a sequential manner with many conditional branches. During execution, the status of the problem is represented by the current values of the variables in the program.

In an expert system, the knowledge base is treated as a separate entity rather than appearing only implicitly as part of the program. It contains facts and rules that are used as the basis for decision-making. The knowledge related to the control of decision-making is collected in the inference engine, which is physically separate from the knowledge base. The inference engine has an interpreter that decides how to select and apply the rules from the knowledge base to infer new information, and a scheduler that determines the order in which the selected rules should be applied. The blackboard is a separate entity that serves as a working memory for the system. It can be viewed as a global database for keeping track of the current problem status and other relevant information during problem solving. The separation of the task-level knowledge (stored in the knowledge base) from the control knowledge (stored in the inference engine), and the addition of a separate working memory (the blackboard), gives expert systems greater flexibility in both the implementation and execution stages. Many applications can benefit from the use of such a system.

9.4.2 Application to Viscoelastic Flow Simulations

One way to approach effectively viscoelastic flow simulations is through computational domain decomposition[23]. For example, the Schur complement method is based on a domain decomposition that leads to a decoupling of the system on a sub-domain basis rather than on a component basis. The advantage of this technique is that all the unknowns in an element (stress, velocity and pressure) exhibit strong local coupling, which makes a decoupling on a component basis less attractive[23].

Another strong advantage of this technique is that it enables the use of the most appropriate rheological model in each region of the flow field or sub-domain. However, the size and boundaries of these sub-domains are not known *a priori*, and they should be allowed to established themselves according to flow conditions through an automated process. This is where knowledge-based expert system based on rule representation become attractive. An expert system would be able to select from a bank of rheological equations the most appropriate model according to the flow conditions calculated in a " start-up element " to get the cycle going[22]. The rules for model selection could be based, for example, on the examination of the velocity gradient. Two main difficulties would have to be overcome: first, the matching of the solutions at the boundaries of neighboring regions, and second the achievement of convergence towards a unique model in each sub-domain, so it would not change from one iteration to the next[24].

The use of a rule-based expert system would enable many simplifications, such as the viscometric approach in flow regions far from flow singularities or in shear-dominated zones. More complete calculations would be done only in complex flow zones, allowing a solution for a small system with a full Newton method, which would facilitate numerical convergence due to its larger radius of convergence.

Some issues have to be explored systematically to develop the expert system. For example, a procedure to determine the number of modes needed, based on the material and the nature of flow. This number could also vary depending on the location of the sub-domain. Also, a method is needed to determine the best approach for use near a singularity. Three possibilities are:

1. The use of a Newtonian model to ensure flow convergence, which is the simplest approach, but would not be valid for extrudate swell.
2. A boundary layer simplification, similar to the boundary layer theory of classical fluid mechanics. An example of such equations are those derived by Renardy[25] for the PTT and Giesekus models for enclosed flows, but they have not been tested in large finite element codes.

3. A coupled macroscopic description of the conservation laws with a kinetic theory of the polymer dynamics, along with a full Newton method to allow convergence. This approach would provide a more realistic description of the flow in these small regions, but would require more computational resources.

The use of a more realistic description would lead to an improvement of the simplified approach by adding to our understanding of material behavior[26].

9.4.3 Incorporation of Other Phenomena

Another advantage of the expert system approach for polymer processing is the possibility of incorporating other phenomena such as slip or fracture that can not be predicted by a continuum mechanics model, but that must be taken into account in the modeling of many industrial forming operations. Since reliable models of these phenomena are not yet available, they could be incorporated into the expert system by means of fuzzy logic[27]. Fuzzy logic or possibility theory[22] is especially suitable for complex, ill-defined, nonlinear phenomena, where human experience is superior to mathematical models[28]. Fuzzy logic represents a mathematical way of looking at vagueness in a form that a computer can deal with. It might be possible in this way to model phenomena such as the wall slip and fracture of molten polymers for which explicit models are not available. The advantage of this approach is that a fuzzy expert system is similar to a conventional rule-based expert system, except that it contains rules with imprecise relationships[29]. Fuzzy-logic could be easily incorporated to the computer program architecture presented earlier.

The essential elements of a possible rule-based expert system for viscoelastic flow simulation are presented in Fig. 9-2. The first calculation might be carried out for a Newtonian fluid in order to insert a start-up solution in the working memory (DATA) to get the cycle of "reasoning" (CONTROL) going.

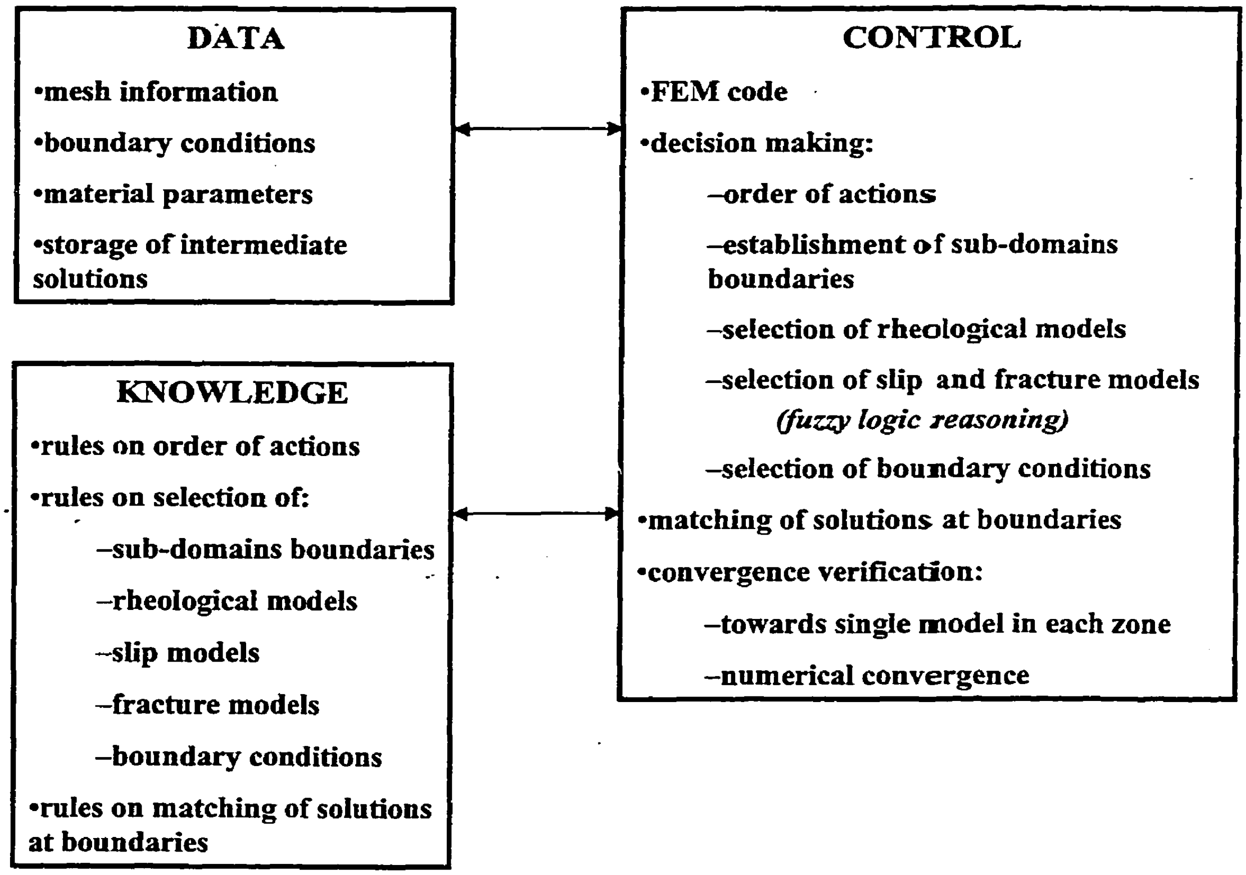

Figure 9-2 Essential Elements of a Possible Rule-Based Expert System for Viscoelastic Flow Simulation.

REFERENCES

[1] Mitsoulis E., Vlachopoulos J., Mirza F.A., " A Numerical Study of the Effect of Normal Stresses and Elongational Viscosity on Entry Vortex Growth and Extrudate Swell ", *Polym. Eng. Sci.*, 25(11), p. 677-689 (1985)
[2] Mitsoulis E., Vlachopoulos J., Mirza F.A., " Simulation of Vortex Growth in Planar Entry Flow of a Viscoelastic Fluid ", *J. Appl. Polym. Sci.*, 30, p. 1379-1391 (1985)
[3] Mitsoulis E., Vlachopoulos J., Mirza F.A., " Numerical Simulation of Entry and Exit Flows in Slit Dies ", *Polym. Eng. Sci.*, 24(9), p. 707-715 (1984)
[4] Mitsoulis E., Vlachopoulos J., Mirza F.A., " Simulation of Extrudate Swell from Long Slit and Capillary Dies ", *Polym. Proc. Eng.*, 2, p. 153-177 (1984)
[5] Larson R.G. " Instabilities in Viscoelastic Flows ", *Rheol. Acta*, 31, p. 213-263 (1992)
[6] McKinley G.H., " Rheological and Geometric Scaling of Purely Elastic Flow Instabilities ", *J. Non-Newt. Fl. Mech.*, 67, p. 19-47 (1996)
[7] Vlček J., Perdikoulis J., Vlachopoulos J., " Extrusion Die Flow Simulation and Design with FLATCAD, COEXCAD and SPIRALCAD ", in *Applications of CAE in Extrusion and Other Continuous Polymer processes*, K.T. O'Brien (ed.), p. 487-504, Carl Hanser Verlag (1992)
[8] Sidiropoulos V., Tian J.J., Vlachopoulos J., " Computer Simulation of Film Blowing ", *J. Plast. Film Sheet*, 12, p. 107-129 (1996)
[9] Ghafur M.O., Koziey B.L., Vlachopoulos J., " Simulation of Thermoforming and Blowmolding: Theory and Experiments ", in *Rheological Fundamentals in Polymer Processing*, J. Covas et al. (eds.), p. 321-383, Kluwer, Netherlands (1995)
[10] Mitsoulis E., Vlachopoulos J., Mirza F.A., " Calendering Analysis without the Lubrication Approximation ", *Polym. Eng. Sci.*, 25, p. 6-18 (1985)
[11] Nassehi V., Salemi R., " Finite Element Modeling of Non-isothermal Viscometric Flows in Rubber Mixing ", *Intern. Polym. Process.*, IX(3), p. 199-204 (1994)
[12] Gupta M., "Effect of Elongational Viscosity on Axisymmetric Entrance Flow of Polymers", *Polym. Eng. Sci*, in review
[13] Gupta M., " Entrance Flow Simulation Using Elongational Properties of Plastics ", presentation at *ANTEC'99, Society of Plastic Engineers*, New York (1999)
[14] Gotsis A.D., Odriozola A., "The relevance of Entry Flow Measurements for the Estimation of Extensional Viscosity of Polymer Melts", *Rheol. Acta*, 37(5), p. 430-437 (1998)
[15] Schunk P.R., Scriven L.E., "Constitutive Equations for Modeling Mixed Extension and Shear in Polymer Solution Processing", *J. Rheol.*, 34(7), p. 1085-1119 (1990)
[16] Seriai M., Guillet J., Carrot C., " A Simple Model to Predict Extrudate Swell of Polystyrene and Linear Polyethylenes ", *Rheol. Acta*, 32, p. 532-538 (1993)
[17] Taylor C.R., Ferry J., " Nonlinear Stress Relaxation of Polyisobutylene in Simple Extension and Recovery After Partial Stress Relaxation ", *J. Rheol.*, 23, p. 533-542 (1979)
[18] Lodge A.S., " A Network Theory of Flow Birefringence and Stress in Concentrated Polymer Solutions ", *Trans. Faraday Soc.*, 52, p. 120-130 (1956)
[19] Vlachopoulos J., " Extrudate Swell in Polymers ", in *Reviews on the Deformation Behavior of Materials*, III(4), P. Feltham (ed.), p. 219-248, Freund Publishing House, Tel-Aviv, Israel (1981)
[20] Bush M.B., " A Method for Approximate Prediction of Extrudate Swell ", *Polym. Eng. Sci.*, 33(15), p. 950-958 (1993)
[21] Crowe E.R., Vassiliadis C.A., " Artificial Intelligence: Starting to Realize its Practical Promise ", *Chem. Eng. Process*, Jan. issue, p. 22-31 (1995)
[22] Lu S. C.-Y., " Knowledge-Based Expert Systems for Materials Processing ", in *Fundamentals of Computer Modeling for Polymer processing*, C.L. Tucker III (ed.), p. 535-573, Carl Hanser Verlag (1989)
[23] Debbault B., Goublomme A., Homerin O., Koopmans R., Liebman D., Meissner J., Schroeter

---

B., Reckman B., Daponte T., Verschaeren P., Agassant J.-F., Vergnes B., Venet C., " Development of High Quality LLDPE and Optimized Processing for Film Blowing ", *Intern. Polym. process.*, XIII(3), p. 262-270 (1998)
[24] Guénette Robert, private communication (June 1999)
[25] Hagen T., Renardy M., " Boundary Layers Analysis of the Phan-Thien/Tanner and Giesekus Models in High Weissenberg Number Flow ", *J. Non-Newt. Fl. Mech.*, 73(1), p. 181-190 (1997)
[26] Keunings R., " Recent Developments in Computational Rheology ", Seminar at the Chemical Engineering Dept. of McGill University (June 1999)
[27] Zadeh L.A., " Fuzzy Sets as a Basis for a Theory of Possibility ", in *Fuzzy Sets and Systems*, North-Holland, Amsterdam (1978)
[28] Rhinehart R.R., Li H.H., Murugan P., " Improve Process Control Using Fuzzy Logic ", *Chem. Eng. Progress*, Nov. issue, p. 60-65 (1996)
[29] Crowe E.R., Vassiliadis C.A., "Artificial Intelligence: Starting to Realize its Practical Promise", *Chem. Eng. Progress*, Jan. issue, p. 22-31 (1995)

10. Conclusions and Recommendations

10.1 Conclusions

The lack of success in the simulation of viscoelastic flows in which there is a strong convergence or divergence of streamlines, or a singularity in the boundary conditions, has been thought to arise from the following sources:

- The inadequacy of the rheological model for the material.
- The presence of the flow singularity.
- The elasticity, i.e., history dependence, of the material.

It is concluded here that the principal source of the problem is the elasticity of the fluid in combination with flow singularities. Numerical difficulties are also encountered with Newtonian fluids in the presence of flow singularities, but since they have no memory the effect of the stress overshoot is not carried into the rest of the flow field. Viscoelasticity, as described by multiple relaxation times, some of which may be quite long, renders even the most advanced numerical methods incapable of modeling industrial flows of melts of typical molten plastics in which elasticity plays an important role.

One of the difficulties encountered in this project was the lack of flexibility to change the numerical algorithms in order to improve convergence. The amount of work involved to change the finite element Fortran code restrained us from trying more powerful (but costly) solvers like the Newton method. For faster progress in the future, new programming methods must be developed to eliminate this restriction.

With regard to the inadequacy of existing rheological models, and in particular the Leonov and PTT models, it is concluded that:

1. With the best constitutive equation from a rheological point of view (Leonov model), solutions for situations of practical importance are impossible, even when one of the most advanced numerical procedure is used. The model also gives conflicting results,

with realistic predictions in planar flow but not in axisymmetric flow. The incorrect prediction of decreasing swell confirms the findings of Rekers[1].

2. Even a model that is thought to be one of the best with regard to convergence (PTT model) is very limited in its capability.

It now seems quite probable that no model expressed solely in terms of continuum mechanics variables will ever be able to provide a universal description of the flow behavior of polymeric liquids, and this observation has given rise to a relatively new area, molecular dynamics simulation. However, it has not been possible up to now to eliminate the problem of numerical convergence by the use of molecular dynamic models even with some of the most advanced numerical methods.

The major conclusions of this work are as follows:

1. The barriers that have arisen in trying to use numerical methods to simulate complex flows of viscoelastic fluids cannot be eliminated using the constitutive equations and numerical techniques that have been applied to date.
2. It is likely that even if more realistic rheological models were available, the basic problem would persist, as it arises from the history dependence of the material. This history dependence leads to an intrinsic instability in numerical solutions.
3. An entirely new approach is needed for the modeling of complex flows. This might be based on a rule-based expert system approach to the problem. By use of such a technique, one could guide the direction of the computation in the neighborhood of singularities, thus ensuring convergence. Such an approach could also readily incorporate models for slip and fracture phenomena.

10.2 Original Contributions to Knowledge

The original contributions to knowledge resulting from this work are derived from the objectives presented in Chapter 3:

1. The determination of the limitations in present numerical methods for the simulation of the flow of viscoelastic materials.

2. The confirmation of the inadequacy of the Leonov model in axisymmetric extrudate swell.
3. The establishment of the cause of these limitations, i.e. the history dependence of the materials.
4. The proposal that a rule-based expert system shows promise for overcoming existing limitations.

10.3 Recommendations for Future Work

Future work should be aimed at developing the new approach described in Chapter 9, a rule-based expert system able to select, from a repertoire of possible models of rheological and slip behavior, the one that is most appropriate in each region of the flow field. The development of an expert system should be the focus of future work in this field rather than continuing the futile effort to elaborate a single model that will be adequate over the entire field of a complex flow.

The use of a multimode spectrum, truncated or not, for nonlinear viscoelastic models is strongly recommended since a single mode can not fit data properly and leads to numerical problems.

Finally, we need not only more efficient numerical methods but also more efficient programming tools that will provide more flexibility for trying various algorithms. An example of such a tool is the program MEF++[2] (Méthode d'Eléments Finis) written in the programming language C++. This code facilitates changes in the mesh, mesh adaptativity, solvers, and upwinding methods in order to improve numerical convergence.

[1] Rekers G., " Numerical Simulation of Unsteady Viscoelastic Flow of Polymers ", Ph.D. Thesis, University of Twente, Twente, The Netherlands (1995)

[2] GIREF (Groupe Interdisciplinaire de Recherche en Elements Finis), Université Laval, Québec, Canada

Bibliography

Agassant J.F., Avenas P., Sergent J.-Ph., Carreau P.J., « Polymer processing. Principles and Modeling », *Hanser Publishers*, New York (1991)

Ahmed R., Liang R.F., Mackley M.R., " The Experimental Observation and Numerical Prediction of Planar Entry Flow and Die Swell for Molten Polyethylenes ", *J. Non-Newt. Fl. Mech.*, 59, p. 129-153 (1995)

Baaijens F.P.T., "Calculation of Residual Stresses in Injection Molded Products", *Rheol. Acta*, 30, p. 284 (1991)

Baaijens F.P.T., Selen S.H.A., Baaijens H.P.W., Peters G.W.M., Meijer H.E.H., " Viscoelastic Flow Past a Confined Cylinder of a LDPE Melt ", *J. Non-Newt. Fl. Mech.*, 68, p.173-203 (1997)

Baaijens, F.P.T., "Mixed Finite Element Methods for Viscoelastic Flow Analysis: a Review", *J. Non-Newt. Fl. Mech.*, 79, p. 361-385 (1998)

Barakos G., Mitsoulis E., "Numerical Simulation of Extrusion through Orifice Dies and Prediction of Bagley Correction for an IUPAC-LDP Melt", *J. Rheol.*, 39(1), p. 193-209 (1995)

Beaufils P., Vergnes B., Agassant J.F., " Characterization of the Sharkskin Defect and its Development with the Flow Conditions ", *Int. Polym. Process.*, IV(2), p. 78-84 (1989)

Béliveau A., « Méthodes de Lesaint-Raviart Modifiées : Applications au Calcul des Surfaces Libres », Ph.D. Thesis, École Polytechnique de Montréal, Montréal, Canada (1997)

Bell T.W., Nyland G.H., Graham M.D., de Pablo J.J., "Combined Brownian Dynamics and Spectral Method Simulations of the Recovery of Polymeric Fluids after Shear Flow", *Macromolecules*, 30, p. 1806-1812 (1997)

Beraudo C., "Méthodes éléments finis pour la simulation numérique d'écoulements de fluides viscoelastiques de type différentiel dans des géométries convergentes", Ph.D. thesis, École Nationale Supérieure des Mines de Paris, Sophia Antipolis, France (1995)

Beraudo C., Fortin A., Coupez T., Demay Y., Vergnes B., Agassant J.F., " A Finite Element Method for Computing the Flow of Multi-Mode Viscoelastic Fluids: Comparison with Experiments ", *J. Non-Newt. Fl. Mech.*, 75, p. 1-23 (1998)

Bernstein B., Kearsley E.A., Zapas L.J., *Trans. Soc. Rheol.*, 7, p. 391-410 (1963)
Bird R.B., Curtiss C.F., Armstrong R.C., Hassager O., "Dynamics of Polymeric Liquids, Vol. 2", Second Edition, *John Wiley & Sons*, New York (1987)

Bird R.B., Curtiss C.F., Armstrong R.C., Hassager O., "Dynamics of Polymeric Liquids, Vol. 1: Fluid Mechanics", Second Edition, *John Wiley & Sons*, New York (1987)

Boger D.V., " Model Polymer Fluid Systems ", *Pure Appl. Chem.*, 57, p. 921 (1985)

Boger D.V., " Viscoelastic Flows through Contractions ", *Ann. Rev. Fluid Mech.*, 19, 157-182 (1987)

Brezzi F., Fortin M., "Mixed and Hybrid Finite Element Methods: Series in Computational Mechanics", *Springer*, New York (1991)

Bush M.B., " A Method for Approximate Prediction of Extrudate Swell ", *Polym. Eng. Sci.*, 33(15), p. 950-958 (1993)

Bush M.B., " Prediction of Polymer Melt Extrudate Swell Using a Differential Constitutive Model ", *J. Non-Newt. Fl. Mech.*, 31, p. 179-191 (1989)

Carreau P.J., Ph.D. Thesis, Univ. of Wisconsin, Madison (1969)

Carrot C., Guillet J., Revenu P., Arsac A., " Experimental Validation of Non Linear Network Models ", in "Rheology of Polymer Melt Processing", J.M. Piau and J.-F. Agassant (eds.), *Elsevier Science*, Amsterdam (1996)

Caswell B., " Report on the IX th International Workshop on Numerical Methods in Non-Newtonian Flows ", *J. Non-Newt. Fl. Mech.*, 62, p. 99-110 (1996)

Coates P.J., Armstrong R.C., Brown R.A., *J. Non-Newt. Fl. Mech.*, 42, p. 141 (1992)

Criminale W.O. Jr., Ericksen J.L., Filbey G.L. Jr., *Arch. Ratl. Mech. Anal.*, 1, p. 410 (1958)

Crochet M.J., Davies A.R., Walters K., "Numerical Simulation of Non-Newtonian Flow", *Elsevier*, Amsterdam (1984)

Crochet M.J., Keunings R., "Finite Element Analysis of Die Swell of Highly Elastic Fluids", *J. Non-Newt. Fl. Mech.*, 10, p. 339-356 (1982)

Crochet M.J., Keunings R., "On Numerical Die Swell Calculations", *J. Non-Newt. Fl. Mech.*, 10, p. 85-94 (1982)

Crochet M.J., Keunings R., "Die Swell of a Maxwell Fluid: Numerical Predictions", *J. Non-Newt. Fl. Mech.*, 7, p. 199-212 (1980)

Crowe E.R., Vassiliadis C.A., " Artificial Intelligence: Starting to Realize its Practical Promise ", *Chem. Eng. Process,* Jan. issue, p. 22-31 (1995)

Curtiss C.F., Bird R.B., "A Kinetic Theory for Polymer Melts. II. The Stress Tensor and the Rheological Equations of State", *J. Chem. Phys.,* 74, p. 2016 (1982)

Dealy J.M., Vu T.K.P., "The Weissenberg Effect in Molten Polymers", *J. Non-Newt. Fl. Mech.,* 3, p. 127 (1977)

Dealy J.M., Wissbrun K.F., "Melt Rheology and its Role in Plastics Processing", *Van Nostrand Reinhold,* New York (1990)

Debbault B., Goublomme A., Homerin O., Koopmans R., Liebman D., Meissner J., Schroeter B., Reckman B., Daponte T., Verschaeren P., Agassant J.-F., Vergnes B., Venet C., " Development of High Quality LLDPE and Optimized Processing for Film Blowing ", *Intern. Polym. process.,* XIII(3), p. 262-270 (1998)

Debbaut B., Crochet M.J., "Further Results on the Flow of a Viscoelastic Fluid Through an Abrupt Contraction", *J. Non-Newt. Fl. Mech.,* 20, p. 173-185 (1986)

Debbaut B., Marchal J.M., Crochet M.J., *J. Non-Newt. Fl. Mech.,* 29, p. 119 (1988)

Demay Y., "Computation of 2D Viscoelastic Flows for a Differential Constitutive Equation", in "Rheology of Polymer Melt Processing", J.M. Piau and J.-F. Agassant (eds.), *Elsevier Science,* Amsterdam (1996)

Doi M., Edwards S.F., " Dynamics of Concentrated Polymer Systems. Part 4.- Rheological Properties ", *J. Chem. Soc., Faraday Trans. II,* 75, p. 38 (1979)

Doi M., Edwards S.F., "Dynamics of Concentrated Polymer Systems. Part 1.- Brownian Motion in the Equilibrium State", *J. Chem. Soc., Faraday Trans. II,* 74, p. 1789 (1978)

Doi M., Edwards S.F., "The Theory of Polymer Dynamics", *Oxford University Press,* Oxford (1983)

Dupont S., Crochet M.J., "The Vortex Growth of a K.B.K.Z. Fluid in an Abrupt Contraction", *J. Non-Newt. Fl. Mech.,* 29, p. 81-91 (1988)

Durst F., Melling A., Whitelaw J.H., " Principles and Practice of laser-Doppler Anemometry ", *Academic Press,* 2nd edition (1981)

Fan Y., Tanner R.I., Phan-Thien N., "Galerkin/Least-Square Finite-Element Methods for Steady Viscoelastic Flows", *J. Non-Newt. Fl. Mech.,* 84, p. 233-256 (1999)

Fano G., *Arch. Fisiol.,* 5, p. 365 (1908)

Fiegl K., Öttinger H.C., " A Numerical Study of the Flow of a Low-Density-Polyethylene Melt in Planar Contraction and Comparison to Experiments ", *J. Rheol.*, 40(1), p. 21-35 (1996)

Fiegl K., Öttinger H.C., " The Flow of a LDPE Melt through an Axisymmetric Contraction: A Numerical Study and Comparison to Experimental Results ", *J. Rheol.*, 38(4), p. 847-874 (1994)

Flaman A.A.M., "Buildup and Relaxation of Molecular Orientation in Injection Molding. Part I: Formulation", *Polym. Eng. Sci.*, 33(4), p. 193 (1993)

Flaman A.A.M., "Buildup and Relaxation of Molecular Orientation in Injection Molding. Part II: Experimental Verification", *Polym. Eng. Sci.*, 33(4), p. 202 (1993)

Fortin A., Béliveau A., "Injection Molding for Charged Viscoelastic Fluid Flow Problems", *PPS-14*, p. 327-328, Yokohama, Japan (1998)

Fortin A., Béliveau A., Heuzey M.C., Lioret A., « Ten Years Using Discontinuous Galerkin Methods for Polymer Processing », to be published in the Proceedings of *Int. Symp. on Discontinuous Galerkin Methods : Theory, Computations and Applications*, Salve Regina College, Newport, RI, USA (1999)

Fortin A., Fortin M., "A Preconditioned Generalized Minimal Residual Algorithm for the Numerical Solution of Viscoelastic Fluid Flows", *J. Non-Newt. Fl. Mech.*, 36, p. 277-288 (1990)

Fortin A., Zine A., Agassant J.F., "Computing Viscoelastic Fluid Flow at Low Cost", *J. Non-Newt. Fl. Mech.*, 45, p. 209-229 (1992)

Fortin M., Fortin A., "A New Approach for the FEM simulation of Viscoelastic Flows", *J. Non-Newt. Fl. Mech.*, 32, p. 295-310 (1989)

Fortin M., Fortin A., "A Generalization of Uzawa's Algorithm for the Solution of Navier-Stokes Equations", *Comm. Appl. Num. Meth.*, 1, p. 205-208 (1985)

Fortin M., Fortin A., "Experiments with Several Elements for Viscous Incompressible Flows", *Int. J. Num. Meth. Fl.*, 5, p. 911-928 (1985)

Fortin M., Guénette R., Pierre R., "Numerical Analysis of the Modified EVSS", *Comp. Meth. Appl. Mech., Eng.*, 143(1), p. 79-96 (1997)

Fortin M., Pierre R., "On the Convergence of the Mixed Method of Crochet and Marchal for Viscoelastic Flows", *Int. J. Numer. Methods Fl.*, 7, p. 1035-1052 (1987)

Garcia-Rejon A., DiRaddo R.W., Ryan M.E., " Effect of Die Geometry and Flow Characteristics on Viscoelastic Annular Swell ", *J. Non-Newt. Fl. Mech.*, 60, p. 107-128 (1995)

Gavrus L., "Étude du comportement des polyéthylenes: Biréfringence d'écoulement et anémometrie laser", rapport d'étape, École Nationale Supérieure des Mines de Paris, Sophia Antipolis, France (1995)

Ghafur M.O., Koziey B.L., Vlachopoulos J., " Simulation of Thermoforming and Blow molding: Theory and Experiments ", in *Rheological Fundamentals in Polymer processing,* J. Covas et al. (eds.), p. 321-383, Kluwer, Netherlands (1995)

Giacomin A.J., Samurkas T., Dealy J.M., " A Novel Sliding Plate Rheometer for Molten Plastics ", *Polym. Eng. Sci.*, 29(8), p. 499 (1989)

Giesekus H., "A Simple Constitutive Equation for Polymer Fluids Based on the Concept of Deformation Dependent Tensorial Mobility", *J. Non-Newt. Fl. Mech.*, 11, p.69-109 (1982)

Gordon R.J., Schowalter W.R., *Trans. Soc. Rheol.*, 16, p. 79 (1972)

Gotsis A.D., Baird D.G., Reddy J.N., " Comparison of Experimental Data with the Numerical Simulation of Planar Entry Flow: Role of the Constitutive Equation ", *Int. J. Num. Meth. Fl.*, 10, p. 373-400 (1990)

Gotsis A.D., Odriozola A., "The relevance of Entry Flow Measurements for the Estimation of Extensional Viscosity of Polymer Melts", *Rheol. Acta,* 37(5), p. 430-437 (1998)

Goublomme A., Crochet M.J., " Numerical Prediction of Extrudate Swell of a High-Density Polyethylene: Further Results ", ", *J. Non-Newt. Fl. Mech.*, 47, p. 281-287 (1993)

Goublomme A., Draily B., Crochet M.J., "Numerical Prediction of Extrudate Swell of a High-Density Polyethylene", *J. Non-Newt. Fl. Mech.*, 44, p. 171-195 (1992)

Guénette R., Fortin M., "A New Mixed Finite Element Method for Computing Viscoelastic Flows", *J. Non-Newt. Fl. Mech.*, 60, p.27-52 (1995)

Guillet J., Revenu P., Béreaux Y., Clermont J.-R., "Experimental and Numerical Study of Entry Flow of Low-Density Polyethylene Melts", *Rheol. Acta,* 35, p. 494-507 (1996)

Gupta M., " Entrance Flow Simulation Using Elongational Properties of Plastics ", presentation at *ANTEC'99, Society of Plastic Engineers,* New York (1999)

Gupta M., "Effect of Elongational Viscosity on Axisymmetric Entrance Flow of Polymers", *Polym. Eng. Sci,* in review

Hagen T., Renardy M., " Boundary Layers Analysis of the Phan-Thien/Tanner and Giesekus Models in High Weissenberg Number Flow ", *J. Non-Newt. Fl. Mech.*, 73(1), p. 181-190 (1997)

Halin P., Lielens G, Keunings R., Legat V., "The Lagrangian Particle Method for Macroscopic and Micro-Macro Viscoelastic Flow Computations", *J. Non-Newt. Fl. Mech.*, 79, p.387-403 (1998)

Hartt W.H., Baird D.G., " The Confined Flow of Polyethylene Melts Past a Cylinder in a Planar Channel ", *J. Non-Newt. Fl. Mech.*, 65, p. 247-268 (1996)

Hassager O., " Working Group on Numerical Techniques ", *J. Non-Newt. Fl. Mech.*, 29, p. 2-5 (1988)

Hatzikiriakos S.G., Mitsoulis E., "Excess Pressure Losses in the Capillary Flow of Molten Polymers", *Rheol. Acta*, 35, p. 545-555 (1996)

Hepperle, J., Saito T., unpublished work, Institute of Polymer Materials, University of Erlangen-Nuremberg, Erlangen, Germany (1998)

Heuzey M.C., " The Occurrence of Flow Marks during Injection Molding of Linear Polyethylene ", Master's Thesis, McGill University, Montreal, Canada (1996)

Hua C.C., Schieber J.D., "Viscoelastic Flow through Fibrous Media Using the CONNFFESSIT Approach", *J. Rheol.*, 42(3), p. 477-491 (1998)

Hulsen M.A., van der Zanden J., "Numerical Simulations of Contraction Flows using a Multi-Mode Giesekus Model", *J. Non-Newt. Fl. Mech.*, 38, p. 183-221 (1991)

Hulsen M.A., van Heel A.P.G., van den Brule B.H.A.A., "Simulation of Viscoelastic Flows Using Brownian Configuration Fields", *J. Non-Newt. Fl. Mech.*, 70, p. 79-101 (1997)

Kaye A., "Non-Newtonian Flow in Incompressible Fluids", *College of Aeronautics*, Cranfield, Note No. 134 (1962)

Keunings R., "On the High Weissenberg Number", *J. Non-Newt. Fl. Mech.*, 20, p. 209-226 (1986)

Keunings R., " Recent Developments in Computational Rheology ", Seminar at the Chemical Engineering Dept. of McGill University (June 1999)

Kiriakidis D.G., Park H.J., Mitsoulis E., Vergnes B., Agassant J.F., " A Study of Stress distribution in Contraction Flows of an LLPDE Melt ", *J. Non-Newt. Fl. Mech.*, 47, p. 339-356 (1993)

Koopmans R.J., " Extrudate Swell of High Density Polyethylene. Part I: Aspects of Molecular Structure and Rheological Characterization Methods, Part II: Time Dependency and Effects of Cooling and Sagging ", *Polym. Eng. Sci.*, 32(23), p. 1741-1754 (1993)

Koran F., "The effect of Pressure on the Rheology and Wall Slip of Polymer Melts", Ph.D. Thesis, McGill University, Montreal, Canada (1998)

Larson R., "Constitutive Equations for Polymer Melts and Solutions", *Butterworths*, Boston (1988)

Larson R.G. " Instabilities in Viscoelastic Flows ", *Rheol. Acta*, 31, p. 213-263 (1992)

Laun H.M., "Polymer Melt Rheology with a Slit die", *Rheol. Acta*, 22, p. 171-185 (1983)

Laun H.M., *Rheol. Acta*, 30, p. 459 (1986)

Legat V., "Computer Modeling of Viscoelastic Flow", in "Rheological Fundamentals of Polymer Processing", J.A. Covas et al. (eds.), *Kluwer Academic Publishers*, The Netherlands, p. 209-229 (1995)

Leonov A.I., "Nonequilibrium Thermodynamics and Rheology of Viscoelastic Polymer Media", *Rheol. Acta*, 15, p. 85-98 (1976)

Leonov A.I., "Viscoelastic Constitutive Equations and Rheology for High Speed Polymer Processing", *Polym. Intern.*, 36(2), p. 187-193 (1995)

Leonov A.I., Lipkina E.H., Paskhin E.D., Prokunin A.N., "Theoretical and Experimental Investigation of Shearing in Elastic Polymer Liquids", *Rheol. Acta*, 15, p. 411-426 (1976)

Lesaint P. Raviart P.A., "On a Finite Element Method for Solving the Neutron Transport Equations", in "Mathematical Aspects of Finite Elements in Partial Differential Equations", C. de Boor (ed.), *Academic Press*, New York, p. 89-123 (1974)

Lioret A., " Méthodes d'Éléments Finis Adaptative pour les Écoulements de Fluides Viscoélastiques », Master's Thesis, École Polytechnique de Montréal, Montréal, Canada (1998)

Liu Y., Shaw M.T., Tuminello W.H., "Optimized Data Collection for Determination of the MWD from the Viscosity Data of Polymer Melts", *Polym. Eng. Sci.*, 38(1), p. 169-176 (1998)

Lodge A.S., "Elastic Liquids", *Academic Press*, London (1969)

Lodge A.S., " A Network Theory of Flow Birefringence and Stress in Concentrated Polymer Solutions ", *Trans. Faraday Soc.*, 52, p. 120-130 (1956)

Lu S. C.-Y., " Knowledge-Based Expert Systems for Materials Processing ", in *Fundamentals of Computer Modeling for Polymer processing*, C.L. Tucker III (ed.), p. 535-573, Carl Hanser Verlag (1989)

Lunsmann W.J., Genieser L., Armstrong R.C., Brown R.A., "Finite Element Analysis of Steady Viscoelastic Flow Around a Sphere in a Tube: Calculations with Constant Viscosity Models", *J. Non-Newt. Fl. Mech.*, 48, p. 63-99 (1993)

Luo X.L., "A Control Volume Approach for Integral Viscoelastic Models and its Application to Contraction Flow of Polymer Melts", *J. Non-Newt. Fl. Mech.*, 64, p. 173-189 (1996)

Luo X.-L., Mitsoulis E., " Memory Phenomena in Extrudate Swell Simulations for Annular Dies ", *J. Rheol.*, 33(8), p. 1307-1327 (1989)

Luo X.-L., Mitsoulis E., "A Numerical Study of the Effect of Elongational Viscosity on Vortex Growth in Contraction Flows of Polyethylene Melts", *J. Rheol.*, 34(3), p. 309-342 (1990)

Luo X.-L., Tanner R.I., " A Streamline Element Scheme for Solving Viscoelastic Flow Problems. Part II: Integral Constitutive Models ", *J. Non-Newt. Fl. Mech.*, 22, p. 71-89 (1986)

Luo X.L., Tanner R.I., *J. Non-Newt. Fl. Mech.*, 21, p. 179-199 (1986)

Luo X.-L., Tanner R.I., *J. Non-Newt. Fl. Mech.*, 31, p. 143 (1989)

Mackay M.E., Boger D.V., *J. Non-Newt. Fl. Mech.*, 22, p. 235 (1987)

Mackay M.E., Petrie C.J.S., "Estimates of Apparent Elongational Viscosity Using the Fibre Spinning and "Pure" Methods", *Rheol. Acta*, 28, p. 281-293 (1989)

Maders H., Vergnes B., Demay Y., Agassant J.F., " Steady Flow of a White-Metzner Fluid in a 2-D Abrupt Contraction: Computation and Experiments ", *J. Non-Newt. Fl. Mech.*, 45, p. 63-80 (1992)

Marchal J.M., Crochet M.J., "A New Element for Calculating Viscoelastic Flows", *J. Non-Newt. Fl. Mech.*, 26, p. 77-114 (1987)

McHugh A.J., Mackay M.E., Khomani B., " Measurements of Birefringence by the Method of Isoclinics ", *J. Rheol.*, 31(7), p. 619-634 (1987)

McKinley G.H., " Rheological and Geometric Scaling of Purely Elastic Flow Instabilities ", *J. Non-Newt. Fl. Mech.*, 67, p. 19-47 (1996)

Meissner J., "Basic Parameters, Melt Rheology, Processing and End-Use Properties of Three Similar Low Density Polyethylene Samples", *Pure Appl. Chem.*, 42, p. 551-612 (1975)

Meissner, J., Hostettler J., " A New Elongational Rheometer for Polymer Melts and Other Highly Viscoelastic Liquids ", *Rheol. Acta*, 33, p. 1-21 (1994)

Mitsoulis E., "Numerical Simulation of Viscoelastic Fluids", in "Polymer Flow Engineering", p. 649-704

Mitsoulis E., Hatzikiriakos S.G., Christodoulou K., Vlassopoulos D., "Sensitivity Analysis of the Bagley Correction to Shear and Extensional Rheology", *Rheol. Acta,* 37, p. 438-448 (1998)

Mitsoulis E., Vlachopoulos J., "The Finite Element for Flow and Heat Transfer Analysis", *Adv. Polym. Techn.,* 4, p. 107 (1984)

Mitsoulis E., Vlachopoulos J., Mirza F.A., " A Numerical Study of the Effect of Normal Stresses and Elongational Viscosity on Entry Vortex Growth and Extrudate Swell ", *Polym. Eng. Sci.,* 25(11), p. 677-689 (1985)

Mitsoulis E., Vlachopoulos J., Mirza F.A., " Calendering Analysis without the Lubrication Approximation ", *Polym. Eng. Sci.,* 25, p. 6-18 (1985)

Mitsoulis E., Vlachopoulos J., Mirza F.A., " Numerical Simulation of Entry and Exit Flows in Slit Dies ", *Polym. Eng. Sci.,* 24(9), p. 707-715 (1984)

Mitsoulis E., Vlachopoulos J., Mirza F.A., " Simulation of Extrudate Swell from Long Slit and Capillary Dies ", *Polym. Proc. Eng.,* 2, p. 153-177 (1984)

Mitsoulis E., Vlachopoulos J., Mirza F.A., " Simulation of Vortex Growth in Planar Entry Flow of a Viscoelastic Fluid ", *J. Appl. Polym. Sci.,* 30, p. 1379-1391 (1985)

Nassehi V., Salemi R., " Finite Element Modeling of Non-isothermal Viscometric Flows in Rubber Mixing ", *Intern. Polym. Process.,* IX(3), p. 199-204 (1994)

Nouatin O.H., Coupez T., Agassant J.F., " Identification of Viscoelastic Rheological Parameters by Inverse Analysis ", Proceedings of *EURORHEO '98,* p. 112-113 (1998)

Orbey N., Dealy J.M., " Determination of the Relaxation Spectrum from Oscillatory Shear Data ", *J. Rheol.,* 35(6), p. 1035-1049 (1991)

Orbey N., Dealy J.M., *Polym. Eng. Sci.,* 24, p. 511 (1984)

Otsuki Y., Kajiwara T., Funatsu K., " Numerical Simulations of Annular Extrudate Swell of Polymer Melts ", *Polym. Eng. Sci.,* 37(7), p. 1171-1181 (1997)

Öttinger H.C., van den Brule B.H.A.A., Hulsen M.A., "Brownian Configuration Fields and Variance Reduced Connffessit", *J. Non-Newt. Fl. Mech.,* 70, p. 255-261 (1997)

Papanastasiou A.C., Scriven L.E., Macosko C.W., "An Integral Constitutive Equation for Mixed Flows: Viscoelastic Characterization", *J. Rheol.,* 27(4), p. 387 (1983)

Park H.J., Kiriakidis D.G., Mitsoulis E., Lee K.J., " Birefringence Studies in Die Flows of an HDPE Melt ", *J. Rheol.*, 36(8), p. 1563-1583 (1992)

Phan Thien N., "A Nonlinear Network Viscoelastic Model", *J. Rheol.*, 22, p. 259-283 (1978)

Phan Thien N., Tanner R.I., "A New Constitutive Equation Derived from Network Theory", *J. Non-Newt. Fl. Mech.*, 2, p. 353-365 (1977)

Picasso M., Laso M., Öttinger H.C., "Two-Dimensional, Time-Dependent Viscoelastic Flow Calculations Using Connffessit", *AICHE J.*, 43, p. 877-892 (1997)

Rajagopalan D., Armstrong R.C., Brown R.A., "Comparison of Computational Efficiency of Flow Simulations with Multimode Constitutive Equations: Integral and Differential Models", *J. Non-Newt. Fl. Mech.*, 46, p. 243-273 (1993)

Rajagopalan D., Armstrong R.C., Brown R.A., "Finite Element Methods for Calculation of Steady, Viscoelastic Flow Using a Constitutive with a Newtonian Viscosity", *J. Non-Newt. Fl. Mech.*, 36, p.159-192 (1990)

Rasmussen H.K., "Time-Dependent Finite-Element Method for the Simulation of Three-Dimensional Viscoelastic Flow with Integral Models", *J. Non-Newt. Fl. Mech.*, 84, p. 217-232 (1999)

Rasmussen H.K., Hassager O., "Simulation of Transient Viscoelastic Flow", *J. Non-Newt. Fl. Mech.*, 46, p. 298-305 (1993)

Rekers G., " Numerical Simulation of Unsteady Viscoelastic Flow of Polymers ", Ph.D. Thesis, University of Twente, Twente, The Netherlands (1995)

Renardy M., "Recent Advances in the Mathematical Theory of Steady Flow of Viscoelastic Fluids", *J. Non-Newt. Fl. Mech.*, 29, p. 11 (1988)

Rhinehart R.R., Li H.H., Murugan P., " Improve Process Control Using Fuzzy Logic ", *Chem. Eng. Progress*, Nov. issue, p. 60-65 (1996)

Rouse P.E. Jr., "A Theory of the Linear Viscoelastic Properties of Dilute Solutions of Coiling Polymers", *J. Chem. Phys.*, 21, p. 1272 (1953)

Samara M.K., " Design and Construction of Computerized Die Swell Apparatus ", Master's Thesis, McGill University, Montreal, Canada (1985)

Schoonen J.F.M., " Determination of Rheological Constitutive Equations using Complex Flows ", Ph.D. thesis, Technische Universiteit Eindhoven, Eindhoven, The Netherlands (1998)

Schunk P.R., Scriven L.E., "Constitutive Equations for Modeling Mixed Extension and Shear in Polymer Solution Processing", *J. Rheol.*, 34(7), p. 1085-1119 (1990)

Sentmanat M.L., Dealy J.M., "Some Factors Affecting Capillary Rheometer Performance", *ANTEC '95, Society of Plastic Engineers*, p. 1068-1072 (1995)

Seriai M., Guillet J., Carrot C., " A Simple Model to Predict Extrudate Swell of Polystyrene and Linear Polyethylenes ", *Rheol. Acta*, 32, p. 532-538 (1993)

Shaw M.T., Tuminello W.H., "A Closer Look at the MWD-Viscosity Transform", *Polym. Eng. Sci.*, 34(2), p. 159-165 (1994)

Sidiropoulos V., Tian J.J., Vlachopoulos J., " Computer Simulation of Film Blowing ", *J. Plast. Film Sheet*, 12, p. 107-129 (1996)

Simhambhatla M., Leonov A.I., "On the Rheological Modeling of Viscoelastic Polymer Liquids with Stable Constitutive Equations", *Rheol. Acta*, 34, p. 259-273 (1995)

Soskey P.L., Winter H.H., " Large Step Shear Strain Experiments with Parallel Disk Rotational Rheometers ", *J. Rheol.*, 28(5), p. 625-645 (1984)

Sridhar T., Gupta R.K., Boger D.V., Binnington R., *J. Non-Newt. Fl. Mech.*, 21, p. 115 (1986)

Sun J., Phan-Thien N., Tanner R.I., " Extrudate Swell Through an Orifice Die ", *Rheol. Acta*, 35, p. 1-12 (1996)

Szady M.J., Salamon T.R., Liu A.W., Bornside D.E., Armstrong R.C., Brown R.A., "A New Mixed Finite Element Method for Viscoelastic Flows Governed by Differential Constitutive Equations", *J. Non-Newt. Fl. Mech.*, 59, p. 215-243 (1995)

Talwar K.K., Khomani B., " Applications of Higher Order Finite Element Method to Viscoelastic Flow in Porous Media ", *J. Rheol.*, 36, p. 1377-1416 (1992)

Tanoue S., Kajiwara T., Iemoto Y., Funatsu K., " High Weissenberg Number Simulation of an Annular Extrudate Swell Using the Differential Type Constitutive Equation ", *Polym. Eng. Sci.*, 38(3), p. 409-419 (1998)

Taylor C.R., Ferry J., " Nonlinear Stress Relaxation of Polyisobutylene in Simple Extension and Recovery After Partial Stress Relaxation ", *J. Rheol.*, 23, p. 533-542 (1979)

Utracki L.A., Catani A., Lara J., Kamal M.R., "Polymer Processing and Properties", G. Astarita and L. Nicolais, eds., Capri, Italy, p. 79 (1983)

Utracki L.A., Lara J., Intern. Workshop on *Extensional Flows*, Mulhouse-La Bress, France (1983)

Vlachopoulos J., " Extrudate Swell in Polymers ", in *Reviews on the Deformation Behavior of Materials,* III(4), P. Feltham (ed.), p. 219-248, Freund Publishing House, Tel-Aviv, Israel (1981)

Vlcek J., Perdikoulis J., Vlachopoulos J., " Extrusion Die Flow Simulation and Design with FLATCAD, COEXCAD and SPIRALCAD ", in *Applications of CAE in Extrusion and Other Continuous Polymer processes,* K.T. O'Brien (ed.), p. 487-504, Carl Hanser Verlag (1992)

Wagner M., "Analysis of Time-Dependent Nonlinear Stress-Growth Data for Shear and Elongational Flow of a Low Density Branched Polyethylene Melt ", *Rheol. Acta,* 15, p. 136-142 (1976)

Wagner M.H., Demarmels A., " A Constitutive Analysis of Extensional Flows of Polyisobutylene ", *J. Rheol.,* 34, p. 943-958 (1990)

Wales J.L.S., " The Application of Flow Birefringence to Rheological Studies of Polymer Melts ", Ph.D. thesis, Delft University of Technology, The Netherlands (1976)

Weissenberg K., *Nature,* 159, p. 310 (1947)

White J.L., Metzner A.B., *J. Appl. Polym. Sci.,* 8, p. 1367 (1963)

White S.A., Baird D.G., " Flow Visualization and Birefringence Studies on Planar Entry Flow Behavior of Polymer Melts ", *J. Non-Newt. Fl. Mech.,* 29, p. 245-267 (1988)

White S.A., Baird D.G., " Numerical Simulation Studies of the Planar Entry Flow of Polymer Melts ", *J. Non-Newt. Fl. Mech.,* 30, p. 47-71 (1988)

Wood-Adams P., "The Effect of Long Chain Branching on the Rheological Behavior of Polyethylenes Synthesized using Single Site Catalysts", Ph.D. Thesis, McGill University, Montreal, Canada (1998)

Wood-Adams P.M., "Determination of Molecular Weight Distribution from Rheological Measurements", Master's Thesis, McGill University, Montreal, Canada (1995)

Yasuda K.Y., Armstrong R.C., Cohen R.E., *Rheol. Acta,* 20, p. 163 (1981)

Zadeh L.A., " Fuzzy Sets as a Basis for a Theory of Possibility ", in *Fuzzy Sets and Systems,* North-Holland, Amsterdam (1978)

APPENDIX: Ultimate Extrudate Swell of LLDPE at 150°C

Apparent Shear Rate (s^{-1})	Ultimate Extrudate Swell
2.22	1.369 ± 0.019
4.44	1.419 ± 0.018
8.88	1.488 ± 0.017
13.3	1.538 ± 0.017
22.2	1.602 ± 0.016
44.4	1.664 ± 0.016
88.8	1.736 ± 0.015